

**The Role of Cytomegalovirus in Organ Transplant
Rejection**

By

Iris K. A. Jones

A DISSERTATION

Presented to the Department of Molecular Microbiology and Immunology
and the Oregon Health & Science University

School of Medicine

in partial fulfillment of
the requirements for the degree of
Doctor of Philosophy

November 2020

School of Medicine
Oregon Health & Science University

CERTIFICATE OF APPROVAL

This is to certify that the Ph.D. dissertation of
Iris K. A. Jones
has been approved

Daniel N. Streblov, Ph.D., *Thesis Advisor*

Ashlee Moses, Ph.D., *Committee Member*

Victor DeFilippis, Ph.D., *Committee Member*

Timothy Nice, Ph.D., *Committee Member*

Jeffrey Nolz, Ph.D., *Committee Member*

Patrizia Caposio, Ph.D., *Committee Member*

Table of Contents

<i>Table of Contents</i>	<i>i</i>
<i>List of Figures</i>	<i>vi</i>
<i>List of Tables</i>	<i>ix</i>
<i>List of Abbreviations</i>	<i>xi</i>
<i>Acknowledgments</i>	<i>xvii</i>
<i>Abstract</i>	<i>1</i>
Chapter 1 – Introduction and Review of the Literature	4
1.1 Biology of herpes viruses	5
1.1.1 Herpesviridae.....	5
1.1.2 Cytomegalovirus is a β -herpesvirus that causes disease in immunocompromised patients.	9
1.1.3 CMV genome and structure.....	17
1.1.4 CMV viral lifecycle	19
1.2 Current status of clinical organ transplantation	31
1.2.1 Ischemia and reperfusion injury.....	32
1.2.2 Hyper-acute and acute rejection.....	32
1.2.3 Chronic rejection	33
1.3 Inflammation and immune-modulation exacerbate CMV-associated transplant vascular sclerosis and chronic rejection	34
1.3.1 The role of chemokines in transplantation.....	34
1.3.2 CMV modulates the host-immune response	39
1.3.3 CMV alters MHC expression and encodes MHC decoys.....	47

1.4 RCMV as a model for HCMV-associated disease following transplantation	50
1.5 Thesis overview and aims.....	52
<i>Chapter 2 – Blocking the IL-1 Receptor Reduces Cardiac Transplant Ischemia and Reperfusion Injury And Mitigates CMV-Accelerated Chronic Rejection.....</i>	55
2.1 Abstract	56
2.2 Introduction.....	57
2.3 Results.....	58
2.3.1 IRI transcriptomic analysis.....	58
2.3.2 Anakinra and Parthenolide reduce IRI-induced tissue damage.....	70
2.3.3 Anakinra reduces inflammatory cytokine production following transplant IRI.....	75
2.3.4 Anakinra prolongs survival of RCMV-infected cardiac allografts.....	77
2.4 Discussion	82
2.5 Materials and methods.....	85
2.6 Acknowledgments	93
<i>Chapter 3 – Rat Cytomegalovirus Virion-associated proteins R131 and R129 are Necessary for Infection of Macrophages and Dendritic cells</i>	94
3.1 Abstract	95
3.2 Introduction.....	95
3.2.1 Regulation of host-cell signaling and trafficking by CMV-encoded chemokine receptors	100
3.2.2 CMV-encoded chemokines regulate cellular migration	102
3.2.3 Role for CMV-encoded chemokines in viral entry	105
3.3 Results.....	107
3.3.1 C’terminal truncations of R131 and R129 fail to incorporate into RCMV particles	107

3.3.2 R131 and R129 are required for entry into bone marrow cells, dendritic cells, and macrophages	115
3.4 Discussion	120
3.5 Materials and methods.....	125
3.6 Acknowledgments	133
 <i>Chapter 4 – Rat and Human Cytomegalovirus ORF116 Encodes a Virion Envelope Glycoprotein Required for Infectivity.....</i>	 <i>135</i>
4.1 Abstract	136
4.2 Introduction.....	136
4.3 Results.....	139
4.3.1 R116 <i>in vitro</i> and <i>in vivo</i> expression profiles	139
4.3.2 RCMV R116 localizes to the virion assembly compartment.....	142
4.3.3 RCMV R116 is a virion associated glycoprotein.....	143
4.3.4 Loss of R116 impairs RCMV infectivity.....	146
4.3.5 UL116 knockdown impairs HCMV infectivity	150
4.3.6 Quantification of UL116 incorporation into HCMV.....	152
4.4 Discussion	153
4.5 Materials and methods.....	156
4.6 Acknowledgments	167
 <i>Chapter 5 – Conclusions and Future Directions</i>	 <i>168</i>
5.1 Summary	169
5.2 Exacerbation of CMV pathogenesis by a pro-inflammatory environment in the host 	169

5.3 CMV-encoded chemokines and other immune-modulatory proteins result in alterations in immune-cell migration	172
5.4 CMV-encoded entry complexes facilitate infection of cells that allow for viral dissemination.....	176
5.5 Conclusions.....	179
<i>References</i>	<i>182</i>
<i>Appendix I – Antibody-Independent Quantification of Cytomegalovirus Virion Protein Incorporation Using HiBiT.....</i>	<i>239</i>
AI.1 Abstract.....	240
AI.2 Introduction	240
AI.3 Materials	243
AI.3.1 RCMV BAC recombineering	243
AI.3.2 Virus rescue.....	248
AI.3.3 RCMV growth and purification.....	248
AI.3.4 Western blotting	249
AI.3.5 HiBiT in-solution detection.....	250
AI.3.6 RCMV viral genome quantification.....	250
AI.4. Methods.....	251
AI.4.1 Generation of RCMV containing R131 or R129 _(short) HiBiT fusion tags.....	251
AI.4.2 Transfection of BAC DNA and rescue of RCMV-R131 and -R129 _(short) HiBiT.....	255
AI.4.3 RCMV purification protocol	257
AI.4.4 Virion protein detection	258
AI.4.5 Trypsin sensitivity of virion-associated R131 and R129 _(short) HiBiT.....	261
AI.4.6 Quantification of virion-associated R131- and R129 _(short) -HiBiT-tagged molecules relative to viral genome copy number.....	263

AI.4.7 Observations.....	267
AI.5 Notes.....	268
AI.6 Acknowledgements	270
<i>Appendix II – Characterizing the RCMV-encoded protein r152.4</i>	<i>271</i>
AII.1 Abstract	272
AII.2 Introduction.....	273
AII.3 Results.....	275
AI.3.1 Characterization of RCMV r152.4.....	275
AI.3.2 r152.4 interacts with the cellular proteins AHNAK, Talin-1, and Pdxdc1	278
AI.3.3 RCMV lacking r152.4 has normal growth kinetics but displays impaired <i>in vivo</i> replication	279
AII.4 Discussion	282
AII.5 Materials and methods	283
<i>Appendix III – RNA Deep Sequencing Data</i>	<i>289</i>

List of Figures

Chapter 1

<i>Figure 1. CMV genome and virion structure.....</i>	<i>18</i>
<i>Figure 2. CMV lifecycle.</i>	<i>19</i>
<i>Figure 3. HCMV viral entry complexes</i>	<i>21</i>
<i>Figure 4. Components of the pentameric entry complex are not strictly conserved between CMV species</i>	<i>27</i>
<i>Figure 5. Modes of rejection in solid organ transplantation.....</i>	<i>31</i>
<i>Figure 6. Chemokine structure</i>	<i>35</i>

Chapter 2

<i>Figure 7. Study design.....</i>	<i>60</i>
<i>Figure 8. IRI causes myocardial tissue damage and PMN infiltration.....</i>	<i>61</i>
<i>Figure 9. RNAseq transcriptomic analysis of cardiac tissue and PBMC following IRI.....</i>	<i>62</i>
<i>Figure 10. IRI results in pro-inflammatory patterns at the transcriptomic level.....</i>	<i>65</i>
<i>Figure 11. IL-1R signaling molecules are up-regulated in graft and PBMC samples following transplantation leading to a pro-inflammatory response.....</i>	<i>67</i>
<i>Figure 12. qRT-PCR validation of expression levels for rat chemokines (a-c), IL-1R (d), MMP12 (e), and SPP-1 (f) in cardiac tissues from non-transplanted control, native, and graft cohorts ...</i>	<i>69</i>
<i>Figure 13. Anakinra suppresses IL-1β signaling in rat PBMC</i>	<i>71</i>
<i>Figure 14. Anakinra treatment of the recipient immediately post-transplantation improves myocardial injury score and PMN infiltrate into cardiac tissue</i>	<i>73</i>
<i>Figure 15. Representative images of cardiac tissue sections from syngeneic transplants or non-transplanted controls.....</i>	<i>74</i>
<i>Figure 16. Gating strategy for leukocytes isolated from heart tissues.....</i>	<i>75</i>
<i>Figure 17. Anakinra reduces pro-inflammatory cytokines elevated during transplantation.....</i>	<i>76</i>

<i>Figure 18. One dose of anakinra at 1-hour post-transplant significantly improves survival time and decreases viral loads at rejection.....</i>	<i>80</i>
<i>Figure 19. Anakinra does not impair viral replication in RFL6 fibroblasts or NR8383 macrophages.....</i>	<i>81</i>

Chapter 3

<i>Figure 20. Construction of RCMV R131 and R129 mutants and HiBiT tag fusions.....</i>	<i>109</i>
<i>Figure 21. R131 is expressed with late viral gene expression kinetics</i>	<i>111</i>
<i>Figure 22. R131 and R129 C' terminal regions are required for viral incorporation</i>	<i>114</i>
<i>Figure 23. R131 and R129 are essential for entry into bone marrow, DC, and macrophages, but not fibroblasts or vSMC</i>	<i>119</i>

Chapter 4

<i>Figure 24. R116 expression profiles differ between in vitro and in vivo infections.....</i>	<i>141</i>
<i>Figure 25. R116 localizes with the trans-Golgi network marker TGN-38 and the viral glycoprotein gB.....</i>	<i>143</i>
<i>Figure 26. R116 is a virion surface envelope glycoprotein.....</i>	<i>145</i>
<i>Figure 27. R116 is necessary for viral entry into fibroblasts</i>	<i>147</i>
<i>Figure 28. HCMV UL116 is required for entry into fibroblasts.....</i>	<i>151</i>

Appendix I

<i>Figure 29. HiBiT tag design for R131 and R129_(short) viral proteins.....</i>	<i>252</i>
<i>Figure 30. Virus purification and analysis workflow diagram.....</i>	<i>257</i>
<i>Figure 31. Detection of virion-associated proteins.....</i>	<i>261</i>
<i>Figure 32. R131 and R129 HiBiT proteins are trypsin sensitive</i>	<i>262</i>
<i>Figure 33. Determination of R131 and R129_(short) HiBiT molecules relative to viral genome copies</i>	<i>264</i>

Appendix II

<i>Figure 34. RCMV r152.4 is heavily glycosylated</i>	<i>277</i>
---	------------

Figure 35. r152.4 is expressed with early viral gene kinetics 278

Figure 36. RCMV viruses with 2x STOP mutations in the r152.4 gene show impaired viral dissemination in vivo, but not in vitro..... 281

List of Tables

Chapter 2

<i>Table 1. Animal cohorts.</i>	60
<i>Table 2. Contribution of molecules predicted to be up-regulated from Figure 10 to pro-inflammatory and immune-cell recruitment associated functions as predicted by IPA in PBMC.</i>	66
<i>Table 3. Pro-inflammatory signaling molecules are up-regulated in graft and PBMC data following transplantation.</i>	68
<i>Table 4. Myocardial injury scoring system used for evaluation of cardiac graft tissue damage.</i>	86
<i>Table 5. qRT-PCR primers and probes</i>	89

Chapter 3

<i>Table 6. CMV encoded chemokines</i>	99
<i>Table 7. CMV encoded chemokine receptors</i>	99
<i>Table 8. CMV pentameric entry complex determinants</i>	124
<i>Table 9. Average number of cells per well counted for RCMV entry assays</i>	133

Chapter 4

<i>Table 10. PEG treatment restores infectivity of RCMV lacking R116</i>	149
<i>Table 11. Primer and probe sets for qRT-PCR</i>	164

Appendix I

<i>Table 12. DNA primers</i>	247
------------------------------------	-----

Appendix III

<i>Table 13. Canonical pathway analysis summary for rat cardiac IRI: up-regulated pathways</i> ...	290
<i>Table 14. Canonical pathway analysis summary for rat cardiac IRI: down-regulated pathways</i>	293
<i>Table 15. Canonical pathway analysis summary for rat PBMC following IRI: up-regulated pathways</i>	294

Table 16. Canonical pathway analysis summary for rat PBMC following IRI: down-regulated pathways..... 299

Table 17. Fold-change data, p-values, and FDR-corrected p-values for all genes and comparisons from RNAseq data..... 300

List of Abbreviations

AHNAK	Neuroblast differentiation-associated protein AHNAK (Desmoyokin)
AIDS	Acquired immunodeficiency syndrome
ANOVA	Analysis of Variance
ATP	Adenosine tri-phosphate
BAC	Bacterial artificial chromosome
BME	β -Mercaptoethanol
bp	Base pairs
BSA	Bovine serum albumin
C'terminal	Carboxy terminal
(CC/CXC/XC)R	(CC/CXC/XC) Receptor
CCL	CC chemokine/ CC ligand
cDNA	Complement deoxyribonucleic acid
Chlor	Chloramphenicol
CMC	Carboxymethyl cellulose
CMV	Cytomegalovirus
CR	Chronic rejection
CREB	cAMP (cyclic adenosine monophosphate) response element-binding protein
CXCL	CXC chemokine/ CXC ligand
Cys	Cysteine
DAMP	Damage associated molecular pattern
DAPI	4',6-diamidino-2-phenylindole
DC	Dendritic cells
DMEM	Dulbecco's modified Eagle's medium
DNA	Deoxyribonucleic acid
DOG plates	2-deoxy-galactose-1-phosphate plates
dpi	Days post-infection
dsDNA	Double stranded deoxyribonucleic acid

(e)GFP	(enhanced) Green fluorescent protein
EBV	Epstein-Barr virus
EGF	Epidermal growth factor
ELISA	Enzyme-linked immunosorbent assay
ELR	Glutamic acid- Leucine- Arginine motif
Endo H	Endoglycosidase H
ER	Endoplasmic reticulum
F-12K	Kaighn's modification of Ham's F-12 medium
FBS	Fetal bovine serum
FCAR	Immunoglobulin alpha Fc-receptor
FDR	False discovery rate
FKBP	FK506 binding protein
g(B/H/N/M/L/O)	Glycoprotein (B/H/N/M/L/O)
GAPDH	Glyceraldehyde 3-phosphate dehydrogenase
gc(I/II/III)	Glycoprotein complex (I/II/III)
gpCMV	Guinea pig Cytomegalovirus
GPCR	G-protein (guanine nucleotide-binding protein) coupled receptor
H&E	Hematoxylin & Eosin
HCMV	Human Cytomegalovirus
HHV-6	Human herpesvirus - 6
HHV-7	Human herpesvirus - 7
HIV	Human immunodeficiency virus
HLA	Human leukocyte antigen
hpi	Hours post-infection
HRP	Horseradish peroxidase
HSPGs	Heparan sulfate proteoglycans
HSV-1	Herpes simplex virus - 1
HSV-2	Herpes simplex virus - 2
i.p.	Intraperitoneal

ICP0	Infected cell polypeptide 0
IE	Immediate early
IFN	Interferon
Ig(G/M)	Immunoglobulin (G/M)
IL	Interleukin
IL-1R	Interleukin-1 receptor
IL-1Ra	Interleukin-1 receptor antagonist
IPA	Ingenuity pathway analysis
IR(L/S)	Internal repeat(long/short)
IRF	Interferon regulatory factor
IRI	Ischemia and reperfusion injury
Kan	Kanamycin
kbp	kilobase pairs
kDa	kiloDaltons
kg	kilogram
KSHV	Kaposi's sarcoma associated herpesvirus
LILRB(1/3)	Leukocyte immunoglobulin-like receptor subfamily B member (1/3)
(m/μ/n)M	(milli/micro/nano) Molar
MCK	Murine cytomegalovirus chemokine
MCMV	Mouse Cytomegalovirus
MCP-1	Monocyte chemoattractant protein - 1
mg	milligram
MHC	Major histocompatibility complex
MIEP	Major immediate early promoter
MIP	Macrophage inflammatory protein
miRNA	Micro ribonucleic acid
MOI	Multiplicity of infection
mRNA	Messenger ribonucleic acid
MuHV8	Murine Herpes virus 8 (English strain of rat cytomegalovirus)

N'terminal	Amino terminal
NF-κB	Nuclear factor kappa-light-chain-enhancer of activated B cells
ng	Nanogram
NI	Neointimal index
NK cells	Natural Killer cells
NKG2D	Natural killer group 2D receptor
NRP-2	Neuropilin-2
NTC	No template control
ORF	Open reading frame
PAMP	Pathogen associated molecular pattern
PBMC	Peripheral blood mononuclear cells
PBS	Phosphate buffered saline
PCR	Polymerase chain reaction
PDGFRα	Platelet-derived growth factor receptor α
Pdxdc1	Pyridoxal-dependent decarboxylase domain-containing protein 1
PEG	Polyethylene glycol
PFA	Paraformaldehyde
PMN	Polymorphonuclear leukocytes
PMSF	Phenylmethylsulfonyl fluoride
PNGase F	Peptide-N-glycosidase F
POD	Post-operation day
pp	Phosphoprotein
PRR	Pattern recognition receptor
PSG	Penicillin, Streptomycin, Glutamine additive
PVDF	Polyvinylidene fluoride
qPCR	Quantitative polymerase chain reaction
qRT-PCR	Quantitative real-time polymerase chain reaction
QS	Quantum sufficit
RCMV	Rat Cytomegalovirus

RFL6 cells	Rat fibroblast lung - 6 cells
RhCMV	Rhesus Cytomegalovirus
RNA	Ribonucleic acid
RNAseq	RNA deep sequencing
RPM	Revolutions per minute
RPMI medium	Roswell Park Memorial Institute medium
RT-PCR	Real time polymerase chain reaction
SDS-PAGE	Sodium dodecyl sulfate - polyacrylamide gel electrophoresis
SEM	Standard error of the mean
SMG	Submandibular glands
SOT	Solid organ transplantation
TAP	Transporter associated with antigen processing
TBST	Tris-buffered saline with 0.1% Tween-20
TCEP	Tris 2-carboxyethyl phosphine
TGFβ1	Transforming growth factor β 1
TGFβRIII	Transforming growth factor β receptor III
TGN	Trans-golgi network
TLR	Toll like receptor
TNE	Tris-Sodium Chloride-Ethylenediaminetetraacetic acid solution
TNF	Tumor necrosis factor
TR_(L/S, L/R)	Terminal repeat _(long/short, left/right)
TRC8	Translocation in renal carcinoma on chromosome 8
TVS	Transplant vascular sclerosis
U/mL	Units per milliliter
UL	Unique long
US	Unique short
UW solution	University of Wisconsin solution
(v)SMC	(vascular) Smooth muscle cells
VZV	Varicella Zoster virus

WT	Wildtype
μg	microgram
μL	microliter
μm	micrometer

Acknowledgments

Like all good science, this dissertation is the product of years of work across multiple collaborations, involving both biological scientists and non-biologists. My thanks must first go to my mentor, Dr. Daniel Streblow for his never-ending support, enthusiasm, and flexibility. Second, I would like to thank the entire Streblow lab for all of their support, discussions, and help over the years. Thanks also go to my advisory committee members for their career guidance and input as my projects evolved. Finally, this work would not have been possible without the non-biologists in my life. Many thanks and much appreciation go to my family and friends for their support leading up to and throughout my graduate education. First and foremost, thanks go to my parents, Cynthia and David Archer, for their support of my education, for giving me opportunities to get away to the farm on the weekends, and for their constant encouragement and sound advice in all things. Most important of all, my eternal gratitude goes to my husband, Mike Jones, for all the emotional support, proof-reading, cooking, and warm hugs over the years.

Abstract

Cytomegaloviruses (CMV) are β -herpesviruses that establish persistent, latent infection in their hosts. Human CMV (HCMV) infection causes significant morbidity and mortality in immunosuppressed patients, including transplant recipients. Additionally, HCMV infection exacerbates the development of transplant vascular sclerosis (TVS) and accelerates chronic rejection (CR) of solid organ transplants. Current therapies to control HCMV do not sufficiently prevent this exacerbation of disease, warranting further research. Here, we examine interactions between the host-immune response and CMV-encoded proteins during pathogenesis and viral dissemination, using a rat CMV (RCMV) infection model of rat cardiac transplantation.

The role of pro-inflammatory host-immune responses as a result of ischemia and reperfusion injury (IRI) in promotion of CMV-exacerbation of TVS and CR are examined in Chapter 2. Utilizing a rat heart isogeneic transplant model, inflammatory pathways involved in IRI are identified as possible therapeutic targets in development of disease. Treatment with two inhibitors of the Interleukin-1 Receptor (IL-1R) pathway significantly reduced graft inflammation and cellular recruitment in the treated recipients relative to non-treated controls. Treatment with an IL-1R antagonist (IL-1Ra) administered at 1-hour post-transplant to recipients of RCMV⁺ cardiac allografts significantly increased the time to rejection. Our results indicate that reducing IRI provides a promising approach for extending survival of cardiac allografts from CMV-infected donors.

Herpesviruses encode multiple glycoproteins required for different stages of viral attachment, fusion, and envelopment. In Appendix I, a novel tagging approach (HiBiT) is described for quantifying incorporation of such proteins into the viral particle. This technique is employed in Chapter 3 to elucidate the role of two RCMV-encoded chemokines with additional roles as entry complex components, R131 and R129. These are putative homologues of HCMV pentamer components UL130 and UL128, but their incorporation, copy number per virion, and role in entry remain to be explored. We demonstrate similar molecular entry requirements for R131 and R129 in a myriad of rat cells as observed for HCMV, and provide evidence that R131 and R129 are part of the viral entry complex required for entry into monocytes.

Chapter 4 discusses the protein encoded by the HCMV open reading frame (ORF) UL116, which forms a stable, virion-associated complex with glycoprotein H (gH), to unknown function. Characterization of the RCMV putative homologue of UL116, R116, reveals similar expression kinetics, post-translational modifications, and roles in viral entry into fibroblasts. A requirement for HCMV UL116 in production of infectious virions is also demonstrated.

In Appendix II, new data on the RCMV glycoprotein r152.4 is discussed. r152.4 is expressed at high levels in multiple tissues post-infection. r152.4 is expressed with early gene kinetics and does not affect viral growth *in vitro*, but r152.4-deficient RCMV exhibits lower viral loads *in vivo*. Although extensive work has detailed major histocompatibility

complex-1 (MHC-I)-like immunomodulatory proteins in mouse CMV (MCMV), this work provides further data towards characterizing a proposed MHC-I-like protein in RCMV.

The experimental data described in this body of work characterizes a variety of factors that contribute to CMV acceleration of CR and development of TVS using an RCMV infection model of rat cardiac transplantation.

Chapter 1 – Introduction and Review of the Literature

1.1 Biology of herpes viruses

1.1.1 Herpesviridae

Herpesviridae are a family of viruses under the order herpesvirales [1]. Other members of this order include alloherpesviridae and malacoherpesviridae. These families all contain herpesviruses, but are differentiated based on host species. Herpesviridae contains mammal, bird, and reptile viruses; alloherpesviridae contains fish and frog viruses; and malacoherpesviridae contains the single-identified bivalve herpes virus *ostreid herpesvirus 1*. Herpesviruses are enveloped, tegumented viruses with a linear double-stranded deoxyribonucleic acid (DNA) genome. For this family of viruses, the genome sizes range from 125-290 kilobase pairs (kbp). The viral genome is encapsulated in a T=16 icosahedral capsid, which is surrounded by a protein layer known as the tegument. This entire particle is enveloped by a lipid bilayer studded with viral proteins that mediate entry. There are over 100 known herpesviruses, however only 8 regularly infect humans [2]. These are herpes simplex virus 1 (HSV-1) and 2 (HSV-2), varicella zoster virus (VZV), HCMV, Epstein-Barr virus (EBV), human herpesviruses 6a, 6b, and 7, and Kaposi's sarcoma-associated herpesvirus (KSHV). Human herpesviruses often have a relatively high seroprevalence globally and cause life-long infection of the host, characterized by a pattern of latency and reactivation, with reactivation often triggered by immunosuppression, inflammation, or stress. Due to the traditionally restricted host range of herpesviruses, only one other herpesvirus is known to occasionally infect humans: macacine herpesvirus 1, more commonly known as simian herpesvirus B. Herpesvirus B infection in humans causes often fatal encephalitis. The Herpesviridae family is sub-divided further into sub-families:

α -, β -, and γ - herpesvirinae [1]. These subfamilies are divided based on host tropism restriction and replication kinetics [2].

I. α -Herpesvirinae

α -Herpesviruses are characterized by a short replicative cycle and broad host tropism [2]. HSV-1 and -2 and VZV are members of the α -herpesvirus sub-family, along with several veterinary herpesviruses such as gallid herpesvirus 2 and 3, the causative agents of Marek's disease in chickens [1]. α -Herpesviruses typically establish latency in the sensory nerve ganglia of hosts following primary infection, which provides their characteristic reactivation patterns. For example, VZV is associated with chickenpox during primary infection and shingles during reactivation from ganglionic neurons [3]. VZV primarily infects T lymphocytes, epithelial cells, and neuronal ganglia. Although chickenpox is considered a common childhood disease, shingles, also known as zoster, can have serious complications including postherpetic neuralgia, myelitis, cranial nerve palsies, meningitis, stroke, retinitis, ulcer, pancreatitis, and hepatitis. Reactivation is believed to occur as host immunity wanes following the primary exposure, warranting vaccination to boost immunity in individuals over 60 years of age. VZV is the only human herpesvirus with an effective vaccine. The live-attenuated strain, vOka, has been used to vaccinate young children against chickenpox and elderly individuals against zoster. Recently, an effective subunit vaccine was developed by GlaxoSmithKline for use in elderly and immunocompromised individuals to provide immunity to zoster in the absence of a replication competent virus [3]. HSV-1 and HSV-2 are α -herpesviruses that establish latency in dorsal root ganglia of the autonomic nervous system [4]. These viruses are

transmitted through close physical contact. Reactivation of both viruses occurs throughout the lifetime of the host, resulting in herpetic lesions. HSV-1 is associated with orofacial infections and encephalitis, whereas HSV-2 is associated with genital infections. Like many herpesviruses, seroprevalence is high and often correlates with socio-economic status globally. HSV-1 seroprevalence ranges from 70-80% in adolescents in under-developed nations compared to 40-60% seroprevalence by 40 years of age in developed nations. HSV-2 has a slightly lower seroprevalence globally with 20-30% of the population infected by age 29 in under-developed nations compared to 35-60% by age 60 in developed nations [4].

II. β -Herpesvirinae

β -Herpesviruses are characterized by a long replicative cycle and a restricted host range [2]. This sub-family includes a number of species-specific CMVs as well as the human herpesvirus 6 (HHV-6) and 7 (HHV-7) [1]. There are 9 known CMV species: human (human herpesvirus 5), rhesus (macacine herpesvirus 3), chimpanzee (panine herpesvirus 2), African green monkey (cercopithecine herpesvirus 5), mouse (murid herpesvirus 1), rat - Maastricht (murid herpesvirus 2), rat - English/Berlin (murid herpesvirus 8), guinea pig (caviid herpesvirus 2), and pig (suid herpesvirus 2) [1,5]. HCMV infection is associated with a mild or asymptomatic infection in healthy individuals [6]. Individuals who develop disease typically present with mononucleosis-like symptoms. However, HCMV can cause severe disease in immunocompromised individuals and during congenital infections, and is associated with skewing of the host T-cell repertoire towards CMV-antigens (covered in detail in section 1.1.2) [6–9]. The other β -herpesviruses that infect humans are HHV-6 and

HHV-7 and are associated with roseola infantum in young children (also known as exanthem subitum or sixth disease) [10]. Primary infection typically results in a high fever followed by a rash. Since cases typically resolve on their own, treatment is supportive. However, like other herpes virus infections, HHV-6 and -7 can reactivate with severe systemic consequences including encephalitis and meningitis in immunocompromised hosts. HHV-6 has a particularly high seroprevalence, infecting 50-60% of children globally by 12 months of age, and nearly 100% of children by age 3. HHV-7 typically infects children a little later in life; however, it also has a high global seroprevalence with 90% of children infected by 10 years of age [10].

III. γ -Herpesvirinae

γ -Herpesviruses are characterized by their extremely restricted host range [2]. EBV and KSHV are the two members of the γ -herpesvirus sub-family that infect humans, and the sub-family also includes Rhesus rhadinovirus (macacine herpesvirus 5), which is commonly used in rhesus macaques as a model of γ -herpesvirus infections [1]. EBV shares several similarities with the β -herpesvirus HCMV. Symptoms of primary infection with EBV are similar to HCMV, with EBV being the primary cause of mononucleosis in patients [11]. However, where HCMV infects a wide variety of cells, EBV primarily infects B lymphocytes and epithelial cells. EBV has similar global seroprevalence to HCMV, with approximately 90% of the global population infected. EBV infection is occasionally associated with more severe disease including Hodgkin and non-Hodgkin lymphomas, nasopharyngeal carcinoma, and Burkitt lymphoma in immunocompromised patients. In transplant recipients, EBV is particularly associated with lymphoproliferative disorders

[11]. KSHV is typically associated with the development of Kaposi sarcoma in immunocompromised patients, with the greatest disease burden seen in Human immunodeficiency virus (HIV)/Acquired immunodeficiency syndrome (AIDS) patients [12].

1.1.2 Cytomegalovirus is a β -herpesvirus that causes disease in immunocompromised patients.

I. Epidemiology

The β -herpesvirus Human herpesvirus 5, more commonly known as HCMV, is ubiquitous in the population, with infection rates ranging from 66-90% of the population [13]. Seroprevalence rates tend to be slightly higher in women of reproductive age and among blood and organ donors; however, this is likely due to the exclusion of children in these groups [13]. In immunocompetent individuals, HCMV infection is typically mild, but viral infection can result in severe disease in immunocompromised individuals and the virus is associated with the development of permanent neurological injuries in developing fetuses following *in utero* infection [8,9]. Following primary infection, HCMV establishes persistent, latent infections in hosts, allowing for reactivation at later time points [6]. In non-immunocompromised patients, this has been associated with increased morbidity and mortality due to cardiovascular disease among aged populations [14,15]. Specifically, HCMV infection is associated with increased systolic blood pressure and rates of cardiovascular death in older populations. In immunosuppressed patients, CMV disease manifests as fever, leukopenia, malaise, and arthralgia, and may also present as a tissue-

invasive disease, with inflammation of the target organ [6]. In the case of tissue-invasive disease, CMV may cause end-stage organ disease, with CMV pneumonia being a particularly serious condition in these patients [6,16,17].

II. Congenital CMV syndrome

Congenital CMV infection affects 20,000-30,000 infants in the US annually, making it the most common cause of congenital infection [9]. Although only 10-15% of infants with congenital CMV infection show symptoms at birth, about 50% of asymptomatic infants will go on to develop sequelae including sensorineural hearing loss. Those infants who are symptomatic exhibit central nervous system abnormalities including microcephaly. Other symptoms include lethargy, jaundice, and hepatosplenomegaly [9]. Previous exposure to CMV does not necessarily protect women from an active infection during pregnancy resulting from super-infection or reactivation [18]. However, infants with congenital CMV infection are less likely to develop severe neurological defects and other sequelae from mothers with previous exposure. Research is on-going to develop a congenital CMV vaccine using live-attenuated, recombinant glycoprotein B (gB), viral vector, and DNA vaccine approaches, along with antibody infusion therapies [18].

III. HCMV in AIDS patients

CMV infection or reactivation associated with development of AIDS in HIV⁺ patients results in severe disease [19]. CMV disease typically manifests in these patients when CD4⁺ T-cell levels drop below 100 cells/microliter (μL). Symptoms in these patients range from fever and malaise to severe end-organ disease, with the most common symptom being

retinitis. CMV disease rates in the HIV⁺ population have been reduced since the introduction of highly-active anti-retroviral therapy to treat HIV [19].

IV. HCMV in transplant recipients

HCMV is the most significant infectious pathogen in organ transplant recipients [6,20]. Transplant recipients face impacts from CMV infection if either the donor or the recipient are infected, with HCMV promoting CR and decreasing graft and patient survival [21,22]. Both solid organ and hematopoietic stem cell transplant recipients are also at increased risk of developing CMV pneumonia post-transplantation, with fatality rates ranging from 30-50% despite therapy [16,17]. HCMV infection decreases cardiac graft survival and increases development of TVS in patients with both HCMV infection and HCMV disease [21]. In the clinic, donor⁺/recipient⁻ solid organ transplantation (SOT) combinations are at the greatest risk of CMV-associated complication and CMV-disease [22]. Graft blood vessels are essential targets in the development of graft injury [20]. HCMV infection results in elevated serum cytokine levels in bone marrow transplant recipients, with Interleukin (IL)-6 correlating with CMV disease [23]. In addition to acute CMV disease, CMV induces the up-regulation of allo-antigens and recruits immune cells to the site of the graft, resulting in allo-reactivity and graft rejection [22]. Human leukocyte antigen (HLA) mismatch between donor and recipient exacerbates these responses [24]. HCMV establishes latency in CD34⁺ bone marrow progenitor cells and monocytes, suggesting that immune cells present in graft organs are key to exacerbation of graft rejection associated with HCMV infection of the donor [21].

V. HCMV mechanism of spread

HCMV is typically spread between hosts via saliva, sexual contact, and breast-feeding [6]. However, it can also spread via blood transfusion, SOT, hematopoietic stem cell transplant, and from mother to fetus during pregnancy. HCMV typically establishes infection via: (1) epithelial cells of the rhino-pharynx or genital tract or (2) endothelial cells of the vascular tree during blood transfusion [25]. Studies of MCMV infection have demonstrated that transmission occurs in olfactory and alveolar epithelial cells [26,27]. The secondary sites of infection are typically macrophages and dendritic cells (DC), which serve to provide a vehicle for viral dissemination throughout the host [26,27]. In addition to infection of tissue resident monocytes, CMV encodes several chemokines to recruit cells to the site of infection to facilitate viral dissemination, as discussed below in section 1.3.2.III. Re-entry of infected DC into the circulation is driven by CMV-encoded chemokine receptors, such as HCMV US28 and MCMV M33. In MCMV, M33 mutants fail to establish infection in the salivary glands following intranasal infection, although the virus readily replicates at the initial site of infection [27,28]. Additionally, M33 promotes extravasation of infected DC into salivary gland tissues, explaining the loss of viral titer in salivary glands in M33-deficient mutants [29]. Importantly, the HCMV chemokine-receptor US28 also promotes infected DC to re-enter circulation from the site of infection [29]. This function appears to be highly conserved across CMV species, as RCMV R33 mutants also fail to show viral replication in salivary glands. However, in the case of R33, trafficking of virus did occur, but the virus failed to establish infection in the salivary gland tissue. R33 mutants also show reduced mortality in immunocompromised rats and delayed progression to cardiac graft CR compared to wildtype (WT) RCMV infections [30,31]. Importantly, these studies

point to slight differences in the functionality of CMV-encoded chemokine receptors. However, US28 and UL33 are partially redundant in function with MCMV M33, since they correct for a loss of MCMV reactivation and viral replication in salivary glands in an M33-signaling deficient infection [32].

VI. Therapeutics

Current therapeutic approaches for CMV typically employ anti-viral prophylactic small molecules. Ganciclovir, valganciclovir, cidofovir, foscarnet, and letermovir are all approved for the treatment of HCMV infections, either as systemic treatments or as a prophylactic therapy [33]. Ganciclovir, valganciclovir, cidofovir, and foscarnet block viral DNA synthesis by targeting the viral DNA polymerase encoded by the HCMV UL54 gene. Ganciclovir and oral pro-drug valganciclovir, are competitive inhibitors of deoxyguanosine triphosphate incorporation into DNA with preferential inhibition of viral DNA polymerases [33,34]. Similarly, cidofovir, which is a deoxycytidine acyclic nucleotide phosphonate analog, also targets UL54 as a competitive inhibitor during DNA elongation [33]. Foscarnet is a trisodium salt of phosphonoformic acid that prevents chain elongation by inhibiting the formation of phosphodiester bonds between nucleoside bases that are incorporated into the growing DNA chain by viral DNA polymerases [35]. Foscarnet is effective against multiple herpesviruses including HCMV, HSV-1 and 2, VZV, and EBV [35]. Letermovir acts slightly later in viral replication by targeting UL56. This compound blocks viral assembly by preventing DNA packaging into viral capsids [33]. All of these small molecules are prone to generation of viral resistance, especially in immune-compromised patients, and they also have several associated drug-related toxicities [33].

Additionally, anti-viral prophylactic therapies do not prevent late-onset HCMV disease in patients [22]. Similarly, in a rat model of cardiac transplant rejection, prophylactic use of ganciclovir failed to protect against CMV-acceleration of CR and development of TVS in latently infected grafts [36].

Other therapies available include Fomivirsen, a 21-mer oligonucleotide, with anti-sense complementarity to the HCMV Immediate Early (IE)-2 messenger ribonucleic acid (mRNA) [37]. Fomivirsen use is typically restricted to intravitreal injection to treat CMV retinitis [37]. Anti-HCMV Immunoglobulin G (IgG) constitutes another therapeutic option. High doses of anti-HCMV IgG have been used in neonates to prevent *in utero* transmission from HCMV-positive mothers [6]. This approach has also shown some promise in reducing disease risk in pregnant women and in renal solid organ transplant recipients [6].

VII. Vaccines

Vaccines offer a proactive, preventative approach to reducing CMV-associated disease [38]. Unfortunately, herpesviruses are notoriously difficult to develop sterilizing immunity against, with VZV being the only human herpesvirus to date with an effective vaccine [3]. However, several vaccine platforms are under investigation including live-attenuated HCMV strains; viral vectored vaccines; gB subunit vaccines; DNA-based vaccines encoding either phosphoprotein (pp) 65 (the primary tegument protein), gB, or IE1; and ribonucleic acid (RNA)-based vaccines against similar targets; virus-like particle vaccines; and dense body vaccines [33]. Several live-attenuated vaccines and a gB subunit vaccine

have reached phase I and II clinical trials, and a DNA-based vaccine has reached phase III clinical trials as of early 2020 [33].

Several live-attenuated vaccine approaches have been tested in clinical trials, typically based on laboratory-attenuated strains. The HCMV strain AD169 was heavily passaged in human fibroblasts, resulting in several attenuating mutations. An early vaccine study compared subcutaneous and intradermal injection of AD169 as a vaccine candidate. Subcutaneous vaccination of individuals with AD169 resulted in neutralizing antibody responses, where intradermal injection did not [39]. More recently, a vaccine strain of AD169 was modified to express the pentamer and further attenuated by the addition of an FK506 binding protein (FKBP)-destabilization domain switch requiring the presence of Shield-1 for production of infectious viral particles. This modified vaccine strain, V160, produced neutralizing antibody titers in rabbits and rhesus macaques, and elicited CD4⁺ and CD8⁺ T-cell responses [40]. Clinical trials with V160 elicited neutralizing antibody responses effective against a range of clinical isolates and induced memory B-cell responses [41]. However, these memory responses were slightly lower than those seen in naturally-infected seropositive individuals. Another laboratory-attenuated HCMV strain, Towne, has also been used in clinical trials. Although the Towne vaccine elicited neutralizing antibodies capable of preventing infection of epithelial cells, patient neutralizing antibody titers were lower than those seen following natural infection with HCMV [42]. A subcutaneous recombinant live-attenuated vaccine generated from Towne and non-attenuated Toledo strains resulted in seroconversion and CD4⁺ and CD8⁺ T-cell responses in some vaccinated individuals [43]. However, neutralizing antibody titers were

low in seroconverted individuals, and the other vaccine chimeras in this study were not as effective. Importantly, none of these studies with live-attenuated viruses reported serious negative reactions indicating a good level of safety, albeit lacking efficacy.

Research *in vitro*, *in vivo* in small animal models, and in clinical trials has suggested that the most effective vaccine targets consist of viral envelope glycoprotein complexes. These include gB, gH and gL, and the pentamer complex consisting of gH/gL/UL128/UL130/UL131A. Analysis of neutralizing antibody targets in hyperimmune globulin from seropositive patients suggested that pentamer-specific antibodies were present at higher concentrations than those against gB or gH/gL, driving researchers to pursue anti-pentamer vaccines [44]. Wussow et al. compared pentamer, gH/gL, and gB as targets using a modified vaccinia Ankara vectored vaccine expressing either complete pentamer, gH/gL, UL128-UL131A, or gB in mice and rhesus macaques [45]. The complete pentamer vaccine elicited significantly greater neutralizing antibody titers in both mice and macaques than the other proteins [45]. Similarly, a modified vaccinia Ankara vectored vaccine expressing the Rhesus CMV (RhCMV) homologues of the pentamer components resulted in similar antibody titers in rhesus macaques as natural infection with RhCMV, whereas vaccines expressing only some of the homologues or gB exhibited minimal neutralizing antibody titers [46]. Animals vaccinated with the complete set of pentamer homologues exhibited lower viral loads following infection with RhCMV [46]. Anti-gB vaccines have also been explored, with gB subunit vaccines tested in clinical trials with some efficacy, but, notably, eliciting lower neutralizing antibody titers than those seen in HCMV seropositive individuals [42,47]. A gB subunit vaccine purified by column

chromatography and given by intramuscular injection was able to elicit neutralizing antibody titers on par with natural infection; however, 4 doses of the vaccine were necessary to establish equivalent responses after 1 year [47]. Although several vaccines targeting viral glycoproteins have shown promise, additional work will be necessary to develop a successful HCMV vaccine.

1.1.3 CMV genome and structure

Like all members of the Herpesviridae family, CMV is an enveloped virus with a T=16 icosahedral capsid. The virus contains a dsDNA genome [1] that can exist as different genome configurations (Figure 1). For example, the HCMV genome contains repeat regions on either side of its two unique regions named Unique long (UL) and Unique short (US) (Figure 1a) [48,49]. In contrast, RCMV consists of only one unique region flanked by terminal repeats [50] (Figure 1a). HCMV viral DNA is encapsulated in a capsid consisting of UL86, UL46, UL85, and UL48A [51]. Surrounding the viral capsid are the inner and outer tegument layers that are composed of a myriad of viral proteins including pp65 and pp150. pp65 is the most abundant tegument protein and pp65-deficient virus results in changes to the incorporation levels of other tegument proteins, suggesting that pp65 serves as a scaffold for other tegument proteins [52,53]. pp150 serves as the binding tegument layer surrounding the viral capsid [54]. Tegument proteins have a variety of functions, but typically either support the structural integrity of the virion, function to improve viral transcription and replication, or promote viral envelopment and egress [52,53,55,56]. The viral envelope of CMV is studded with glycoproteins. To date, 19 glycoproteins have been identified as being incorporated into the viral particle [53]. Some

of these have roles in entry, however, not all do. Those that are involved in viral entry include gM, gN, gB, gH, gL, gO, UL128, UL130, UL131A, and UL116. These glycoproteins form a variety of complexes discussed below in 1.1.4.I (CMV Viral Entry). Proteomics analyses of HCMV viral particles revealed incorporation of a number of viral capsid, tegument, and glycoproteins, as well as other viral and host proteins not previously recognized as being incorporated into virions [53]. Similar findings were described for MCMV, with incorporated proteins including the MCMV DNA packaging protein, assembly protein, DNA polymerase proteins, glycoproteins, and capsid and tegument proteins [55].

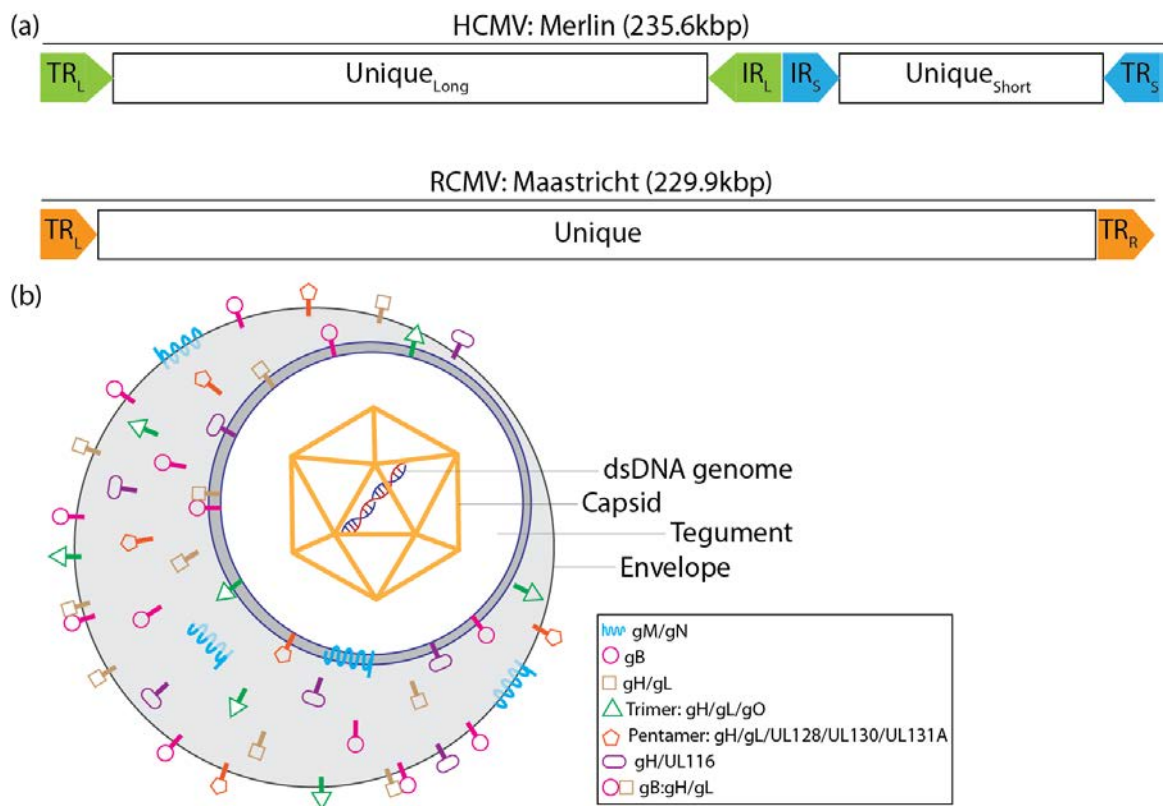


Figure 1. CMV genome and virion structure. (a) The HCMV Merlin genome contains unique long and unique short regions bracketed by their associated terminal and internal repeats (TR_L , TR_S , IR_L , IR_S). The RCMV Maastricht genome contains a single unique region bracketed by a terminal repeat left (TR_L) and a terminal

repeat right (TR_R). (b) The CMV viral particle is an enveloped, tegumented viral particle containing a double stranded (ds) DNA genome in a viral protein capsid.

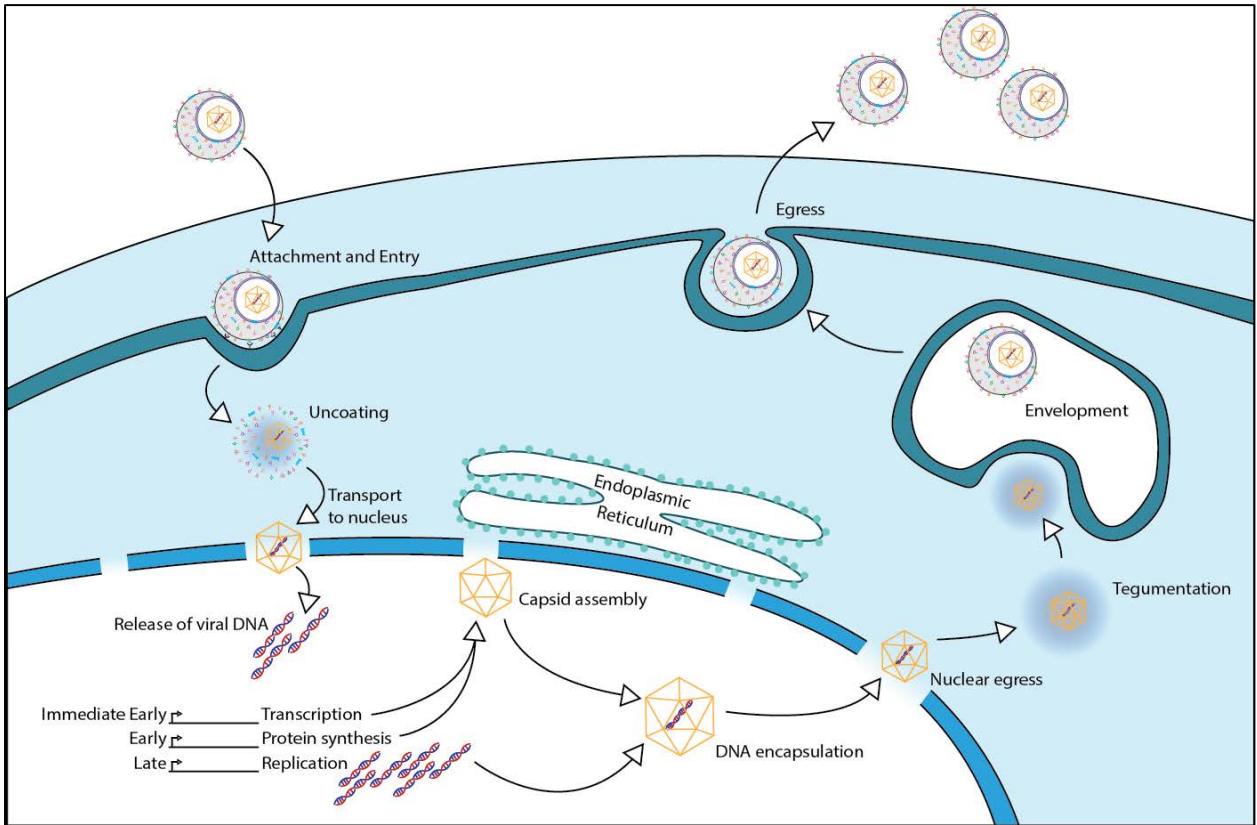


Figure 2. CMV lifecycle.

1.1.4 CMV viral lifecycle

CMV infects a variety of cell types, including fibroblasts, epithelial cells, endothelial cells, macrophages, and DC, and can establish infection in many organs of the body. The CMV lifecycle consists of entry, uncoating and trafficking of the viral capsid to the nucleus, viral gene expression and DNA replication, capsid assembly and DNA encapsulation, nuclear egress, tegumentation, envelopment, and egress (Figure 2). These processes are discussed in detail below (1.1.4.I-V).

I. CMV viral entry

Given the broad cellular tropism of CMV, entry is an important step in the viral lifecycle. CMV enters cells through two primary processes – pH-independent fusion and pH-dependent fusion – determined by cell type and virion associated receptor binding complexes. This process begins by tethering of the virus to the host cell membrane via binding of viral glycoproteins to heparan sulfate proteoglycans; followed by endocytosis, macropinocytosis, or membrane fusion involving a variety of cellular receptors and viral protein complexes. CMVs encode 19 known structural glycoproteins that are incorporated into the mature virion. However, not all of these glycoproteins participate in the viral entry process [53]. Of those that do, gB, gH, gL, gM, gN, gO, UL128, UL130, and UL131A are the most well characterized for their roles in virion assembly and virus entry. These glycoproteins form several identified complexes known as glycoprotein complex (gC) I, gCII, gCIII, gH/UL116, and the pentamer and consist of gB, gM/gN, gH/gL/gO, gH/UL116, and gH/gL/UL128/UL130/UL131A, respectively [57,58]. These complexes promote entry through either pH-independent entry by macropinocytosis or membrane fusion, or pH-dependent entry via endocytosis or macropinocytosis (Figure 3). Many cellular receptors have been proposed as having a role in these HCMV entry processes, but further work remains to be done to detail the mechanisms through which they promote entry.

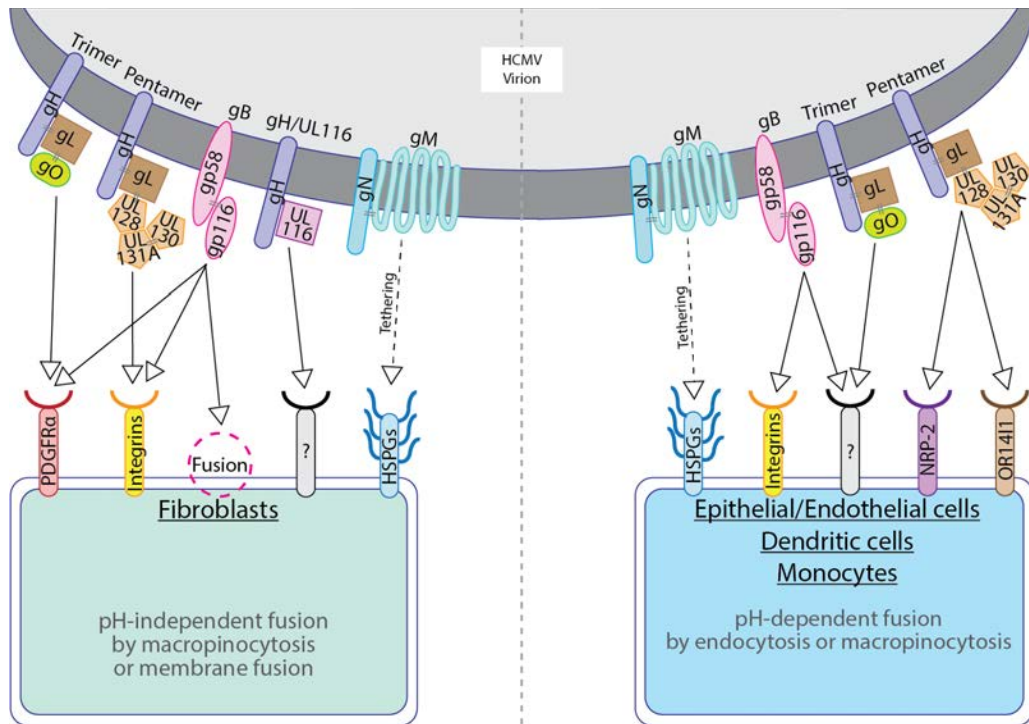


Figure 3. HCMV viral entry complexes. Known binding partners include heparan sulfate proteoglycans (HSPGs), platelet-derived growth factor α (PDGFR α), Neuropilin-2 (NRP-2), Integrins, and OR1411.

a. Viral tethering

The gM/gN complex (gCII) is the most abundant glycoprotein complex on virions, and has roles in both viral entry and viral assembly [53,59–61]. At the beginning of the entry process, gM/gN tethers to heparan sulfate proteoglycans on cells [59]. Prior work has shown that gM and gN mutants are either non-viable or have severe replication deficiencies [60,61]. Carboxy-terminal (C’terminal) deletion mutants of gM result in unstable gM proteins and fail to produce viable virus, while mutations in structural domains of the protein produce replication-deficient virus [61]. C’terminal deletion mutants of gN are also replication-deficient and fail to be enveloped [60]. This suggests that the gM/gN complex is necessary for appropriate viral assembly, in addition to its role in viral tethering.

b. gB

gCI consists of a functional trimer formed by gB, which permits entry via pH-independent membrane fusion [62,63]. gB has also been shown to interact with platelet-derived growth factor receptor α (PDGFR α), and cellular integrins [64–67]. There has been some debate over the direct involvement of gB with the epidermal growth factor (EGF) receptor, but the most recent evidence suggests that the two do not interact directly [68]. The α 2, α 6, and β 1 integrins interact with gB during the fusion process [65]. Membrane fusion occurs via a process requiring both gH/gL and gB, which is not enhanced by pentamer components [69].

c. gH/gL

gH/gL forms the covalently-bonded scaffold for the two entry complexes associated with viral tropism – the gH/gL/gO trimeric complex and the gH/gL/UL128/UL130/UL131A pentameric complex [57,70–73]. These two complexes compete for the same binding site on gL for assembly and their relative expression levels are regulated by UL148 [74,75]. Disruption of UL148 leads to a loss of mature trimer and promotes infection of epithelial cells, while rescue of UL148 expression decreases levels of the pentamer and decreases infection of epithelial cells [75].

In addition to their role in formation of the trimer and pentamer complexes, gH/gL may have additional roles in binding of cellular receptors. Recently, it was shown that treatment of cell surfaces with heparinase prevented gH/gL binding to cells [76]. The gH/gL complex

has also been shown to interact with several integrins [67]. $\alpha 2\beta 1$ and $\alpha 6\beta 1$ interact with gH/gL as entry receptors into fibroblasts, and $\alpha V\beta 3$ interacts with gH/gL as an entry receptor in fibroblasts and trophoblasts. CD90 (THY-1) has been shown to interact with gH and gB [77,78]. In these interactions, CD90 recruits Paxillin, which is important during HCMV entry into monocytes [79], and interacts with $\alpha V\beta 3$ integrins, which function as gH-dependent co-receptors [80]. Additionally, CD151, a tetraspanin, functions as a co-receptor for entry into endothelial cells and fibroblasts, although the precise mechanism involved in this process remains unclear [81]. Tetraspanin-enriched microdomains have been implicated as having potentially redundant roles in viral entry [82].

Although it was previously thought that gH and gL were necessary for proper trafficking of each other, gH has recently been shown to interact with another protein UL116 [72], forming a complex, which we showed is necessary for virus entry into fibroblasts [83] (Chapter 4). However, gH appears to preferentially associate with gL over UL116 [72] and co-expression of gH and gL stabilizes both proteins, protecting them from degradation by the endoplasmic reticulum (ER)-associated degradation pathway [84].

d. Trimer

The trimer (gCIII) is essential for entry into fibroblasts, epithelial cells, and endothelial cells, and abundance of trimer incorporated into the virion associates with infection levels in both fibroblasts and epithelial cells [76,85–87]. Trimer-associated entry into fibroblasts involves binding of PDGFR α , followed by recruitment of gB [88–90]. However, the precise role of trimer in entry into epithelial cells and endothelial cells is unclear, as viruses

lacking pentamer have impaired entry into these cells and PDGFR α is not highly expressed on these cell types [89,91–93]. Additionally, although soluble trimer bound to the surface of both fibroblasts and epithelial cells and blocked entry into fibroblasts, epithelial, and endothelial cells, expression in trans of trimer components only interfered with entry into fibroblasts [76,85]. The trimer has also been shown to interact with Transforming Growth Factor β Receptor III (TGF β RIII) and Neuregulin-2, although the precise role of these interactions in entry will require further investigation [94].

e. Pentamer

In contrast to the trimer, pentamer-associated entry occurs in a pH-dependent manner [95]. The pentamer is not necessary for entry into fibroblasts, but is necessary for entry into epithelial cells, endothelial cells, DC, and monocytes [91–93,96–98]. Cellular receptors for the pentamer are still actively being described, but pentamer associated entry processes have been shown to involve activation of integrin/Src/Paxillin signaling pathways [98]. Two receptors have recently been described for the pentamer – Neuropilin 2 in epithelial and endothelial cells and OR14I1 in epithelial cells [94,99]. Thrombomodulin, Leukocyte immunoglobulin-like receptor subfamily B member (LILRB) -3 , and Immunoglobulin alpha Fc-receptor (FCAR) were also identified as interacting with the pentameric complex [94]. CD46 was also identified, however it showed a lower affinity association for the pentamer than the other identified proteins [94]. CD147 has also been shown to be involved in pentamer-dependent epithelial cell entry [100]. In addition, several integrins have been implicated as entry receptors involving binding by the pentameric complex [67]. α 1 β 1 and α 3 β 1 have been implicated as entry receptors in trophoblasts for the pentameric complex.

Similarly, $\beta 1$ and $\beta 3$ have a role as entry receptors, interacting with both the pentamer and gB to facilitate entry into monocytes, and interacting with the pentamer alone to facilitate entry into epithelial cells and endothelial cells [67].

f. Comparison of entry complexes between CMV species

The functional components of the entry complexes are not strictly conserved across CMV species, making it difficult to interrogate *in vivo* models of CMV entry (Figure 4). Both RhCMV and guinea pig CMV (gpCMV) entry complexes closely mirror those of HCMV [101–103]; however, MCMV does not show as much functional homology [104,105]. Variants of the gM/gN, pentameric, and trimeric complexes have been identified in RhCMV, gpCMV and MCMV [101,102,105–111]. The RhCMV pentamer consists of gH/gL/Rh157.5/Rh157.4/Rh157.6 and is required for entry into epithelial cells, but not fibroblasts [101,112,113].

gpCMV encodes five putative homologues to the HCMV pentamer members, gH/gL/GP129/GP131/GP133. The gpCMV pentamer is required for entry into monocytes and endothelial cells, and loss of the complex yields impaired entry into epithelial cells [102,103,114–116]. Although initial reports showed the gpCMV pentamer to be essential for entry into fibroblasts [102], later work has shown that GP129 mutants and deletion mutants of GP129-GP133 enter fibroblasts and exhibit normal growth kinetics in fibroblasts [103,115–117]. Recent work demonstrated that this may be due to differences in PDGFR α expression in the fibroblasts used, as pentamer mutants fail to enter fibroblasts lacking PDGFR α , but will enter WT fibroblasts [111]. Furthermore, PDGFR α expression

was sufficient to permit pentamer-deficient mutants to enter pentamer-restricted cell types, suggesting that trimer-mediated entry was able to replace pentamer-mediated entry in the presence of PDGFR α . Interestingly, this work also demonstrated further functional homology between the gpCMV and HCMV entry complexes, by demonstrating that guinea pig PDGFR α co-immunoprecipitated with gpCMV gH, along with other trimer components. gB also co-immunoprecipitated with gH and the other trimer components, suggesting a similar trimer-mediated entry process in gpCMV. This is similar to HCMV, where trimer has been shown to bind PDGFR α , followed by gB-mediated membrane fusion [88–90,111]. Additionally, expression of gpCMV trimer and guinea pig PDGFR α in neighboring cells is sufficient to allow for cell-cell fusion. This work supports a similar interaction between gpCMV trimer and guinea pig PDGFR α and HCMV trimer and human PDGFR α [88–90,111].

Where HCMV and gpCMV have five known members of the pentamer, MCMV only has three, gH/gL/murine cytomegalovirus chemokine (MCK)-2. MCK-2 is a fusion product of the m129 and m131 genes [105]. A fifth gene involved in this complex has yet to be identified, although m133 has positional homology to HCMV UL131A and gpCMV GP133, and MCMV mutants lacking m133 have lower viral titers in salivary glands *in vivo* [118,119]. The MCMV gH/gL/MCK-2 complex is not required for entry into fibroblasts, but is required for entry into macrophages [105,120]. In contrast to the HCMV pentamer, gH/gL/MCK-2 is not required for entry into epithelial cells, and mutants show an increased capacity to infect epithelial cells [105].

Interestingly, all pentamer CMV mutants have the same phenotype *in vivo*, where they show low viral titers in salivary glands [102,104,118,121–124]. Additionally, MCMV, gpCMV, and HCMV pentamer genes are all expressed with late viral gene kinetics [125–128]. The locus encoding the pentamer components appears to be unstable in multiple CMV species, and is often mutated in CMV strains that have been serially passaged in fibroblasts [98,101,117,128–130]. Maintenance of the pentamer during growth in fibroblasts may be unfavorable due to the inhibitory effect of the pentamer on integrin/Src/Paxillin signaling in fibroblasts [98,128]. Interestingly, loss of a single member of the pentamer appears to impair formation of the entire complex in both HCMV and gpCMV [117,131].

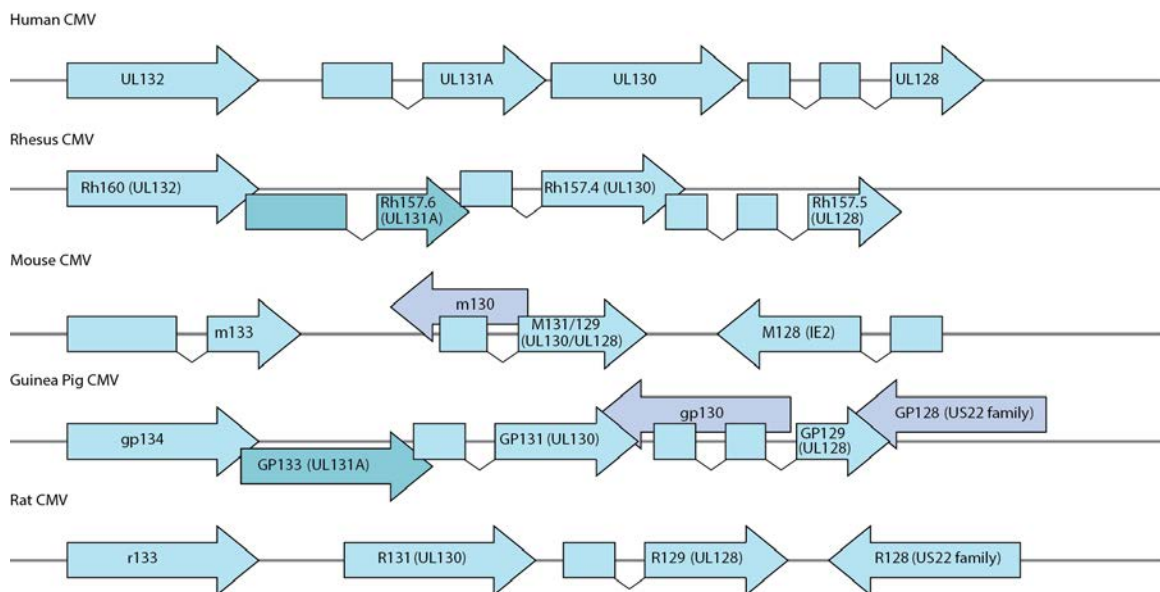


Figure 4. Components of the pentameric entry complex are not strictly conserved between CMV species. Homology to HCMV genes is indicated in parentheses.

Little is known about the RCMV Maastricht entry complexes, although homologues of gH, gL, gB, gO, and gM have been identified [132]. We have also recently described a homologous complex to the HCMV gH/UL116 complex in RCMV consisting of gH/R116

[83] (Chapter 4). Importantly, no homologous complex to the HCMV pentamer has been characterized. RCMV R129 and R131 are considered to be putative homologues to the HCMV pentamer components UL128 and UL130 as they share chemotactic functions and positional homology with pentamer components from other CMV species [123,132,133]. UL128 and UL130 are predicted to adopt a traditional chemokine fold and UL128 has been shown to have chemotactic activity [134,135]. However, other work has suggested that UL128 may also function to impair response of monocytes to chemotactic stimuli [131,136]. MCMV m131 and m129 gene products MCK-1 and MCK-2 are putative chemokines, with evidence suggesting that MCK-2 can be secreted and that MCK-1 promotes adherence in murine peritoneal macrophages *in vitro* and trafficking of leukocytes *in vivo* [125,137]. Similarly, R129 is chemotactic [133]. R131 has been proposed to be a homologue of the MCMV pentamer genes m131/m129, with mutants having a similar phenotype *in vivo*, exhibiting less foot-pad swelling and lower viral loads in salivary glands [104,123,132]. Additionally, R131 has 41.1% sequence similarity with HCMV UL130 [135], although it is predicted to be a CC-chemokine, rather than a XC-chemokine, and therefore may more closely resemble HCMV UL128 in function. Although further work remains to be done to determine if R129 and R131 do form a similar entry complex to the HCMV pentamer in RCMV, work presented in Chapter 3 and Appendix I supports functional homology between R129 and UL128 and R131 and UL130. Additional work will be necessary to determine the chemotactic properties of R131.

II. Uncoating and trafficking to the nucleus

Upon entry the virion is uncoated and the capsid is trafficked along microtubules to the nucleus, where the viral DNA is injected through the nuclear pore complex [138,139]. Much of the work on herpesvirus lifecycles has been performed in HSV-1, and forms the basis for our current understanding of CMV replication. Following membrane fusion, HSV tegument proteins are released to the cytosol [140]. The viral capsid is then targeted to the nuclear membrane by a combination of the HSV-1 capsid protein UL35, the tegument protein UL14, and infected cell polypeptide 0 (ICP0) [141]. Although the identity of these proteins varies among herpesviruses, the functionality is likely conserved. The capsid is trafficked along microtubules via dynein motors to the nuclear pore where the packaged viral DNA genome is injected into the cell nucleus and the capsid is disassembled [142].

III. Viral gene expression and DNA replication

CMV DNA replication occurs from an OriLyt element, with IE2 and UL84 initiating viral replication via responsive elements [143]. CMV gene expression occurs in three phases: IE (immediate early), early, and late. IE genes are typically associated with initiation of viral transcription. The early genes are associated with viral DNA synthesis, and late genes are associated with viral replication and virion assembly.

IV. Viral assembly

Following protein synthesis and genomic DNA replication the viral capsid is assembled. The HCMV major capsid protein, UL86, is guided to the cell nucleus by the precursor assembly protein (pAP) [144]. Viral DNA is then organized as head-to-tail concatemers and loaded into capsids through the viral portal protein (UL104). Loading of viral DNA is

terminated by UL52 and the terminase complex (UL89, UL56, and UL51) [51]. Assembled viral capsids bud from the inner nuclear membrane to the perinuclear space and then the enveloped capsids are de-enveloped as they fuse with the outer nuclear membrane to move into the cytoplasm [145]. This process is facilitated by UL50 through the formation of a nuclear egress complex involving UL53 and UL97 that promotes reorganization of the nuclear envelope [146–148]. Once the capsid reaches the cytoplasm, the remaining assembly steps occur in the cytoplasmic virion assembly compartment, formed by CMV manipulation of the endosecretory pathway [149]. As part of this process, tegument and envelope proteins co-localize to the trans-golgi network (TGN) and microtubule organizing center [150]. Tegumentation and secondary envelopment then occur in a process requiring UL47 and UL48 [151].

V. Egress

Once the viral particle is enveloped in the endosecretory pathway the endosomes are trafficked to the cell membrane where membrane fusion of these two membranes permits virus egress [152]. This process requires the tegument protein, UL103, loss of which impairs both production of dense-bodies as well as cell-free virus [153].

VI. Latency

Following entry, HCMV enters either a lytic or latent life-cycle. Latency is characterized by a lack of viral genome replication with maintenance of the viral genome in the cell [154]. HCMV establishes latency in CD34⁺ hematopoietic stem cells and CD14⁺ monocytes [155–158]. The regulators of latency and reactivation, while not yet fully

understood, are currently under intense investigation. Several cellular pathways are known to be regulated during the establishment of latency, including EGF receptor and integrin signaling [154]. The viral protein US28 is essential for regulation of latency and reactivation, with the effects of US28 on major immediate early promoter (MIEP) activation being dependent on the differentiation state of the infected cell [156,159,160]. Additionally, ligand binding activity of US28 is required to maintain latency [156]. Interestingly, other viral G-protein coupled receptors (GPCRs) are not necessary for establishment of latency [160]. IE gene expression is the earliest event in reactivation. However, recent work has raised some debate over whether IE gene expression is associated with activation of the MIEP, or if expression occurs via promoter switching using cryptic intronic promoter sites [154]. Reactivation is intimately tied to myeloid lineage cellular differentiation, a process that is, in part, driven by the promotion of myeloid lineage cellular differentiation by US28 [156].

1.2 Current status of clinical organ transplantation

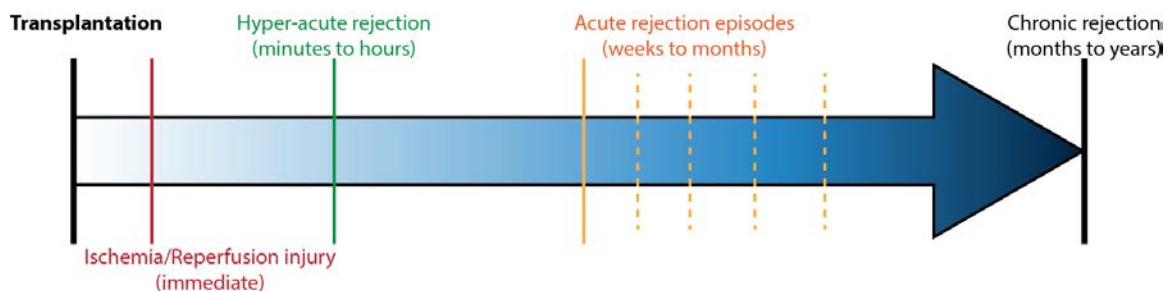


Figure 5. Modes of rejection in solid organ transplantation.

Transplantation is the current standard of care for patients with end-stage organ failure. However, transplantation is a complex process with a variety of complicating factors that decrease patient survival. Factors that can impact success of the graft include cause of

donor death, organ transport time, infection status of the recipient, HLA matching of donors and recipients, blood type of donor and recipient, and compatibility of body size, among others [161]. Organ transport typically occurs in University of Wisconsin (UW) solution to minimize tissue damage associated with ischemia. UW solution contains reagents intended to prevent swelling of cells, as well as glutathione and adenosine to improve cellular recovery upon reperfusion [162]. There are four major types of injury and rejection following transplantation: ischemia and reperfusion injury (IRI), hyper-acute rejection, acute rejection, and CR (Figure 5).

1.2.1 Ischemia and reperfusion injury

IRI are inherent to the transplant procedure. During IRI, oxygen and glucose deprivation, combined with physical stress, result in cell damage and the initiation of apoptotic signaling cascades involving Caspase-1 activation, IL-1 β signaling, and Nuclear factor kappa-light-chain enhancer of activated B cells (NF- κ B) activation. The resultant pro-inflammatory cascade includes activation and up-regulation of cytokines and chemokines that promote macrophage and neutrophil recruitment [163,164]. IRI-induced inflammation promotes acute rejection, leading to tissue fibrosis and an increase in the risk of CR. Preservation solutions and the limitation of graft cold ischemia time have reduced, but not eliminated, IRI-induced inflammation in the clinic [163]. However, to date there are no standardized therapies to block IRI.

1.2.2 Hyper-acute and acute rejection

Hyper-acute rejection is mediated by anti-donor specific antibodies and results in severe graft dysfunction within hours of transplantation [165]. Risk of hyper-acute rejection increases with prior transplantation, over-reactive antibody responses, and HCMV infection, but is currently moderated by donor and recipient antibody cross-matching [165]. For the life of the transplanted organ, recurring episodes of acute rejection also occur. These are typically mediated by T-cells and macrophages as they infiltrate the transplanted tissue and cause cellular damage or death [165]. Acute rejection is controlled with immunosuppressive therapies such as cyclosporin A. Cyclosporin A, and other calcineurin inhibitors, function by inhibiting transcription of IL2, which suppresses T-lymphocyte expansion and differentiation [165].

1.2.3 Chronic rejection

IRI, hyper-acute rejection, and acute rejection episodes all contribute to the development of CR. Additionally, donor age, hyper cholesterolemia, insulin resistance, and HCMV infection are known risk factors for CR [161,166,167]. The exact mechanism of CR varies according to the graft type; however, CR is typically characterized by a loss of graft function. In cardiac grafts, CR is characterized by the development of TVS with diffuse concentric narrowing of coronary arteries and small branch vessels due to intimal thickening [165]. Development of TVS is significantly associated with inflammation of the endothelial lining of blood vessels, complement deposition, and development of circulating anti-donor antibodies [168]. TVS resulting in CR is the leading cause of death in transplant patients greater than 5 years post-transplant [167,169]. Re-transplantation presents an approximate 71% increase in the risk of organ rejection and death over the long-term, but

remains the only available therapeutic intervention for organ failure, making prevention of CR essential to decreasing morbidity and mortality for transplant recipients [161].

1.3 Inflammation and immune-modulation exacerbate CMV-associated transplant vascular sclerosis and chronic rejection

1.3.1 The role of chemokines in transplantation

Chemokines and their cognate receptors participate in a variety of biological processes including development, inflammation, and immunity by directing targeted cellular migration. Dysregulation of the chemokine signaling network is implicated in the pathogenesis of a number of inflammatory diseases including transplant rejection. There are 47 identified chemokines that are subdivided into 4 groups based upon the specific spacing and composition of the first Cysteines (Cys) present at the amino (N') terminus of the molecule. These groups are the CC-, CXC-, XC-, and CX₃C-chemokines (Figure 6) [170–172]. All of these chemokine groups share a related tertiary structure that is held together through disulfide bonds between the N'terminal Cys residues and internal Cys residues. These common chemokine folds promote the formation of conserved domains within this family of proteins. For example, the N'loop domain interacts with chemokine receptors and helps to define receptor-binding specificity [172].

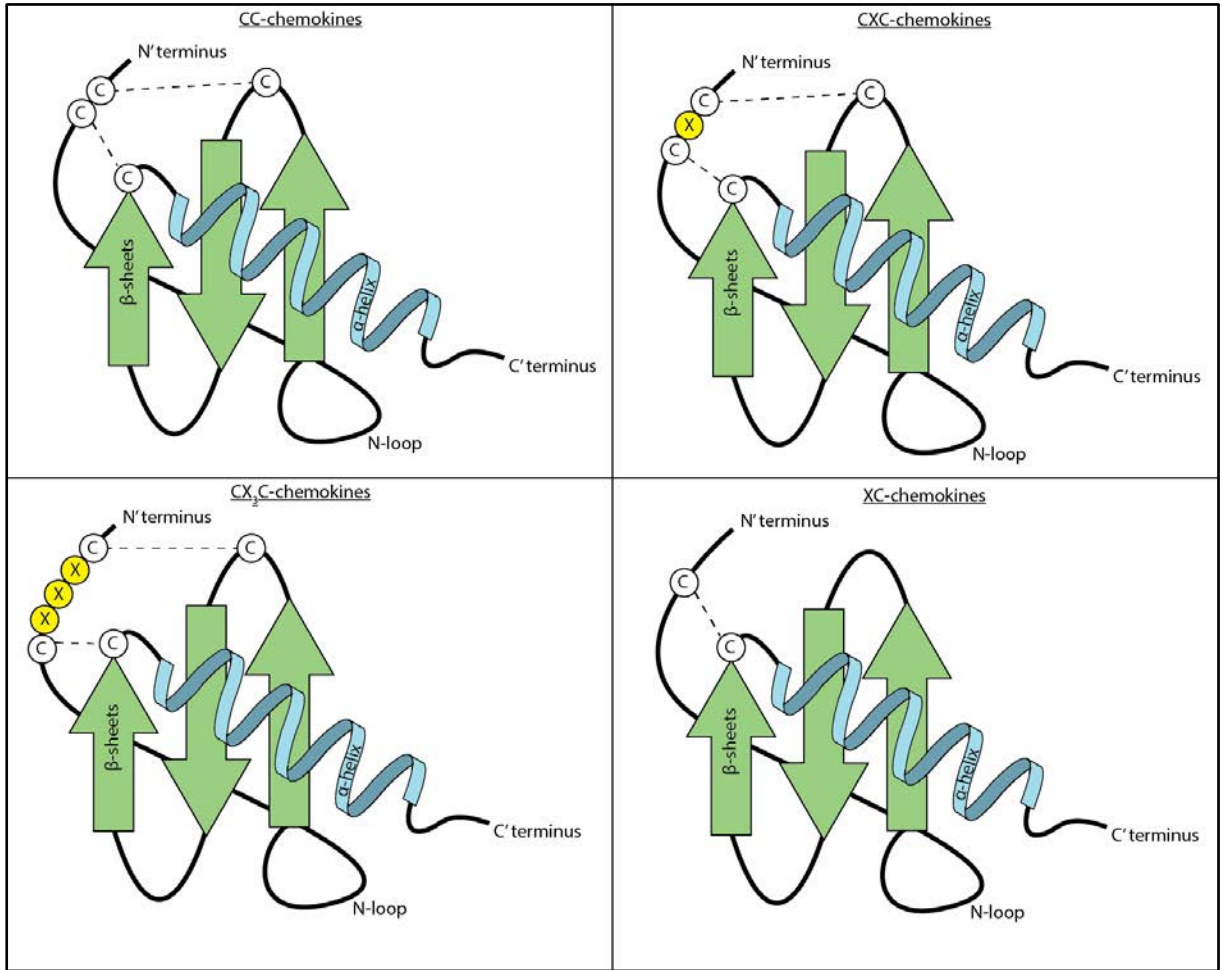


Figure 6. Chemokine structure.

I. Chemokine classifications

Of the four chemokine classes (CC, CXC, XC, and CX₃C), the CC-chemokine group is the largest [170,172]. This group consists of 27 members that contain two adjacent Cys residues. In contrast, the seventeen CXC-chemokines have one amino acid that separates their two Cys residues. Additionally, the CXC-chemokine group is subdivided based upon the presence or absence of a Glutamic acid-Leucine-Arginine (ELR) motif [172]. CXC-chemokines containing an ELR motif direct neutrophil migration via interactions with one of two chemokine receptors: CXC Receptor (CXCR) 1 and CXCR2 [164]. There are fewer

known members of the two remaining chemokine families: the XC-chemokines and the CX₃C-chemokines [173]. The two XC-chemokines in mammals, which include lymphotactin- α and β (XCL1/XCL2) contain only one Cys residue, which is sufficient to promote the classical chemokine fold and interactions with their receptors. The single CX₃C-chemokine family member, CX₃CL1/Fractalkine, has three amino acids that separate the two N'terminal Cys residues. Fractalkine exists in two molecular forms: a secreted form and a form that is tethered to the surface of cells, such as endothelial cells. Fractalkine has been implicated in a variety of inflammatory diseases [174].

II. Chemokine receptor classifications

Chemokine receptors are 7-transmembrane spanning proteins that interact with G proteins in order to activate shared and unique downstream signaling events. Chemokine receptors are similarly divided into 4 different families based upon the ligands they bind and are designated as CC Receptor (CCR), CXC Receptor (CXCR), XC Receptor (XCR), and CX₃C Receptor (CX₃CR). These receptors have an extracellular N'terminus that binds their respective ligands, and an intracellular C'terminus that contains phosphorylation sites involved in chemokine receptor signaling.

III. Chemokines in transplant rejection

Many chemokines have been identified as being predictors and promoters of transplant rejection. Following cardiac allograft transplantation recruitment and accumulation of T-cells and monocytes to the transplanted tissue is typically associated with an increased risk of rejection. Several chemokines are known to regulate this process. For example, CC

ligand (CCL) 5 is elevated in patients experiencing TVS, and is therefore predicted to be involved in this characteristic recruitment of T-cells and monocytes to the transplant tissue, promoting the development of TVS [175]. Blockade of another chemokine, monocyte chemoattractant protein-1 (MCP-1), via an anti-MCP-1 L-ribonucleic acid aptamer was used successfully in a mouse heart transplant model to extend graft survival [176]. A similar pharmacological approach was used to inhibit CXC ligand (CXCL) 12 signaling through the chemokine receptors CXCR4 and CXCR7 and was shown to reduce proliferation of vascular smooth muscle cells (vSMC) *in vitro* as well as impair development of TVS in mice [177]. More recently, it was shown that CXCL12/CXCR4 signaling is regulated by Transforming growth factor β 1 (TGF β 1), and is necessary for TGF β 1 promotion of mesenchymal stem cell homing to sites of IRI following cardiac transplantation [178].

IV. Chemokine receptors in transplant rejection

A variety of chemokine receptors have also been implicated as promoters of accelerated immune response to graft tissues, and are involved in the inflammatory cell recruitment to transplant tissues. For example, the chemokine receptors CCR4, CCR5, and CXCR3 promote T-cell recruitment specifically to inflamed and transplanted cardiac tissue in murine models [179–181]. Expression of CCR1, CCR3, CCR5, and CXCR3 are also correlated with CD3⁺ T-cell infiltration following cardiac transplantation [182]. Additionally, CCR5 inhibition in a mouse transplant model has been shown to reduce development of TVS [183]. Of the chemokine receptors mentioned above as being implicated in promotion of transplant rejection, CXCR3 has been shown in several studies

to be of particular interest in allograft rejection scenarios and CXCR3 ligands (CXCL9, CXCL10, CXCL11) have been shown to be up-regulated following transplantation. For example, CXCL10 was induced, in conjunction with CXCL11 and CXCL9, upon cardiac allograft transplantation in mice [184]. In this same study, while CXCL10 was induced in both isografts and allografts, allografts from donors lacking CXCL10 did not undergo acute allograft rejection. CXCL9 and CXCL10 were shown to regulate alloreactive T-cell responses in a murine model of cardiac transplantation [185]. Specifically, absence of CXCL9 reduced the production of Interferon (IFN) γ and increased the production of IL-17A by CD8⁺ T-cells. The absence of CXCL10 still promoted the production of IFN γ by CD8⁺ T cells [185]. Additionally, anti-CXCR3 antibodies improved cardiac transplant survival in a mouse model [186]. Combined anti-CXCL9, anti-CXCL10, and immunosuppressive therapy has been shown to improve cardiac allograft rejection and reduce T-cell infiltration into graft tissue in a mouse model [187]. Recently, the efficacy of anti-CXCL10 therapy in preventing infiltration and accumulation of T-cells in graft tissues was also demonstrated in a rat cardiac re-transplantation model [188]. This study showed that in the re-transplantation model anti-CXCL10 antibodies abrogated accelerated rejection and improved graft survival [188]. CXCL10 is increased in the transcriptome of inflamed cardiac tissue in mice and rats [36,179]. Similarly, CXCL10 and CXCR3 mRNA expression following renal allograft in patients have been shown to be a functional predictor for acute rejection [189]. CXCR3 and CXCL10 have previously been shown to be predictors of acute rejection in cardiac transplants in the clinic [182]. CXCR3 and its ligands have also been implicated in a variety of cardiovascular diseases, in addition to their roles in solid organ transplant rejection, as reviewed previously [190].

V. Chemokine signaling leads to CMV reactivation

In addition to their involvement in immune cell recruitment to transplanted tissues, chemokine receptor expression on host cells can be a functional predictor indicative of increased risk of CMV reactivation following transplantation, which may lead to an increased rate of transplant rejection. For example, CCR6 has been identified as a potential predictor of CMV reactivation following cessation of prophylactic therapy after SOT, since it has been shown that high levels of CCR6 expression on CD4⁺ T-cells is indicative of CMV reactivation [191]. Additionally, CMV viremic transplant recipients showed a correlation between CCL8 and CXCL10 expression and ability to control viral replication. Correspondingly, patients with a polymorphism in the promoter for CCL8 exhibited an increased risk of viral reactivation upon termination of prophylactic therapy [192].

1.3.2 CMV modulates the host-immune response

CMV uses a variety of techniques to modulate the host immune response to establish life-long infection of the host. These techniques are complex, and many still remain to be fully elucidated. However, they tend to focus on two key portions of the immune response: (1) regulation of chemokines and chemokine receptors and (2) altering MHC-mediated detection of infected cells. Additionally, the characteristic life-long latent infection established by CMV results in skewing of T-cell responses over the life-time of the host. Recent work identified a correlation between latent HCMV genome copies and the breadth and magnitude of IFN γ T-cell responses to HCMV antigens [7]. However, donor age and latent HCMV genome copies did not correlate, suggesting that although latent HCMV

infection does cause an expansion of CMV-specific T-cell responses, these responses do not detrimentally impact host T-cell responses in healthy individuals [7]. These responses tend to be targeted to pp65 and IE peptides [193].

I. HCMV manipulates host chemokine synthesis and function

CMV infection causes increased pro-inflammatory cytokine and chemokine expression, which drives CMV-mediated disease. HCMV induces the expression of MCP-1, RANTES and macrophage inflammatory protein (MIP) -1 α [194,195]. Proteomics analysis of supernatants from HCMV infected cells found that a number of chemokines were induced upon infection including CCL3, CCL5, CCL7, CCL20, CXCL1, CXCL5, and CXCL16. The mechanism by which CMV up-regulates chemokine expression remains unclear; however, CMV entry induces anti-viral responses including activation of NF- κ B, interferon regulatory factor (IRF) 3, and other transcriptional activators that may induce chemokine expression. In addition, CMV encodes a number of proteins and micro RNAs (miRNA) that affect chemokine expression and function. For example, it was recently shown that the HCMV tegument protein pp71 induces CCL2 expression *in vitro*. However, increased CCL2 expression was abrogated by replicative viral infection, suggesting that HCMV encodes additional factors to reduce immune-cell attraction at later time-points of infection [196,197].

Another approach CMV uses to modulate the host response to chemokines is degradation of necessary host proteins for immune cell migration. HCMV US2 acts as an immune modulator by targeting MHC-I and MHC-II for degradation. US2 requires the cellular

ubiquitin ligase translocation in renal cancer from chromosome 8 (TRC8) for this activity. Recent work utilizing a proteomics approach has expanded on our knowledge of US2 as an immune modulator by describing its role in collaboration with TRC8 to cause degradation of a number of α -integrins, thereby reducing THP-1 monocyte migration in response to the chemokine MCP-1 (CCL2) [198].

II. CMV regulation of host chemokine receptors

HCMV infection also modulates chemokine receptor expression and function. For example, HCMV encodes UL111A, the viral homologue of IL-10. UL111A increases response from the CXCR4 signaling network upon the host ligand CXCL12 binding to the receptor [199]. Additionally, monocytes exhibited down-regulation of CCR1, CCR2, CCR5, and CXCR4 at the cell surface upon infection with the endotheliotropic strain TB40e of HCMV [136]. Similarly, TB40e infection of DC and macrophages resulted in down-regulation of CCR1 and CCR5 by internalization of the receptors [200,201]. Notably, in these studies there were multiple chemokine receptors that were unaltered following infection, suggesting that CMV down-regulates specific chemokine receptors [136,200,201].

CMV modulation of chemokine receptors also contributes to CMV's role in recruitment of T-cells and monocytes to transplant tissues, impacting rejection. Recent work built off of the role of CXCR3 in recruitment of inflammatory cells to transplant tissues in an MCMV salivary gland infection model [202]. This study demonstrated that MCMV infection increased expression of CXCR3 and CCR5 ligands in salivary glands. However, CXCR3

and CCR5 did not appear to be necessary for T-cell recruitment to salivary glands *in vivo* during MCMV infection, despite CXCR3 being necessary for recruitment in uninfected animals [202]. This suggests that MCMV modulates the CXCR3 T-cell recruitment pathways, which remains to be explored.

III. Cytomegalovirus encodes chemokines and chemokine receptors

CMV uses host-chemokine and host-chemokine-receptor like molecules to evade and modulate the host immune response. The β -herpesviruses encode an assortment of host-chemokine and host-chemokine-receptor like molecules. For example, HCMV is known to encode homologues of at least four chemokines and four chemokine receptors: chemokines UL128, UL130, UL146 (vCXCL-1), and UL147 (vCXCL-2), and chemokine-receptor homologues US27, US28, UL33, and UL78. A current list of the CMV-encoded chemokines and chemokine receptors is presented in Table 6 and Table 7, respectively (Chapter 3). CMV-encoded chemokine and chemokine-receptor homologues have been implicated as having roles in cellular entry and recruitment of other cells to the site of infection during CMV pathogenesis.

a. CMV encoded chemokines and chemokine receptors in viral entry

CMV encoded chemokine homologues have been shown to have roles in cell migration and entry. For example, HCMV UL128 and UL130 chemokines have been implicated in mediating CMV entry into cells. HCMV UL128 and UL130 are part of the pentameric complex vital for productive infection during CMV pathogenesis, and required for transmission of virus to leukocytes [74,93], as discussed above (1.1.4.I.e). Work by Ciferri

et al. demonstrated that soluble UL128 interferes with viral entry [74]. Likewise, CMV encodes several chemokine receptor homologues that appear to have a role in viral entry. For example, the chemokine receptor homologue UL78 is required between the binding and entry phases of viral infection in epithelial cells. However, UL78 does not appear to be necessary for viral entry in fibroblasts [203]. Prior work had also demonstrated that RCMV lacking R78, the RCMV homologue of UL78, displayed lower replication efficiency *in vitro* and a lower lethality *in vivo* [204]. These studies suggest that CMV-encoded chemokine and chemokine-receptor homologues function to increase viral dissemination and play a role in pathogenesis.

b. CMV-encoded chemokines and chemokine receptors alter immune cell recruitment

CMV encoded chemokine homologues also display functions in regulating immune-cell recruitment in response to infection. In addition to its role in entry, HCMV-encoded UL128 has been shown to exhibit β -chemokine like functions in its ability to recruit peripheral blood mononuclear cells (PBMC) [134]. In contrast, Straschewski *et al.* demonstrated that UL128 can inhibit host-chemokine driven motility of monocytes and can cause monocyte paralysis [131]. The HCMV-encoded UL146 has been shown to activate CXCR1 and CXCR2 in a process that promotes migration of neutrophils [205,206]. UL146 induces Ca^{2+} flux and integrin expression on target cells, upon binding to host CXCR1 [207]. Furthermore, Heo *et al.* showed that there is a hyper-variability associated with UL146, which correlates with high functional selectivity in the recruitment and activation of neutrophils to infected tissues. *In vivo* studies in rats have demonstrated that RCMV chemokine homologues mediate immune cell migration to the site of infections, promoting

further spread of the virus, in a manner similar to that seen with HCMV-encoded chemokine homologues. For example, Kaptein *et al.* showed that R131 is involved in the recruitment of macrophages to the site of RCMV infection in rats. While the lack of R131 does not significantly affect viral replication, null mutations in R131 correlate with a lack of a high titer of infection in the salivary glands of immunocompromised rats and a significant decrease in footpad swelling upon inoculation of RCMV [123]. Furthermore, R129, the RCMV homologue of UL128, binds rat chemokine receptors CCR3, CCR4, CCR5, and CCR7 [133]. Additionally, migration of lymphocytes and naïve CD4⁺ T-cells was shown to be induced by R129 [133]. The m131/129 chemokine homologue is also involved in regulating the inflammatory response. In a study by Fleming *et al.*, an m131/129-mutant MCMV failed to produce high-titers in salivary glands *in vivo* and had improved clearance rates during acute infection from spleen and liver in a Natural Killer (NK) and T-cell dependent manner, suggesting that m131/129 has pro-inflammatory properties and is necessary for immune evasion. The authors suggest the mechanism of m131/129 may involve regulation of NK and T-cells [122]. Later, Saederup *et al.* utilized recombinant viruses to demonstrate that MCK-2, the secreted product of m131/129, is sufficient to induce inflammation [104]. Further work in mice confirmed that MCK-2 enhances recruitment of myeloid progenitors to the site of infection, which may aid in viral dissemination [208]. Additional *in vivo* studies in mice suggested that MCK-2 mediates recruitment of pro-inflammatory monocytes via CCR2 in order to impair CD8⁺ T-cell anti-viral responses, which slows viral clearance [209]. Together these studies depict a clear relationship between the murine CMV encoded 131/129 chemokine homologues and the promotion of pro-inflammatory conditions to promote viral dissemination. However, it has

recently been shown that MCMV self-regulates MCK-2 expression during infection via the virally-encoded M48 deubiquitinating enzyme. This process regulates excessive inflammation associated with viral infection [210]. In a guinea pig model of CMV infection, deletion of gp1, a gpCMV homologue of the host chemokine MIP, allowed generation of an immunogenic attenuated vaccine strain of gpCMV that reduced viremia in non-pregnant guinea pigs and reduced DNAemia in the third trimester of pregnancy in guinea pig dams [211]. Intriguingly, recent work by Geyer *et al.* identified a novel XC chemokine in the English RCMV viral isolate (Murine Herpesvirus 8 (MuHV8)). This chemokine homologue vXCL1 recruits XCR1⁺ CD4⁻ DC in rats, which was suggested to allow MuHV8 to undermine the traditional cytotoxic immune response [212]. Overall, regulation of leukocyte recruitment by CMV-encoded chemokines appears to promote viral dissemination and inhibit viral clearance.

In addition, CMV encoded chemokine-receptor homologues function to alter immune cell recruitment to infection. For example, US28 has been implicated in the suppression of IL-8 secretion and the sequestering of cellular/host chemokines and exogenously expressed chemokines during CMV infection, thus regulating the immune response to virally-infected cells [213]. The mechanism of action of US28 was shown to involve binding of G α_{16} and G α_i subunits of the GPCR to mediate cell responses to chemokines, including RANTES. The authors suggested a role for US28 in viral persistence, macrophage activation, and monocyte proliferation given its ability to bind with the G α_{16} subunit [214]. However, further work demonstrated that although US28 is involved in the sequestration of MCP-1, it is not involved in the modulation of MCP-1 during HCMV infection of human

fibroblasts *in vitro* [197,215]. Additionally, US28 promotes migration of macrophages and vSMC in a chemokine-dependent manner [216,217]. While US28 binds multiple chemokine ligands, signaling and migration are affected by ligand specificity [217]. Specifically, US28-induced migration of vSMC is driven by CC chemokine binding and is inhibited by Fractalkine. The opposite effect is observed in macrophages, wherein US28 migration is promoted by Fractalkine [217]. Coupling to G α 12/13 G proteins is critical for vSMC migration, as is signaling through Src and FAK [218,219]. Stable expression of US28 has also been shown to increase migration of HEK293 cells over HEK293 cells expressing CX₃CR1 in response to CX₃CL1. Interestingly, this increase in migration is competitively inhibited by the CC chemokines CCL2 and CCL5, but not by CCL3 [220], which would support binding of multiple chemokines by US28. Recent work aimed to further examine the chemokine receptor US28, along with US27, by phylogenetic comparison to human chemokine receptors [221]. The authors concluded that both US28 and US27 were the result of a gene-capture event of CX₃CR1 from the host, followed by gene duplication within the virus. US28 has retained significant homology with human CX₃CR1 and binds the host ligand CX₃CL1. However, US27 has experienced a significant amount of mutation and no longer binds any known ligands. It's function remains unclear, although it was found to carry some resemblance to human CCR1 [221]. In addition, US27 was revealed to enhance CXCL12/CXCR4 signaling, suggesting that this protein has a role in promoting monocyte recruitment and viral dissemination [199]. However, further work remains to be done to clearly elucidate the functions of US28 and US27, along with the remaining CMV encoded chemokine-receptor homologues.

M33, a mouse-encoded functional homologue of US28, was shown to be required for recruitment of mouse vSMC, but not mouse fibroblasts, in a mRANTES dependent manner [222]. Similarly, RCMV R33 is necessary for migration of infected vSMCs in the development of TVS during CR of rat cardiac transplants [31]. Additional work demonstrated that US28 and M33 also have a role in regulating host gene transcription via constitutive activation of the cyclic-AMP response element binding protein (CREB) and NF- κ B. However, the HCMV-encoded structural homologue of M33, UL33, was not constitutively active towards NF- κ B, and was only slightly constitutively active with respect to CREB, indicating varying levels of host-transcription regulation by different chemokine-receptor homologues [223]. US28 and UL33 are, nonetheless, partially redundant in function with M33 since they correct for a loss of MCMV reactivation and viral replication in salivary glands in M33-signaling deficient MCMV [32].

1.3.3 CMV alters MHC expression and encodes MHC decoys

HCMV encodes several immune-modulation genes that affect or mimic MHC-I. The most notable of these is UL18, which adopts an MHC-I-like fold [224] but has only approximately 25% sequence similarity to classical MHC-I [225]. UL18 binds LILRB-1 on NK cells [224,226,227], and presents peptide similar to host MHC-I [228]. HCMV UL18 contains 13 potential N-linked glycosylation sites, that allow for most of the protein to be shielded by carbohydrate groups, preventing protein-protein interactions beyond binding LILRB-1 and peptide presentation [224]. UL18 was initially proposed to block NK cell-mediated killing; however, further work revealed its function to be more nuanced [229]. LILRB1⁺ NK cells were inhibited by UL18 expressing fibroblasts, whereas LILRB1⁻

NK cells were activated [230]. Importantly, UL18 is not essential for HCMV replication *in vitro* [231], and is not expressed until approximately 72 hours post-infection (hpi) with late gene expression kinetics [232]. Additional immune-modulators encoded by HCMV include US3 and US6, which block MHC-I trafficking to the cellular membrane. US3 prevents trafficking of MHC-I out of the ER, resulting in perinuclear accumulation of MHC-I heavy chains [233]. US6 blocks MHC-I antigen presentation by binding to transporter associated with antigen processing (TAP) [234]. UL18 interacts with US6 to restore TAP function for loading of peptides on to UL18, but still prevents interaction of MHC-I molecules with TAP [235].

Loss of MHC-I expression on the cell surface associated with the HCMV genes US2-US11, prevents cytotoxic CD8⁺ T-cell responses against infected cells [193,236]. These genes use a variety of mechanisms to down-regulate MHC class I expression at the cell surface, including targeting HLA class Ia molecules to the proteasome and altering TAP conformation to prevent loading [193]. However, this results in an increase in NK-cell targeting of infected cells. To circumvent NK-cell targeting, HCMV up-regulates MHC-E expression [237]. Loss of MHC class I and II restricted CD8⁺ T-cell responses, and the corresponding increase in MHC-E restricted CD8⁺ T-cell responses appear to require loss of a family of chemokine genes encoded by CMV, as shown with loss of RhCMV homologues to UL128-UL131A, and cannot be recapitulated by inhibition of TAP alone [238,239]. However, loss of only UL128-UL131A was not sufficient to drive these responses in patients vaccinated with attenuated HCMV strains [240]. Recent work has suggested that loss of an additional region containing several other chemokine homologues

is necessary to elicit these responses, suggesting that CMV modulates MHC responses to establish life-long infection in the host.

Similarly, MCMV encodes a family of genes consisting of m145, m146, m150-m155, m157, m158, and m17 that are involved in immune modulation [241,242]. Similar to HCMV UL18, MCMV m145 family members typically include a signal peptide, a transmembrane domain, and several N-linked glycosylation sites [242]. Several of these genes are predicted to adopt an MHC-I-like fold [243], and the solved structures of m144 (a relative of the m145 family), m153, and m157 all exhibit MHC-I-like folds [244–246]. RCMV encodes several predicted homologues of these genes including r145, r149, r150, r151, r151.3, r152, r152.2, r152.3, r152.4, r155, and r157 [132,242]. One of these, RCMV r152.4, is of particular interest because it is highly expressed in multiple tissues during *in vivo* infections [247] and is most closely related to m152 [132], which has multiple immune-modulation functions reviewed previously [242]. Briefly, MCMV m152 has been shown to down-regulate Rae-1, a ligand of the activating NK cell receptor NKG2D (Natural Killer group 2D receptor). In addition, m152 has been shown to down-regulate MHC-I gene expression by retaining the MHC-complex to the ER, similar to the function of US3 in HCMV. This blockade of antigen presentation provides a resistance to cytotoxic T-lymphocyte attack of infected cells, a process that is regulated by m152 in conjunction with m04 and m06, two additional genes that alter antigen presentation on infected cells [248–250]. These functions provide selective advantage for the virus as an m04, m06, m152-deficient MCMV had a 10-fold reduction in viral titers in salivary glands of mice [251]. However, m152 appears to have no impact on the ability of the virus to infect,

persist, or establish latency [252]. Interestingly, transfection experiments showed that m152 is poorly expressed on the cell surface, but is rather primarily expressed intracellularly [242], suggesting a role in retaining MHC-I rather than as an MHC-mimic.

1.4 RCMV as a model for HCMV-associated disease following transplantation

Due to the high species specificity of CMV several model systems are commonly used to study CMV pathogenesis including MCMV, RCMV, RhCMV, and gpCMV models in their respective host species [253]. Each CMV/host species combination has unique properties making them suited for models of different CMV-associated pathologies.

Although RhCMV is the most closely related to HCMV, work in rhesus macaques is prohibitively expensive and requires isolated CMV-free colonies [254]. Furthermore, rhesus macaques lack the in-bred characteristics of small animal CMV models [254], making experimental consistency difficult to achieve.

gpCMV is typically used to model congenital CMV infections as it is the only small animal model that recapitulates congenital CMV pathology seen in the clinic [107,115,117,211]. The gpCMV model bears a greater phylogenetic similarity to primate CMVs than the other rodent CMVs [255]. Of particular interest to viral infection and dissemination models, gpCMV appears to contain entry complexes with greater homology to those of HCMV than does MCMV [102,107,114–117,127], as discussed in section 1.1.4.I.f.

MCMV infection of mice is a common model system used to elucidate both viral pathogenesis and immune interactions due to the availability of mouse reagents, highly inbred mouse lines, and genetically modified mouse lines. MCMV models in SCID mice present a viable model for CMV infections of immunocompromised patients, and acute and chronic infections can be obtained in other mouse lines [253]. MCMV models have been used to model MCMV-mediation of host immunity including memory inflation in response to long-term infection with CMV, immune cell recruitment by CMV-encoded proteins, and regulation of antigen presentation [208,250,256]. However, MCMV does not appear to encode an entry complex with close structural homology to the HCMV pentameric complex [105] and the small animal size of mice can make organ transplant models difficult.

There are four unique RCMVs – Maastricht, Malaysian, Berlin, and English [5,132,257–260]. However, the Berlin and English strains more closely resemble MCMV isolates and, along with the Malaysian strain, constitute a unique evolutionary clade from RCMV Maastricht [5,259,261]. Maastricht RCMV infection in rats recapitulates the acceleration of TVS and CR of allografts seen with HCMV in the clinic [36,194,262]. RCMV infection results in an increase in early inflammatory cell responses, substantial endothelial cell proliferation and intimal thickening [262]. The up-regulation of chemokine expression correlates with development of intimal thickening and an increase in infiltration of T-cells and macrophages to the graft [194]. Additionally, in latently infected animals RCMV infection produces tertiary lymphoid structures containing macrophages and T-cells in heart tissue [36]. In this model, latent infection of donors shows an acceleration of CR

following transplantation with similar kinetics to those seen in acutely infected recipient animals [36].

We have previously published extensively using a heterotopic cardiac allograft model with F344 rats as donors and Lewis rats as recipients [31,36,133,194,263–265]. F344 and Lewis rats only differ partially at MHC I and II loci, and a few non-MHC loci. This allows for the study of CR, but substantially decreases risk of acute rejection episodes in animals [266]. This model uses Cyclosporin A for 10 days post-operation at 5 milligram/kilogram (mg/kg) per day by subcutaneous injection to suppress acute rejection. Loss of anti-donor alloreactivity, as seen in syngeneic grafts and bone-marrow chimeras, results in failure to develop TVS and CR, regardless of CMV infection [265]. Although orthotopic transplantation is almost exclusively used in the clinic today, in the lab the heterotopic transplant procedure circumvents the need for extensive circulatory and respiratory equipment during the transplant procedure [169]. However, it is important to note that heterotopic transplants fail to provide appropriate volume loading of the left ventricle, resulting in decreased ejection volume from the grafted heart [169]. For the heterotopic allograft procedure, the donor cardiac ascending aorta is sutured to the recipient abdominal aorta and the donor pulmonary artery is sutured to the recipient inferior vena cava [169]. The development of TVS is measured using the neointimal index (NI) at time of sacrifice ($((\text{intimal area} - \text{luminal area})/\text{intimal area}) * 100$) and CR is determined based on palpation of the graft heart for loss of heart beat.

1.5 Thesis overview and aims

CMVs are β -herpesviruses that establish persistent latent infection in their hosts. HCMV infection causes significant morbidity and mortality in immunosuppressed patients, such as transplant recipients. Additionally, HCMV infection exacerbates the development of TVS and accelerates CR of solid organ transplants. Current therapies to control HCMV do not sufficiently prevent this exacerbation of disease. As such, further research is needed to identify new therapies to prevent CMV-accelerated graft rejection.

Ethical considerations limit human experimentation and therapeutic testing until validated for safety and efficacy in relevant animal models. A major limiting factor in performing such studies in these animal models is the high-species specificity of herpesviruses that requires the use of model systems with the appropriate host-specific CMV. In order to determine the role of viral and host genes/pathways in pathogenesis and chronic allograft rejection, we have developed a model of rat cardiac transplantation infected with RCMV. We have used this model to identify novel therapy modalities to mitigate the acceleration of transplant rejection.

First, we demonstrate the utility of the RCMV/rat cardiac transplant model system for identifying novel therapeutic approaches for cardiac transplant rejection (Chapter 2). This work incorporates transcriptomic and proteomic profiling to identify novel targets for reducing tissue damage following transplantation-induced cardiac graft IRI. The therapeutic potential of these targets will be determined in two RCMV⁺ models - an IRI model and a CR model.

Second, we will describe a novel approach to studying virion incorporation of tagged viral proteins (Appendix I). CMV has multiple entry complexes; however, it is unclear which complexes are required for entry into specific cell types *in vitro* and *in vivo*, and whether they function similarly across CMV species. Here, we detail the involvement of two proteins (R129 and R131) in the formation of the RCMV pentameric entry complex, and determine which rat cell types require this complex for viral entry (Chapter 3). These results are discussed in the context of CMV mediation of immune responses to aid in viral dissemination.

Finally, in Chapter 4, we discuss the characterization of another RCMV proposed entry complex component. R116 is expressed with late viral gene expression kinetics and produces several molecular weight variants. Additionally, R116 is incorporated into the viral envelope and is required for production of infectious virions. We compare our characterization of R116 with HCMV UL116, and demonstrate that UL116 is similarly required for production of infectious virus.

Chapter 2 – Blocking the IL-1 Receptor Reduces Cardiac Transplant Ischemia and Reperfusion Injury And Mitigates CMV-Accelerated Chronic Rejection

Iris K. A. Jones¹, Susan Orloff^{2,3}, Jennifer M. Burg², Nicole N. Haese¹, Takeshi F. Andoh^{1,2}, Ashley Chambers¹, Suzanne S. Fei⁴, Lina Gao⁴, Craig N. Kreklywich¹, Zachary J. Streblow¹, Kristian Enesthvedt², Alan Wanderer⁵, James Baker⁶, and Daniel N. Streblow^{1,3}

¹ *Vaccine and Gene Therapy Institute, Oregon Health & Science University, Beaverton, Oregon, USA*

² *Department of Surgery, Oregon Health & Science University, Portland, Oregon, USA*

³ *Department of Molecular Microbiology and Immunology, Oregon Health & Science University, Portland, Oregon, USA*

⁴ *Bioinformatics & Biostatistics Core, Oregon National Primate Research Center, Oregon Health & Science University, Beaverton, Oregon, USA*

⁵ *University of Colorado Medical Center, Aurora, CO USA*

⁶ *Baker Allergy Asthma and Dermatology, Portland, OR USA*

This chapter is adapted from:

American Journal of Transplantation (2020), DOI: 10.1111/ajt.16149

2.1 Abstract

IRI is an important risk factor for accelerated cardiac allograft rejection and graft dysfunction [163]. Utilizing a rat heart isogeneic transplant model, we identified inflammatory pathways involved in IRI in order to identify therapeutic targets involved in disease. Pathway analyses identified several relevant targets, including cytokine signaling by the IL-1R pathway and inflammasome activation. To investigate the role of IL-1R signaling pathways during IRI, we treated syngeneic cardiac transplant recipients at 1-hour post-transplant with Anakinra, an FDA approved IL-1R antagonist, or parthenolide, a Caspase-1 and NF- κ B inhibitor that blocks IL-1 β maturation. Both Anakinra and parthenolide significantly reduced graft inflammation and cellular recruitment in the treated recipients relative to non-treated controls. Anakinra treatment administered at 1-hour post-transplant to recipients of cardiac allografts from CMV-infected donors significantly increased the time to rejection and reduced viral loads at rejection. Our results indicate that reducing IRI by blocking IL-1R signaling pathways with Anakinra, or inflammasome activity with parthenolide, provides a promising approach for extending survival of cardiac allografts from CMV-infected donors.

2.2 Introduction

SOT remains the standard of care for patients with end-stage organ failure. However, CR remains a barrier to long-term transplant success. The defining feature of CR in cardiac transplants is development of TVS, affecting approximately 30% of transplant patients. The disease is characterized by a subendothelial low-grade inflammatory process resulting in narrowing of graft coronary vessels and leading to graft loss [167]. Several risk factors are associated with CR including: donor age, IRI, acute rejection episodes, hypercholesterolemia and HCMV infection [161,166,167]. The only effective treatment for CR is re-transplantation. Hence, identifying mechanisms involved in this process is critical to prevent cardiac allograft disease.

IRI is a primary activator of graft inflammation leading to increased risk for both acute and chronic allograft rejection [163]. During IRI, oxygen and glucose deprivation combined with physical stress result in cell damage and the initiation of apoptotic signaling cascades involving Caspase-1 activation, IL-1 β signaling, and NF- κ B activation. The resultant pro-inflammatory cascade includes activation and up-regulation of cytokines and chemokines that promote macrophage and neutrophil recruitment [163]. IRI-induced inflammation promotes acute rejection, leading to tissue fibrosis and increasing the risk of CR. Preservation solutions and limiting graft cold ischemia time have reduced, but not eliminated, IRI-induced inflammation [163]. Potential strategies to reduce IRI include pre-conditioning of donor tissue or blocking cytokine/chemokine signaling in the recipient immediately after transplantation [163].

CMV infection has many deleterious effects on SOT outcomes [6,21,167]. Importantly, HCMV infection occurs in 75% of the solid organ donor/recipient population. Both active and latent CMV infections promote allograft rejection [6,22,36,167]. Currently, prophylactic therapies such as Valganciclovir are used to control CMV infection in transplant recipients. However, this therapy does not prevent late onset CMV disease, and efficacy is attenuated by drug resistance [22]. A rat transplant model with latent RCMV donor infection significantly accelerates TVS development and CR [36]. Latent CMV is reactivated by pro-inflammatory signals that are associated with IRI [22,267]. CMV infection increases donor graft passenger lymphocyte loads prior to transplantation, which we hypothesize results in a double hit during transplantation [165]. Despite the similar clinical manifestations of disease associated with IRI and CMV infection, we do not understand the signaling networks that promote IRI-induced graft rejection. Identification of these pathways may identify therapeutic targets to improve graft survival. In this report, we profiled the IRI pro-inflammatory environment that promotes CMV-accelerated rejection. Inflammasome and IL-1R signaling pathways constituted the central node in IRI-induced cardiac allograft injury. Reduction of IRI by treatment of transplant recipients with a single dose of Anakinra improved allograft outcomes and delayed RCMV-infected donor graft CR.

2.3 Results

2.3.1 IRI transcriptomic analysis

IRI induces cellular responses that promote TVS and accelerate CR. To characterize these responses, a rat model of syngeneic heart transplantation was used to evaluate early graft

injury (Figure 7, Table 1). The degree of cardiac graft IRI at post-operation day (POD) 3 was measured by histological evidence of disease and scored for myocardial injury score, size of myocardial injury area, and level of polymorphonuclear leukocyte (PMN) infiltrate. Significant myocardial injury was observed in transplanted hearts versus non-transplanted controls, with no substantial difference between RCMV-infected and uninfected heart syngeneic grafts (Figure 8). This is consistent with previous findings that CMV acceleration of TVS and CR requires an allogeneic environment [265,268]. To identify molecular pathways involved in IRI, RNA deep sequencing (RNAseq) transcriptomics was performed on PBMC and heart tissues from animals in Cohorts 1 and 2 lacking RCMV infection. Differential gene analysis revealed changes in the expression of 5,518 genes in graft heart tissues and 647 genes in PBMC at POD3 (Figure 9). However, fewer genes were transcriptionally altered in syngeneic recipient native hearts (Cohort 2) versus the native hearts of non-transplanted animals (Cohort 1), indicating that the cardiac transplantation surgery causes IRI and its associated transcriptomic changes (Figure 9a,c).

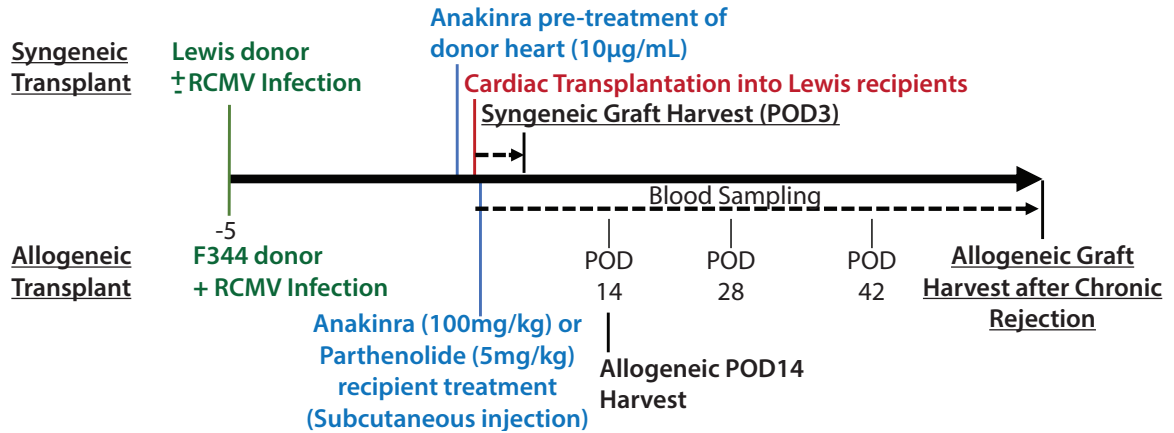


Figure 7. Study design. Syngeneic donors (Lewis) were either mock infected or infected with RCMV at 1×10^5 PFU/animal 5 days prior to transplantation. One cohort of syngeneic cardiac grafts were perfused with UW solution containing 10µg/mL anakinra during the 4-hour cold ischemia time. At 1-hour post-transplantation, groups of recipients were treated by subcutaneous injection with either anakinra (100mg/kg) or parthenolide (5mg/kg) or their respective vehicles. Syngeneic cohorts were harvested at POD3. Allogeneic donors (F344) were infected with RCMV at 1×10^5 PFU/animal 5 days prior to transplantation. Allogeneic cohorts were treated subcutaneously with anakinra at 100mg/kg or vehicle by subcutaneous injection at 1 hour post-transplantation. Blood samples were taken at POD 14, 28, and 42. Animals were sacrificed at two time-points for analyses: POD14 and at the time of CR.

Cohort	n	Graft Type	Donor	Recipient	RCMV Infection	Drug treatment	Harvest POD
1	4-5	None	-	Lewis	-	-	3
2	4-8	Syngeneic	Lewis	Lewis	-	-	3
3	4	Syngeneic	Lewis	Lewis	Donor +	-	3
4	4	Syngeneic	Lewis	Lewis	-	Anakinra, Donor Tissue	3
5	4-8	Syngeneic	Lewis	Lewis	-	Anakinra, Recipient	3
6	4	Syngeneic	Lewis	Lewis	Donor +	Anakinra, Recipient	3
7	5	Syngeneic	Lewis	Lewis	-	Parthenolide, Recipient	3
8	5	Syngeneic	Lewis	Lewis	Donor +	Parthenolide, Recipient	3
9	6, 10	Allogeneic	F344	Lewis	Donor +	-	14, CR
10	6, 10	Allogeneic	F344	Lewis	Donor +	Anakinra, Recipient	14, CR

Table 1. Animal cohorts.

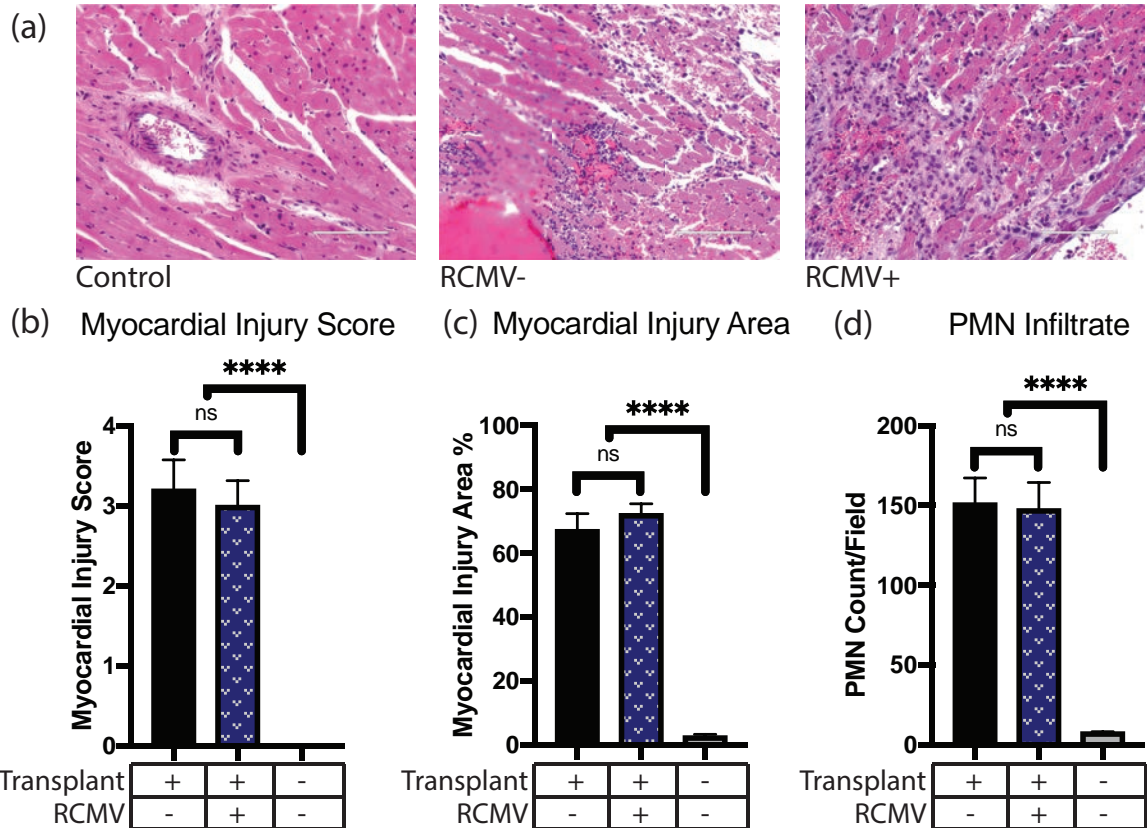


Figure 8. IRI causes myocardial tissue damage and PMN infiltration. Graft or control hearts were harvested at POD3 from isogeneic transplants, fixed in formalin, sectioned, and H&E stained. Tissue sections were then examined and graded for severity of myocardial injury, percent of examined area showing myocardial injury, and PMN infiltrate counts. (a) Representative images of control and I/R injured cardiac tissue at POD3 with or without prior RCMV infection. Control tissue was obtained from a non-transplanted animal. Scale bars represent 100 μ m. (b) Myocardial injury scores on a scale of 0 (no damage) to 4 (severe damage) as described in Table 4, (c) Myocardial injury area determined as percent of examined area showing any degree of myocardial injury, (d) PMN infiltrate as measured by number of PMN cells per field of view at 400x magnification. $n=4$ for all groups. Error bars represent standard error of the mean (SEM).

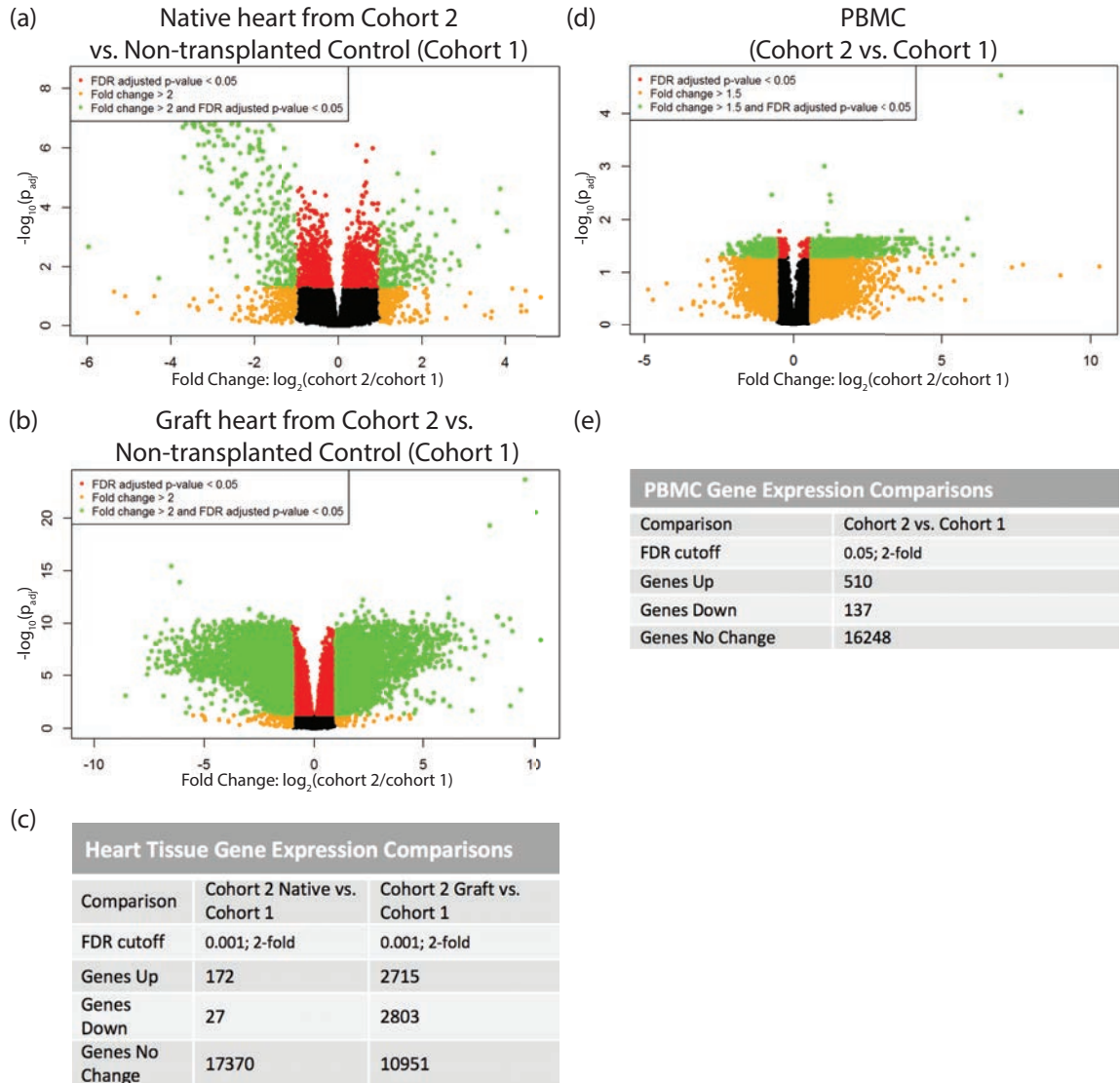


Figure 9. RNAseq transcriptomic analysis of cardiac tissue and PBMC following IRI. Heart tissues were homogenized in Trizol. PBMC were isolated over lymphocyte separation media and resuspended in Trizol. RNA was extracted from heart and PBMC samples by Trizol preparation with isopropanol precipitation. One μg of total RNA was used for RNAseq. (a) Native heart from RCMV- transplant recipient at POD3 (cohort 2) compared to a non-transplanted control heart (cohort 1), (b) Graft heart from RCMV- transplant recipient at POD3 (cohort 2) compared to a non-transplanted control heart (cohort 1), (c) FDR-cutoffs and regulated gene counts for heart tissue comparisons. (d) PBMC isolated from whole blood of a RCMV- transplant recipient at POD3 (cohort 2) compared to PBMC isolated from whole blood of a non-transplanted control animal (cohort 1), (e) FDR-cutoffs and regulated gene counts for PBMC heart tissues. Genes showing fold-

change greater than 2 (Heart) or 1.5 (PBMC) with an FDR adjusted p-value of 0.05 are shown in green in volcano plots (a, b, d) and were selected for further investigation.

Genes showing differential expression following IRI were organized into functional and disease pathways revealing cellular migration, chemotaxis, and inflammation pathways were altered in Cohort 2 versus Cohort 1 hearts (Table 13, Table 14). Top up-regulated hits in graft hearts included acute phase response signaling; NF- κ B signaling; and inflammasome pathway. In PBMC samples, up-regulated pathways included NF- κ B signaling; acute phase response signaling, and interleukin-signaling (Table 15, Table 16). Consideration of upstream regulators and predicted downstream effects revealed that IL-1R up-regulation in recipient PBMC predicted increased expression of interleukins, chemokines, Tumor necrosis factor (TNF)-associated molecules, and IFN factors, matching our RNAseq findings (Figure 10). Causal analysis for molecules within these networks predicted increases in the activation of leukocytes, the inflammatory response, leukocyte migration, leuko-/lympho-poiesis, and recruitment of myeloid cells (Table 2). Further analysis revealed that members of the IL-1 cytokine family pathway were upregulated in both cardiac grafts and PBMC following IRI (Table 3, Figure 11).

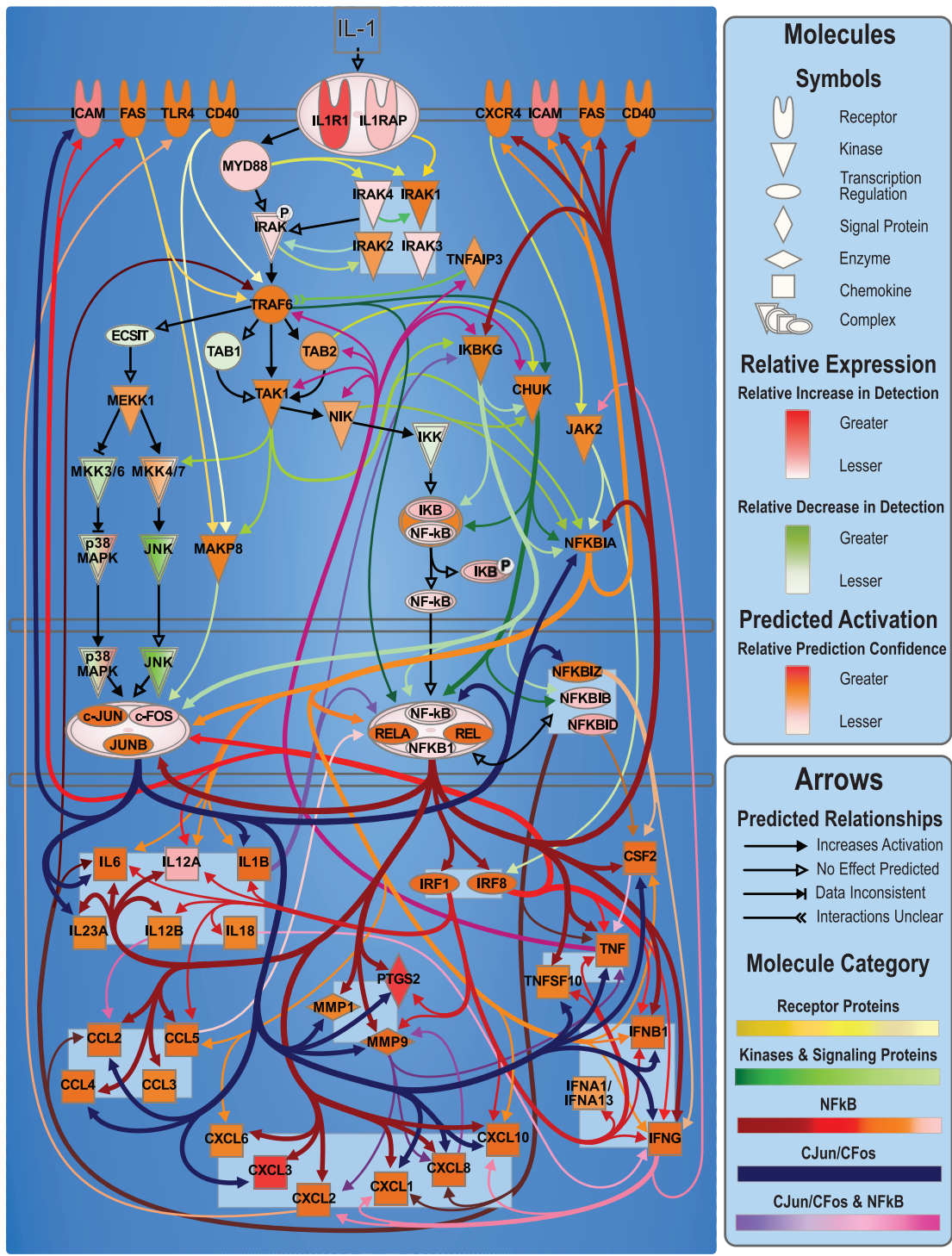


Figure 10. IRI results in pro-inflammatory patterns at the transcriptomic level. Ingenuity pathway core analysis was used to identify downstream effects of IL-1R activation seen in PBMC samples following transplantation (cohort 2 vs. cohort 1). Genes are represented by labeled shapes depending on their molecular function. Expression and predicted activation levels determined by fold-change between cohort 2 and cohort 1 are presented using the following convention on color scales with increasing saturation associated with an greater absolute fold-change value: red = increased detection; green = decreased detection; orange=predicted activation. Predicted relationships are indicated by arrow-heads as follows: (increases activation) molecule at beginning of arrow is predicted to increase the activation of the molecule at the end of the arrow-head; (no effect predicted) molecules are part of the canonical IL-1 signaling pathway, but do not have any direct effect on each other transcriptionally; (data inconsistent) interacting signaling networks made it impossible to determine what the predicted outcome of these relationships was in our dataset; (interactions unclear) these molecules have been shown to effect each other, but the direction and extent of these interactions is unclear. Predicted transcriptional regulatory networks are indicated based on molecule categories: (receptor proteins) Green - predicted activation is initiated from a receptor molecule; (kinases & signaling proteins) Yellow- predicted activation is initiated from a kinase or other signaling protein; (cJun/cFOS) Blue – predicted activation is initiated from cJun/cFOS; (NF- κ B) Red – predicted activation is initiated from NF- κ B; and (cJun/cFOS & NF- κ B) Purple – predicted activation is initiated from both cJun/cFOS and NF- κ B transcription complexes.

Values	Activation of Leukocytes	Inflammatory response	Leukocyte migration	Leukopoiesis	Lymphopoiesis	Recruitment of myeloid cells
Combined p-Value	1.31E-55	1.06E-42	1.35E-43	8.70E-57	2.05E-54	1.06E-42
CCL2	✓	✓	✓	✓	-	✓
CCL3	✓	✓	✓	✓	✓	✓
CCL4	✓	✓	✓	-	-	✓
CCL5	✓	✓	✓	✓	✓	✓
CD40	✓	✓	✓	✓	✓	✓
c-FOS	✓	✓	✓	✓	✓	-
CHUK	✓	✓	✓	✓	✓	-
c-JUN	-	-	✓	✓	✓	-
CSF2	✓	✓	✓	✓	✓	✓
CXCL1	✓	✓	✓	✓	✓	✓
CXCL10	✓	✓	✓	✓	✓	✓
CXCL2	-	✓	✓	-	-	✓
CXCL3	✓	✓	✓	-	-	✓
CXCL6	✓	✓	✓	-	-	-
CXCL8	✓	✓	✓	✓	-	✓
CXCR4	-	✓	✓	✓	✓	✓
FAS	✓	-	✓	✓	✓	-
ICAM1	✓	✓	✓	✓	✓	✓
IFNA1/IFNA13	✓	✓	-	✓	✓	-
IFNB1	✓	✓	✓	✓	✓	-
IFNG	✓	✓	✓	✓	✓	✓
IKBKKG	✓	✓	✓	✓	✓	-
IKK	-	-	-	✓	✓	-
IL-1	✓	✓	✓	✓	✓	✓
IL12A	✓	-	✓	✓	✓	-
IL12B	✓	✓	✓	✓	✓	-
IL18	✓	✓	✓	✓	✓	✓
IL1B	✓	✓	✓	✓	✓	✓
IL1R1	✓	✓	✓	✓	✓	✓
IL23A	✓	✓	✓	✓	✓	-
IL6	✓	✓	✓	✓	✓	✓
IRAK1	✓	✓	-	✓	✓	-
IRAK3	✓	✓	-	✓	✓	-
IRAK4	✓	-	✓	-	-	-
IRF1	✓	-	-	✓	✓	-
IRF8	✓	-	-	✓	✓	-
JAK2	✓	✓	✓	✓	-	-
JNK	✓	✓	✓	✓	✓	-
JUNB	-	-	-	✓	✓	-
MAPK8	✓	✓	✓	✓	✓	✓
MMP1	-	✓	✓	-	-	✓
MMP9	✓	✓	✓	-	-	✓
MYD88	✓	✓	✓	✓	✓	✓
NFKB1	✓	✓	✓	✓	✓	-
NFKBIA	✓	✓	✓	✓	✓	✓
NFKBIB	-	✓	-	-	-	-
NFKBID	✓	-	-	✓	✓	-
NFKBIZ	✓	✓	✓	✓	✓	-
NF-κB	✓	✓	✓	✓	✓	-
NIK	-	-	✓	✓	✓	-
p38MAPK	✓	✓	✓	✓	✓	✓
PTGS2	✓	✓	✓	✓	✓	-
REL	✓	✓	✓	✓	✓	-
RELA	✓	✓	✓	✓	✓	-
TAB2	✓	-	-	✓	✓	-
TAK1	✓	-	-	✓	✓	-
TLR4	✓	✓	✓	✓	✓	✓
TNF	✓	✓	✓	✓	✓	✓
TNFAIP3	✓	✓	✓	✓	✓	-
TNFSF10	✓	-	✓	✓	✓	-
TRAF6	-	-	✓	✓	✓	-

Table 2. Contribution of molecules predicted to be up-regulated from Figure 10 to pro-inflammatory and immune-cell recruitment associated functions as predicted by IPA in PBMC. Combined p-values of prediction for each function are listed underneath each function heading. Molecules contributing to each function are marked with green check-marks. Molecules not contributing to the functions are marked with a grey dash.

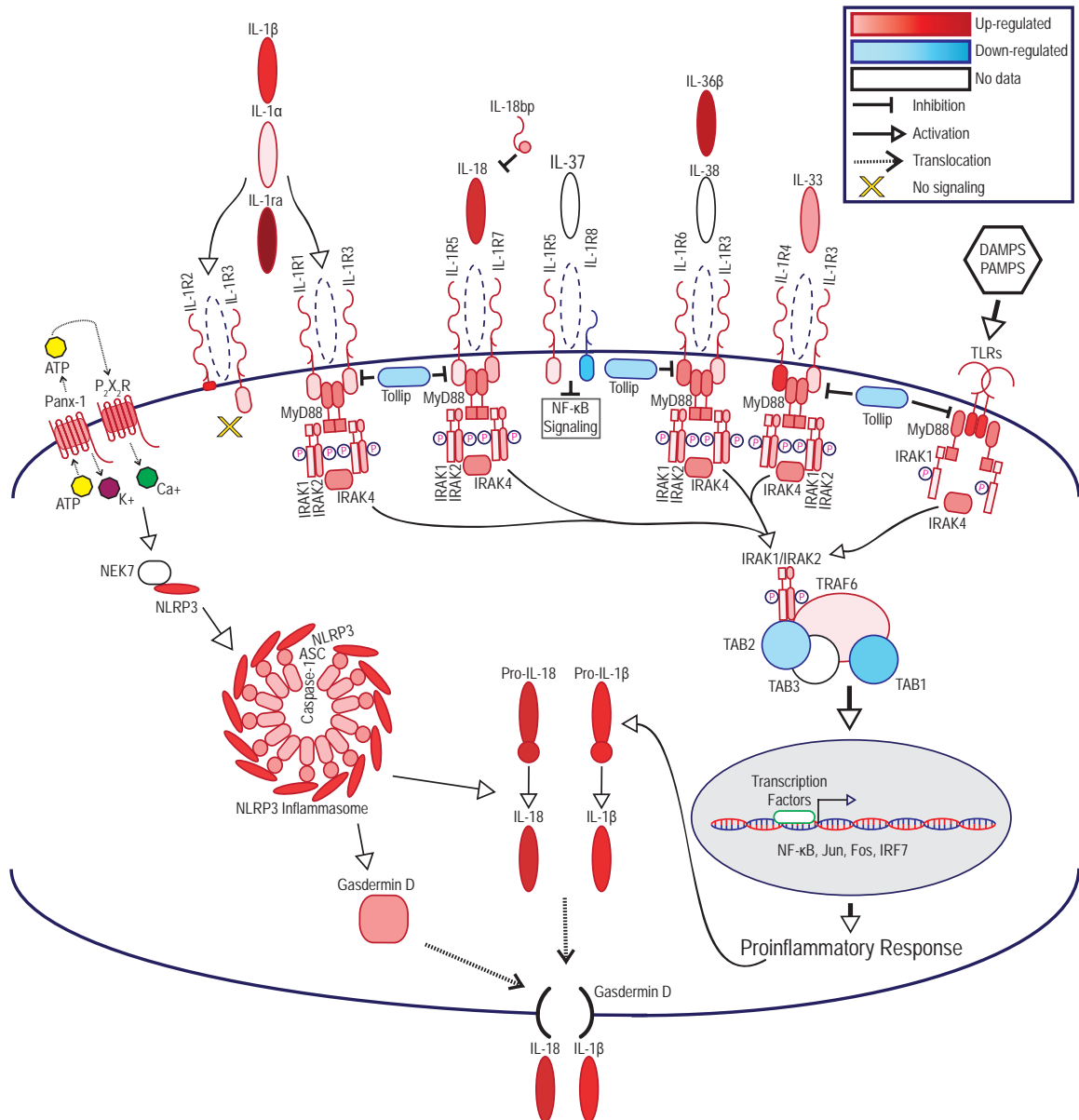


Figure 11. IL-1R signaling molecules are up-regulated in graft and PBMC samples following transplantation leading to a pro-inflammatory response. Statistically significant alterations in gene expression from RNAseq analysis of graft tissues are represented by red (up-regulation) and blue (down-regulation). Molecules which did not meet statistical significance, or for which mapping was unavailable in the rat genome are shown in white. $FDR-p < 0.05$. FDR-corrected p -values and Cohort 2 versus Cohort 1 ratios are listed in Table 3. Abbreviations are as follows: DAMPs (damage associated molecular patterns), PAMPs (pathogen associated molecular patterns), TLRs (Toll like receptors).

Gene	Heart: Cohort 2 Graft/Cohort 1	FDR p-value	PBMC: Cohort 2/Cohort 1	FDR p-value	Function
IL-1 α	1.66	0.4812			Cytokine, Inflammation
IL-1 β	19.57	0.0000	3.63	0.4305	Cytokine, Inflammation
IL1rn/IL1ra	127.41	0.0000	4.06	0.0845	Cytokine, Inhibitor
IL-18	29.50	0.0000	2.11	0.6595	Cytokine, Inflammation
IL-18bp	2.18	0.0014	1.76	0.6741	Cytokine, Inhibitor
IL36 β	95.31	0.0000	3.48	0.0739	Cytokine, Inflammation
IL33	3.40	0.0000	1.17	0.9715	Cytokine, Inflammation
IL1R1	1.87	0.0181	12.32	0.0503	Receptor, Inflammation
IL1R2	41.12	0.0000	21.46	0.1209	Decoy Receptor, Inhibitor
IL1RAP	1.88	0.0028	2.36	0.1481	Receptor, Inflammation
IL18r1	1.69	0.0233	0.86	0.9050	Receptor, Inflammation
IL18R β	2.56	0.0000	1.95	0.4543	Receptor, Inflammation
IL1R8	0.56	0.0014	0.73	0.6399	Receptor, Inhibitor
IL1rl1	23.25	0.0000	2.32	0.5777	Receptor, Inflammation
IL1rl2	4.86	0.0001	2.49	0.4433	Receptor, Inflammation
Myd88	5.19	0.0000	1.84	0.0755	Signaling Adaptor, Inflammation
IRAK1	1.29	0.0000	1.20	0.5414	Signaling Adaptor, Inflammation
IRAK2	2.81	0.0000	1.24	0.7535	Signaling Adaptor, Inflammation
IRAK4	4.47	0.0000	1.64	0.0728	Signaling Adaptor, Inflammation
TRAF6	1.65	0.0006	1.26	0.8759	Signaling Adaptor, Inflammation
Tollip	0.80	0.0010	1.32	0.5129	Signaling Adaptor, Inhibitor
Pannexin-1	2.32	0.0018	0.46	0.3481	ATP Release Channel
P2X2R	6.16	0.0001			DAMP, ATP Sensor
TLR2	22.85	0.0000	3.39	0.1182	PRR, Inflammation
TLR3	1.87	0.0007	1.01	0.9981	PRR, Inflammation
TLR4	4.95	0.0000	2.00	0.5758	PRR, Inflammation
TLR5	4.63	0.0005	7.24	0.0170	PRR, Inflammation
TLR6	6.51	0.0000	2.17	0.1580	PRR, Inflammation
TLR7	22.94	0.0000	2.25	0.3191	PRR, Inflammation
TLR8	26.43	0.0007	2.22	0.0443	PRR, Inflammation
TLR9	11.48	0.0240	0.76	0.7868	PRR, Inflammation
TLR10	20.00	0.0000	2.24	0.2805	PRR, Inflammation
TLR11	3.08	0.0099			PRR, Inflammation
TLR12	3.83	0.0015	0.40	0.6166	PRR, Inflammation
TLR13	6.92	0.0000	2.76	0.0691	PRR, Inflammation
NLRP3	12.35	0.0000	7.79	0.1089	Sensor, Inflammasome Formation
ASC	3.75	0.0000	1.15	0.8267	Adaptor, Inflammasome Formation
Caspase-1	2.75	0.0000	0.81	0.6099	Enzyme, Inflammasome
Gasdermin D	4.21	0.0000	0.95	0.9080	Membrane Pore, Cytokine Release

Cohort 1 = Non-transplanted, non-infected
Cohort 2 = Syngeneic transplant, non-infected
p < 0.05 is significant

Table 3. Pro-inflammatory signaling molecules are up-regulated in graft and PBMC data following transplantation. Selected RNAseq data showing graft hearts from transplant recipients (cohort 2) versus non-transplanted native hearts (cohort 1) and PBMC samples from cohort 2 versus cohort 1. Up-regulated genes are color coded in red, down-regulated genes are color coded in blue. Those values that were found to be statistically significant (FDR-p < 0.05) are bolded. Functions of each signaling molecule are listed.

Abbreviations are as follows: ATP (adenosine trip-phosphate), DAMP (damage associated molecular pattern), PRR (pattern recognition receptor).

Regulated genes from cardiac grafts appearing in multiple pathways were selected for validation by quantitative real time polymerase chain reaction (qRT-PCR) (Figure 12). The up-regulation of MMP12, SPP1, CXCL6, CXCL2, and CXCL3 supported our RNAseq analysis. While IL-1R1 and IL-1R2 were both up-regulated in PBMCs by RNAseq, RNAseq showed only a minor change in POD3 transcriptional expression of IL1R in cardiac grafts (Table 3). We validated IL-1R expression in cardiac grafts by qRT-PCR and, similarly, found no change between Cohort 2 and Cohort 1 (Figure 12). These findings indicate that transplant IRI initiates inflammation in the cardiac grafts; and lymphocytes, through their response to IL-1, consequently exacerbate this inflammatory process.

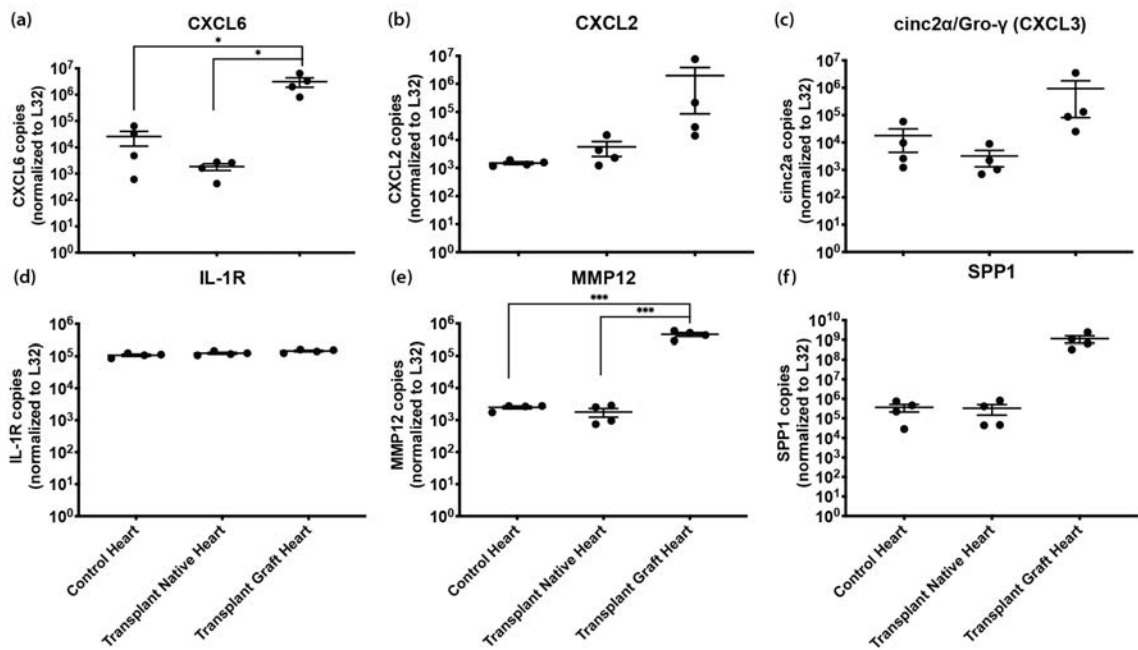


Figure 12. qRT-PCR validation of expression levels for rat chemokines (a-c), IL-1R (d), MMP12 (e), and SPP-1 (f) in cardiac tissues from non-transplanted control, native, and graft cohorts. Statistical significance determined by one-way ANOVA with Tukey's multiple comparison, * $P < 0.05$, *** $P < 0.001$.

2.3.2 Anakinra and Parthenolide reduce IRI-induced tissue damage

Transcriptomic analysis suggested a key role for IL-1 signaling in IRI in syngeneic heart transplants. Our data, and prior work by others [269–271], implicated NF- κ B signaling and the inflammasome as other targets for reducing IRI (Figure 11, Table 3). Two different therapeutics were tested to assess the role of IL-1 signaling in IRI. The first approach used the clinically-approved IL-1R1/2 antagonist Anakinra, which reduces neutrophil and macrophage activation in multiple disease states and in rat models [272–275]. Additionally, NLRP3 was increased 12.35-fold in cardiac grafts and 7.79-fold in PBMC during transplant-induced IRI (Figure 11, Table 3). The NLRP3 inflammasome activates Caspase-1, which proteolytically activates pro-IL-1 β and pro-IL-18. Our second treatment used parthenolide, an inhibitor of Caspase-1/NF- κ B, with known anti-inflammatory activity in rats [270,276,277].

To determine efficacy of Anakinra two treatment regimens were used: 1) syngeneic donor cardiac grafts during the 4-hour cold ischemia period at a concentration determined to be effective *in vitro* (Figure 13) (Cohort 4); or 2) the recipient at 1-hour post-transplant (Cohort 5) (Figure 7, Table 1). Syngeneic graft hearts were harvested at POD 3 and analyzed by immunohistochemistry and flow cytometry. Pre-transplant donor cardiac graft treatment (Cohort 4) resulted in minimal decreases in myocardial injury (score and area) and PMN infiltration compared to vehicle treated controls (Cohort 2) (Figure 14a-d). In contrast, recipients treated with Anakinra at 1-hour post-transplant (Cohort 5) had a significant decrease in myocardial injury score and PMN and macrophage graft infiltration compared to vehicle treated controls (Cohort 2) (Figure 14a,c,d). Flow cytometric analysis

of graft and native heart cellular infiltrates demonstrated that neutrophils and macrophages were the predominant infiltrating immune cell types in the grafts at POD3, which were significantly reduced by Anakinra treatment and absent in native hearts (Figure 14e,f). For parthenolide studies, syngeneic transplant recipients were treated subcutaneously at 1-hour post-transplantation with 5mg/kg (Cohort 7) or vehicle (Cohort 2). Similar to Anakinra, parthenolide significantly reduced POD3 myocardial injury score, as well as PMN and macrophage graft infiltration (Figure 14a-d). RCMV infection did not influence these early events in syngeneic graft hearts (Cohorts 6 and 8), which is consistent with our previous findings that CMV affects allograft rejection starting at POD7 [263]. Our findings demonstrate that syngeneic grafts from RCMV-infected donors respond equally to Anakinra and parthenolide treatments with a reduction in myocardial injury and inflammatory cell infiltration.

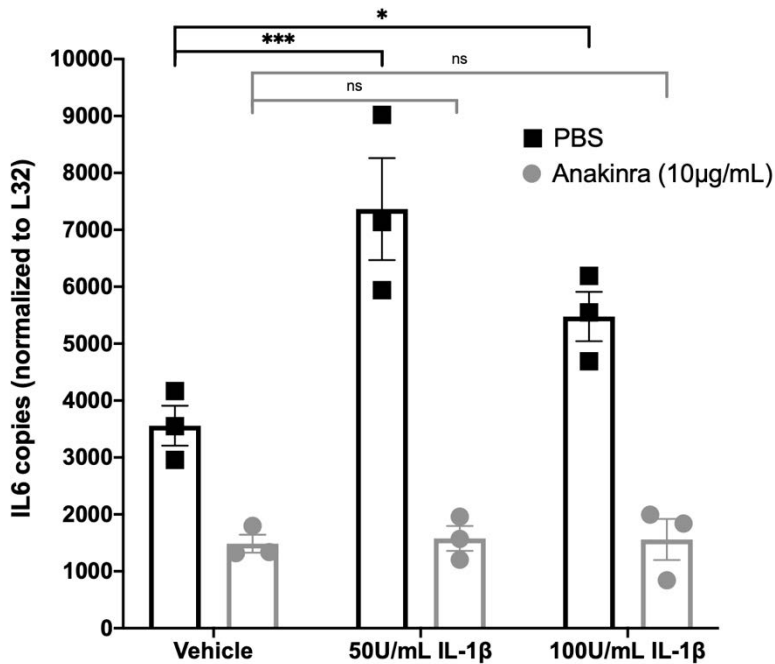


Figure 13. Anakinra suppresses IL-1 β signaling in rat PBMC. Rat PBMC were isolated from blood of a naïve lewis rat and treated with Anakinra at 10 μ g/mL or PBS (control) at 37 $^{\circ}$ C for 1 hour. Following incubation, IL-1 β at 50U/mL or 100U/mL or PBS (control) was added to cells. Treatment groups were incubated at 37 $^{\circ}$ C for 24

hours and harvested in Trizol. RNA was extracted and qRT-PCR was performed for rat IL-6 and L32. IL-6 copies were normalized against copies of L32. Treatments were performed in triplicate. * p <0.05, *** p <0.001.

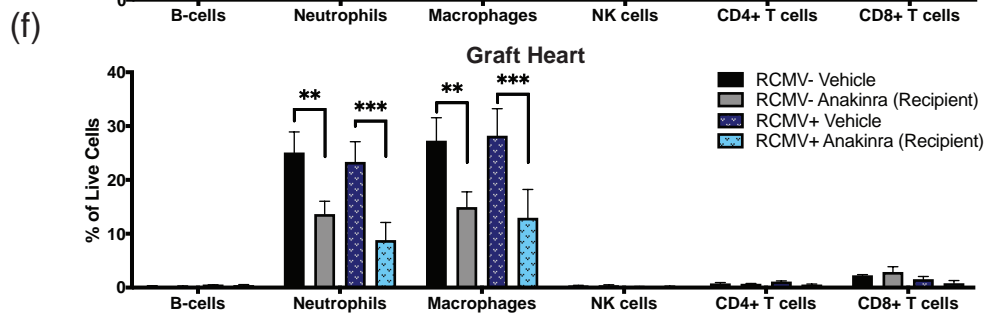
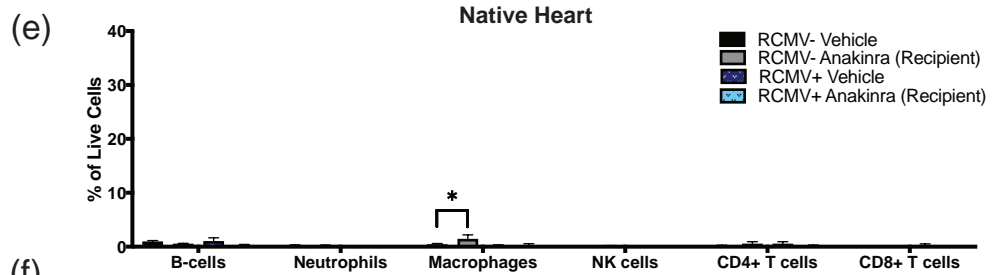
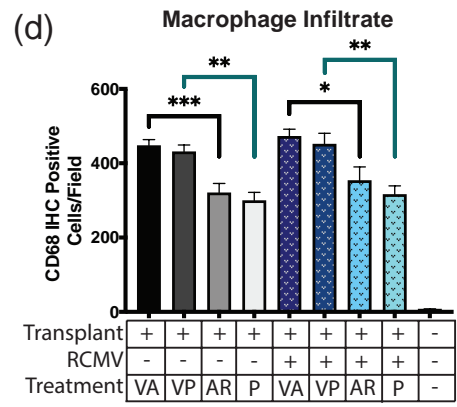
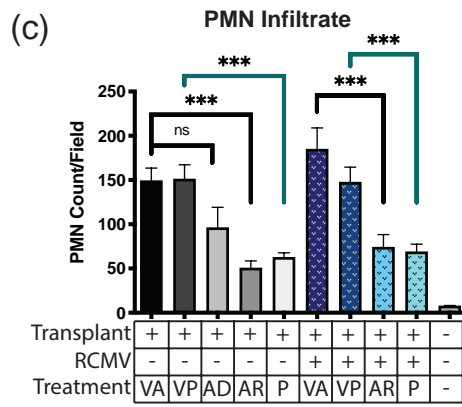
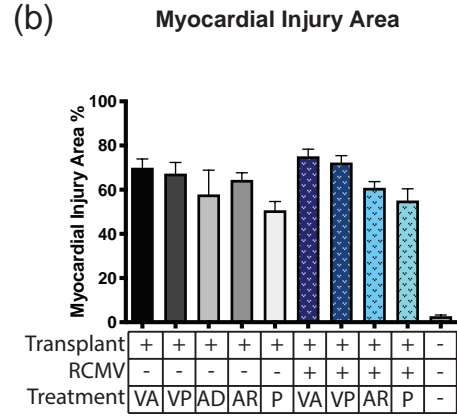
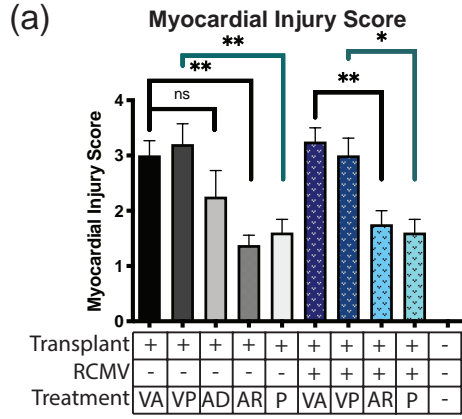


Figure 14. Anakinra treatment of the recipient immediately post-transplantation improves myocardial injury score and PMN infiltrate into cardiac tissue. (a-d) Myocardial injury score (a), myocardial injury area (b), PMN infiltrate (c), and macrophage infiltrate (d). Error bars represent SEM. Statistical significance determined by one-way ANOVA with Tukey's multiple comparison, * $P < 0.05$, ** $P < 0.01$, *** $P < 0.001$ versus vehicle transplant. Representative images are shown in Figure 15. Fields counted for (c) and (d) were viewed at magnification equal to 400x. Groups are labeled (Transplant-/RCMV-/Treatment-) Native heart from a non-transplanted, uninfected animal (n=5); (Transplant+/RCMV-/VA) Graft heart from RCMV donor with anakinra vehicle injection of recipient animals 1-hour post-transplant (n=4); (Transplant+/RCMV-/VP) Graft heart from RCMV donor with parthenolide vehicle injection of recipient animals 1-hour post-transplant (n=5); (Transplant+/RCMV-/AD) Graft heart from RCMV donor with anakinra treatment of donor organ pre-transplantation (n=4); (Transplant+/RCMV-/AR) Graft heart from RCMV donor with anakinra treatment of recipient 1-hour post-transplant (n=4); (Transplant+/RCMV-/P) Graft heart from RCMV donor with parthenolide treatment of recipient 1-hour post-transplant (n=5); (Transplant+/RCMV+/VA) Donor infected i.p. with 1×10^5 PFU RCMV 5 days prior to transplant, with anakinra vehicle injection of recipients 1-hour post-transplant (n=4); (Transplant+/RCMV+/VP) Donor infected i.p. with 1×10^5 PFU RCMV 5 days prior to transplant, with parthenolide vehicle injection of recipients 1-hour post-transplant (n=4); (Transplant+/RCMV+/AR) Donor infected i.p. with 1×10^5 PFU RCMV 5 days prior to transplant followed by anakinra treatment of recipient 1-hour post-transplant (n=4); (Transplant+/RCMV+/P) Donor infected i.p. with 1×10^5 PFU RCMV 5 days prior to transplant with parthenolide treatment of recipient 1-hour post-transplant (n=5). (e,f) Native (e) and graft (f) heart tissues were harvested at 3 days post-transplant from RCMV⁻ PBS treated (cohort 2), RCMV⁻ Anakinra treated (cohort 4), RCMV⁺ PBS treated (cohort 5), and RCMV⁺ Anakinra treated (cohort 6) recipients and processed for flow cytometry staining. Antibodies were directed against cellular markers for T-cells (CD3⁺, CD4⁺/CD8⁺), B-cells (CD45ra⁺, CD3⁻, CD161a low), Neutrophils (CD43⁺, CD3⁻, CD161a low, CD45ra⁺), macrophages (CD68⁺, CD3⁻), and NK cells (CD161a high, CD3⁻). Gating strategy as in Figure 16. (e) Native heart tissues from transplant recipients at POD3, cell percentages reported as percent of total live cells. (f) Graft heart tissues from transplant recipients at POD3, cell percentages reported as percent of total live

cells. Statistical significance determined by two-way ANOVA with Tukey's multiple comparison, $*P < 0.05$, $**P < 0.01$, $***P < 0.001$. $n = 4$. Error bars represent SEM.

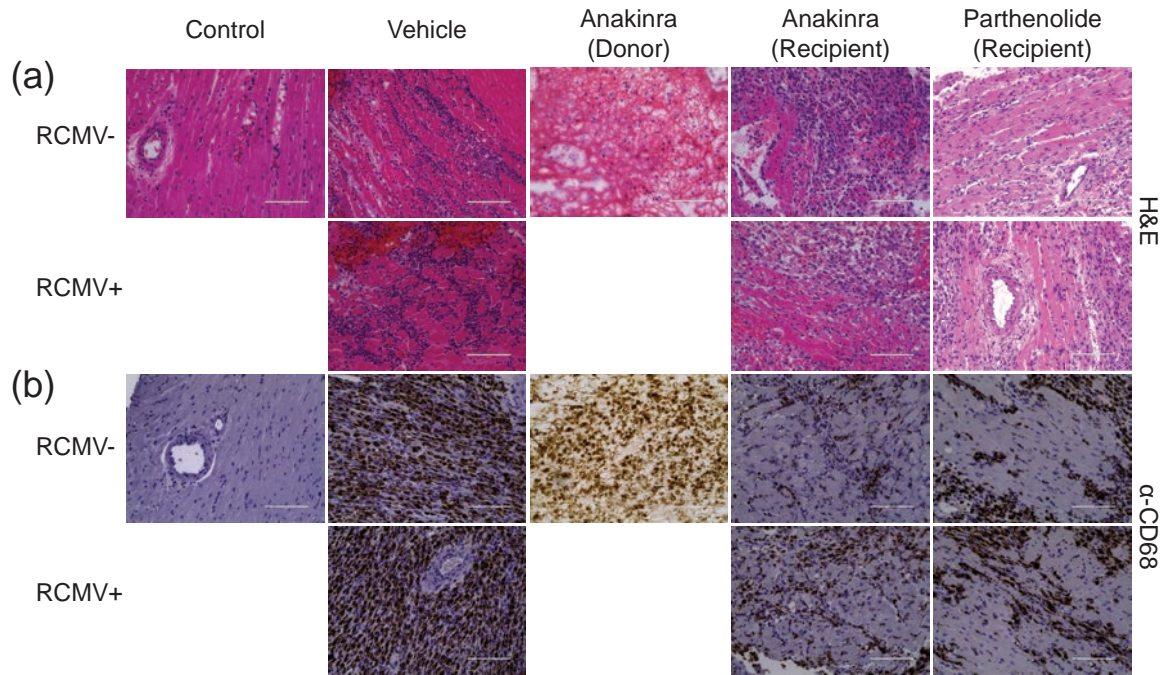


Figure 15. Representative images of cardiac tissue sections from syngeneic transplants or non-transplanted controls (Figure 14) are shown with (a) H&E staining to visualize PMN infiltrate and myocardial injury, and (b) anti-CD68 staining for macrophage infiltrate. Scale bars represent 100 μm .

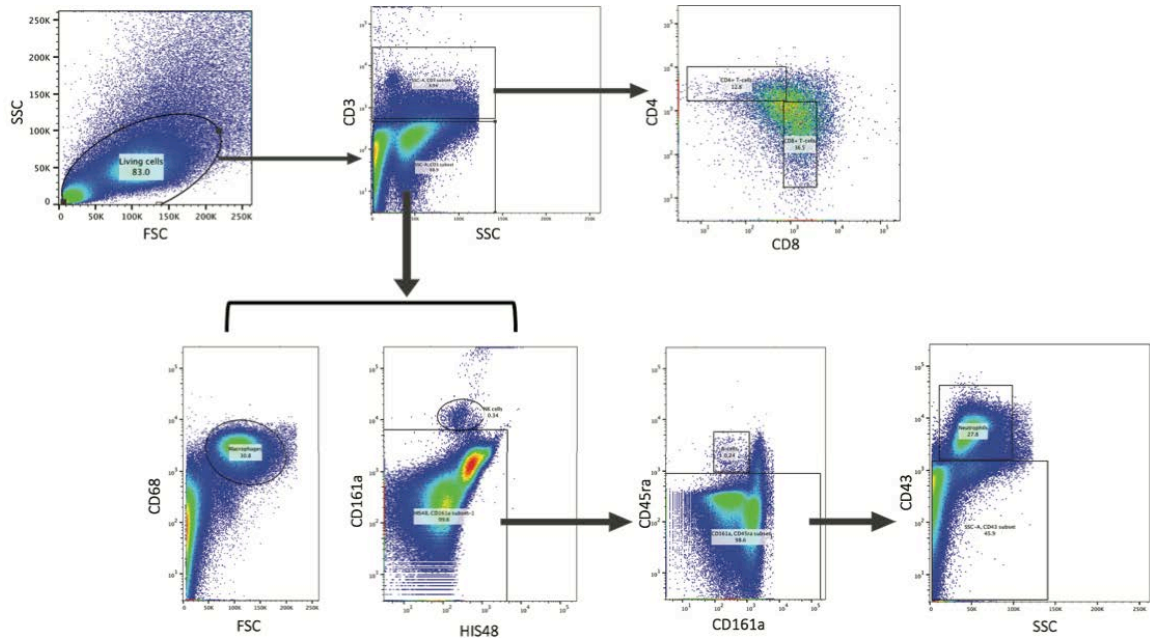


Figure 16. Gating strategy for leukocytes isolated from heart tissues. Antibodies were directed against markers for B cell, neutrophil, macrophage, NK cell, CD4⁺ T-cell, and CD8⁺ T-cell populations.

2.3.3 Anakinra reduces inflammatory cytokine production following transplant IRI

To determine the anti-inflammatory pathways that are activated by IRI and targeted by Anakinra, we performed rat cytokine/chemokine assays on POD3 plasma and graft heart homogenates (Figure 17). Following transplantation, plasma concentrations were elevated above pre-transplant levels for cytokines IL-1 β , IL-2, IL-5, IL-10, IL-13, IL-17A, IFN γ , G-CSF, and TNF α ; chemokines CCL2, CCL5, CXCL1, CXCL2, and CXCL10; and EGF. Cardiac graft cytokine levels were also increased above those detected in non-transplanted control hearts for IL-1 α , IL-1 β , IL-2, IL-6, IL-13, IL-18, IFN γ , and TNF α ; chemokines CCL2, CCL3, CXCL1, CXCL10; and EGF. Interestingly, while Anakinra treatment reduced the IRI-induced levels of IL-1 β , IL-2, TNF α , CXCL1 and EGF, the drug did not have a global effect on all of the upregulated factors and some were differentially affected in plasma versus tissue. For example, IL-18 and CXCL10 were increased in grafts from

treated animals compared to transplanted controls whereas plasma levels of CXCL10 were reduced upon treatment. Treatment reduced IL-5, IL-10, IL-13, IL-17A, G-CSF, and CCL2 in plasma. By contrast, graft levels of CCL2 were increased in the treated animals. IL-1 α , IL-6, IFN γ , CCL3, and CXCL2 graft levels were reduced as a result of Anakinra treatment. These data indicate that Anakinra reduces plasma and graft cytokine expression associated with IL-1R-driven inflammation.

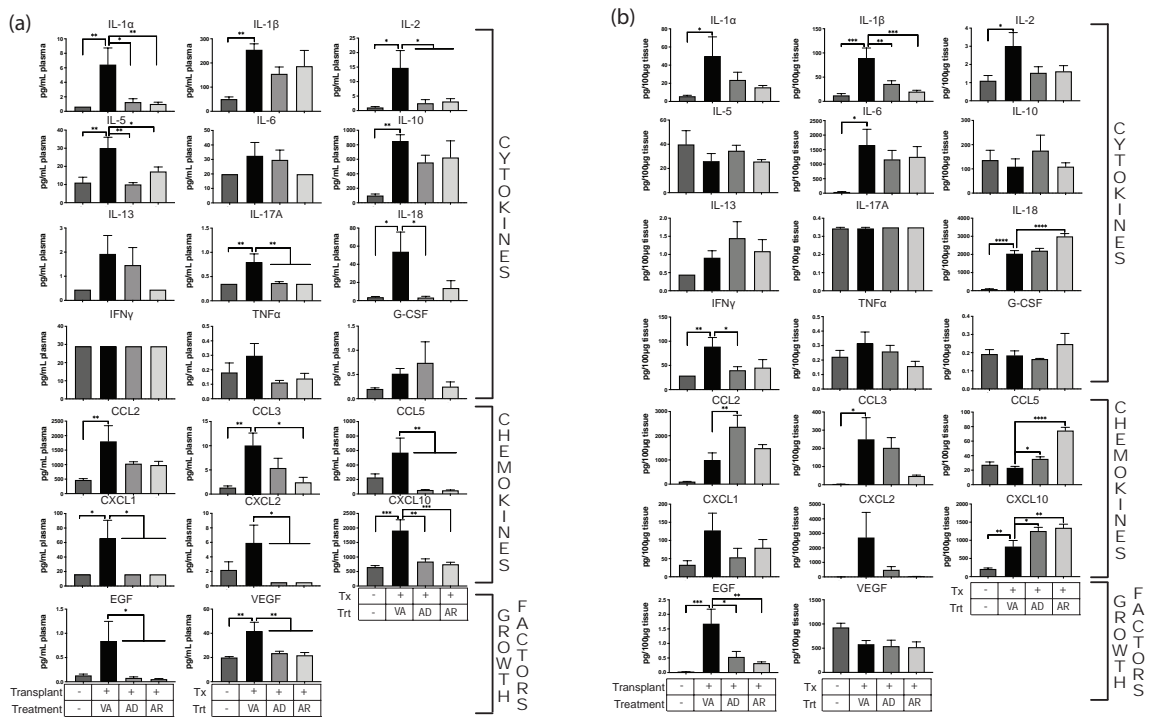


Figure 17. Anakinra reduces pro-inflammatory cytokines elevated during transplantation. Luminex cytokine profiling of serum and heart tissue homogenates was analyzed following IL-1R antagonist treatment of recipients compared to non-treated controls and non-transplanted controls. Treatment groups are as indicated with (Transplant-/Treatment-) Native heart from a non-transplanted, uninfected animal (n=5); (Transplant+/VA) Graft heart from RCMV⁻ donor with anakinra vehicle injection of recipient animals 1-hour post-transplant (n=4); (Transplant+/AD) Graft heart from RCMV⁻ donor with anakinra treatment of donor organ pre-transplantation (n=4); (Transplant+/AR) Graft heart from RCMV⁻ donor with anakinra

*treatment of recipient 1-hour post-transplant (n=4). Error bars represent SEM. Statistical significance determined by one-way ANOVA with Dunnett's correction for multiple comparisons, *P<0.05, ***P<0.001.*

2.3.4 Anakinra prolongs survival of RCMV-infected cardiac allografts

Our findings suggest neutrophil and macrophage infiltration following transplantation is a crucial component of IRI, which may contribute to graft CR. In light of IL-1R signaling blockade to reduce IRI and PMN infiltrate at POD3 from an RCMV⁺ donor, we determined whether Anakinra immediately following transplantation would improve long-term graft survival in RCMV⁺ allogeneic cardiac grafts. RCMV-infected F344 donors were transplanted into naïve Lewis rats and the recipients were treated with 100mg/kg Anakinra (Cohort 10) or vehicle (Cohort 9) at 1-hour post-transplantation. Animals were monitored daily for diminishing heart beat as an indicator of graft failure (CR). Time to CR was significantly increased ($p<0.001$) in Anakinra treated animals (66 days) compared to vehicle controls (51 days) (Figure 18a). Anakinra treatment also reduced the development of TVS (NI measured at rejection) (Figure 18b,c). To assess kinetics of TVS reduction by Anakinra treatment, we harvested allografts (Cohorts 9 and 10) at POD14. Anakinra treatment reduced neointima formation to near RCMV-naïve transplanted grafts (Figure 18d,e), suggesting that Anakinra abrogates RCMV-induced early graft damaging TVS [263].

A possible mechanism behind Anakinra's reduction in TVS and improved graft survival may be effects on CMV replication because CMV-accelerated TVS/CR are linked to active viral replication [278,279]. We assessed the effect of Anakinra on RCMV replication and immune response. Serum from RCMV infected graft recipients at 2, 4, and 6 weeks post-

transplantation were quantified for RCMV-specific IgG and IgM antibody responses. No significant differences were observed in IgM titers (Figure 18f) at any timepoint, indicating no effect of Anakinra on early antibody responses. However, anti-RCMV IgG antibody levels were reduced with Anakinra versus controls (Figure 18g). Anti-donor IgG antibody responses were very low in all animals, and were not significantly different between treatment groups (Figure 18h). The reduction in antiviral IgG titers may be the result of decreased viral loads due to the impaired recruitment of macrophages into the graft heart or a direct antiviral effect. Accordingly, we first measured RCMV viral DNA loads in native heart, graft heart, spleen, and submandibular glands (SMG) at the time of rejection. Viral DNA levels in SMG tissues of Anakinra treated animals were reduced compared to controls, with a significantly greater number of animals with undetectable levels in SMG tissues (Figure 18i). Additionally, native heart, graft heart, and spleen tissues from Anakinra-treated animals trended towards decreased detectable levels (Figure 18i). Unexpectedly, Anakinra treatment only modestly reduced viral loads at POD14 in all tissues tested (Figure 18j). To rule out whether Anakinra directly inhibits viral replication, we infected rat macrophages and fibroblasts with RCMV and treated them with Anakinra at 10 microgram/milliliter ($\mu\text{g}/\text{mL}$). Treatment did not significantly alter viral titers at any timepoint in fibroblasts (Figure 19), or reduce viral genomes present in macrophages at 7 days post-infection (dpi) (Figure 19). These results suggest Anakinra treatment in the early post-transplant period improves graft survival from RCMV-infected donors transplanted into naïve recipients by limiting RCMV dissemination, rather than directly impairing viral replication.

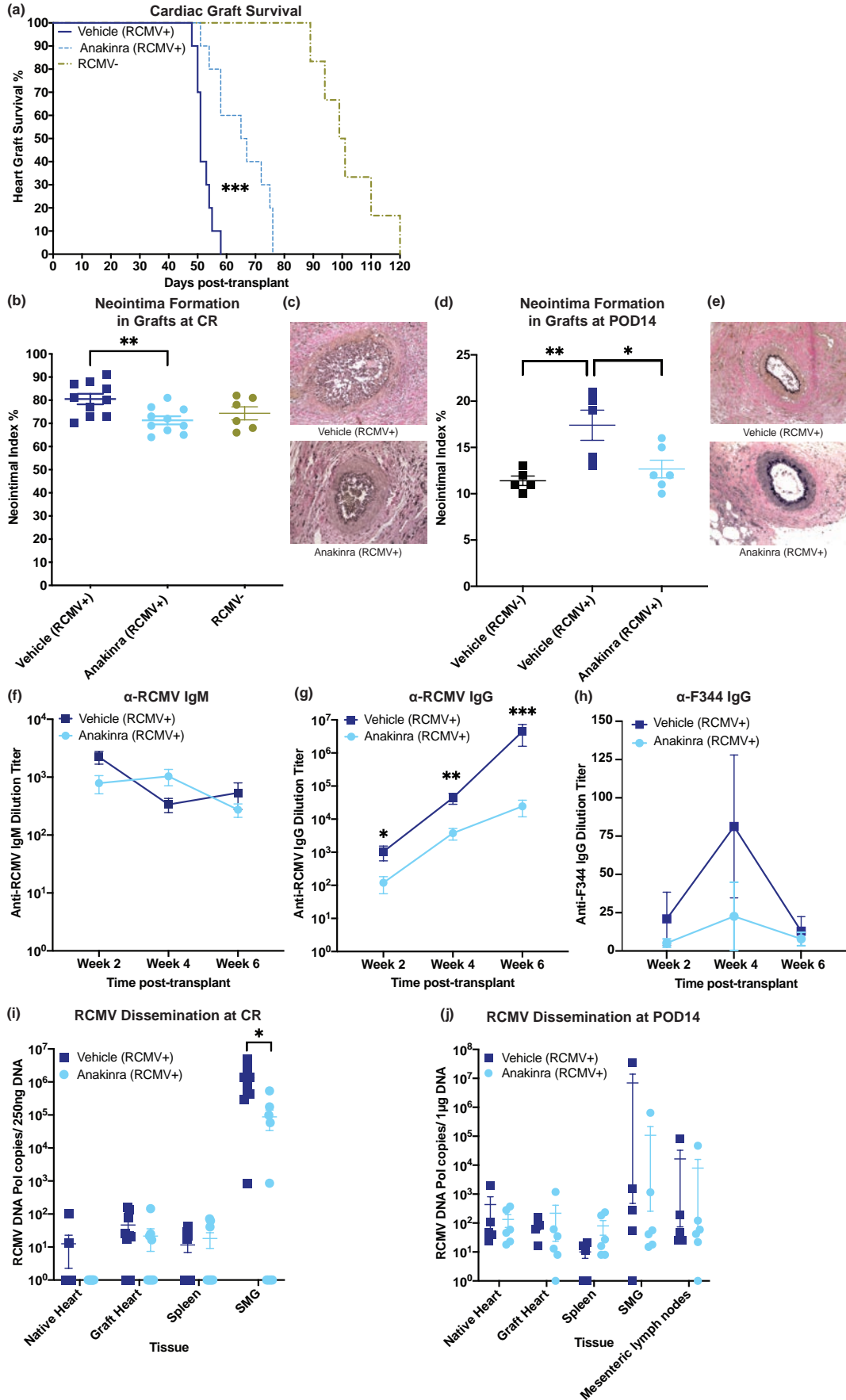


Figure 18. One dose of anakinra at 1-hour post-transplant significantly improves survival time and decreases viral loads at rejection. Donor animals were infected with RCMV 5 days prior to transplantation. Recipients were then treated with vehicle or with anakinra at 1-hour post-transplantation. (a) Time to rejection was significantly improved by recipient treatment with anakinra following transplantation. Graft heart rejection was monitored by palpation for heart beat. Animals were sacrificed and tissues were harvested at the time of rejection. Vehicle treated animals had a mean survival time of 52 days and Anakinra treated animals had a mean survival time of 65 days. Statistical significance determined by Mann-Whitney test, $***P < 0.001$ vs. Vehicle-control, $n=10$. PBS-treated RCMV- historical controls included for references (light green) (b,c) NI of coronary arteries in graft hearts at CR was decreased in Anakinra-treated cohorts. Tissue sections were taken from graft hearts at the time of rejection and fixed in formalin. Tissue sections were stained with H&E and Elastin staining and the NI was determined as an average of 6 coronary artery sections per animal (b). Representative images are shown in (c). Statistical significance was determined by Mann-Whitney test, $**P < 0.01$, $n=10$. PBS-treated RCMV- historical controls included for references (light green). (d,e) NI of coronary arteries in graft hearts at POD14 was decreased in Anakinra-treated cohorts. Tissue sections were stained and the NI was scored as in (b/c). NI scores are summarized in (d). Representative images are shown in (e). Statistical significance was determined by one-way ANOVA with Tukey's correction for multiple comparisons, $*P < 0.05$, $**P < 0.01$, $n=6$. (f-h) Anti-RCMV IgG antibody responses were reduced in Anakinra treated animals. Blood was taken from transplant recipients at 2, 4, and 6 weeks post-transplant until graft rejection. Enzyme-linked immunosorbent assays against anti-RCMV IgM (f) and IgG (g) antibodies and anti-F344 cardiac tissue IgG (h) antibodies were performed on serum samples and dilution titers were calculated for each sample. Averages for each cohort at 2, 4, and 6 weeks post-transplant are shown. $n=10$. Error bars represent SEM. Statistical significance determined by Mann-Whitney test, $*P < 0.05$, $**P < 0.01$, $***P < 0.001$ vs. Vehicle-control. (i) Viral loads in tissues at rejection showed a significant decrease in the number of animals with detectable viral loads in SMG following Anakinra treatment. Tissues were harvested at time of cardiac graft rejection in RNAlater. Tissues were then homogenized in DNAzol and DNA was extracted. qPCR for RCMV viral DNA polymerase was used to quantitate RCMV genome copies in tissues. Error bars represent SEM. Statistical significance determined by fisher's exact test, $*p=0.0325$ (two-tailed). (j) Viral

loads in tissues at POD14 did not yet show significant impairment in viral loads in Anakinra-treated cohorts. Tissues were harvested as in (i). n=6.

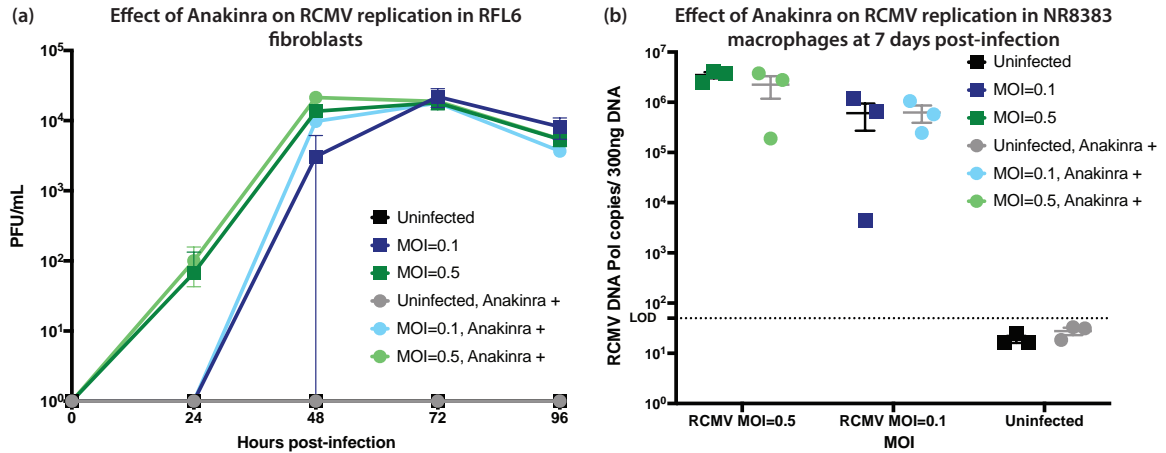


Figure 19. Anakinra does not impair viral replication in RFL6 fibroblasts or NR8383 macrophages. (a) RFL6 fibroblasts were treated with Anakinra at 10 μ g/mL or vehicle for 2 hours, and then infected in triplicate in the presence of the treatment with RCMV at an MOI=0.1 or 0.5 for 2 hours. Cells were then washed three times with PBS and fresh media containing Anakinra or vehicle was added to the cells. Supernatant samples were taken every 24 hours, starting at time 0, and were frozen at -80°C. Samples were titered over RFL6 fibroblasts. (b) NR8383 rat macrophages were treated in triplicate with Anakinra at 10 μ g/mL or vehicle for 2 hours, and then infected in the presence of treatment with RCMV at an MOI=0.1 or 0.5 for 2 hours. Cells were then washed three times with PBS and fresh media containing Anakinra or vehicle was added to the cells. At 7 dpi cells were washed 3 times in PBS and harvested in DNAzol. DNA was extracted, diluted to 60ng/ μ L and qPCR was performed for RCMV DNA polymerase. Two-way ANOVAs with Tukey's multiple comparison (RFL6 growth curve) or Sidak's multiple comparison (NR8383 viral loads) were used to test for statistically significant differences between Anakinra and PBS treated infection groups and no significant differences were found in either RFL6 growth curves or in NR8383 macrophage viral loads.

2.4 Discussion

CR is a major impediment to long-term graft and patient survival in SOT recipients. Alloimmunity, CMV infection, and IRI following transplantation are factors that contribute to acceleration of TVS. Recent work in murine kidney transplants demonstrated that IRI can initiate CMV reactivation, whereas immunosuppression promotes viral dissemination following transplantation [268], supporting the hypothesis that IRI combines with CMV-associated pathogenesis to accelerate CR. Reducing transplant-induced IRI has the potential to improve transplant survival rates related to CMV infection; however, IRI lacks specific effective therapies. To develop targeted strategies toward reducing IRI, we identified pathways that contribute to IRI in the absence of alloimmunity in syngeneic cardiac transplants. Importantly, syngeneic grafts, in the setting of CMV infection, do not undergo CR due to the lack of alloimmune responses [265]. In our current study, we introduced a 4-hour cold ischemia time to improve the clinical relevance of our cardiac transplant model. We identified biological changes associated with transplant-induced IRI that included pro-inflammatory cytokines and then utilized targeted therapeutics to enhance graft survival in the context of RCMV infection.

IRI is a multifaceted disease process involving initial injury followed by a cascade of inflammatory steps that mediate further tissue damage. The goal of this study was to identify possible inflammation signaling nodes that, when inhibited, could target the multiple downstream effects of IRI, particularly as they relate to CR. One such node is the IL-1 pathway, which plays an important role in defense against pathogens and immunopathogenic disease [271]. The IL-1 family includes IL-1 α/β , IL-18, IL-33, IL-37,

and IL-38, their receptors and downstream activated transcriptional factors that produce other inflammatory molecules. We found upregulation of IL-1 inflammatory pathway members in both PBMC and cardiac grafts that included IL-1 α , IL-1 β , IL-18, IL-33, and IL-36 β ; their cognate receptors IL-1R1, IL-1R3-6; and their downstream signaling molecules IRAK1,2,4, MyD88, and TRAF6. Interestingly, IL-1R8, an IL-1R that inhibits NF- κ B signaling, was transcriptionally down regulated. Thus, the IL-1 family is highly dysregulated following IRI. The IL-1 pathway has previously been identified as key to development of IRI [272,280,281]. For example, elevation of IL-1 α levels have previously been linked to activation of alloreactive T-cells, suggesting that IL-1 α , in addition to our data implicating IL-1 β , may be a prominent component of early allograft injury [282]. Our pathway analysis builds on previous data, but the methods outlined here could be used to identify other targetable pathways for therapy.

Natural mechanisms limit IL-1-induced immunopathogenesis and promote adaptive immunity and wound healing. Soluble IL-1R antagonists and membrane decoys have been exploited for therapeutics that target IL-1 cytokine function during rheumatoid arthritis, autoinflammatory disease, cardiovascular disease, restenosis following angioplasty, systemic sclerosis, IRI, and diabetes [280,283,284]. In our IRI model, the natural rat IL-1R antagonist (IL-1Ra) was upregulated at POD3, but this is likely too late to prevent immune-mediated damage. However, Anakinra presents a prime candidate for clinical intervention by targeting IRI early inflammatory processes. Anakinra is approved for clinical use and has a short half-life, allowing us to interrogate the impact of a single-treatment on IRI and allograft CR. Parthenolide also targets the IL-1 signaling node, and

has previously been tested as an anti-inflammatory drug in a rat myocardial reperfusion injury model [270]. Our model incorporates a CMV⁺ donor with active CMV infection of the donor tissue [285], as previous studies have shown that CMV infection accelerates CR [21], and IL-1Ra therapies have shown promise in other transplant models in the absence of CMV infection [286–288]. We targeted IRI in the setting of CMV infection in SOT, and demonstrated a reduction in accelerated cardiac graft CR. While the impact of Anakinra on chronic cardiac allograft rejection in the absence of CMV remains to be tested, Anakinra and parthenolide treatments both decreased tissue injury and graft macrophage and PMN recruitment, reducing the downstream events that promote acute and CR. Given the higher toxicity of parthenolide, Anakinra was a better therapeutic option and it improved graft survival and reduced CMV tissue viral loads at rejection. While Anakinra reduced anti-RCMV IgG responses there was no major impact on anti-donor IgG responses, suggesting that the reduction in inflammation reduced viral load rather than impacting global humoral responses. However, a remaining area to be explored is effect of Anakinra on the role of T-cell responses to viral and/or donor antigens and how this affects TVS and CR. Further work in this area would provide a better understanding of the disease mechanisms at work with and without treatment.

Anakinra solely targets the receptor for IL-1 α / β . Thus, our finding that Anakinra did not completely inhibit graft IRI or restore the timing of CR to levels observed for uninfected allografts would suggest that additional IL-1 signaling components may be involved in the tissue injury process. This theory is consistent with our observation that IL-18, IL-33, IL-36, and their receptors are highly expressed during IRI. We hypothesize that combination

therapy utilizing Anakinra and newly developed inhibitors of IL-18, IL-33, and IL-36 may have greater impact on reducing graft injury. Furthermore, graft survival may be enhanced with IL-1R antagonists, targeting early events leading to graft dysfunction, in combination with ganciclovir, to prevent CMV-driven, long-term events [278,289,290]. Future studies will focus on determining the role of Anakinra in CMV-naïve transplants as well as improving our understanding of the effect that Anakinra treatment has on T-cell-mediated immune responses during CR.

2.5 Materials and methods

Rat Cardiac Transplantation: OHSU West Campus Small Laboratory Animal Facility is AAALAC accredited and complies with USDA and HHS animal care requirements. Heterotopic syngeneic heart transplantation was performed in Lewis rats in order to characterize IRI without alloimmunity. Heterotopic allogeneic heart transplantation of F344 hearts into Lewis recipients was performed to assess the effect of treating IRI on CR. Rat donor hearts (Lewis syngeneic or F344 allogeneic) were surgically removed, placed in 4°C UW solution for 4 hours, and then transplanted [36,265] (Figure 7 and Table 1). Phosphate buffered saline (PBS) served as vehicle for Anakinra (SOBI), whereas 10% Ethanol/90% corn oil served as the parthenolide vehicle (Cayman Chemical). Donor rats for Cohorts 3, 6, and 8-10 were infected at 5 days before transplantation with RCMV Maastricht strain (1×10^5 pfu by intraperitoneal injection (i.p.)). Donor rats for Cohorts 1, 2, 4, 5 and 7 were uninfected. Animals were examined daily for overall health and CR was determined by monitoring graft heartbeat grade [265]. Blood and tissues from Cohorts 1-8 were harvested at POD3; whereas Cohorts 9-10 were harvested at POD14 or at the time of

allograft CR. Blood was separated into plasma and PBMC using lymphocyte separation media (Corning). Portions of heart tissues were: fixed for histological evaluation; snap frozen for immunohistochemistry and nucleic acid analysis; and harvested for flow cytometry.

Histological Assessment: Paraffin embedded heart tissue sections were stained with hematoxylin and eosin (H&E) and evaluated by microscopy. Lymphocytic infiltration and extent of tissue damage were quantified using a graded scale (Table 4). Paraffin embedded allograft heart tissue sections were stained with H&E and elastic van Gieson stain. TVS was calculated as the neointimal index ($NI = (\text{intima area} / \text{lumen} + \text{intima area}) \times 100$) [133,194,291].

Myocardial Injury Score	
0	No damage
1	Mild interstitial lymphocytic infiltrate and rupture of myocardial fibers
2	Moderate interstitial lymphocytic infiltrate, edema, myocardial cell swelling and necrosis
3	Severe necrosis with contraction band, neutrophil infiltrate and compressed capillaries
4	Highly severe diffused necrosis with contraction band, neutrophil infiltrate and hemorrhage

Table 4. Myocardial injury scoring system used for evaluation of cardiac graft tissue damage.

Transcriptomics: Total RNA was isolated from PBMC and homogenized graft and native hearts using Trizol. RNA deep sequencing analysis (RNASeq) was performed on 1 µg of polyA-fractionated RNA utilizing the TruSeq Stranded mRNA library prep kit (Illumina). Library was validated using Agilent DNA 1000 kit on bioanalyzer according to manufacturer's protocol. RNA libraries were sequenced by the OHSU Massively Parallel

Sequencing Shared Resource Core using their Illumina HiSeq-2500. Bioinformatics analyses and biostatistical comparisons were performed by the Bioinformatics & Biostatistics Core at Oregon National Primate Research Center. The quality of the raw sequencing data was evaluated using FastQC [292] combined with MultiQC [293] (<http://multiqc.info/>). The files were imported into ONPRC's DISCVR-Seq [294], LabKey [295] Server-based system. PRIME-Seq Trimmomatic [296] removed remaining Illumina adapters. Reads were aligned to the *Rattus_norvegicus* Rnor_6 genome in Ensembl along with its corresponding annotation, release 90. STAR [297] (v020201) aligned reads to the genome using the Two-pass mode with default parameters. STAR calculated the number of reads aligned to each gene. RNA-SeQC [298] (v1.1.8.1) ensured alignments were of sufficient quality. Samples had an average of 56M mapped reads, an average exonic rate of 76%, and an average of 15.6K genes detected (>5 raw reads) per sample. Gene-level differential expression analysis was performed in open source software R [299]. Gene-level raw counts were filtered to remove genes with extremely low counts following the published guidelines [300] normalized using the trimmed mean of M-values method (TMM) [301] and transformed to log-counts per million with associated sample-wise quality weight and observational precision weights using the Voom method [302]. Gene-wise linear models comparing the groups were employed for differential expression analyses using Limma with empirical Bayes moderation [303] and false discovery rate (FDR) adjustment [304]. Pathway analysis was performed using Qiagen's Ingenuity Pathway Analysis (IPA) software.

Pathway Analysis: IPA was used to evaluate expression data and determine predicted gene interactions. Analysis parameters excluded p-values >0.1, FDR >0.01, and log₂ fold-change values between -0.9 and 0.9, providing 7,579 (PBMC) and 7,899 (Heart) analysis ready molecules. P-values were calculated via the Fisher exact test and corrected via the Benjamini-Hochberg procedure. Significantly impacted canonical pathways were explored via IPA core analysis and path explorer to develop a map of predicted down-stream effects from genes regulated following transplantation.

RCMV Quantitative PCR: Viral genome copies in rat tissues were quantified using real-time PCR with standard cycling parameters with an RCMV DNA polymerase-specific primer and probe set: P1:CCTCACGGGCTACAACATCA; P2:GAGAGTTGACGAAGAACCGACC; Probe:VIC-CGGCTTCGATATCAAGTATCTCCTGCACC-TAMRA. Tissue DNA was extracted using DNazol (ThermoFisher Scientific 10503027) and diluted to 50ng/μL DNA. Quantitative polymerase chain reaction (qPCR) was performed using TaqMan Fast Advanced Master Mix (Invitrogen). RCMV viral DNA served as the quantification standard. Samples were analyzed using an ABI StepOne Real-Time PCR system.

Quantitative RT-PCR: Gene expression was quantified by qRT-PCR using primer and probe sets shown in Table 5. RNA (1μg total RNA for Anakinra cohorts or 5μg for Parthenolide cohorts) was isolated from approximately 20mg of rat heart tissues using Trizol (ThermoFisher Scientific) and DNase treated using TURBO DNase-free kit (Ambion). Complement DNA (cDNA) was generated using Superscript IV (Invitrogen)

and analyzed by real-time PCR. Cloned gene amplicons were used as quantification standards. qRT-PCR was performed using TaqMan Fast Advanced Master Mix. Samples were analyzed using a QuantStudio 7 Flex Real-Time PCR system and data was normalized to the gene encoding ribosomal protein L32.

Gene	Forward Primer	Reverse Primer	Probe	Dye	Quencher
CXCL6	CTGTTACACTGCCACAGCAT	CAGCGTAGCTCCGTTGCAA	TGTCCTTTCTCGGCCA	FAM	MGBNFQ
CXCL2	TGAACAAAGGCAAGGCTAACTGA	CTCTTTGATTCTGCCCGTTGA	AAGAACATGGGCTCCTG	FAM	MGBNFQ
Cinc2 α	GCACTGCACCCAGACAGAAG	CTGGGAGCTTGAGGGTTGAG	TAGCCACTCTCAAGGAT	FAM	MGBNFQ
IL-1R	GATTATGAGCCACGGAATGA	GACGTTGCAGATCAGTTGTATCG	ATGGAAGCTGACCCAGG	FAM	MGBNFQ
MMP12	GAAAGGAGCTGGCACAAATGAAG	GCCCCACAGGCAGATACCT	TCCTCGTGCTGGTGCT	FAM	MGBNFQ
SPP1	CTCACCTCCCGCATGAAGAG	TCAGACGCTGGGCAACTG	AGTCCGATGAGGCTAT	FAM	MGBNFQ
IL-6	GGAACGAAAGTCAACTCCATCTG	AAGGCAACTGGCTGGAAGTCT	ACAGCTATGAAGTTTCTC	FAM	MGBNFQ
L32	GAAGATTCAAGGCCAGATCC	GTGGACCAGAACTTCCGGA	CGGGAGTAACAAGAAAACCAAGCACATGC	VIC	TAMRA

Table 5. qRT-PCR primers and probes.

Multiplex Cytokine Assay: A 27-Plex rat cytokine assay (Millipore) was performed on POD3 serum samples and heart tissue lysates. Tissues samples weighing 0.1g were homogenized by bead-beating in cold PBS containing 1 millimolar (mM) phenylmethylsulfonyl fluoride (PMSF). Samples were centrifuged at 10,000 revolutions per minute (RPM) in a microcentrifuge at 4°C for 10 minutes. The supernatants were collected for use in the assay.

Flow Cytometry: Native and graft hearts were harvested from rats at POD3 and digested in PBS containing Collagenase D (200 units/milliliter (U/mL)) (Millipore Sigma) at 37°C for 45 minutes. Digested heart tissues were macerated and strained through 70 μ m nylon

cell strainers (Fisher). Lymphocytes were isolated by centrifugation over lymphocyte separation media (Corning). For each sample, 2×10^6 cells were stained for 20 minutes at 4°C with fluorescently labeled anti-rat antibodies directed against CD3-APC (BD Biosciences), CD4-APC-Cy7 (BioLegend), CD8-PerCP (BD Biosciences), CD161a-V450 Biotinylated (BD Biosciences), CD68-A700 (Bio-Rad), CD45rA-PE-Cy7 (Invitrogen), His48-FITC (Invitrogen), CD43-PE (BioLegend). Cells were analyzed using an LSRII flow cytometer and data were analyzed using FlowJo software (FlowJo v10.5.3).

Enzyme-linked Immunosorbent Assays (ELISA): High-binding ELISA plates (Corning 9018) were coated overnight at 4°C with RCMV-infected cellular lysates (10µg/mL) or F344 heart homogenates diluted in PBS. To assess anti-graft antibody levels, hearts from RCMV-naïve F344 rats were homogenized in 2mL/heart of cell lysis buffer (Cell Signaling Technology) containing HALT protease inhibitor (ThermoFisher). A 1/64 dilution of heart homogenate in PBS was used to coat high binding ELISA plates. Plates were blocked with 2% milk in wash buffer (0.05% Tween-PBS) for 2 hours at room temperature. Plates were washed three times with wash buffer and then incubated for 1.5 hours with 2-fold serial dilutions of plasma. After washing, the plates were incubated for 1 hour with horseradish peroxidase (HRP)-conjugated anti-rat IgG (Invitrogen) or IgM (ThermoScientific) antibodies. Detection and quantification of bound secondary antibodies was performed by adding o-phenylenediamine dihydrochloride substrate (ThermoFisher Scientific). Dilution titers were calculated based on log-log transformations of the linear portion of the dilution curve for each sample.

Stimulation of Rat PBMC by IL-1 β with and without Anakinra treatment in vitro: PBMC from a naïve lewis rat were isolated over lymphocyte separation media and plated in 24-well cell culture plates at 2.5×10^6 cells/well in Roswell Park Memorial Institute (RPMI) media (Fisher) with 10% Fetal Bovine Serum (FBS) plus penicillin, streptomycin, and glutamine additives (PSG). Cells were allowed to recover for 15 minutes at 37°C. Cells were then treated with Anakinra at 10 μ g/mL or PBS for 1 hour at 37°C. At the end of 1 hour IL-1 β or PBS was added to the cells at 50U/mL or 100U/mL and incubated at 37°C for 24 hours. Cells were washed once at 4°C in PBS, harvested in Trizol, and RNA was extracted. cDNA was prepared as described above for qRT-PCR, and qRT-PCR was performed for rat IL-6 and L32. IL-6 copies were normalized against L32 copies for each sample.

RCMV Viral Replication Analysis: NR8383 rat macrophages (ATCC) were maintained in Kaighn's modification of Ham's F-12 (F-12K) media (Fisher) with 10%FBS plus PSG. Rat fibroblast lung -6 (RFL6) fibroblasts (ATCC) were maintained in Dulbecco's modified Eagle's Medium (DMEM) (Fisher) with 5%FBS and PSG. Triplicate wells of macrophages or fibroblasts, plated in 24-well plates at 6.5×10^5 or 1×10^5 cells/well, respectively, were treated with Anakinra at 10 μ g/mL or PBS for 2 hours and then mock infected or infected with RCMV-enhanced green fluorescent protein (eGFP) [133] at multiplicity of infection (MOI)=0.1 or 0.5 (n=3). Cells were washed and cultured +/-Anakinra (10 μ g/mL) for 7 days. Supernatant samples from fibroblasts were collected at 24-hour intervals and viral loads were determined by plaque assay. Infected NR8383 macrophages were collected at 7 dpi and virus was quantified by qPCR as described above.

Viral plaque Assays: RFL6 fibroblasts were plated at confluency in 24 well plates. Serial dilutions from 10^{-1} to 10^{-6} of viral supernatants were performed in round-bottom 96 well plates. Media was aspirated from RFL6 fibroblasts and 100 μ L of each viral dilution was added per well. After a 2-hour incubation on a rocker at 37°C, 250 μ L of carboxymethyl cellulose (CMC) (0.25% low viscosity/0.25% high viscosity (Sigma) in complete DMEM) [285] was added to each well and cells were cultured at 37°C. At 7 days, cells were fixed and stained with methylene blue, and plaques were counted to determine viral titers.

Statistical Tests: A one-way Analysis of Variance (ANOVA) with Tukey's multiple comparisons was used to identify statistically significant differences in histological, qPCR, and POD14 NI data. A one-way ANOVA with Dunnett's multiple comparisons was used to analyze Luminex assay data. A two-way ANOVA with Tukey's multiple comparisons was used to analyze flow cytometry results and RCMV RFL6 growth curves. Statistical significance of RCMV NR8383 viral load data and qRT-PCR expression data was determined using two-way ANOVA with Sidak's multiple comparisons or Dunnett's multiple comparisons, respectively. Two-way ANOVA with Dunnett's multiple comparisons was used to determine statistical significance of IL-1 β stimulation compared to control for *in vitro* verification of Anakinra dosage. Mann-Whitney test was used to analyze CR survival, NI data, and antibody titers. For all tests *(p<0.05), **(p<0.01), ***(p<0.001), ****(p<0.0001). Statistical analysis of animal viral loads was determined as the number of animals with detectable versus non-detectable viral loads by Fisher's exact test.

2.6 Acknowledgments

This work was supported by a grant from the National Institutes of Health NIAID R01 AI116633. NH and IJ were supported by the OHSU Molecular Microbiology and Immunology Interactions at the Microbe/Host Interface training grant NIH 2T32 AI007472. IJ received additional support from the grant NIH F31 1F311AI145193-01. Short read sequencing assays were performed by the OHSU Massively Parallel Sequencing Shared Resource. The authors acknowledge the support of the Oregon National Primate Research Center Bioinformatics & Biostatistics Core, which is funded in part by NIH grant OD P51 OD011092.

Chapter 3 – Rat Cytomegalovirus Virion-associated proteins R131 and R129 are Necessary for Infection of Macrophages and Dendritic cells

Iris K. A. Jones¹, Nicole N. Haese¹, Philippe Gatault², Zachary J. Streblow¹, Takeshi F. Andoh^{1,3}, Michael Denton¹, Cassilyn E. Streblow¹, Kiley Bonin¹, Craig N. Kreklywich¹, Jennifer M. Burg³, Susan L. Orloff^{3,4}, Daniel N. Streblow¹

¹ *Vaccine & Gene Therapy Institute, Oregon Health & Science University, Portland OR 97239*

² *Renal Transplant Unit, 10 Boulevard Tonnellé, University Hospital of Tours, Tours 37032, France*

³ *Department of Surgery, Oregon Health & Science University, Portland, Oregon, USA*

⁴ *Department of Molecular Microbiology & Immunology, Oregon Health & Science University, Portland, Oregon, USA*

This chapter is adapted from:

Pathogens (2020), DOI: 10.3390/pathogens9110963

3.1 Abstract

CMV establishes persistent, latent infection in hosts, causing disease in immunocompromised patients, transplant recipients, and neonates. CMV infection modifies the host chemokine axis by modulating chemokine and chemokine receptor expression and by encoding putative chemokine and chemokine receptor homologues. The viral proteins have roles in cellular signaling, migration, and transformation, as well as viral dissemination, tropism, latency and reactivation. Herein, we review the contribution of CMV-encoded chemokines and chemokine receptors to these processes, and further elucidate the viral tropism role of RCMV R129 and R131. These homologues of the HCMV-encoded chemokines UL128 and UL130 are of particular interest because of their dual role as chemokines and members of the pentameric entry complex required for entry into cell types essential for viral transmission and dissemination. The contributions of UL128 and UL130 to acceleration of solid organ transplant CR are poorly understood, requiring an effective *in vivo* model system to elucidate. We demonstrate similar molecular entry requirements for R129 and R131 in rat cells as observed for HCMV, and provide evidence that R129 and R131 are part of the viral entry complex required for entry into macrophages, DC, and bone marrow cells.

3.2 Introduction

CMV is a β -herpes virus that establishes persistent latent infection in hosts, and causes severe disease in immunocompromised patients. Transplant recipients, in particular, face impacts from CMV infection if either the donor or the recipient are infected [21,22]. Although anti-viral prophylactic therapies, such as ganciclovir, are used clinically to control CMV in transplant recipients, these therapies are prone to generation of resistance

mutants and do not protect against CMV-induced acceleration of CR and development of TVS in latently infected grafts [22,36]. As such, a more thorough understanding of CMV dissemination and latency is necessary to guide development of novel therapies and vaccines candidates. CMV dissemination within the host is a complex process involving regulation of host immune cells and cell-specific entry mechanisms. In order to regulate trafficking of host immune cells to promote its dissemination, CMV uses virally encoded homologues of host chemokines and chemokine receptors. Hence, the focus of this research is to better elucidate the pathways involved in CMV viral entry into key immune cell populations that impact viral dissemination.

Chemokines (chemotactic cytokines) are a group of inducible cytokines that promote cellular migration and activation through binding to their respective GPCRs. The major chemokine groups are the CC chemokines, which include MCP-1, MIP-1 α , MIP-1 β , and RANTES; the CXC chemokines, which include IL-8, IP-10, and SDF-1 α ; the CX₃C chemokines, which includes Fractalkine; and the C chemokines which includes lymphotactin. Chemokines are generally involved in most aspects of immunity and their binding to receptors increases the cellular production of other cytokines and growth factors, and increases the expression of integrins promoting cellular adhesion to the vascular endothelia. Chemokines are present in the vascularized graft at all stages post-transplantation including, during IRI, acute rejection, CR, and during the healing processes [305]. By contrast, long-term graft acceptance has been attributed to the absence of chemokines, thus substantiating a major role for chemokines in allogeneic graft rejection and during the development of TVS [306]. Both the CC and CXC chemokines have been

detected in human and experimentally induced animal models of graft rejection (reviewed previously [305]). The CC-chemokines are produced as a result of vessel injury, which promote cellular adhesion to the endothelium, transmigration of immune cells, cellular activation and migration. Chemokine receptors are present on all classes of immune and inflammatory cells and act as barcodes to direct immune responses. Chemokine ligand binding promotes signaling through G proteins and other signaling molecules to activate a diverse set of functional responses including transcriptional activation and migration of the critical cells involved in inflammation and graft rejection.

All the members of the β -herpesviruses encode chemokine and chemokine receptor homologues [307–313]. These modify host signaling and facilitate viral dissemination via their roles in entry and recruitment of cells to the site of infection during CMV pathogenesis. A current list of the CMV-encoded chemokines and chemokine receptors are listed in Table 6 and Table 7, respectively. HCMV contains four putative GPCRs, which are encoded in the ORFs UL33, US27, US28, and UL78 [311]. RCMV and murine CMV (MCMV) only contain two putative chemokine receptor homologues R33 and R78 and M33 and M78, respectively. Interestingly, RhCMV contains 7 chemokine receptors including 5 US28 homologues, a UL33 homologue, and a UL78 homologue. In addition, the β -herpesviruses HHV-6 and HHV-7 each encode UL12 (CC) and UL51 (CC) chemokine receptors. CMVs also encode at least four chemokine homologues including UL128, UL130, UL146 (vCXCL-1), and UL147 (vCXCL-2).

Name	Known receptors	Possible homologues	Functions	Classification	References
UL128	(R129 receptors: CCR3, CCR4, CCR5, CCR7)	R129/m129	Entry, regulation of leukocyte recruitment	CC	[132–134]
UL130	Unknown	R131/m131	Entry, Macrophage recruitment, promotion of inflammation, viral dissemination	XC	[123,132,135]
UL146	CXCR1, CXCR2	No known homologues in RCMV or MCMV	Neutrophil recruitment, viral dissemination	CXC	[205,206,212]
UL147	Unknown	No known homologues in RCMV or MCMV	No known function	CXC	[212]
RCMV- vXCL1	XCR1		Dendritic Cell Recruitment	C	[212]

MCMV	CCR-2	eCK-2,	Slow viral	CC	[132,209,314]
- MCK-2		RCK-2	clearance		
RCK-3	Unknown		Unknown	CC	[123,128,132, 314]

Table 6. CMV encoded chemokines.

Name	Known ligands	Possible homologues	Function	References
US27	Unknown	RhCMV -214, -215, -216, -218, -220	No known functions	[315]
US28	CCL2, CCL3, CCL4, CCL5, CX3CL1	RhCMV -214, -215, -216, -218, -220	Immune modulation, viral entry or cell tropism, cellular migration, signaling, viral latency and reactivation	[315,316]
UL33	β -chemokine receptor; m33 ligands: mCCL5	R33/M33	CREB activation, cell migration, necessary for replication <i>in vivo</i>	[132,222,223]
UL78	Unknown	R78, M78, homologues present in all CMVs	Viral replication	[132,204]

Table 7. CMV encoded chemokine receptors.

3.2.1 Regulation of host-cell signaling and trafficking by CMV-encoded chemokine receptors

The CMV encoded chemokine-receptor homologues are multi-functional, operating to promote viral infection through several unique mechanisms. CMV encoded chemokines and chemokine receptors display signaling functions that help to regulate cellular migration and immune-cell recruitment. Importantly, CMV encodes several chemokine and chemokine-receptor homologues that recruit or direct movement of macrophages and DC, which may provide the virus with a vehicle for transmission and viral dissemination. Oral transmission of MCMV occurs through the infection of olfactory and alveolar epithelial cells. Infection of these cells then establishes infection of tissue-resident DC and macrophages [26,27]. Re-entry of these infected DC into the circulation is driven by the MCMV-encoded chemokine receptor M33. MCMV containing mutations in M33 fails to establish infection in the salivary glands following intranasal infection, although the virus is capable of readily replicating at the initial site of infection [27,28]. Additionally, M33 promotes extravasation of infected DC into salivary gland tissues, explaining the loss of viral titer in salivary glands for M33-deficient mutants [29]. Importantly, replacement of M33 with the HCMV chemokine-receptor US28 also promotes infected DC to re-enter circulation from the site of infection [29]. This function appears to be highly conserved across CMV species, as RCMV R33 mutants also fail to show viral replication in salivary glands [30]. However, in the case of R33, trafficking of virus did occur, but the virus failed to establish infection in the salivary gland tissue. R33-deficient RCMV also show reduced mortality in immunocompromised rats and delayed progression to CR in rat heart transplant recipients compared to recipients infected with WT RCMV [30,31]. Importantly,

these studies point to slight differences in the functionality of CMV-encoded chemokine receptors. However, US28 and UL33 are, notably, partially redundant in function with MCMV M33 since they correct for a loss of MCMV reactivation and viral replication in salivary glands in an M33-signaling deficient infection [32].

CMV chemokine receptors promote migration in other cell types as well. For example, US28 also promotes the migration of macrophages and vSMC in a chemokine-dependent manner [216,217]. While US28 binds multiple chemokine ligands, signaling and migration are affected by ligand specificity [217]. Specifically, US28 induced migration of vSMC is driven by CC chemokine binding and is inhibited by Fractalkine. The opposite effect is observed in macrophages, wherein US28 migration is promoted by Fractalkine [217]. Coupling to G α 12/13 G proteins is critical for vSMC migration as is signaling through Src and FAK [218,219]. Stable expression of US28 has also been shown to increase migration of HEK293 cells over HEK293 cells expressing CX₃CR1 in response to CX₃CL1. Interestingly, this increase in migration is competitively inhibited by the CC chemokines CCL2 and CCL5, but not by CCL3 [220], which would support binding of multiple chemokines by US28. M33 also drives migration of infected cells, specifically mouse vSMCs, but not fibroblasts, in a mRANTES dependent manner [222]. Similarly, RCMV R33 is necessary for migration of infected vSMCs in the development of TVS during CR of rat cardiac transplants [31]. Furthermore, US27 enhances CXCL12/CXCR4 signaling, suggesting that this protein may also have a role in monocyte recruitment and viral dissemination [199]. Interestingly, UL78 and homologues in other CMV species have not

been demonstrated to promote cellular migration, although R78 is expressed in macrophages and required for efficient infection in the spleen [204].

In addition to its role in cellular migration, US28 has been shown to be critical for HCMV latency and reactivation [156,159,160]. US28 ligand binding activity is critical for maintaining the virus in a latent state but ligand specificity is still unknown. Interestingly, the viral GPCR is also required to promote reactivation, which may be driven by the ability of US28 to promote myeloid lineage cellular differentiation [156]. US28 has also been implicated in the suppression of IL-8 secretion and the sequestering of cellular/host chemokines and exogenously expressed chemokines during CMV infection, thus regulating immune response to virally-infected cells [213]. UL33 has been shown to facilitate cell-cell spread of HCMV, and loss of UL33 reduces viral titers *in vitro* in fibroblasts; however, the precise function of UL33 in this process is still unclear [317]. Additionally, UL78 is required for a step between virus binding and entry phases in epithelial cells. However, UL78 does not appear to be necessary for viral entry in fibroblasts [203]. Prior work has also demonstrated that an RCMV virus expressing a null mutant form of R78 displayed lower replication efficiency *in vitro* and a lower lethality *in vivo* [204]. These studies suggest that CMV-encoded chemokine-receptor homologues function to increase viral dissemination via multiple potential mechanisms.

3.2.2 CMV-encoded chemokines regulate cellular migration

HCMV UL128 and UL146 have been shown to exhibit chemotactic activity. UL128 exhibits β -chemokine like functions in its ability to recruit PBMC [134]. In contrast, Straschewski *et al.* demonstrated that UL128 inhibits host-chemokine driven motility of

monocytes and can cause monocyte paralysis [131]. This highlights the fact that even the viral chemokines are responsive to cell-type specific differences. UL146 has been shown to activate CXCR1, and, with a lower affinity, CXCR2, which may promote migration of neutrophils to the site of infection [205,206]. Furthermore, Heo *et al.* showed that there is a hyper-variability associated with UL146, which correlates with high functional selectivity in the recruitment and activation of neutrophils to infected tissues. UL146 induces Ca²⁺ flux and integrin expression on target cells, upon binding to host CXCR1 [207].

Studies in rats and mice have demonstrated that CMV chemokine homologues contribute to immune cell migration to the site of infections, promoting further spread of the virus, in a manner similar to that seen with HCMV-encoded chemokines. Kaptein *et al.* showed that the putative UL130 homologue, R131, is involved in the recruitment of macrophages to the site of RCMV infection in rats [123]. Although lack of R131 does not seem to affect replication of RCMV in fibroblasts, null mutations in R131 correlate with a lack of a high titer of infection in the salivary glands of immunocompromised rats and a significant decrease in footpad swelling upon inoculation with RCMV [123]. It is worth noting that R131 has 41.1% sequence similarity with HCMV UL130 [135] and is predicted to be a CC-chemokine, rather than a XC-chemokine, and therefore, its chemokine functionality more closely resembles HCMV UL128. R129, the RCMV homologue of UL128, binds rat chemokine receptors CCR3, CCR4, CCR5, and CCR7 [133]. Additionally, migration of lymphocytes and naïve CD4⁺ T-cells were induced by r129 in *in vitro* transwell-migration assays [133]. RCMV containing an R129 mutation that lacks chemokine activity also failed

to accelerate TVS and CR in a rat heart transplant model, indicating that the chemokine promotes CMV transplant disease through either its role as a chemokine or through participation in the pentamer receptor complex [133]. While deletion of the viral chemokines in RhCMV strain 68.1 allows the virus to act as a potent viral vaccine vector [238], the role that these chemokines play in this process (chemotaxis vs. entry) has yet to be fully elucidated.

MCMV encodes a fusion product, MCK-2, from the MCMV genes m129 and m131, which are homologues of RCMV R129 and R131. MCK-2 also regulates the inflammatory response by inducing inflammation [104]. In a study by Fleming *et al.*, Δ m131/129 MCMV *in vivo* failed to produce high-titers in salivary glands and had improved clearance rates during acute MCMV infection from the spleen and liver in an NK cell- and T-cell-dependent manner. This finding suggests that m131/129 has pro-inflammatory properties and is necessary for immune evasion by regulating NK and T-cells [122]. Further work in mice confirmed that MCK-2 enhances recruitment of myeloid progenitors to the site of infection, which may aid in viral dissemination [208]. However, whether the effect of viral dissemination is limited to MCK-2's ability to promote cellular migration or involves other mechanisms has yet to be determined. Additional *in vivo* studies suggested that MCK-2 mediates recruitment of pro-inflammatory monocytes via CCR2 in order to impair CD8⁺ T-cell anti-viral responses, thereby slowing viral clearance [209]. Together these studies depict a clear relationship between the murine CMV encoded 131/129 chemokine homologues and the promotion of pro-inflammatory conditions to promote viral dissemination. However, it has recently been shown that MCMV self-regulates MCK-2

expression during infection via the virally-encoded M48 deubiquitinating enzyme, in order to regulate excessive inflammation associated with viral infection [210]. In a guinea pig model of CMV infection, deletion of gp1, a gpCMV homologue of the host chemokine MIP, allowed generation of an immunogenic attenuated vaccine strain of gpCMV that reduced viremia in non-pregnant guinea pigs and reduced DNAemia in the third trimester of pregnancy in guinea pig dams [211]. Intriguingly, work by Geyer *et al.* identified a novel XC chemokine (vXCL1) in the English strain of RCMV. vXCL1 recruits XCR1⁺ CD4⁻ DC in rats. Geyer *et al.* hypothesized that this allowed MuHV8 to undermine the traditional cytotoxic immune response [212]. In aggregate, regulation of leukocyte recruitment by CMV-encoded chemokines appears to promote viral dissemination and to inhibit viral clearance.

3.2.3 Role for CMV-encoded chemokines in viral entry

As mentioned above, CMV encoded chemokines play a role in viral entry through participation in the viral pentameric entry complex. Expression of different viral entry complexes determine cell tropism and can impact viral dissemination. HCMV encodes approximately 19 structural glycoproteins that are incorporated into the mature virion. However, not all of these glycoproteins participate in the viral entry process [53]. Of those that do, gB, gH, gL, gM, gN, gO, UL128, UL130, and UL131A are the most well characterized for their roles in virion assembly and virus entry. These glycoproteins form several identified complexes including gB, gM/gN, gH/gL/gO (trimer), gH/UL116, and gH/gL/UL128/UL130/UL131A (pentamer) [57,58].

The gM/gN complex has roles in both viral entry and viral assembly, and mutants are either non-viable or have severe replication deficiencies [53,59–61]. gB forms a functional homotrimer, which interacts with integrins and permits entry via pH-independent membrane fusion [62,63,65]. gH/gL form the basis for two HCMV entry complexes, the trimer (gH/gL/gO) and pentamer (gH/gL/UL128/UL130/UL131A), that also function with gB to promote membrane fusion [69,74,318]. The trimer is essential for entry into fibroblasts, epithelial cells, and endothelial cells. The abundance of trimer incorporated into the virion correlates with infection levels in both fibroblasts and epithelial cells [76,85–87]. Trimer associated entry into fibroblasts involves binding of PDGFR α , followed by recruitment of gB [88–90]. The pentameric entry complex is unique among these glycoprotein complexes in that it contains the viral chemokines, UL128 and UL130, as well as UL131A. Pentamer-associated entry occurs in a pH-dependent manner [95]. The pentamer is not necessary for entry into fibroblasts, but is necessary for entry into epithelial cells, endothelial cells, DC, and monocytes [91–93,96,97]. Two receptors have recently been identified for the pentamer – Neuropilin-2 in epithelial and endothelial cells and OR14I1 in epithelial cells [94,99].

While the pentameric entry complexes have been studied for HCMV, little is known about the role of RCMV-encoded chemokines in viral entry. The RCMV 129 and 131 proteins are predicted to be putative homologues to the HCMV pentamer components UL128 and UL130 because they share chemotactic functions and positional homology with pentamer components from other CMV species [123,132,133]. In this report, we investigate the role that R129 and R131 play in viral entry and demonstrate that while the C' terminal domains

(non-chemokine domain) are required for incorporation into RCMV particles, the R131 CC-domain is critical for mediating entry, suggesting a potential role in receptor binding of the R131 chemokine domain.

3.3 Results

3.3.1 C'terminal truncations of R131 and R129 fail to incorporate into RCMV particles

HCMV entry complex components are incorporated into the viral particle in order to facilitate viral dissemination. In order to monitor viral protein incorporation of R129 and R131, we tagged each of these proteins with the 11 amino acid component (HiBiT) of the split NanoLuc protein-Lumit. The large portion can be added in trans solution- or membrane-based assays to reconstitute the enzyme and activate luminescence. We have previously quantified the levels of R131 and R129 HiBiT incorporation into virus particles, and demonstrated that virion incorporated R131 and R129 are trypsin sensitive, suggesting that both R131 and R129 are incorporated into the viral envelope [319]. However, the effect of further structural mutations and deletions on incorporation of R131 and R129 require additional study.

The HCMV homologues of R131 and R129, UL130 and UL128, have two unique domains including an N'terminal chemokine fold and a C'terminal region that interacts with other components of the pentamer entry complex. Charged clusters in UL128 and UL130 mediate incorporation of the proteins into viral particles and their mutation alters entry phenotypes in human endothelial cells [320,321]. Structural data on the HCMV pentamer

from Chandramouli *et al* and phenotypic data on entry mutants from Schuessler *et al* demonstrate that mutations in the $\alpha 2$ α -helix and β -sheets $\beta 4$, 5, and 6 of UL128 are involved in interactions between UL128 and UL130. Mutation of the HSLTR sequence immediately preceding $\alpha 2$ or the EADGR sequence between $\beta 4$ and $\beta 5$ of UL128 result in severe entry impairments. Similarly, mutation of the UL128 KKHKR sequence following $\alpha 3$ and preceding Cys¹⁶², which interacts with gL, results in impaired entry into endothelial cells. In UL130, His¹⁵⁰ in $\alpha 4$ allows for proper folding of UL130 and association with UL131A. Additionally, $\beta 4$, and $\beta 5$ interact with UL128 and UL131A and deletion of the DGTR sequence between the β -sheets and the HVFRD sequence partially contained in $\beta 5$ result in severe entry impairments. His²⁰⁹ in the disordered C' terminal region of UL130 interacts with UL128 and Tyr¹¹³ in $\alpha 2$ of UL130 interacts with UL131A. There are charged residue clusters in both R131 and R129 that show homology to these charged regions of UL130 and UL128, respectively. To determine if loss of these regions altered incorporation of R131 and R129 into viral particles or viral tropism, truncation mutants were constructed by bacterial artificial chromosome (BAC) recombineering that excluded the acidic clusters and putative entry domains of the proteins and added an in-frame HiBiT tag to the C' terminus of the proteins (Figure 20, Δ CT HiBiT). These truncations exclude predicted homologous regions in R129 corresponding to the EADGR sequence, $\beta 5$, $\beta 6$, KKHKR sequence, and disordered region containing Cys¹⁶² of UL128; or in R131 corresponding to $\alpha 4$ containing His¹⁵⁰, $\beta 4$, $\beta 5$, the DGTR sequence, the HVFRD sequence, and the conserved His²⁰⁹ residue of UL130. To determine whether the loss of the CC-chemokine fold is necessary for virion incorporation and/or modulates cell tropism we also constructed an

HCMV, MCMV and gpCMV express their pentameric entry complex proteins with late viral gene expression kinetics [125–128]. Previously, we demonstrated that RCMV R129 was also expressed with late viral expression kinetics and expression was sensitive to foscarnet, an antiviral that targets the viral polymerase and prevents late gene expression [133]. In order to characterize R131 protein expression, we performed western blots to detect the R131 HiBiT fusion protein in infected fibroblasts. R131 protein was detected by 24 hpi and accumulated up to 48 hpi (Figure 21a). Treatment with 0.5 mM foscarnet blocked R131 HiBiT expression at 48 hpi, suggesting the protein is expressed with late viral gene expression kinetics (Figure 21b). Northern blots and polymerase chain reaction (PCR) for R131 transcripts with RNA from infected RFL6 fibroblasts harvested at 8, 24, or 48 hpi also confirmed late viral gene expression at 48 hpi; and again, the expression was sensitive to treatment with foscarnet (Figure 21c,d). Northern blot analysis demonstrated that the viral gene is expressed as a single transcript at the predicted size of 700 nucleotides (Figure 21c).

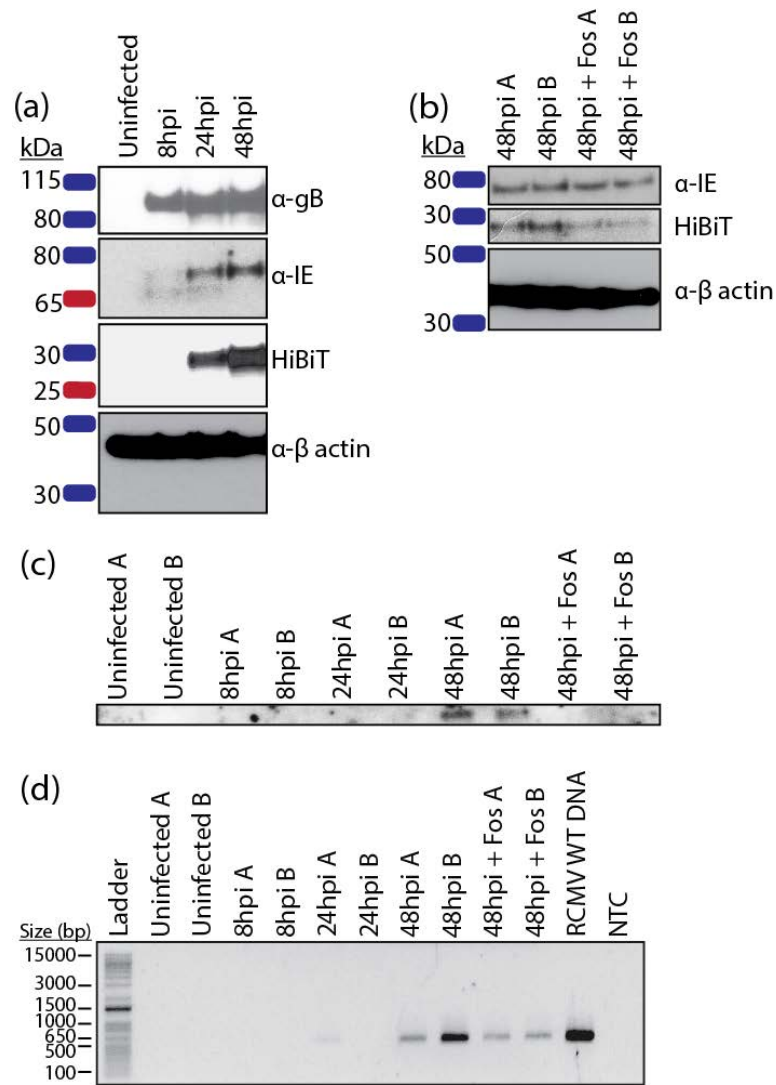


Figure 21. R131 is expressed with late viral gene expression kinetics. (a) Rat fibroblasts were infected with RCMV R131-HiBiT at a MOI=1. Samples were washed with PBS and harvested in cell lysis buffer at 8, 24, and 48 hpi. Western blots for gB, RCMV IE, β -actin, and HiBiT (R131) were performed. (b) Rat fibroblasts were infected with RCMV R131-HiBiT at a MOI=1 with or without foscarnet (0.5mM) and samples were harvested in cell lysis buffer at 48hpi. (c) Duplicate wells (A and B) of rat fibroblasts were infected in duplicate with WT RCMV at an MOI=1 with or without foscarnet (0.5mM) and harvested in Trizol at 8, 24, and 48 hpi. RNA was isolated and northern blots were performed probing for R131. (d) cDNA was made from RNA samples from (c) and PCR for R131 was performed. RCMV WT DNA was used as a positive control, water was used as the no template control (NTC). Size of select ladder bands are listed in base pairs (bp).

Next, we sought to confirm expression of the HiBiT-tagged proteins R129 and R131 for the recombinant RCMV viruses containing mutations in the C' terminal domain and CC motif. Rat fibroblasts were infected and lysates and supernatants were collected at the time of maximum cytopathic effect. Cell lysates and virus particles purified from supernatants of the infected cells were analyzed by western blotting for HiBiT. This analysis confirmed the presence of R129 and R131 HiBiT tagged viruses in the cell lysates and verified the deletion of the C' terminal domains (Figure 22a, upper panel). Interestingly, while the tagged proteins were detected for all of the viral mutants in the cell lysates, the C' terminal truncation mutants failed to be detected in the viral particle preparations (Figure 22a, lower panel). If R131 and R129 are members of the pentamer complex, we would expect that they should co-precipitate. Consequently, to determine whether R129 and R131 co-precipitate in samples of virus particles, we utilized a novel technique of HiBiT-based precipitation [322]. For this approach a Halo-tag reagent was used to couple LgBiT to magnetic beads that can be used to capture HiBiT tagged R131. R129 was detected in the pull-downs using our previously generated polyclonal mouse antiserum that recognizes R129 [133]. Antibodies directed against gB were used to normalize levels of WT, R131 HiBiT and R129 HiBiT RCMV preparations. Equal quantities of gB-containing viral particles were lysed and incubated with LgBiT-HaloTag protein and immunoprecipitation was performed using HaloTag beads. Using this method both R131 and R129 could be pulled-down and detected using HiBiT (Figure 22b). Importantly, despite the lower dynamic range of detection seen with the anti-R129 antibody, R129 was immunoprecipitated in both the R129 HiBiT control and the R131 HiBiT, demonstrating that R129 co-precipitated with R131. gB was not detected in the precipitated samples for

WT, R131 HiBiT, or R129 HiBiT and R129 did not bind to the HaloTag beads in the WT (negative control) samples. Since R131 and R129 were incorporated into viral particles and associated with each other, we next asked how many molecules of R131 and R129 mutants were incorporated into each virion relative to viral genomes. To address this subject, we performed the HiBiT lytic quantification assay on 3 different volumes of virus preparations (7.5 μ L, 3.75 μ L, and 1.875 μ L) of each virus in triplicate. We developed a standard curve of a known number of molecules of HiBiT control protein available from Promega (Figure 22c). For each mutant, molecules of HiBiT-tagged protein per microliter of virus preparation was determined. Genome copies per μ L of each virus preparation were then determined by qPCR using primers directed against the RCMV DNA polymerase gene (R54) (Figure 22d). Molecules of HiBiT-tagged protein per genome were calculated. R131 and R129 were incorporated at 2.6×10^4 and 1.0×10^5 copies per viral genome, respectively. Importantly, our quantification supported our earlier findings that the Δ CT mutants of R131 and R129 were not incorporated into the virion (Figure 22e) indicating that, similar to UL128 and UL130, the charged cluster rich C-terminal domain is necessary for incorporation into the pentamer complex [320,321]. Interestingly, both the R131 C36A and R129_(short) structural mutants are incorporated at slightly lower levels than the R131 and R129 WT proteins.

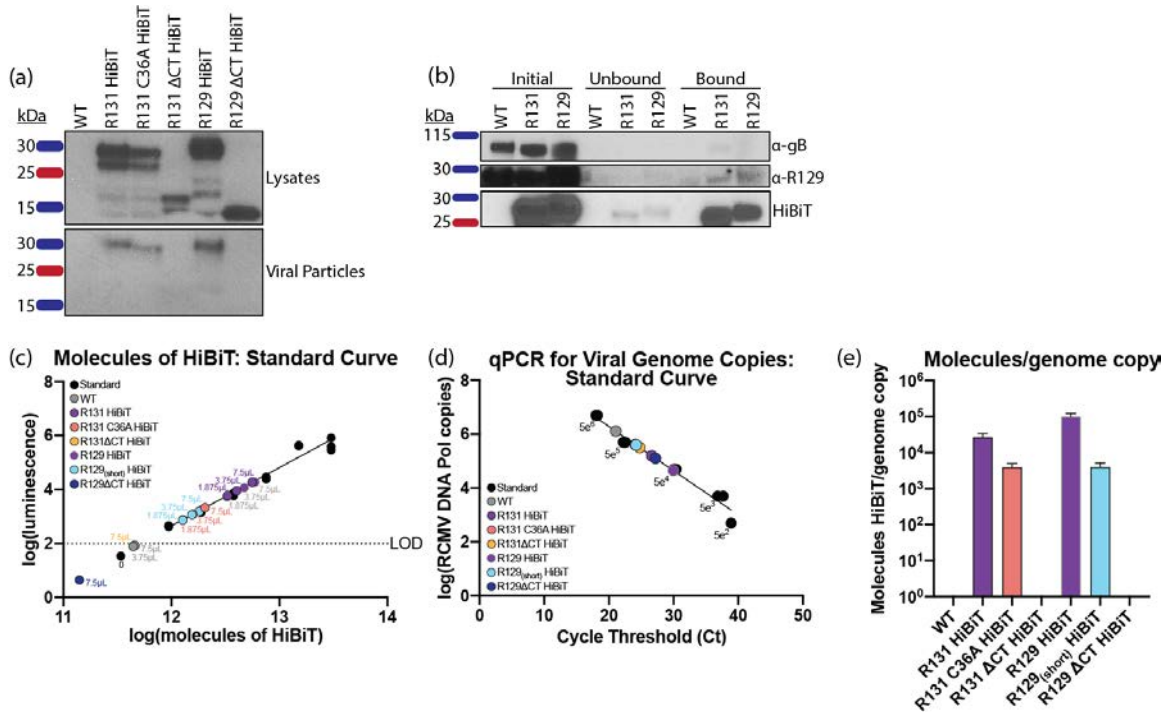


Figure 22. R131 and R129 C-terminal regions are required for viral incorporation. (a) Viral incorporation of R129 and R131 was assessed for wild type RCMV and viral mutants containing R129 and R131 HiBiT tags. The viruses were grown in rat fibroblasts. At the time of maximum cytopathic effect, supernatants were harvested and cellular debris was removed by centrifugation. Viral particles were then pelleted by ultracentrifugation over a 10% sorbitol gradient, and the resuspended virus pellet was additionally purified by banding over a discontinuous histodenz gradient. The banded virus was collected by ultracentrifugation over a 10% sorbitol gradient. Purified viral particles were resuspended in PBS and equivalent quantities of viral particles were determined by blotting for gB. Lysates of rat fibroblasts infected with RCMV HiBiT-tagged mutants were harvested in cell lysis buffer with protease inhibitors. Equal quantities of protein, as determined by BCA assay, were loaded on SDS-Page gels and detected by HiBiT blot with LgBiT. HiBiT tagged R129 and R131 was detected in infected cell lysates (upper panel) for all viruses including mutants. While WT HiBiT tagged R129 and R131 as well as the R131 C36A mutant were present in viral particles, the C-terminal deletion mutants were excluded from the purified viruses indicating that they were not incorporated (lower panel). (b) Viral particles were prepared as described in (a) for WT RCMV and the R129 and R131 HiBiT tagged viruses. The samples were normalized to amount of gB using western blot (initial sample). Equal quantities of gB-containing viral particles were subjected to pull downs utilizing

LgBiT-Halo Tag protein bound to Halo-Tag magnetic beads. The unbound fractions and bead bound fractions were analyzed by western blotting for gB, R129, and HiBiT. (c-e) C-terminal deletions of R131 and R129 are not incorporated into viral particles. (c) Three different volumes of each virus preparation (7.5 μ L, 3.75 μ L, 1.875 μ L) were assayed in triplicate against a standard curve by HiBiT lytic detection assay. Molecules of HiBiT per μ L of virus preparation was determined using a commercially available standard HiBiT tagged protein. (d) Viral DNA was extracted from 12.5 μ L of each virus preparation and DNA was diluted 1:1000 and analyzed in triplicate by qPCR using primers and probe directed against the RCMV DNA polymerase. A standard curve of known concentration RCMV DNA was used to determine viral genome copies in each of the samples. (e) Molecules of HiBiT over viral genome copies in each sample was compared. Data from (c) and (d) were normalized per μ L of the initial virus preparations.

3.3.2 R131 and R129 are required for entry into bone marrow cells, dendritic cells, and macrophages

Other CMV pentamer complex mutants exhibit varying impacts on cellular entry and tropism, raising the question of which cell types require the RCMV pentamer complex for entry. A panel of RCMV viral mutants was generated using BAC recombineering, including an R131 2xSTOP, R131 C36A, R131 Δ CT, R129 2xSTOP, R129 Δ CT, and a double mutant R131 2xSTOP/ R129 2xSTOP (Figure 20, Pentamer mutants). In order to determine the role of R131 and R129 in cellular entry this panel of mutants was used. The R131 2xSTOP and R129 2xSTOP mutants allow for determination of the impact of complete loss of each of these proteins on cellular entry. Comparing these mutants to the R131 2xSTOP/R129 2xSTOP mutant identifies redundancy in the functions of R129 and R131 with regard to viral entry. Finally, the R131 Δ CT, R131 C36A, and R129 Δ CT are expected to exhibit inappropriate protein structure which are predicted to impair protein-protein interactions. Notably, viral incorporation data indicate that the C36A R131 mutant

protein is still incorporated into the viral particle, albeit at lower levels than WT, whereas R131 Δ CT and R129 Δ CT are not likewise incorporated (Figure 22a,e). Multistep growth curves were used to determine whether any of the viral mutations affected replication in rat fibroblasts relative to wild type virus. All of the viral mutants demonstrated normal replication kinetics in fibroblasts, suggesting no replication defect generated by the R131 or R129 mutations (Figure 23a). CMV pentamer complexes dictate cell-type specific entry. In order to identify the cell types in which R129 and R131 are required for cellular entry, we performed an immunofluorescence-based assay that quantifies the percentage of cells expressing the viral IE protein relative to total cell number at 20 hpi. WT RCMV and RCMV R131 and R129 viral mutants were used to infect rat fibroblasts, vSMC, epithelial cells, bone marrow, DC, and macrophages. R131 and R129 mutants show significantly increased entry into fibroblasts compared to WT, suggesting improved entry for these mutants (Figure 23b). WT RCMV infected 53.6% of fibroblasts in this assay. Similarly, entry into vSMC was not significantly impacted by mutations in either R131 or R129, with WT infecting 82.0% of all cells (Figure 23c). All R131 and R129 mutants were substantially lower in entry into bone marrow cells, DC, and macrophages, where WT infected 6.1%, 19.5%, and 34.9% of cells, respectively (Figure 23e-g). Additionally, the R131 Δ CT and R129 Δ CT mutants exhibited impaired entry into epithelial cells, and entry of the R131 C36A mutant was reduced, although not significantly (Figure 23d). In epithelial cells, WT infected 36.3% of cells. Since none of the 2xSTOP mutants exhibited impaired entry into epithelial cells, this suggests that R131 and R129 structural mutants disrupt cellular entry mediated by other entry complexes by competing with gH during viral assembly. Correspondingly, complete loss of the pentamer complex in deletion of

R131 or R129 appears to be void of an impact in viral entry via this pathway. Further work will be necessary to determine if competition for gH results in a significant impact on competition between viral entry complexes.

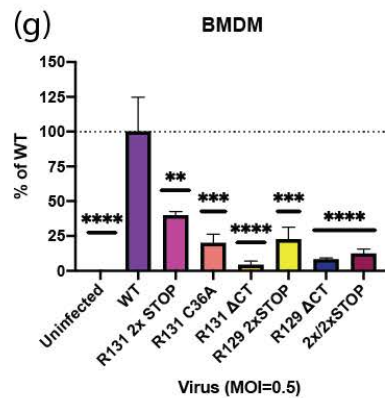
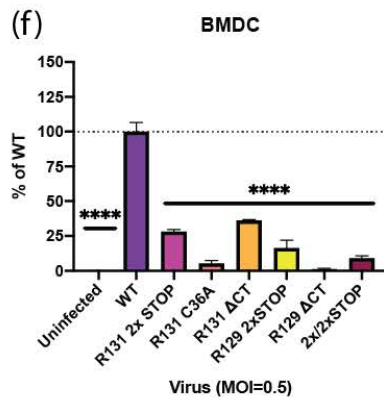
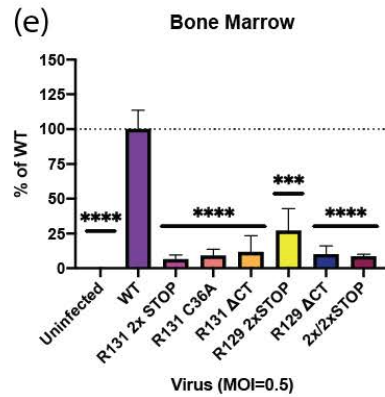
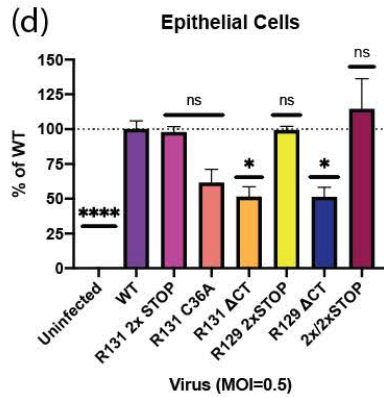
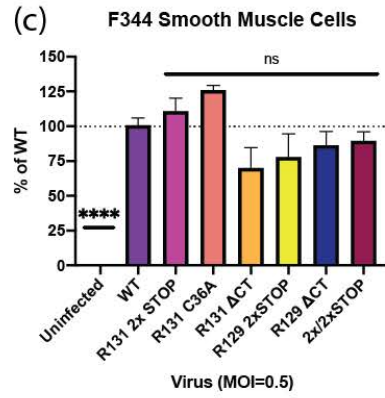
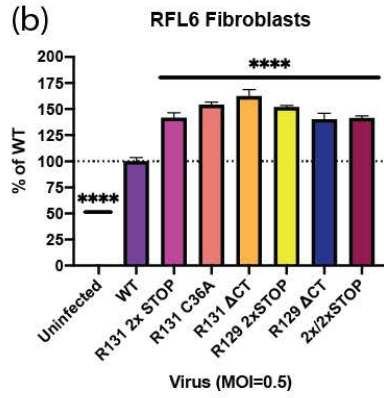
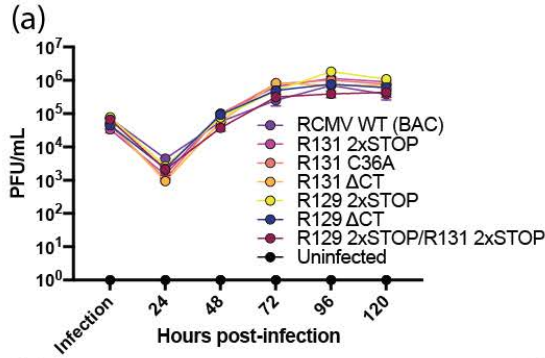


Figure 23. R131 and R129 are essential for entry into bone marrow, DC, and macrophages, but not fibroblasts or vSMC. (a) Multistep growth curves were performed in triplicate wells by infecting rat fibroblasts with RCMV WT, R131 mutants, or R129 mutants at an MOI=0.1. At 2 hpi, cells were washed three times with PBS and fresh medium was added to each well. Supernatant samples were collected at the time of infection and every 24 hpi until 120 hpi. The supernatants were titered by limiting dilution plaque assays in 24 well plates containing confluent monolayers of rat fibroblasts. The plates were fixed and stained after 7 days and viral titers were calculated. (b-g) For entry assays, 96 well plates containing rat fibroblasts (b), vSMC (c), SMG-derived epithelial cells (d), bone marrow cells (e), bone-marrow derived DC (f) and macrophages (g) were infected with RCMV WT, R131 mutants, or R129 mutants at a MOI=0.5 in triplicate wells. At 20 hpi cells were fixed and stained with an anti-RCMV IE polyclonal antibody and counterstained with DAPI in order to count cell nuclei. Percent infection was determined by counting the number of IE positive cells divided by the number of cell nuclei. Percent of infection relative to WT virus was determined for each cell type. Data are representative of two independent experiments, each performed in triplicate. Statistical significance compared to infection levels with WT RCMV was determined for each viral mutant by one-way ANOVA using Dunnett's correction for multiple comparisons. ns=not significant, * $p<0.05$, ** $p<0.01$, *** $p<0.001$, **** $p<0.0001$.

3.4 Discussion

In addition to modulating host chemokine and chemokine receptor expression, CMV also encodes many of its own viral associated factors. While viral chemokines and chemokine receptors are thought to have had their function and evolution derived from host gene capture events, their functions have been modified and enhanced in order to increase fitness and promulgation of the virus. These modifications include altered signaling patterns, enhanced chemokine binding breadth, and facilitate incorporation into cellular entry complexes. The overlapping roles of CMV-encoded chemokines and chemokine receptors in CMV cellular entry and virus transmission further complicates the study of this sophisticated pathogen. This virus expresses chemokines and associated receptors that play roles in infection of epithelial cells and monocytes, leading to enhanced virus persistence and dissemination, as well as downstream damage to infected tissues and transplanted organs. Prior animal and *in vitro* studies with MCMV have demonstrated that epithelial cells and monocytes are crucial for appropriate viral dissemination and subsequent downstream sequelae [26–28,323]. Given that the HCMV pentamer is required for entry into these cell types, further investigation of this complex in functional disease models is warranted.

The HCMV pentamer consists of the gH/gL scaffold, UL128, UL130, and UL131A [71]. The functions and components of the pentamer are not strictly conserved across CMV species, making it difficult to establish *in vivo* models of CMV cellular entry. Importantly both Rhesus and Guinea pig CMV entry complexes seem to mirror those of HCMV closely [101–103]; however, MCMV shows less functional homology [104,105]. Variants of the

gM/gN, pentameric, and trimeric complexes have been identified in RhCMV, gpCMV and MCMV [101,102,105–111]. The RhCMV pentamer consists of gH/gL/Rh157.5/Rh157.4/Rh157.6 and is required for entry into epithelial cells, but not fibroblasts [101,112,113]. Similarly, the gpCMV pentamer consists of gH/gL/GP129/GP131/GP133 and is essential for entry into monocytes and endothelial cells, but not fibroblasts [102,103,114–116]. Additionally, gpCMV pentamer mutants show impaired entry into epithelial cells [114]. The predicted homologous complex in MCMV contains three known members, gH, gL, and MCK-2, where MCK-2 is a fusion product of the m129 and m131 genes [105]. The MCMV gH/gL/MCK-2 complex is not required for entry into fibroblasts, but is required for entry into macrophages [105,120]. In contrast to the HCMV pentamer, gH/gL/MCK-2 is not required for entry into epithelial cells, and mutants show an increased capacity to infect epithelial cells [105]. Although RCMV homologues of gH, gL, gB, gO, and gM have been identified [132], the pentamer components remain to be experimentally determined. The data we present supports the predicted role of R131 and R129 in formation of a functionally homologous pentamer cellular entry complex, which results in significant impacts on infected hosts with respect to RCMV's pathogenesis and other associated pathologic effects.

Our studies show that R131 and R129 were both incorporated into viral particles at near equivalent molecular levels. Importantly, charged cluster domains within UL130 and UL128 are involved in appropriate formation of the HCMV pentamer, and mutation of these clusters results in impaired entry into endothelial cells [320,321]. Prediction of similar charged clusters in R131 and R129 resulted in recognition of acidic clusters

following the predicted chemokine N-loop domains of the proteins (Figure 20). Deletion of the acidic cluster regions present in the C' terminal domains of R129 and R131 resulted in failure of the proteins to be incorporated into viral particles. In contrast, partial removal of the C' terminal region of an R129 mutant that retains the two acidic clusters (R129_(short)) shows only a minor decrease in viral incorporation. This data demonstrates that the C' terminal region is required for virion incorporation. Interestingly, a mutant of the CC-motif of R131 (C36A) was incorporated into virions but failed to enter macrophages and dendritic cells, indicating that a functional R131 is required for entry. This may indicate that either gross structural changes of either R131 or the complex as a whole exist for this mutant and/or that the chemokine domain of R131 is necessary for entry receptor binding. NMR and cryo-EM studies aimed at determining structural changes resulting from the mutations made here would provide further insight into the role of the chemokine fold in complex formation and binding.

In order to determine if R131 and R129 associate in a complex, we performed HiBiT/HaloTag Co-precipitation experiments from purified viral particles. R129 successfully precipitated with R131, supporting formation of a complex containing R131 and R129. Importantly, gB did not associate with either R129 or R131 in pull-downs. Although R131 and R129 were incorporated into the virion, a role for both proteins in entry remained to be demonstrated. The panel of R131 and R129 mutants exhibited normal growth kinetics in fibroblasts, as seen with other CMV pentamer mutants. R131 and R129 mutants also exhibited slightly above normal entry in fibroblasts and vSMC. Entry was significantly reduced for all R131 and R129 mutants in DC, macrophages, and bone

marrow cells, which is consistent with pentamer mutants in other CMV species (Table 8). Previous studies have identified CD34⁺ progenitor cells in bone marrow as a site of CMV latency [324,325]. Further work will be necessary to determine if pentamer mutants show impaired abilities to establish latency. Of particular interest are the inconsistencies in epithelial cell entry requirements across CMV species. Although HCMV and RhCMV require the pentamer for epithelial cell entry, gpCMV and RCMV exhibit partial impairment to entry, while MCMV shows enhanced entry into epithelial cells following mutation of MCK-2 [101–105,112–116,120]. Our data highlight an interesting difference in complete loss mutants of R131 and R129 and misfolded or C' terminal deletion mutants, where the complete loss mutants enter epithelial cells at similar levels to WT but the C' terminal mutants show impaired entry. These findings suggest the potential for multiple entry mechanisms in epithelial cells that may be impaired by competition for gH/gL scaffolds in the case of structural mutants of R131 and R129. Such multiple mechanisms for epithelial cell entry might explain the differences seen in epithelial cell entry across different pentamer mutations and CMV species. Importantly, whether a fifth member of the RCMV pentamer exists remains to be determined. Positional homology with the gpCMV genome would suggest R133 as a putative fifth member; however, this remains to be confirmed for RCMV.

	Putative pentamer components	Fibroblasts	Macrophages & Monocytes	Endothelial Cells	Epithelial Cells
HCMV	gH/gL/UL128/ UL130/UL131A	Not required	Required	Required	Required
RhCMV	gH/gL/Rh157.5/ Rh157.4/Rh157.6	Not required	?	Required	Required
gpCMV	gH/gL/GP129/ GP131/GP133	Not required	Required	Required	Impaired entry
MCMV	gH/gL/MCK-2	Not required	Required	?	Not required
RCMV	gH/gL/R129/R131/ ?	Not required	Required	?	Impaired entry

Table 8. CMV pentameric entry complex determinants.

CMV encoded chemokines and chemokine receptors mediate multiple functions important for viral transmission and pathogenesis. Here, we demonstrated similar molecular entry requirements for R131 and R129 in rat cells as observed for HCMV, supporting the use of the RCMV rat cardiac transplant model to study solid organ transplant rejection. Our data demonstrate a role for R131 and R129 as part of the viral entry complex required for entry into macrophages, DC, and bone marrow cells, depicting the evolution of viral chemokines to facilitate viral dissemination. These data advance comparisons between pentamer viral entry complexes amongst the common CMV model systems (Table 8).

3.5 Materials and methods

Generation and Maintenance of cell cultures: The RFL6 rat fibroblast cell line (ATCC, CCL-192) were maintained in DMEM (ThermoFisher) supplemented with 5% FBS and 100U Penicillin/ 100µg Streptomycin/ 292µg/mL Glutamine (Fisher) at 37°C in 5% CO₂.

Generation of SMG-derived epithelial cells: Epithelial cells were isolated from F344 rat SMG using a protocol adapted from Beucler, M & Miller, W. 2019 [326]. Briefly, rat SMG were minced and digested in Dispase & Collagenase III (Sigma) at 37°C for 3 hours. The resulting cell suspension was filtered through a 70 micrometer (µm) filter and cells were centrifuged at 216 x g for 5 minutes. Red blood cells were lysed and cells were washed in PBS. Cells were cultured in epithelial cell growth media (Cell Biologics) on a basement membrane matrix in 6-well plates. Salisphere growth was monitored, and at 5 days the basement membrane matrix was digested with dispase/collagenase III solution. The cells were dissociated with trypsin and single cells were plated in epithelial cell growth media on tissue culture treated plates for viral entry assays.

Generation of F344 bone marrow derived macrophages: Macrophages were differentiated from bone marrow collected from the femurs of naïve F344 rats. Bone marrow was collected by flushing bones with RPMI media (ThermoFisher). The resulting cell suspension was filtered through a 70µm filter and cells were pelleted at 1500RPM for 10 minutes. Red blood cells were lysed and cells were washed once in RPMI. Cells were plated in 10% FBS RPMI with 25ng/mL M-CSF (R&D Systems) at 1x10⁶cells/mL. Cells

were allowed to differentiate for 7 days before being scraped from plates and plated for viral entry assays.

Generation of F344 bone marrow derived dendritic cells: DC were differentiated from bone marrow as reported previously [327]. Briefly, filtered bone marrow cells were plated in 10% FBS RPMI with 5ng/mL IL4 (R&D Systems) and 10ng/mL GMCSF (R&D Systems) at 1×10^6 cells/mL. Cells were allowed to differentiate for 7 days before being scraped from plates and plated for viral entry assays.

Generation of F344 vascular smooth muscle cells: vSMC cells were isolated from F344 rat aorta as previously described [31]. Briefly, a F344 rat aorta was minced in DMEM containing 10% FBS plus PSG (DMEM-10) and plated in 6-well dishes. The vSMCs vacated the tissue pieces and adhered to the tissue culture dish. Cells were expanded in DMEM-10 culture medium. Cells were stained with an anti-SMC actin antibody to verify purity of the culture.

RCMV Bacterial Artificial Chromosome: The RCMV Maastricht strain genome was captured as a BAC containing enhanced eGFP using homologous recombination by replacing ORFs r144-r146 with a BAC cassette [133,319]. A two-step recombination protocol was used to create all viral mutants. The 2xSTOP mutants were created by insertion of 2 STOP codons into the N' terminus of the appropriate ORF. Viruses containing in frame fusions with the HiBiT tag (a small component of the split Nanoluciferase complex [322]) were constructed by insertion of the 11 amino acid tag at the C' terminus

of the protein or as indicated in Figure 20. Following rescue and expansion of RCMV, virus preparations were aliquoted and stored at -80°C. Viral manipulations were confirmed by sequencing and HiBiT-tag expression was verified by western blotting. Viruses were titered by limiting dilution plaque assay as described below.

Isolation of purified viral particles: RCMV viruses were expanded on RFL6 fibroblasts. At the time of maximum cytopathic effect, supernatants were harvested and clarified by ultracentrifugation (46676.5 x g) followed by filtration through a 70µm filter. Virus was then pelleted over a 10% sorbitol cushion, resuspended in Tris-sodium chloride-ethylenediaminetetraacetic acid (TNE) buffer (50mM Tris [pH 7.4], 100mM NaCl, 10mM EDTA), banded via density gradient ultracentrifugation over a discontinuous 10-50% Histodenz gradient, and the banded virus was removed from the gradient. The virus fraction was then resuspended in PBS and pelleted over a 10% Sorbitol cushion. Pelleted virus was resuspended in a minimal volume of PBS, aliquoted, and stored at -80°C until use.

Plaque Assays: Viral supernatants and stocks were quantified by making serial dilutions ranging from 10⁻¹ to 10⁻⁶. Confluent monolayers of RFL6 cells in 24-well plates were incubated with the viral dilutions for 2 hours on a rocker at 37°C. After 2 hpi, 250µL of CMC diluted in culture medium was added to each well and cells were placed in a 37°C incubator. At 7 dpi the cells were fixed with 3.7% formalin in PBS (ThermoFisher) and stained with methylene blue. The viral plaques were counted to determine viral titers.

RCMV multi-step viral growth curve: RCMV growth was assessed by multistep growth analysis in fibroblasts. Cells were plated at 1.5×10^5 cells/well in 6-well plates and allowed to adhere overnight. Cells were infected at an MOI equal to 0.1 with RCMV WT, RCMV R131 and R129 mutants, or left uninfected as a control. At 2 hpi, cells were washed 3 times with PBS to remove unbound virus and fresh DMEM-10 was added to the cells. At 24-hour intervals beginning with 0 hpi, 100 μ L samples of supernatant were taken. Plaque assays were performed on supernatants to quantify virus growth over the time-course. Infections were performed in biological triplicates. Statistical differences were determined by two-way ANOVA with Tukey's correction for multiple comparisons.

Antibodies: Rabbit anti-RCMV-IE polyclonal antibody, mouse anti-R129 polyclonal antibodies, and rat anti-RCMV gB monoclonal antibody were previously described [133,263,328]. All primary antibodies were used at a dilution of 1:1,000 overnight at 4°C. HRP-conjugated secondary antibodies (TrueBlot Rabbit anti-Rabbit; TrueBlot Mouse anti-Mouse; Southern Biotech anti-Rat) were used at 1:10,000 dilution overnight at 4°C with blocking in 5% Bovine Serum Albumin (BSA) in 0.1% Tween-20 in tris buffered saline TBST. An HRP-conjugated anti- β actin antibody was used at a dilution of 1:10,000 with blocking in 5% BSA-TBST as a loading control for western blots.

Protein detection by western blotting: RFL6 cells were plated in 6-well dishes at 5×10^5 cells/well and infected with RCMV at an MOI=1 or left uninfected as a control. At 48 hpi cell lysates were harvested in cell lysate buffer (Cell Signaling Technologies) with 1x HALT (ThermoFisher Scientific) and clarified by centrifugation at 9,167 x g for 10 minutes

at 4°C. Virus particles were prepared as described above. Cell lysates and viral particles were combined 1:1 with NuPage SDS running buffer (ThermoFisher) + 2% β -Mercaptoethanol (BME) and boiled for 7 minutes, then centrifuged briefly to pellet debris. Proteins were separated on sodium dodecyl sulfate -polyacrylamide gel electrophoresis (SDS-PAGE) BOLT gels at 165V for 40 minutes and transferred to a polyvinylidene fluoride (PVDF) membrane (Millipore) using a semi-dry transfer system at 25V for 25 minutes. The membrane was dried overnight and then blocked with 5% BSA in TBST and proteins were detected with anti-IE, anti-gB, and anti-glyceraldehyde 3-phosphate dehydrogenase (GAPDH) antibodies. The membrane was detected by autoradiography with chemiluminescent solution (ThermoFisher, West Pico Plus Solution). For the detection of HiBiT tagged proteins, blots were washed for 1 minute in TBST, and placed in HiBiT detection buffer with LgBiT protein (Promega) at a 1:200 dilution and rocked at room temperature for 1 hour. NanoBiT substrate (1:500) was then added to the solution and the blot was rocked at room temperature for 5 minutes. Luminescent signal was detected by autoradiography.

HiBiT lytic detection system: Samples of viral or cellular lysates (25 μ L) were combined with 25 μ L of HiBiT lytic detection mix (1x buffer, 1:100 LgBiT, 1:50 substrate; Promega) in a black-walled 96-well plate and rocked in the dark at room temperature for 10 minutes. Luminescence of samples was determined using a Synergy HTX multi-mode microplate BioTek plate reader with a gain of 135.

HiBiT Co-precipitation: Equal quantities of isolated viral particle preparations, normalized to gB, were incubated for 15 minutes at 4°C in 1mL 1x cell lysis buffer (Cell Signaling) without protease inhibitors to lyse the viral particles. An untreated aliquot was kept for determining input levels of protein by western blotting. Following incubation samples were vortexed thoroughly and spun at 9,167 x g at 4°C for 10 minutes. Clarified lysates were transferred to clean 1.5mL tubes and HaloTag-LgBiT protein (ProMega) was added at 1:100. Samples were incubated with occasional mixing for 1 hour at 4°C. Prior to addition Magne HaloTag beads (ProMega) were washed 4 times in 0.05% NP-40 in TBS with 1mL/wash. The HaloTag-LgBiT viral lysate mixture was added to the HaloTag beads (40µL/sample) and rocked overnight at 4°C. Following incubation, supernatants were removed and kept as the unbound fraction. Beads were washed 4 times in 0.05% NP-40 in TBS with 1mL/wash. Excess wash buffer was removed and 40µL of 2x NuPage loading buffer with 2% BME was added to the beads. Initial samples as well as bound and unbound fractions were mixed 1:1 with 4x NuPage loading buffer with 2% BME. All samples were boiled for 10 minutes. Samples were then loaded onto 4-12% BOLT SDS-Page gels and transferred via a semi-dry transfer system to PVDF membranes. Western blots were performed as described above for gB, R129, and HiBiT.

Viral DNA detection: Equal volumes of isolated viral particle preparations were diluted to 200µL with PBS. DNA was extracted with the GeneJet Viral DNA and RNA purification kit (Thermo Scientific) and resuspended in 50µL of eluent. Serial 10-fold dilutions of extracted DNA were prepared with molecular grade water; and qPCR was performed using primers and probe that target the RCMV DNA polymerase gene (R54): forward primer:

CCTCACGGGCTACAACATCA; reverse primer:
GAGAGTTGACGAAGAACCGACC; probe:
CGGCTTCGATATCAAGTATCTCCTGCACC. qPCR was performed using TaqMan Fast Advanced Master Mix (ThermoFisher 4444963). RCMV viral DNA at known genome concentrations served as the quantification standard. Samples were analyzed using a QuantStudio 7 Flex Real-Time PCR system.

Northern blot analysis: RFL6 cells were plated in 6-well dishes at 5×10^5 cells/well and infected in duplicate with RCMV at an MOI=1 or left uninfected as a control. Additional duplicates were treated with Foscarnet at 0.5mM and infected with RCMV at an MOI of 1. At 8, 24, and 48 hpi cell lysates were harvested in TRIzol. RNA was extracted from infected cells using the Trizol method. Briefly, cells were washed and then incubated with 1mL TRIzol; and then the sample was collected. The Trizol samples were loaded onto phase-lock tubes with 200 μ L of 2-bromo-3-chloropropane and mixed by inversion. Tubes were centrifuged for 5 minutes at 20,000 x g. Aqueous phase was transferred to a fresh Eppendorf tube with 500 μ L isopropanol and 2 μ L linear acrylamide. Samples were incubated at room temperature for 10 minutes and centrifuged at 4°C for 30 minutes at 20,000 x g to pellet nucleic acids. Pellets were washed twice in 75% ethanol and resuspended in molecular-biology grade water. RNA samples were treated with TURBO DNase (Invitrogen) using the manufacturer's protocol and then analyzed by spectrophotometry. Equal quantities of RNA were loaded onto a 1% agarose/formaldehyde gel and electrophoresed. RNA was transferred to positively charged nylon transfer membranes (GE Healthcare) and then subjected to UV-crosslinking. The membrane was

pre-hybridized in DIG easy Hyb (Roche). The blots were hybridized with a probe specific for R131 generated using a PCR DIG probe labeling kit (Roche) in DIG easy Hyb. The blots were washed with low stringency wash (2xSSC with 0.05% SDS) followed by high stringency wash (0.1xSSC with 0.1% SDS). Anti-DIG antibody was detected after exposure to autoradiography film using intensifying screens.

Detection of R131 transcripts by PCR: RNA samples were generated as described above for Northern blot analysis and cDNA was generated. 800ng of RNA was DNase treated using TURBO DNase-free kit (Ambion) and cDNA was generated using Superscript IV (Invitrogen). 0.5µL of cDNA was used for a PCR reaction with 25 cycles and an extension time of 1 minute with Platinum HiFi PCR master mix (ThermoFisher), using 1µL of each primer at 10 micromolar (µM). R131 primers were P1: 5'-GCTTTGGGTATCGTTCGAATG-3' and P2: 5'-AGAATAGCCGTTTCGGAATAG-3'. Ladder used was 1kb plus protein ladder (ThermoFisher). RCMV DNA extracted as described above for viral DNA detection was used as a positive control and PCR-grade water was used for the no template control.

Viral entry assays: Cells were plated at 2×10^4 (RFL6), 4×10^4 (vSMC) and 5×10^4 cells/well (DC, Bone Marrow, Macrophages), 1×10^4 cells/well (Epithelial cells) and allowed to recover overnight. Cells were infected with RCMV WT or mutants in triplicate wells at a MOI=0.5. At 20 hpi cells were fixed with 3.7% paraformaldehyde (PFA), permeabilized with 0.15% Triton X-100, and stained with anti-IE (1:250). After washing the cells were incubated with an anti-Rabbit secondary conjugated to AlexaFluor 594 (1:1000) and

counterstained with 4',6'-diamidino-2-phenylindole (DAPI). Cells were imaged using an EVOS scanning scope at 10x magnification. Total cells per field of view were counted based on DAPI staining of nuclei, with average number of cells per well counted shown in Table 9, and RCMV positive cells were determined via anti-IE staining. The percentage of positive cells was determined for each field of view and all samples were normalized against WT infection for the specific cell type. Statistical significance was determined by one-way ANOVA against WT with Dunnett's multiple comparisons. *p<0.05, **p<0.01, ***p<0.001, ****p<0.0001.

	RFL6	vSMC	Epithelial cells	Bone Marrow	Dendritic cells	Macrophages
Uninfected	806.3	550.0	395.3	151.3	586.7	77.7
WT	801.0	524.3	429.3	270.3	528.3	78.0
R131 2xSTOP	614.0	457.0	411.0	154.3	560.7	163.7
R131 C36A	804.3	12.3	434.7	269.7	747.7	88.7
R131 ΔCT	781.0	645.0	466.7	123.7	563.0	63.3
R129 2xSTOP	813.7	14.3	392.7	55.0	676.3	241.7
R129 ΔCT	735.3	468.7	394.3	153.7	671.3	87.7
2x/2x STOP	839.0	403.7	424.3	203.3	601.3	228.0

Table 9. Average number of cells per well counted for RCMV entry assays.

3.6 Acknowledgments

This research was funded by grants from the National Institutes of Health NIAID R01 AI116633 and AI127335. IKAJ was supported by the OHSU Molecular Microbiology and Immunology Interactions at the Microbe/Host Interface training grant NIH 2T32 AI007472

and NIH F31 1F311AI145193-01. NNH was supported by the OHSU Molecular Microbiology and Immunology Interactions at the Microbe/Host Interface training grant NIH 2T32 AI007472.

Chapter 4 – Rat and Human Cytomegalovirus ORF116 Encodes a Virion Envelope Glycoprotein Required for Infectivity

Iris K. A. Jones^{1*}, Philippe Gatault^{2*}, Christine Meyer^{1*}, Craig N. Kreklywich¹, Timothy Alexander¹, Patricia P. Smith¹, Michael Denton¹, Josh Powell¹, Susan L. Orloff³, and Daniel N. Streblow¹

¹ *Vaccine & Gene Therapy Institute, Oregon Health & Science University, Portland OR 97239*

² *Renal Transplant Unit, 10 Boulevard Tonnellé, University Hospital of Tours, France*

³ *Department of Surgery, Oregon Health & Science University, Portland OR 97239*

**Co-first authors*

This chapter is adapted from:

A submission to Elsevier Virology (Sept. 2020)

4.1 Abstract

Herpesviruses encode multiple glycoproteins required for different stages of viral attachment, fusion, and envelopment. The protein encoded by the HCMV ORF UL116 forms a stable complex with gH that is incorporated into virions. However, the function of this complex remains unknown. Herein, we characterize R116, the RCMV putative homologue of UL116. Two R116 transcripts were identified in fibroblasts with three proteins expressed with molecular weights of 42, 58, and 82 kiloDaltons (kDa). R116 is N-glycosylated, expressed with late viral gene kinetics, and is incorporated into the virion envelope. RCMV lacking R116 failed to result in productive infection of fibroblasts and siRNA knockdown of R116 substantially reduced RCMV infectivity. Complementation *in trans* of an R116-deficient virus restored ability of the virus to infect fibroblasts. Finally, UL116 knockdown also decreased HCMV infectivity indicating that R116 and UL116 both contribute to viral infectivity.

4.2 Introduction

HCMV is ubiquitous in the human population, with primary infections resulting in life-long infection. Although HCMV is generally mild or asymptomatic in immunocompetent individuals, immunocompromised patients suffer severe acute disease and *in utero* infection can result in permanent neurological injuries [329]. In addition, HCMV replication within transplanted tissues promotes CR and affects patient and graft survival despite use of prophylactic anti-CMV strategies [330–333]. Therefore, the development of an effective HCMV vaccine remains a high-priority [334]. Previous vaccine candidates have targeted CMV envelope glycoproteins with varying efficacy [335–338].

CMVs encode approximately 19 structural glycoproteins that are incorporated into the mature virion. However, not all of these glycoproteins directly participate in the viral entry process [53]. gB, gH, gL, gM, gN, gO, UL128, UL130, and UL131A are the most well characterized for their roles in virion assembly and the virus entry process. These glycoproteins form several identified complexes (gB homotrimers, gM/gN, gH/gL/gO, and gH/gL/UL128/UL130/UL131A) that promote entry through either pH-independent entry by macropinocytosis or membrane fusion, or pH-dependent entry via endocytosis or macropinocytosis. Many cellular receptors have been proposed as having a role in these HCMV entry processes, but further work remains to be done to detail the mechanisms through which they promote entry [57,58].

The HCMV gB complex is a functional trimer that mediates viral membrane fusion with the host membrane [62,63]. This glycoprotein complex has also been implicated in binding of PDGFR α and several integrins to help facilitate entry [64–66]. However, no additional evidence has supported these interactions to date. The glycoproteins gN and gM form the most abundant glycoprotein complex on the virion surface [53]. The precise role of the gM/gN complex is not yet known; however, the complex has been identified as binding heparan sulfate proteoglycans, suggesting a role in the initial tethering step [59]. Interestingly, viral mutants containing a gM C' terminal deletion result in unstable gM proteins and fail to produce viable virus, and similarly mutations in the structural domains of gM generate replication-deficient virus [61]. C' terminal deletion mutants of gN are also

replication-deficient and fail to be enveloped, suggesting a further role for the gM/gN complex in viral assembly [60].

The gH and gL glycoproteins form a scaffold for the two known HCMV entry complexes: the gH/gL/gO heterotrimer and the pentameric complex consisting of gH/gL/UL128/UL130/UL131A [57,70,73,74]. These two complexes compete for the same binding region on the gH/gL scaffold [74]. The levels of trimer and pentamer incorporated into viral particles are influenced by HCMV UL148 [75]. Disruption of UL148 leads to a loss of mature trimer and promotes infection of epithelial cells, whereas rescue of UL148 expression decreases levels of the pentamer and decreases infection of epithelial cells. The trimeric gH/gL/gO complex is essential for entry into fibroblasts via binding of PDGFR α and for entry into epithelial cells [85,87,89,90,339]. However, the precise role of trimer in entry into epithelial cells and endothelial cells is unclear, as PDGFR α is not highly expressed on these cell types and viruses lacking pentamer have impaired entry efficiency into these cells [89,91–93]. In addition to being necessary for entry into endothelial and epithelial cells, the pentamer is also essential for entry into DC and monocytes [96,98]. The Integrin/Src/Paxillin signaling pathway is activated in pentamer associated entry processes [98]. Furthermore, Neuropilin-2 and OR14I1 were recently identified as cellular receptors for the pentamer [94,99].

An additional gH complex has been recently shown to exist that contains the viral glycoprotein UL116. UL116 is incorporated into the HCMV viral envelope complexed with gH [72]; however, the function of this complex and its influence on viral infectivity

remain unknown. Proteomics analysis also indicated that the MCMV homologue, M116, was present in MCMV particle preparations [55]. To better define the role of UL116, we described the role of a putative homologue of UL116 in RCMV, and we have previously reported that the R116 gene is highly expressed in many different rat tissues following infection with RCMV [247]. In the present study, we investigated R116 expression, virion association and requirement for entry. We demonstrate that R116 is a virion-associated glycoprotein that is required for efficient viral infection of fibroblasts, and trans-complementation of R116 restored infectivity. Similarly, we also demonstrate here that HCMV UL116 is required for efficient production of infectious HCMV.

4.3 Results

4.3.1 R116 *in vitro* and *in vivo* expression profiles

R116 transcription kinetics were determined by Northern blot analysis using a double stranded DNA probe to identify all transcripts sharing the R116 sequence. Two transcripts, measuring 1kb and 3kb in length, were detectable at 48 hpi, with a faint band detected at 24 hpi. R116 mRNA expression was blocked by treatment with the viral DNA synthesis inhibitor foscarnet, suggesting that R116 is expressed with late viral gene expression kinetics (Figure 24a). Using a cDNA library generated from RCMV infected fibroblasts harvested at 48 hpi, we observed that the 3 kb transcript contained R116, R115 (gL), and R114, but that the 1 kb transcript contained only R116 sequences. A truncated form of R116 (880 base pairs (bp)) was additionally identified at 24 hpi, corresponding to the shifted northern bands observed at 24 hpi. Analysis of these three R116 transcripts revealed a common splice event such that 84 base pairs are removed from 355 to 436 bp of the gene

(Figure 24e). A recombinant R116 protein based on the mid-sized transcript and encoding amino acid residues 19-222 of the protein, excluding the predicted signal peptide (residues 1-18), was used to generate a rabbit polyclonal anti-R116 antibody. The predicted molecular weight of R116 is 42 kDa; however, four different molecular weight R116 protein species were detected under denaturing conditions with this polyclonal serum (Figure 24b). The lowest molecular weight band was detected by 24 hpi corresponding to the small transcript, and expression of the low molecular weight version was unaltered by foscarnet treatment at 48 hpi. In contrast, the larger R116 isoforms (42, 58, and 82 kDa) were expressed with late viral expression kinetics, as their expression was first detectable at 48 hpi and was sensitive to foscarnet. Interestingly, western blot analysis on solubilized salivary gland tissue from mock-infected and RCMV-infected rats at 28 dpi revealed that only the two higher molecular weight species of R116 were detected in salivary gland lysates (Figure 24c). The 82 kDa R116 band was the most abundant *in vivo*, whereas the 58 kDa band was the most abundant *in vitro*. The presence of R116 in the salivary glands was confirmed by immunofluorescence staining of frozen sections from rats infected with RCMV-GFP at 21 dpi (Figure 24d).

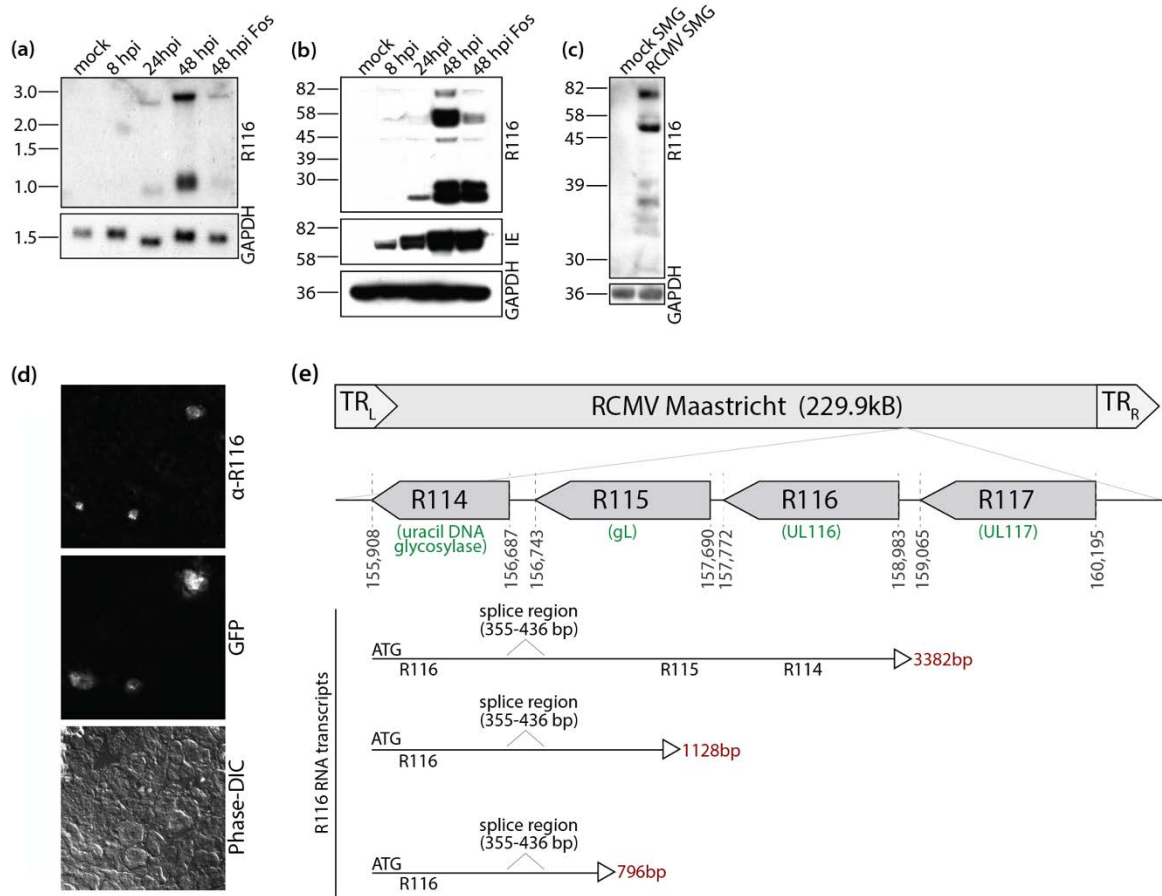


Figure 24. *R116* expression profiles differ between *in vitro* and *in vivo* infections. (a) *R116* is a spliced message expressed on two viral transcripts with late viral gene expression kinetics. Rat fibroblasts were mock infected or infected with RCMV (MOI=1) and harvested at 8, 24, and 48 hpi. One infected cell sample was treated with foscarnet (100 μ g/ml) and harvested at 48 hpi. RNA was separated by electrophoresis utilizing a 1% formaldehyde agarose gel. RNA was transferred to nitrocellulose membranes and probed for *R116*. The blot was then stripped and re-probed for *GAPDH*. The Northern blots were visualized by autoradiography. (b) *R116* protein is expressed with early and late viral kinetics *in vitro*. Rat RFL6 fibroblasts were mock infected or infected with RCMV (MOI=1) and harvested at 8, 24, and 48 hpi in Laemmli's sample buffer. An additional infected cell sample was treated with foscarnet (100 μ g/ml) upon infection and harvested at 48 hpi. The blot was probed with antibodies directed against the RCMV proteins *R116* and immediate early proteins 1 and 2 (IE1&2) as well as *GAPDH*. (c) Only high molecular weight *R116* proteins are expressed in the salivary gland of RCMV infected rats. Salivary glands were harvested from RCMV infected rats at 28 dpi. Salivary glands from uninfected rats served as a control. The salivary

glands were homogenized in RIPA buffer, analyzed by SDS-PAGE and probed using the anti-R116 polyclonal antibody. Equal loading was confirmed by staining for the cellular protein GAPDH. Western blots were visualized by autoradiography. (d) R116 protein expression is limited to glandular infected cells. Salivary glands were harvested from rats infected with RCMV-GFP RCMV at 21 dpi. Embedded frozen tissues were cut and sections were fixed with 2% PFA, washed and stained with antibodies directed against R116. Infected cells were detected by GFP expression. Deconvolution microscopy was used to visualize the stained cells. Mag=60X. (e) The RCMV R116 gene is expressed as three transcript variants with the largest containing transcripts for R115 (gL) and R114. A short transcript corresponding to the low molecular weight protein identified by western blots in (b) is shown.

4.3.2 RCMV R116 localizes to the virion assembly compartment

The cellular localization of R116 was identified using immunofluorescence microscopy by co-staining RCMV-infected RFL6 fibroblasts (48 hpi) for R116 and either the ER marker KDEL, the TGN marker TGN-38, or the lysosomal marker LAMP-1. R116 protein localized to the TGN, but not within the ER or lysosomes in infected fibroblasts (Figure 25a). In order to chase R116 to its natural final compartment, cells infected for 48 hours were treated with cycloheximide and fixed and stained at 0, 1, 2, or 4 hours post treatment. Virion-associated glycoprotein gB translocates from the surface into the assembly compartment within 4-6 hours (Figure 25b). While R116 does not relocate to the same extent as gB, by 6 hours a portion of the cellular R116 protein localizes with gB to a perinuclear site, reminiscent of the virion assembly compartment.

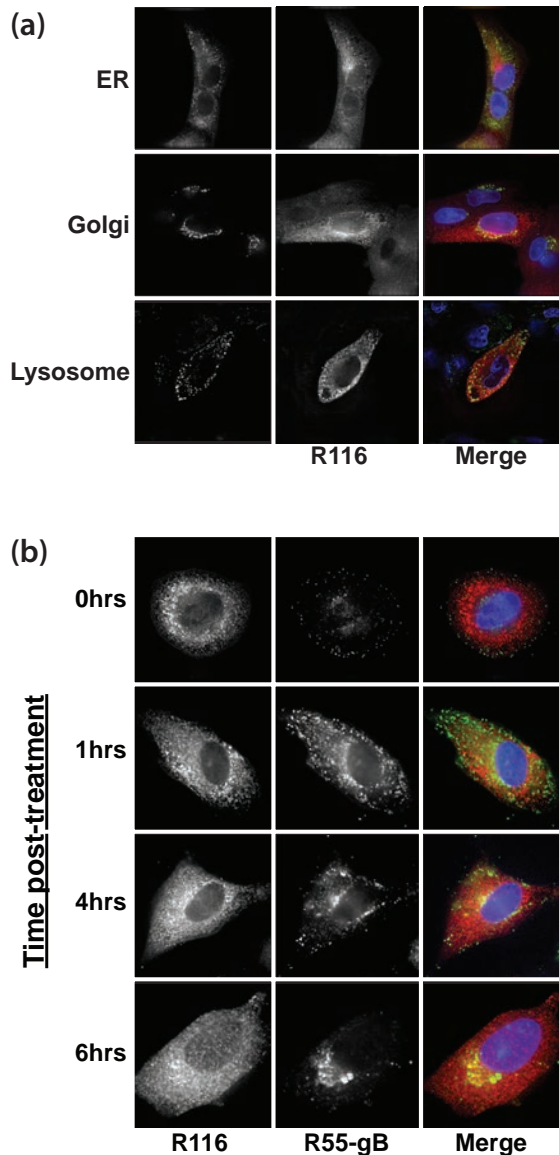


Figure 25. R116 localizes with the trans-Golgi network marker TGN-38 and the viral glycoprotein gB. Rat fibroblasts were infected with RCMV (MOI=1). (a) At 48 hpi the cells were fixed with 2% PFA diluted in PBS. The fixed cells were stained for R116 (red) and antibodies to the cellular ER, TGN or lysosomal compartments using antibodies directed against KDEL, LAMP-1 or TGN-38 (green), and DAPI (blue). (b) To confirm the cellular localization of R116 (red) in relationship to the viral glycoprotein gB (green), RCMV infected fibroblasts were fixed in 2% PFA at 0, 1, 2, 4, and 6 hours post treatment with Cycloheximide (100 μ g/ml) that was initiated at 48 hpi. Deconvolution microscopy was used to visualize the stained cells. Mag=60x.

4.3.3 RCMV R116 is a virion associated glycoprotein

Since R116 localized to the virus assembly compartment, it was possible that R116 was incorporated into RCMV particles. Western blot analysis of gradient purified virions indicated that the high molecular weight species of R116 are preferentially enriched in RCMV virions, whereas the lowest molecular weight species was excluded from the virions (Figure 26a). RCMV IE and GAPDH are present in infected cell lysates but not

incorporated into virions, and were used as controls. To determine whether R116 was incorporated into the virion as part of the viral envelope, aliquots of gradient purified RCMV virions were treated with either 2% NP40 or PBS and centrifuged to separate the virion envelope from the capsid/tegument fraction (Figure 26b). The pellet and supernatant fractions were analyzed by western blot with anti-R116 and anti-gB antibodies. Similar to the viral glycoprotein gB, R116 protein was present in the pellet fraction of the PBS-treated virus preparation and in the supernatant fraction when treated with NP40 (Figure 26c). This finding suggests that R116 is part of the viral envelope. In addition, R116 in gradient purified virions was sensitive to trypsin degradation indicating that R116 was present on the surface of the viral particle (Figure 26c).

Examination of the R116 amino acid sequence indicates that the protein contains three predicted N-glycosylation sites. Virion associated R116 and gB were treated with endoglycosidase H (Endo H) and Peptide N Glycosidase F (PNGase F) to trim off sugar moieties. Endo H removes high mannose and some hybrid types of N-linked carbohydrates, whereas PNGase F cleaves all N-linked carbohydrates without regard to type. Similar to gB, both enzymes reduced the molecular weight of R116, from the 82kDa and 58 kDa bands to 42 kDa (Figure 26d). The predicted size of R116 without glycosylation is 42 kDa. However, PNGase F had a greater effect than Endo H, suggesting that R116 is N-linked glycosylated with a mixture of high mannose or hybrid and complex glycans.

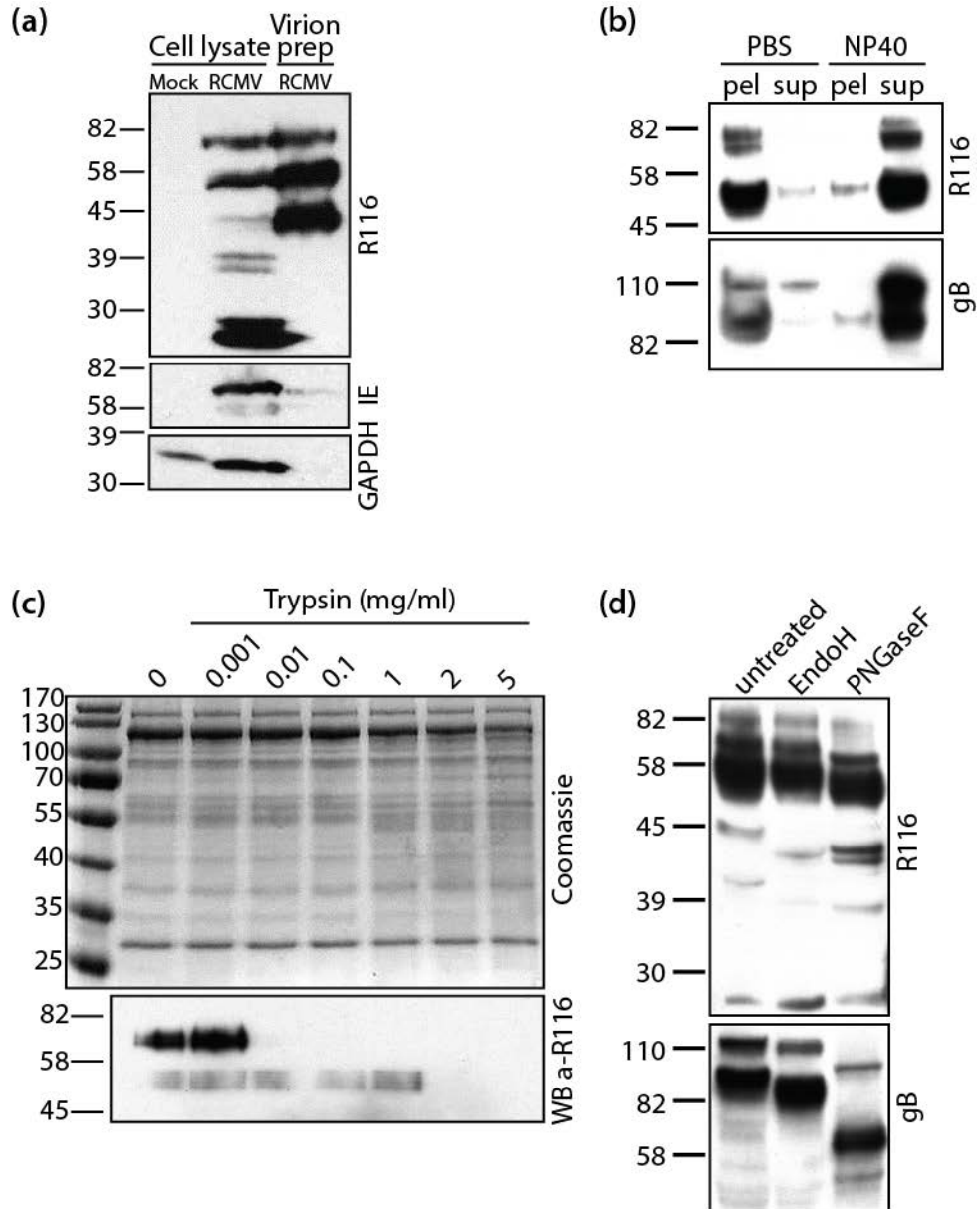


Figure 26. R116 is a virion surface envelope glycoprotein. RCMV virus particles were purified over a discontinuous 10-to-50% Nycodenz gradient and then resuspended and pelleted through a 10% sorbitol cushion. (a) The RCMV virion preparation, infected fibroblast lysate, and lysate from mock-infected fibroblasts were analyzed by SDS-PAGE for R116, IE1&2 and GAPDH by Western blot. (b) RCMV virion preparation was split into two samples. One sample was treated with 1% NP-40 and the control sample with an equal volume of PBS. Both samples were pelleted at 100,000 x g for 30 minutes. The pellet and supernatant

fractions were analyzed by SDS-PAGE and probed for RCMV R116 and gB. (c) RCMV virion preparations was subjected to increasing concentrations of trypsin (0-5 μ g) for 15 minutes at 37°C. The samples were analyzed on two separate SDS-PAGE gels; one was stained with Coomassie Brilliant Blue and the other was probed for R116. (d) RCMV particles was treated with either Endo H or PNGase F and analyzed by SDS-PAGE. The Western blot was stained for RCMV R116 and gB and visualized by chemiluminescence.

4.3.4 Loss of R116 impairs RCMV infectivity

Since R116 is a virion envelope glycoprotein, we hypothesized that R116 plays a role in virus entry. A BAC was generated containing a GFP reporter and the RCMV genome. BAC recombineering was then used to generate a mutant virus containing a 2xSTOP mutation at the beginning of the R116 coding sequence. RFL6 cells transfected with recombinant BACs containing the R116 2xSTOP mutation produced GFP and the viral IE proteins indicating successful transfection of the BAC DNA and viral gene expression. However, exhaustive transfection experiments with multiple BAC clones and preparations failed to rescue infectious virus (data not shown).

As an alternative approach, R116 knockdown experiments were performed in WT RCMV-infected fibroblasts using two different siRNAs specific for R116. Western blot analysis of cell lysates validated that both R116 specific siRNAs, but not a control siRNA, reduced R116 protein production (Figure 27a). Titration of supernatant virus from this experiment revealed that knockdown of R116 reduced RCMV infectivity by nearly 10-fold when compared to the negative control siRNA or non-transfected controls (Figure 27b). To determine whether R116 knock-down affects viral genome replication or the release of genome containing particles, viral DNA levels in supernatants and cell pellets from siRNA

treated cells were analyzed by qPCR. Knockdown of R116 did not decrease viral genomic DNA levels in the infected cells indicating that the R116 knockdown did not decrease the production of infectious virus by preventing DNA replication (Figure 27c). Furthermore, knockdown of R116 did not decrease the release of viral genome containing particles into the supernatant suggesting that R116 deficient viruses display a reduced infectivity per particle ratio, rather than a reduction in the production of viral particles (Figure 27c).

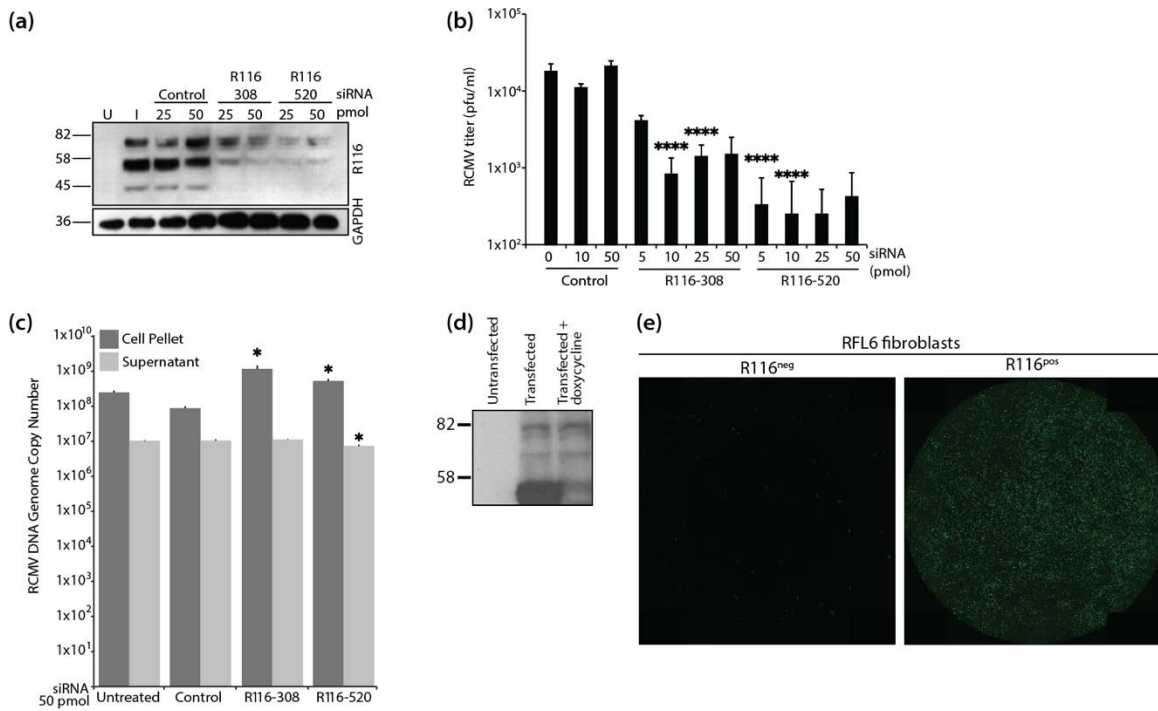


Figure 27. R116 is necessary for viral entry into fibroblasts. (a-c) In triplicate wells RFL6 fibroblasts were transfected with a control siRNA or siRNAs targeting sequences present within the R116 gene. At 24 hours post transfection, the cells were infected with RCMV (MOI=1.0) and allowed to incubate for 4 hours at which time the virus inocula were removed and the cells were washed twice with fresh medium. At 48 hpi, supernatants and cell pellets were collected and analyzed by: (a) Western blotting for R116 and GAPDH; (b) Plaque assay for the presence of infectious virus. Statistical significance was determined by Student's *t*-test [control vs R116 siRNA at 10 and 50pmol $p < 0.001$, $n = 3$]; and (c) qPCR for the presence of viral DNA genomes. Statistical significance was determined by Student's *t*-test [control vs. siRNA R116-308 cell pellet

*p=0.02 and supernatant p=0.33, n=3; control vs. siRNA R116-520 cell pellet and supernatant p=0.01, *p<0.05, n=3]. (d-e) R116 expression by RFL6 cells restores infectivity of Δ R116-RCMV. (d) RFL6 fibroblasts were harvested in lysis buffer containing protease inhibitor, analyzed by SDS-PAGE and probed using the anti-R116 polyclonal antibody. Western blots were visualized by autoradiography. (e) GFP expression 5 days after infection with Δ R116-RCMV in triplicate wells of wild-type RFL6 fibroblasts (left) or R116-expressing RFL6 fibroblasts (right). Representative images are shown.*

We next investigated whether the reduced infectivity per particle ratio was due to a defect in an entry process or a post-entry step. For these experiments, cells were treated with polyethylene glycol (PEG) following infection with WT RCMV collected from cells treated with the anti-R116 or control siRNA. PEG is a fusogenic substance, known to promote viral and cell membrane fusion. PEG restored infectivity of the R116-deficient virus to PEG-treated control siRNA levels (Table 10). While PEG treatment increased the infectivity of virus from both control and R116 siRNA treated cells, the effect of PEG was greatest in cells infected with the R116-deficient virus, wherein PEG increases the infectivity by 10-12-fold. This result indicates there were similar numbers of RCMV virions present in the R116 knockdown supernatants compared to controls and confirms our findings of equal viral genome levels in the R116-deficient virions. Thus, R116-deficient viral particles have a reduced infectivity per particle ratio and lack the necessary entry machinery to complete early entry steps.

	# plaque		fold increase with PEG ^a
	no treatment	PEG	
Control siRNA	725 +/- 199	2417 +/- 736	3.3
R116-308	158 +/- 143^b	1950 +/- 421^c	12.3
R116-520	208 +/- 174^d	2183 +/- 640^e	10.5

a=PEG treatment increases infectivity for all siRNA (p<0.005)

b, d=siRNA to R116 decreases infectivity vs. control (p<0.0003, p<0.0008 respectively)

c, e=PEG restores infectivity of RCMV lacking R116 to control levels (p=0.21, p=0.57 respectively)

Table 10. PEG treatment restores infectivity of RCMV lacking R116.

Since R116 is necessary for virus entry into fibroblasts, we hypothesized that trans-complementation may permit the rescue of recombinant RCMV lacking expression of R116. For this experiment, fibroblasts were constructed that express R116 in a doxycycline-inducible manner using a Tet OFF system. R116 expression was confirmed by western blot of lysates from transfected fibroblasts (Figure 27d). To evaluate whether trans-complementation was possible for viruses lacking R116, these cells expressing R116 were transfected with the RCMV-GFP-116-2xStop BAC, in the absence of doxycycline. Supernatants were collected at 7 days post transfection and titered on fibroblasts by GFP expression. Importantly, virus was recovered from the R116 expressing cells, which was used to infect WT or R116 expressing cells to assess viral entry and support of viral replication. Cells were infected with a low MOI (0.1) and visualized by fluorescence microscopy at 5 dpi for the presence of virus as indicated by GFP. R116 complementation restored infectivity of RCMV (Figure 27e) and the RCMV-GFP-116-2xStop virus was

capable of spreading in the cells expressing R116 but not in cells that did not express R116. This data confirms that R116 is required for the production of infectious virus.

4.3.5 UL116 knockdown impairs HCMV infectivity

Previously it has been reported that UL116 binds to gH but the function of this complex remains unknown [72]. To examine whether UL116 is required for HCMV infectivity, we utilized a UL116 knockdown technique in WT HCMV infected cells, which was similar to our approach for R116. For this experiment, UL116 was knocked-down with 2 unique siRNAs targeting different regions of the UL116 gene and then infected with HCMV-TB40EgfpUL116-HiBiT. This virus contains a C' terminal in-frame fusion of UL116 with an 11 amino acid epitope that binds to Large BiT in trans for luminescence detection (Figure 28a). Comparison of multistep growth curves of HCMV WT and UL116 HiBiT viruses revealed no impairment of viral replication in NHDF in the HiBiT-tagged virus (Figure 28b). For the siRNA experiments, culture supernatants were collected at 5 dpi and titered to determine viral infectivity. siRNA knockdown of UL116 with 50pmol siRNA significantly decreased viral loads at 5 dpi with HCMV TB40e UL116-HiBiT (MOI=0.3) in NHDF fibroblasts (Figure 28c). Knock-down of UL116-HiBiT in this experiment was confirmed by HiBiT lytic assay of supernatants (Figure 28d). This assay detects HiBiT-tagged proteins in the environment of a membrane-dissociation buffer, in this case in media supernatants from infected cells. These data indicate that UL116 contributes to the production of infectious HCMV.

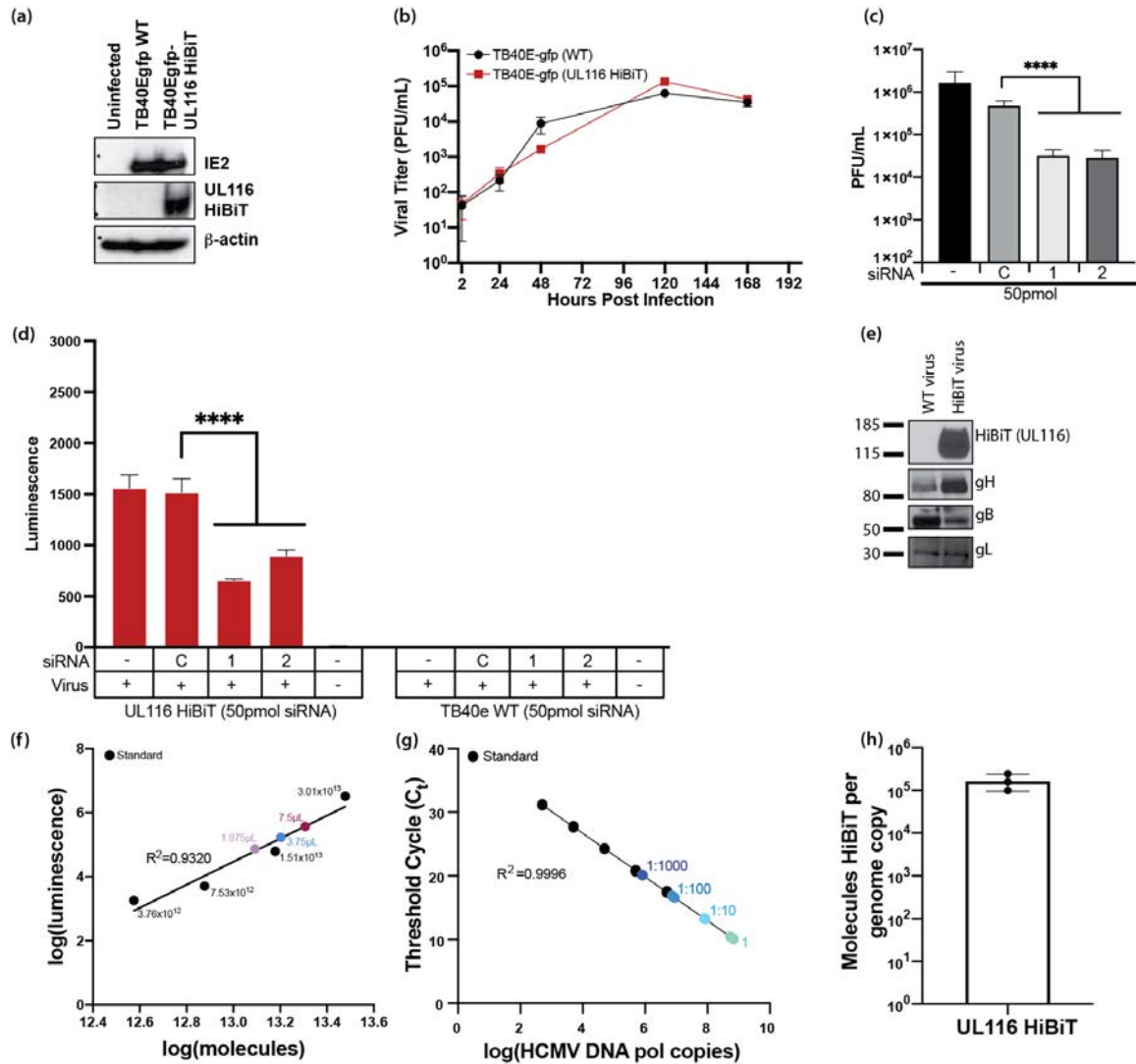


Figure 28. HCMV UL116 is required for entry into fibroblasts. HCMV UL116 was molecularly tagged with the HiBiT tag using BAC recombineering in a TB40e background. (a) NHDF fibroblasts were infected with TB40e GFP HCMV or TB40e GFP UL116-HiBiT HCMV and were harvested in lysis buffer. Western blots were performed for IE2, HiBiT, and β -actin to confirm expression of UL116-HiBiT. (b) NHDF fibroblasts were infected at an MOI=0.3 using a UL116-HiBiT tagged HCMV or TB40e WT HCMV for 2 hours, at which time the virus inoculums were removed and cells were washed with PBS and fresh media was added. Supernatants were harvested at 24, 48, 120, and 168 hpi and titered over NHDF fibroblasts. (c) NHDF fibroblasts were plated in 24-well plates and treated in quadruplicates. NHDF fibroblasts were transfected with a control siRNA or siRNAs targeting sequences present within the UL116 gene at 50pmol/well. At 24 hours post transfection, the cells were infected with HCMV (MOI=0.3) and incubated for 2 hours at which

time the virus inoculums were removed and the cells were washed twice with fresh medium. At 5 dpi, supernatants and cell pellets were collected and analyzed by plaque assay for the presence of infectious virus. Statistical significance was determined by one-way ANOVA with Dunnett's correction for multiple comparisons [**** $p < 0.0001$, $n = 4$]. (d) NHDF fibroblasts were seeded in 96-well black plates and transfected with control siRNA or siRNAs targeting sequences present within the UL116 gene. Cells were infected at an MOI=0.3 using a UL116-HiBiT tagged HCMV or TB40e WT HCMV for 2 hours, at which time the virus inoculums were removed and cells were washed with PBS and fresh media was added. At 3 dpi cells were harvested and analyzed by HiBiT lytic detection assay. Statistical significance was determined by two-way ANOVA with Dunnett's correction for multiple comparisons [**** $p < 0.0001$]. (e) gH, gB, and gL are incorporated into viral particles of UL116-HiBiT HCMV. WT and UL116-HiBiT HCMV were expanded over NHDF fibroblasts. Viruses were harvested at the time of maximum cytopathic effect and pelleted over 20% sorbitol. UL116-HiBiT HCMV viral particles were further purified over a 10-50% histodenz gradient. Purified viral particles were run on SDS-PAGE gels and western blots for gH, gB, gL, and HiBiT were performed. (f-h) UL116 is incorporated into HCMV virions at 1.06×10^5 molecules/HCMV genome. HCMV UL116 HiBiT viral particles were isolated over a histodenz gradient and molecules of HiBiT was determined against a standard curve by HiBiT lytic detection assay (f) and genome copies were determined by qPCR for HCMV DNA polymerase (g). HiBiT control protein (Promega) and known genome copies of HCMV TB40e were used as respective assay controls. Ratio of UL116-HiBiT molecules over genome copies was calculated (h).

4.3.6 Quantification of UL116 incorporation into HCMV

To determine the number of UL116 molecules incorporated into viral particles, we isolated UL116-HiBiT tagged virus particles by serial centrifugation over a 20% sorbitol cushion, a discontinuous 10-50% histodenz gradient, and a 20% sorbitol cushion. Gradient purified HCMV incorporation of UL116-HiBiT was detected by western blot analysis and compared to HCMV TB40e WT virus (Figure 28e). Glycoproteins gH, gL and gB were

detected in the UL116-HiBiT tagged virus (Figure 28e). Molecules of HiBiT tagged protein in three different volumes of virus were determined by HiBiT lytic detection assay relative to a tagged control protein purchased from Promega (Figure 28f). Viral genome copies in the virus preparations were determined by qPCR using primers and probes directed against *UL54* gene sequences and this data was used to calculate the number of viral genomes per μL of the virus preparation (Figure 28g). By directly comparing the number of HCMV genome copies with HiBiT molecules per volume, it was calculated that, on average, 1.06×10^5 molecules of UL116-HiBiT per viral genome are incorporated into virus particles (Figure 28h).

4.4 Discussion

The UL116 proteins are incorporated into multiple CMVs including HCMV, MCMV and RCMV. In this report, we demonstrate that RCMV ORF R116 is a virion surface envelope glycoprotein required for an early step of virus entry. R116 protein localizes to the TGN in a compartment that co-stains with RCMV glycoprotein gB. From this data and given the incorporation of R116 into the virion, we predict that this compartment is the virion assembly compartment. Transfection with a RCMV BAC containing a disrupted R116 gene was unable to spread in fibroblasts *in vitro*. Similarly, siRNA knockdown of R116 decreased RCMV infectivity of fibroblasts by approximately a log but did not alter viral genome replication or release of viral genome containing particles. PEG treatment promotes the fusion of membranes and as such restored the infectivity of virus lacking R116, indicating that the R116-deficient particles are otherwise intact. R116 complementation restored RCMV infectivity in fibroblasts. Finally, knockdown of UL116

decreased HCMV infectivity in human fibroblasts by approximately a log. Importantly, we determined that UL116 is incorporated at 1.06×10^5 molecules per genome copy. Taken together the data presented in this manuscript demonstrate that CMV ORF 116 encodes a virion glycoprotein involved in the production of infectious virus.

Despite a low identity (18%) with UL116, the RCMV R116 protein shares many structural characteristics with its HCMV homologue. Both proteins contain predicted 18 amino-acid signal peptides in their N-terminal regions, with a cleavage site between position 18 and 19 for R116 (www.cbs.dtu.dk/services/SignalP/). Additionally, both proteins are expressed with late viral gene expression, as observed for UL116 [72]. Multiple variants of UL116 have been described, with a 35 kDa, a 76 kDa, and a 125 kDa form accumulating after 3 dpi [72]. Similarly, we found two distinct R116 forms of about 82 and 58 kDa expressed *in vivo*. R116 is glycosylated, and post-translational modification prediction reveals 3 N-linked glycosylation sites at positions 98, 134 and 335 and more than 60 O-glycosylation sites (<http://www.cbs.dtu.dk/services/NetNGlyc>), while UL116 contains 14 N-glycosylation sites and numerous O-glycosylation sites. Therefore, we suggest that the function of ORF 116 might be conserved between RCMV, MCMV and HCMV. Notably, treatment of cell lysates with PNGase F decreased the size of R116, but a large proportion of R116 was not reduced to the un-glycosylated size of 42kDa. Since PNGase F treatment had significantly more effect on reducing the size at which gB migrates, this suggests alternative post-translational modifications beyond N-linked glycosylation of R116. The requirement for R116 and UL116 in the production of infectious virus suggests that either the protein encoded by ORF116 is a member of a putative entry complex or is involved in

regulation of other entry complexes. A putative entry complex containing UL116 has been proposed previously for HCMV, consisting of gH/UL116 [72]. So far, gH/gL/gO has been described as the primary gH based complex for entry into fibroblasts, and is believed to function with gB to create the core fusion machinery for entry [57]. Importantly, the decrease in production of infectious CMV via UL116/R116 knockdown may alternatively be due to effects on an mRNA also containing UL115/R115 (gL); however, our trans-complementation of RCMV deficient of R116 would indicate that expression of only R116 is sufficient to regain infectivity.

Interaction between gH and gB to form gB:gH/gL complexes is essential to induce cell-to-cell fusion [69,340]. The crystal structure for HCMV gH was recently described in complex with the other pentamer components [341]. This crystal structure showed substantial similarities to previous descriptions of gH for EBV and HSV-2 [341–345]. Based on mechanistic studies involving different neutralizing antibodies, some studies determined that binding of gH/gL to gB depends on N-terminal domain H1 of gH [342,344,345], which is supported by the inability of MSL-109 (an anti-CMV neutralizing antibody binding domain H2 of gH) to prevent the generation of gB:gH/gL [343]. Here, we found that gB and R116 are colocalized, but formation of a gB:gH/R116 (or gB:gH/UL116) complex remains to be explored.

Numerous receptors of CMV envelope glycoproteins have been identified, conferring a broad cell tropism to CMV, including fibroblasts, endothelial cells, epithelial cells and myeloid cells [64–66,68,94]. PDGFR α is known as the main receptor of gH/gL/gO, while

neuropilin-2 and OR14I1 are known as the main receptors of the pentameric complex [89,94,99]. Calo *et al.* showed that UL116 competes with gL for gH binding, leading to the formation of a stable gH/UL116 complex, which is transported to the plasma membrane [72]. How UL116 interacts with gH remains unknown, but UL116 does not contain the necessary Cys residues to form disulfide bonds with gH. Further work remains to be done to identify binding partners of the gH/UL116 complex and to determine whether UL116 limits CMV cell tropism beyond fibroblasts. Additional studies are required to determine whether UL116/R116 acts a chaperone promoting gH complex formation. In conclusion, ORF 116 encodes a CMV envelope glycoprotein essential for production of infectious virus in both HCMV and RCMV, and should be considered as an attractive therapeutic target when developing vaccines and monoclonal antibodies against CMV.

4.5 Materials and methods

Antibodies: Rabbit polyclonal antibodies were generated to ORF R116 by immunizing rabbits with a HIS tag R116 (19-222aa) fusion protein. Rabbit anti-RCMV-IE polyclonal antibody was previously described [263]. A rat anti-RCMV gB monoclonal antibody was produced by Dan Cawley at the OHSU-VGTI Monoclonal Antibody Facility from splenocytes derived from RCMV-infected rats. Mouse monoclonal antibodies directed against GAPDH (ab8245), KDEL (ab12223), LAMP-1 (ab13523), and TGN-38 (ab16059) were purchased from AbCAM. Secondary anti-mouse and anti-rabbit HRP-conjugated antibodies (NA934V and NA931V) were purchased from Amersham and rabbit anti-rat HRP (6180-05) was purchased from Southern Biotech. Secondary anti-mouse (A11020),

anti-rabbit (A11046) and anti-rat (A21470) fluorescently tagged antibodies were purchased from BioSource International.

RCMV: The RCMV Maastricht strain genome was captured as a BAC using homologous recombination by replacing ORFs r144-r146 with a BAC cassette expressing eGFP under the HCMV MIEP [133]. Two-step recombination was used to mutate RCMV ORFs in the creation of the R116 2xSTOP mutant. The first recombination step incorporated a gene cassette expressing *galK* and Kanamycin (Kan) resistance genes into the RCMV BAC genome at the genomic site for introduction of the mutation, via PCR amplification of a 100bp homology region flanking the *galK*/Kan gene cassette. The amplified DNA was treated with Dpn1, purified, and then electroporated into competent RCMV-BAC SW102 cells. Clones were positively selected for gain of resistance against Kan, screened by PCR and sequenced to identify clones with the proper insertion. PCR was used to generate DNA fragments containing RCMV sequences with the desired mutation. This amplicon was electroporated into competent bacteria and negatively selected for *galK* replacement on 2-deoxy-galactose-1-phosphate (DOG) negative selection plates. BAC clones were verified by PCR and the gene containing the mutation was sequenced for correct incorporation of mutations. DNA from correct clones was transfected into RFL6 fibroblasts (RFL6, ATCC) to rescue the virus. RCMV mutants and WT were then expanded on RFL6 fibroblasts and purified over a 10% sorbitol cushion by ultracentrifugation at 25,000 RPM (SW32) for 1 hour. Purified virus was then titered over RFL6 fibroblasts in serial dilutions to determine viral titer as measured in PFU/mL.

HCMV: In order to evaluate the efficiency of UL116 knockdown using specific siRNA, we modified a GFP-expressing BAC of wild type HCMV clinical isolate TB40E using galK positive/negative selection as described for RCMV. The HiBiT tag (5'-GTGAGCGGCTGGCGGCTGTTCAAGAAGATTAGC-3') was inserted between nucleotides 1026 and 1027 in the *UL116* gene, corresponding to the C-terminal region of the protein. Correct insertion of the tag was confirmed by sequencing.

Identification of RCMV R116 transcripts: An RCMV cDNA library was constructed from rat RFL6 fibroblasts infected with RCMV at an MOI of 1 for 24 and 48 hpi using the Superscript Plasmid System with Gateway Technology for cDNA synthesis and cloning (Invitrogen). The cDNA was ligated into the plasmid pSPORT and screened by Southern blotting using an R116 DNA probe. The R116-positive clones were sequenced using oligonucleotides corresponding to Sp6 and T7 binding sites present in the plasmid flanking the cDNA insert. The predicted splicing of R116 was confirmed by real time polymerase chain reaction (RT-PCR) using flanking primers. The products were analyzed by gel electrophoresis and the products were sequenced.

Northern blot: RFL6 fibroblasts plated on 10cm dishes were infected with RCMV (MOI=1). At 8, 24 and 48 hpi the cells were washed and lysed with Trizol for 5 min at room temperature. Subsequently, the samples were scraped and stored at -80°C. RNA was isolated per the manufacturer's instructions and electrophoresed through a 1% agarose/formaldehyde gel and transferred to GeneScreen Plus nylon membranes (Dupont/NEN). The blots were hybridized with probes specific for R116 and GAPDH

generated from 500bp *Bam*HI fragments of plasmids containing R116 or GAPDH using Roche Random Prime Labeling kit. Alternatively, single stranded probes were made by end labeling DNA oligonucleotides complementary for R116 or GAPDH sequences using T4 polynucleotide kinase (New England Bio). The Northern blots were hybridized in Express Hybe (Clontech) and washed with low stringency wash (2xSSC with 0.05% SDS) followed by high stringency wash (0.1xSSC with 0.1% SDS). The blots were exposed to autoradiography film (Kodak Biomax MS) using intensifying screens at -80°C, developed, and visualized.

Western blots: Cells were placed on ice, washed once with 4°C PBS, and 1x cell lysis buffer (cell signaling) containing HALT protease inhibitor (ThermoFisher) was added. Cells were incubated on ice for 15 minutes and scraped. Cell nuclei were pelleted out at 10,000 RPM for 10 minutes at 4°C and clarified supernatants were transferred to new Eppendorf tubes. NuPage loading buffer with 2% BME was added to cell lysates at a final concentration of 2x. Samples were boiled for 5 minutes and loaded on 4-12% SDS-PAGE protein gels. Proteins were transferred using a semi-dry transfer system to PVDF membranes and membranes were probed with the appropriate antibodies with membrane blocking in 5% milk-TBST (10mM Tris, pH 7.2, 100mM sodium chloride, 0.1% Tween-20). HiBiT blots on PVDF membranes were washed in TBST for 15 minutes at room temperature, incubated with 1:200 LgBiT in 1x HiBiT blotting buffer for 1 hour at room temperature, and HiBiT substrate was added at 1:500 for 5 minutes at room temperature. Blots were then developed by chemiluminescence.

Salivary gland protein isolation: R116 in vivo protein expression was performed on approximately 100µg of protein extracted from flash frozen salivary gland tissue from uninfected control rats and rats infected with RCMV for 28 days (n=3). Tissues were homogenized in RIPA buffer (50mM Tris HCl pH7.4, 150mM NaCl, 5mM MgCl₂, 0.5% NP-40, 1mM PMSF and protease inhibitor cocktail) using a Precellys tissue homogenizer. Lysates were analyzed by SDS-PAGE and Western blotted for R116 and GAPDH as described above.

Cellular localization of R116 assessed by immunofluorescence microscopy: Fibroblasts grown in 4-well chamber slides were infected with RCMV (MOI=0.5) for 48 hpi and then treated with cycloheximide (100µg/ml) for an additional 0, 1, 2, 4 and 6 hpi to block new protein synthesis. At the indicated time points, cells were fixed in 2% PFA in PBS and then permeabilized with Saponin buffer (0.2% saponin, 1% BSA, PBS) blocking with normal goat serum. Localization of viral and cellular proteins was determined by immunofluorescence microscopy utilizing primary antibodies directed against R116, gB, KDEL, LAMP-1, and TGN-38. Samples were then incubated with appropriate fluorescently-labeled species-specific secondary antibodies and DAPI DNA stain. Frozen, thin-sections of rat salivary glands from rats infected with RCMV-GFP at 21 dpi were fixed and stained with antibodies directed against R116 using the same protocols described above. Deconvolution microscopy was used to visualize the stained cells in the 4-well chamber slides and tissue sections (mag=60X).

Virion localization and glycosylation of R116: The protein composition of the pelleted virus was analyzed by Western blotting to determine whether R116 was incorporated into virions. We analyzed samples of RFL6 fibroblasts infected with RCMV (MOI=1.0), salivary gland tissue homogenates, or different preparations of virus pellets. RCMV virus particles were purified by layering over a discontinuous 10-to-50% Nycodenz gradient and centrifuged at 110,000xg for 2 hours at 4°C. Virus banded at 20-30% Nycodenz was brought up in PBS and pelleted at 59,439xg for 1 hr through a 10% sorbitol cushion. The virus pellet was resuspended in a minimal volume of PBS. First, to determine whether RCMV R116 was an envelope protein, the resuspended viral pellet was split into 2 samples. One sample was treated with 1% NP-40 in PBS added in a 1:1 ratio and the second half of the original sample was treated with an equivalent volume of PBS. The samples were incubated for 30 minutes at 4°C and centrifuged in a mini-ultracentrifuge at 100,000 xg for 30 minutes to acquire both the pellet and supernatant fractions. Second, to determine whether R116 was on the virion surface, an additional preparation of gradient banded virus particles was incubated with increasing concentrations of trypsin and incubated at 37°C for 15 minutes. Laemmli's sample buffer was added to the virus/protease mixture to stop the reaction and the samples were analyzed by SDS-PAGE in combination with either Coomassie brilliant blue staining or Western blotting for R116. Third, to determine whether virion-associated R116 was glycosylated, RCMV particles were treated with PNGase F (NEB) or Endo H (Roche). The treated virus samples were analyzed by SDS PAGE and Western blotting for R116 and gB.

siRNA transfection and infection: Two R116-specific siRNAs (R116 ORF positions 308-326 nt and 520-538 nt) and a control siRNA were purchased from Dharmacon. The sequences of the R116 siRNA were: R116-308 5'-CTACATTACCCTCGCAAAT-3' and siRNA R116-520 5'-GCGACGAGGCGATACGTTT-3'. Two UL116-specific siRNA were purchased from Horizon having the following sequences: UL116-1 5'-ACAAGAAACACAAGGAAUAUU-3' and UL116-2 5'-CCGUCAUCGUCGCGGGUAAUU-3'. RFL6 fibroblasts and NHDF fibroblasts seeded in 24-well plates were transfected twice with each siRNA using Lipofectamine RNAiMAX Reagent (Invitrogen) according to the manufacturer's protocol. At 24 hours after the initial transfection step, the cells were infected with RCMV (MOI=1) or HCMV (MOI=0.3). The cells and supernatants were collected and titered using a standard plaque assay at 2 and 5 dpi for RCMV and at 5 dpi for HCMV. For HCMV, protein levels were determined by HiBiT lytic detection, as described below. For RCMV, the triplicate samples of cells were lysed in either DNazol (viral DNA analysis), Trizol (mRNA analysis) or Laemmli's buffer (viral protein analysis). Host cell production of the viral mRNAs was quantified by RT-PCR Taqman. R116 protein expression levels were determined by Western blotting. Viral genomic DNA was analyzed by qPCR for R54 (viral DNA polymerase) as described below.

Plaque Assays: Serial dilutions (10^{-1} to 10^{-6}) of viral supernatant were performed in complete DMEM and 100 μ L were added to confluent 24-well plates of rat fibroblasts or NHDF fibroblasts as appropriate. Viral solutions were incubated for 2 hours at 37°C. CMC (500 μ L per well) was overlaid onto the cells and cells were incubated for 7 days for RCMV

or 14 days for HCMV at 37°C. Titer plates were fixed in 3.7% PFA and stained with methylene blue and plaques were counted using a dissecting microscope. HCMV titers were counted by GFP fluorescence microscopy.

Viral Entry Assays: A 1:10 dilution of supernatant from siRNA treated cells infected with RCMV was allowed to bind for 1 hour and then treated with the fusogenic substance PEG 6000 (Calbiochem) diluted in PBS (44%) for 30 seconds at 37°C using a protocol designed by Ryckman *et al.* for the study of HCMV entry [71,97]. Following PEG treatment, the cells were washed once with PBS, twice with media and then overlaid with CMC and incubated for 5 days to allow for plaquing of virus. Cells were then fixed with 3.7% PFA and stained with methylene blue and plaques were counted.

Quantitative PCR detection of RCMV genomic DNA and viral gene expression: For the quantification of RCMV DNA in virus particles and infected cells treated with siRNA, total genomic DNA was extracted from cells and supernatants using DNazol (Invitrogen). A total of 0.5 µg of DNA was analyzed using a Taqman probe/primer set recognizing a RCMV R54 DNA polymerase sequence as previously described [194,247]. PCR reactions were set up using the TaqMan Universal PCR Master Mix (Applied Biosystems). Following thermal activation of AmpliTaq Gold (10 min. at 95°C), a total of 40 cycles were performed (15 sec. at 95°C and 1 min. at 58°C) using an ABI StepOnePlus RT-PCR machine. The sensitivity of detection for this assay was <100 copies.

RT-PCR was used to quantify expression levels of RCMV R114, R115 and R116 from infected cells collected following treatment with siRNA [247]. cDNA was generated from mRNA using Superscript III RT (Invitrogen) and analyzed by real-time PCR techniques using primer sets recognizing RCMV gene sequences. RT-PCRs were performed using the SYBR Green PCR Master Mix (Applied Biosystems) as previously described using an ABI StepOnePlus RT-PCR machine [247,263]. Plasmid clones containing each gene fragment were used as positive controls and quantification standards. The sensitivity of detection of this assay was <100 plasmid copies for all of the tested RCMV genes. Quantitative PCR data were analyzed by ANOVA and student's t-test.

	Forward Primer	Reverse Primer	Probe
R54	5'-CCTCACGGG CTACAACATCA -3'	5'-GAGAGTTGACGA AGAACCGACC-3'	5'- CGGCTTCGATATCAA GTATCTCCTGCACC- 3'
R114	5'- ACCTTTACGGA ACCGGAGTTG- 3'	5'- ACGGACAAGGTCGAT AGGGA-3'	N/A
R116	5'- TCCGGCTGAA TAAGACCTCG- 3'	5'- CCCATCCTCAACAGC ACACA-3'	N/A

Table 11. Primer and probe sets for qRT and RT-PCR.

Fibroblast R116 transfection and infection: The entire R116 gene was ligated into the plasmid pGEM®-T easy (PROMEGA). Briefly, we combined 22ng of amplified modified R116 gene (forward primer 5'-TCCACGAACACACATACGTA-3', reverse primer 5'-TTCGACATCTGTTGGCGAAT-3'), 50 nanograms (ng) of pGEM®-T easy vector and 5µl of rapid ligation buffer in a total volume of 10 µL. After incubation for 1 hour at room temperature, we carried out transformation of high-efficiency competent cells using 10µL of ligation reactions. Mix was successively incubated for 20 minutes on ice, heat-shocked for 45 seconds at 42°C, and chilled for 2 minutes on ice. Transformed competent cells were then recovered in 500 µl of LB media for 1 hour at 37°C with shaking (300 RPM) and transformants were selected on carbenicillin-containing 2xYT agar plates. Colonies were PCR screened and positive colonies were expanded in carbenicillin-containing 2xYT broth. DNA was purified from pGEM-T easy R116 positive clones and empty pB vector and digested with Kpn1 and Xho1. Purified DNA was then isolated by gel electrophoresis, followed by gel extraction. The R116 gene was then ligated into the pB expression vector and transformed into chemically competent cells as above. Colonies were screened by PCR and sequenced to confirm R116 insertion. Sequence-confirmed constructs were transfected into rat RFL6 fibroblasts. The pB vector is a TET-Off system, so treatment with doxycycline (250µg/ml) was used to silence R116 gene expression. R116 production in absence of doxycycline was confirmed by western blot. R116-expressing RFL6 cells were infected with RCMV-116-2xStop to produce a R116 complemented RCMV. Spreading of infection was monitored by GFP detection.

Virion purification of UL116 HiBiT: HCMV UL116 HiBiT was expanded over NHDF fibroblasts. Supernatants were pelleted at 76,755xg for 2 hours over a 20% sorbitol cushion. Viral particles were then resuspended in TNE buffer (50mM Tris [pH 7.4], 100mM NaCl, 10mM EDTA) and layered over a discontinuous 10-to-50% Histodenz gradient and centrifuged at 111,132 xg for 2 hours at 4°C. Virus banded at 20-30% Histodenz was brought up in PBS and pelleted at 76,755 xg for 2 hours through a 20% sorbitol cushion. The virus pellet was resuspended in a minimal volume of PBS.

qPCR for genome copies of UL116 HiBiT: DNA was extracted from histodenz-purified virus with the GeneJet viral DNA and RNA purification kit (ThermoFisher). Dilutions of DNA were prepared (Undiluted, 1:10, 1:100, 1:1000) and qPCR against HCMV DNA pol (UL54) was performed in triplicate. HCMV TB40e of known genome copies was used to create a standard curve in triplicate. UL54 primers and probe were as follows: (P1: CGCTGCGAGTCCACCTTATAC, P2: ACCGGTTACAACATCAACTCTTTTG, Probe: CGCGTGAGGATGTACT). Genome copies per μL of the histodenz-purified virus preparation was determined for use in calculating UL116-HiBiT molecules/genome copy.

HiBiT lytic detection assay for UL116-HiBiT: For infection of NHDF with UL116 HiBiT, supernatants were removed from cells and 25 μL per well of fresh media was added to cells. For detection of virion incorporated proteins, three quantities of histodenz-purified HCMV UL116 HiBiT (7.5 μL , 3.75 μL , 1.875 μL) were diluted with PBS to 25 μL in a black 96-well plate and assayed in triplicate. A standard curve was generated using HiBiT control protein (ProMega) from 1000 to 15.625 nanomolar (nM). For all assays, 25 μL per well of HiBiT

lytic detection reagent with LgBiT and substrate was then added to wells as per the manufacturer's protocol. Plates were incubated at room temperature for 10 minutes on an orbital shaker. Luminescence was read on a 96-well plate reader with a gain setting of 135.

4.6 Acknowledgments

The authors would like to thank Drs. Jeremy P. Kamil (LSU) and Brent Ryckman (MSU) for their critical reading of the manuscript and constructive discussion over the course of these studies. This work was supported by a grant from the National Institutes of Health NIAID R01 AI116633. IKAJ was supported by the OHSU Molecular Microbiology and Immunology Interactions at the Microbe/Host Interface training grant NIH 2T32 AI007472 and NIH F31 1F311AI145193-01.

Chapter 5 – Conclusions and Future Directions

5.1 Summary

CMV continues to be a major health concern for patients experiencing long-term immunosuppression, such as those receiving treatment for bone marrow or solid organ transplants. The work included in this dissertation illustrates the many mechanisms by which CMV accelerates cardiac allograft rejection. In Chapter 2, we identified an effective therapeutic administered early following transplantation that successfully inhibits IRI in the graft. This ultimately improves graft survival and reduces CMV-acceleration of graft rejection. A number of CMV genes are required to establish persistent, latent infections. In Chapter 3, we defined the role of two RCMV-encoded chemokines in viral entry. We developed a novel approach for quantification of protein incorporation into viral particles (Appendix I), and used this approach in Chapter 3 to identify key features of R129 and R131 proteins in regulation of entry, including the C' terminal and CC-domains of these proteins. We also identified a new protein, R116, and characterized its role in the production of fully infectious virus (Chapter 4). These data also demonstrated functional homology between RCMV R116 and HCMV UL116. Overall, the data presented here highlight the role of CMV in transplant rejection, with an emphasis on elucidating the mechanisms, encompassing both viral proteins and host-immune responses, that contribute to pathogenesis in CMV-accelerated allograft rejection, in order to develop new therapeutic approaches for SOT recipients. Our work improves our current understanding of the mechanisms behind CMV infection in SOT.

5.2 Exacerbation of CMV pathogenesis by a pro-inflammatory environment in the host

In solid organ transplant recipients, graft inflammation increases risk of acute and chronic allograft rejection [163]. As discussed in Chapter 2, both IRI and CMV infection are associated with an increase in this inflammatory response. Following IRI, a variety of inflammation-related pathways are activated, while cellular metabolism pathways are typically down-regulated (Table 13, Table 14, Table 15, Table 16). Here we have shown that inhibition of one of the key inflammatory pathways, the IL-1R signaling pathway, immediately following IRI reduces acceleration of cardiac transplant rejection associated with CMV infection. Interestingly, this was achieved with a single dose of an IL-1R antagonist, suggesting that early responses following transplantation have a significant impact on CMV-associated acceleration of rejection and development of TVS. Previous work would suggest that a reduction in IRI-associated inflammatory signaling post-transplantation is effective because CMV is reactivated by pro-inflammatory signals induced by IRI [22,267]. Importantly, we did not perform transcriptomic analysis comparing CMV⁺ versus CMV⁻ transplant recipient PBMC or graft hearts. It is likely that such data would provide additional avenues for therapeutic intervention. However, comparison of Anakinra-treated animals versus vehicle-treated animals (data not shown) did not reveal substantial alterations in the transcriptome, despite having significant impact on cytokine production and myocardial injury. Since Anakinra treatment specifically targets IL-1R signaling, it is possible that alternative pro-inflammatory pathways hid treatment-related alterations in the global transcriptomic analysis. Similarly, it may be difficult to identify CMV-associated transcriptomic changes on-top of transplantation-associated transcriptional regulation, especially given the tissue-specific nature of CMV

gene-expression and the necessity of separating infected cells from uninfected cells in order to identify transcriptomic changes associated with infection [285].

Transcriptomic and proteomic data presented several additional targets not explored here for therapeutic intervention in CMV⁺ transplant recipients. Additional targets in inflammatory pathways provide an intriguing approach to treat both CMV-associated CR and IRI damage in transplant patients without inducing escape mutants with direct anti-viral therapies. Targets of particular interest include IL-18R, IL36 β /IL38R, and toll-like receptor antagonists. It is possible that a combination approach targeting multiple inflammatory pathways would yield better results with regard to minimizing TVS and CR than the single approaches we employed here. Additionally, anti-viral therapies, such as ganciclovir, combined with anti-inflammatory therapies should be explored. Furthermore, kinase inhibitors present an intriguing avenue for therapeutic intervention, as several kinase pathways were identified in our transcriptomic data. Many of these compounds are already licensed for use in humans for the treatment of cancer [346–349], making them particularly favorable therapeutic options. Kinase inhibitors have been considered previously for other viral infections that are associated with hyper-inflammatory pathogenesis, such as influenza and SARS-CoV-2 [350–352]. In these cases, kinase inhibitors can either be used to target host proteins necessary for viral replication or entry to block viral replication and dissemination, or to target host proteins involved in cytokine signaling and antiviral responses. Combination therapies involving IL-1 inhibitors and kinase inhibitors have also been proposed to more effectively reduce cytokine signaling [352]. However, these viruses do not establish latency, adding a complicating factor to targeting of anti-viral pro-

inflammatory pathways during CMV infections. In immunosuppressed patients, suppression of pro-inflammatory signaling pathways must be effectively balanced with direct anti-viral strategies to prevent viral reactivation [353]. Previous work has considered the use of mTOR inhibitors to control viral infections in solid organ transplant recipients, finding mTOR a promising target in reducing TVS and CMV reactivation [354]. As proposed for other viral infections, in which the host immune response plays a role in pathogenesis, kinase inhibitors alone or in combination, present a potential therapeutic target for reducing CMV-associated TVS and CR.

5.3 CMV-encoded chemokines and other immune-modulatory proteins result in alterations in immune-cell migration

CMV infection results in further long-lasting alterations to the host immune response through encoding its own immunomodulatory proteins. These include chemokines, chemokine-receptors, and MHC-I-like molecules, as well as viral proteins that target various proteins involved in host-immune responses [58,355]. Chapter 3 contains a review of the functions of CMV-encoded chemokines and chemokine-receptors in CMV infection. A common point between CMV-encoded immunomodulatory proteins and host-immune responses that exacerbate CR and TVS in transplant recipients is the presence of macrophages and DC. DC play a key role in viral dissemination and both mouse and human CMV encode chemokine receptors (M33 and US28 respectively) that promote tissue resident DC to re-enter circulation, permitting establishment of infection in salivary glands and spread of the virus from host to host [27–29,323]. US28 is also involved in migration of macrophages and vSMC [216,217], key cell types in the development of TVS following

transplantation. Homologues in MCMV and RCMV, M33 and R33, also promote migration of vSMC [31,222]. Previous work has shown that CMV infection of the donor results in an increase in donor graft passenger lymphocyte loads prior to transplantation [165]. In conjunction with these findings, recent work from our group demonstrated the utility of macrophage depletion from donors prior to transplantation for improving TVS and CR in recipient animals, moderately reducing viral loads in tissues following transplantation [356]. Animals that received transplants from macrophage-depleted donors showed moderately reduced viral loads in tissues following transplantation [356]. Taken together, these studies suggest that alteration of CMV-directed host cell migration presents a viable therapeutic option in transplant recipients. Additionally, impairment of CMV-entry into monocytes is likely to reduce viral dissemination and improve CR rates in transplant recipients. Prior work with a mutant of the RCMV-encoded chemokine, R129, improved development of TVS and time to CR [133]. Furthermore, a mutant of another RCMV-encoded chemokine, R131, resulted in reduced viral loads in salivary glands [123]. The work presented here (Chapter 3), demonstrates that both R129 and R131 mutants fail to enter macrophages and DC. Previous work in gpCMV suggests that loss of the gpCMV homologues to these proteins, GP129 and GP131, also results in lower titers in salivary glands and a reduction in pathogenicity in both primary and congenital infection models [102,114,117]. Importantly, as discussed in Chapter 3, the R129 and R131 proteins, and their homologues, have dual roles in entry and as chemokines, making it difficult to differentiate which functionality plays a larger role in pathogenesis and dissemination. However, our data in Chapter 3 demonstrate that deletion of the C' terminal (entry domain) of R129 and R131 or mutation of the CC-domain of R131 results in failure of RCMV to

enter monocytes. This suggests the distinct possibility that the two functions are inseparable, as the chemokine fold may be necessary for binding of a host-cellular entry receptor or for proper protein structure. Further investigation will be required to determine the role of host chemokine-receptors in mediating viral entry.

Since normal host immune responses would preclude viral dissemination via infected cells, CMV encodes several proteins aimed at altering host recognition of infected cells. Appendix II discusses the role of CMV-encoded proteins in altering host antigen-presentation and characterizes a putative RCMV homologue of the MHC-I-like family of proteins. HCMV encodes several MHC-I-like molecules that down-regulate NK cell activity, including UL16, UL17, UL18, UL40, UL140, and UL142 [236]. In addition, the HCMV-encoded proteins US2, US3, US6, and US11 down-regulate MHC-I to evade CD8⁺ T-cell killing of infected cells [357,358]. RCMV r152.4, discussed in Appendix II, is a predicted m145 family member with the greatest predicted homology to MCMV m152 [132]. m152 is an immunoevasion gene with functional homology to US2-US11 in that it blocks antigen presentation to allow MCMV to evade cytotoxic T-cell responses [248,249]. MCMV encodes several other known regulators of MHC expression, including m04 and m06 [248–252].

RCMV r152.4 homology to m152, and other m145 family members, is primarily based on sequence prediction of MHC-I-like folds in these molecules. We identified similarities in predicted protein structure between r152.4 and m145 family members, including a predicted signal peptide, multiple N-linked glycosylation sites, and a predicted trans-

membrane domain (Figure 34) [242]. However, where m152 was expressed with IE gene kinetics and was absent by early gene expression, r152.4 was expressed with early gene kinetics (Figure 35) [242]. In contrast, UL18 is expressed with late gene expression kinetics, suggesting that expression of immunomodulatory genes may not occur consistently across all genes [232]. Notably, deletion of the MCMV m145 family members m152, m04, and m06 had little effect on infection, persistence, or latency *in vivo*, except to lower viral loads in salivary glands compared to WT infection [251,252]. Similarly, we saw a decrease in viral loads *in vivo* for an r152.4-deficient mutant at 5 dpi (Figure 36).

The high degree of N-linked glycosylation of r152.4 (Figure 34), was of particular interest to us. Various viral glycoproteins function as immunoevasions in a variety of ways, with three of the most common being glycan shielding, antagonism of antigen presentation, and antagonism of NK cell killing [193,236,242,359]. Current evidence suggests that m152 is more directly involved in antagonism of antigen presentation and NK cell killing than glycan shielding, through down-regulation of both MHC-I and the NK cell receptor ligand Rae1 [242]. However, this does not preclude a function for r152.4 in glycan shielding. Further work including determination of the structure of r152.4, verification of binding partners, and cellular localization studies will be necessary to elucidate the function of r152.4. Due to high glycosylation, molecular tagging approaches may be necessary to provide sufficient accuracy of detection for cellular localization and further co-immunoprecipitation studies.

5.4 CMV-encoded entry complexes facilitate infection of cells that allow for viral dissemination

CMV encodes components for multiple different entry receptors, which allows CMV to regulate entry dependent on the tissues it infects. HCMV has two traditional entry complexes that determine cell tropism: the trimer complex consisting of gH/gL/gO and the pentamer complex consisting of gH/gL/UL128/UL130/UL131A. The ratios of these two complexes are regulated by an additional HCMV gene UL148 [75]. Here, we discussed two RCMV entry complexes, the RCMV pentamer homologue consisting of gH/gL/R129/R131 and an unknown potential member, as well as the proposed gH/R116 complex.

R131 and R129 had been proposed as putative members of an RCMV pentamer due to predicted structural homology with UL130 and UL128, as well as positional homology with pentamer members in MCMV, gpCMV, and HCMV. However, their role in viral entry remained to be demonstrated. In Chapter 4 and Appendix I, we showed that R131 and R129 are incorporated into viral particles within the viral envelope. Furthermore, we were able to quantify the incorporation of WT R131 and R129 in viral particles compared to mutant proteins constructed through BAC recombineering. These experiments demonstrated that loss of the charged-clusters and C-terminal tails of R131 and R129 resulted in loss of incorporation into the viral particle. Interestingly, mutation of C36 in R131, which is necessary for formation of the protein's chemokine-fold, and a lesser C-terminal truncation of R129 resulted in lower quantities of protein incorporated into the viral particles. Notably, all of the R131 and R129 mutants, including 2x STOP mutants failed to enter rat DC,

macrophages, and mixed bone marrow cultures. However, only the structural mutants, and not the 2xSTOP mutants, showed reduced entry into epithelial cells. The role of R131 and R129 in entry into rat endothelial cells remains to be determined. Further *in vitro* work will be necessary to explore the role of these mutations in altering virion incorporation of other entry complex components such as gH, gL, gO, and gB. Additionally, loss of UL128 in HCMV results in loss of the other associated proteins, UL130 and UL131A [131]. However, a mutant UL131A virus still incorporated UL128, but showed substantially decreased levels of UL130 [71]. Considering the structure of the HCMV pentamer [341], it is not surprising that loss of UL128 resulted in a greater loss of the other members of the complex than a UL131A-deficient mutant. As such, it will be important to determine if loss of R129 results in failure to incorporate R131 and vice versa. Importantly, our data strongly support a role for R131 and R129 in a functionally homologous entry complex to the HCMV pentamer. Taken with findings from other CMV models (ie. gpCMV) this suggests a high degree of conservation of viral entry complexes and mechanisms across CMV species. This is of significance to the field due to the high reliance on species models to study CMV. Further work on R131 and R129 could build on this data and previous studies by Farrell *et al* [26,28,29,323] to study the role of monocytes in viral dissemination *in vivo*, especially within the context of SOT. For example, previous work has shown that an N-terminal deletion mutant of R129, R129 Δ NT, shows reduced exacerbation of TVS and CR compared to WT RCMV in a rat cardiac transplant model [133]. Furthermore, RCMV⁺ donors show an increase in macrophage and T-cell infiltrates compared to uninfected animals, similar to that seen in humans with HCMV infection [22,36]. Additional studies

showing impacts on recruitment of immune cells to cardiac tissue prior to transplantation might further explain the role of R131/UL130 and R129/UL128 in CR processes.

As discussed in Chapter 4, RCMV R116 constitutes another viral glycoprotein with a role in production of infectious virus. We demonstrate a role for both RCMV R116 and HCMV UL116 in production of virus capable of infecting fibroblasts. Current discussion in the field is investigating two distinct possibilities for the role of UL116 in HCMV entry: (1) UL116 serves as a chaperone for gH while gL binds the additional trimer or pentamer components, or (2) UL116 forms a unique entry complex separate from the gH/gL scaffold, associating only with gH. UL116 has been shown to associate with gH, but not gL [72]. However, it is possible this is a fraction of associated proteins from the viral assembly process that are incorporated into the virion. Additionally, knock-down or knock-out of UL116 may impair entry through effects on UL115 (gL) due to a common transcriptional frame. In contrast, trans-complementation of R116, the RCMV homologue of UL116, was sufficient to generate a virus capable of infecting fibroblasts. This would suggest that the presence of R116, rather than an effect on R115 (RCMV gL), is responsible for changes in viral entry. Additionally, when the molecules of UL116-HiBiT incorporated per viral genome (Figure 28h) were quantitated, we saw levels of incorporation on par with what we had quantified for R131 and R129 (Figure 22e). Since R131 and R129 also have roles in an entry complex, this may suggest that UL116 is intentionally trafficked to the assembled viral particle, rather than being incorporated as a side-effect of gH incorporation. However, replicates of these experiments revealed there is some variability between viral preparations despite normalization to viral genome copies. Further

improvements on this technique will need to focus on normalizations between individual virus preparations in order to offer consistent results between experiments. Ongoing work on UL116 by others includes identification of other interacting proteins and further investigation of the mechanism by which UL116 affects viral entry into fibroblasts.

5.5 Conclusions

Interactions between CMV and the host result in pathogenesis in immunosuppressed patients, including SOT recipients, that is not observed in immunocompetent hosts. However, upon closer inspection, CMV's regulation of its host's immune response lays the ground-work for future disease enhancement in transplant recipients. Here, we have detailed the attenuation of CMV-acceleration of TVS and CR through blockade of host pro-inflammatory signaling associated with IRI. We have also discussed the role of several glycoproteins in viral entry into pathologically relevant cell types, and the role of viral proteins in regulation of host immune cell migration to permit viral dissemination and transmission between hosts. Together these data present a compelling illustration of the complexity of the interactions between CMV and host immune responses that combine to decrease graft and patient survival in SOT recipients.

The work here further details a model in which the pro-inflammatory environment produced by IRI results in an increase in passenger-CMV viral replication and reactivation, including production of virally-encoded chemokines. These virally-encoded chemokines, along with host chemokines produced following IRI, function to recruit recipient macrophages, dendritic cells, and neutrophils to the graft tissue. Recruitment of these

immune cells exacerbates acute rejection episodes, causing further tissue damage and accelerating chronic rejection. Furthermore, virally encoded chemokines and chemokine-receptors facilitate development of the neointima in graft vessels through induction of vSMC migration, contributing to the development of TVS. The macrophages and DC recruited to the graft also serve as vehicles for viral dissemination throughout the new host, with CMV encoding chemokine receptor-like molecules capable of directing macrophage and DC migration from the site of initial infection to the salivary glands, allowing for spread to other hosts.

The attenuation of CMV-accelerated chronic rejection by inhibition of pro-inflammatory responses supports the “two-hit” hypothesis currently being developed in the field of CMV-associated transplant rejection, whereby IRI is sufficient and necessary to induce CMV reactivation, and immunosuppression of the host permits for viral dissemination. Inhibiting pro-inflammatory responses offers a novel approach for minimizing CMV-associated pathogenesis. By targeting the pathogenic host responses in this model, we have avoided eliciting viral escape mutants, as well as shown a successful impact on long-term graft survival that current anti-viral therapies lack in model systems. Combining this approach with a better understanding of viral entry mechanisms allows us to propose approaches to minimizing CMV-acceleration of CR that target both the host immune response and viral dissemination. There are a wide variety of interesting approaches to pursue further, many of which we have discussed above, but which generally fall into two categories: (1) targeting of the host pro-inflammatory responses, through inhibition of interleukin and TLR pro-inflammatory pathways, or apoptosis and pyroptosis pathways;

and (2) inhibition of viral dissemination and spread through targeting of viral proteins necessary for viral entry or manipulation of host cells. The study of CMV has greatly expanded the fields of both virology and immunology due to the virus' capacity for modulation of the host-immune response, including its role as an opportunistic pathogen. Further work will improve our understanding of viral latency determinants, viral dissemination determinants, and the interplay between IRI, allogeneic immune responses, and viral pathogenesis.

References

1. Davison, A.J.; Eberle, R.; Ehlers, B.; Hayward, G.S.; McGeoch, D.J.; Minson, A.C.; Pellett, P.E.; Roizman, B.; Studdert, M.J.; Thiry, E. The order Herpesvirales. *Arch. Virol.* **2009**, *154*, 171–177, doi:10.1007/s00705-008-0278-4.
2. Whitley, R.J. Herpesviruses. In *Medical Microbiology*; Baron, S., Ed.; University of Texas Medical Branch at Galveston: Galveston, 1996 ISBN 0-9631172-1-1.
3. Gershon, A.A.; Breuer, J.; Cohen, J.I.; Cohrs, R.J.; Gershon, M.D.; Gilden, D.; Grose, C.; Hambleton, S.; Kennedy, P.G.E.; Oxman, M.N.; et al. Varicella zoster virus infection. *Nat. Rev. Dis. Prim.* **2015**, *1*, 15016, doi:10.1038/nrdp.2015.16.
4. Whitley, R.J.; Roizman, B. Herpes simplex virus infections. *Lancet* **2001**, *357*, 1513–1518, doi:10.1016/S0140-6736(00)04638-9.
5. Geyer, H.; Ettinger, J.; Möller, L.; Schmolz, E.; Nitsche, A.; Brune, W.; Heaggans, S.; Sandford, G.R.; Hayward, G.S.; Voigt, S. Rat cytomegalovirus (RCMV) English isolate and a newly identified Berlin isolate share similarities with but are separate as an anciently diverged clade from Mouse CMV and the Maastricht isolate of RCMV. *J. Gen. Virol.* **2015**, *96*, 1873–1882, doi:10.1099/vir.0.000109.
6. Crough, T.; Khanna, R. Immunobiology of human cytomegalovirus: from bench to bedside. *Clin. Microbiol. Rev.* **2009**, *22*, 76–98, doi:10.1128/CMR.00034-08.
7. Jackson, S.E.; Sedikides, G.X.; Okecha, G.; Poole, E.L.; Sinclair, J.H.; Wills, M.R. Latent Cytomegalovirus (CMV) Infection Does Not Detrimentally Alter T Cell Responses in the Healthy Old, But Increased Latent CMV Carriage Is Related to Expanded CMV-Specific T Cells. *Front. Immunol.* **2017**, *8*, 1–20, doi:10.3389/fimmu.2017.00733.

8. Azevedo, L.; Pierrotti, L.; Abdala, E.; Costa, S.; Strabelli, T.; Campos, S.; Ramos, J.; Latif, A.; Litvinov, N.; Maluf, N.; et al. Cytomegalovirus infection in transplant recipients. *Clinics* **2015**, *70*, 515–523, doi:10.6061/clinics/2015(07)09.
9. Boppana, S.B.; Ross, S.A.; Fowler, K.B. Congenital Cytomegalovirus Infection: Clinical Outcome. *Clin. Infect. Dis.* **2013**, *57*, S178–S181, doi:10.1093/cid/cit629.
10. Stone, R.C.; Micali, G.A.; Schwartz, R.A. Roseola infantum and its causal human herpesviruses. *Int. J. Dermatol.* **2014**, *53*, 397–403, doi:10.1111/ijd.12310.
11. Nowalk, A.; Green, M. Epstein-Barr Virus. *Microbiol. Spectr.* **2016**, *4*, 1–16, doi:10.1128/microbiolspec.DMIH2-0011-2015.
12. Mesri, E.A.; Cesarman, E.; Boshoff, C. Kaposi's sarcoma and its associated herpesvirus. *Nat. Rev. Cancer* **2010**, *10*, 707–719, doi:10.1038/nrc2888.
13. Zuhair, M.; Smit, G.S.A.; Wallis, G.; Jabbar, F.; Smith, C.; Devleeschauwer, B.; Griffiths, P. Estimation of the worldwide seroprevalence of cytomegalovirus: A systematic review and meta-analysis. *Rev. Med. Virol.* **2019**, *29*, e2034, doi:10.1002/rmv.2034.
14. Firth, C.; Harrison, R.; Ritchie, S.; Wardlaw, J.; Ferro, C.J.; Starr, J.M.; Deary, I.J.; Moss, P. Cytomegalovirus infection is associated with an increase in systolic blood pressure in older individuals. *QJM* **2016**, *109*, 595–600, doi:10.1093/qjmed/hcw026.
15. Savva, G.M.; Pachnio, A.; Kaul, B.; Morgan, K.; Huppert, F.A.; Brayne, C.; Moss, P.A.H. Cytomegalovirus infection is associated with increased mortality in the older population. *Aging Cell* **2013**, *12*, 381–387, doi:10.1111/accel.12059.
16. Fonseca Brito, L.; Brune, W.; Stahl, F.R. Cytomegalovirus (CMV) Pneumonitis:

- Cell Tropism, Inflammation, and Immunity. *Int. J. Mol. Sci.* **2019**, *20*, 3865, doi:10.3390/ijms20163865.
17. Travi, G.; Pergam, S.A. Cytomegalovirus Pneumonia in Hematopoietic Stem Cell Recipients. *J. Intensive Care Med.* **2014**, *29*, 200–212, doi:10.1177/0885066613476454.
 18. Bialas, K.M.; Permar, S.R. The March towards a Vaccine for Congenital CMV: Rationale and Models. *PLOS Pathog.* **2016**, *12*, e1005355, doi:10.1371/journal.ppat.1005355.
 19. Springer, K.L.; Weinberg, A. Cytomegalovirus infection in the era of HAART: fewer reactivations and more immunity. *J. Antimicrob. Chemother.* **2004**, *54*, 582–586, doi:10.1093/jac/dkh396.
 20. Baron, C.; Forconi, C.; Lebranchu, Y. Revisiting the effects of CMV on long-term transplant outcome. *Curr. Opin. Organ Transplant.* **2010**, *15*, 492–498, doi:10.1097/MOT.0b013e32833bd3b5.
 21. Johansson, I.; Andersson, R.; Friman, V.; Selimovic, N.; Hanzen, L.; Nasic, S.; Nyström, U.; Sigurdardottir, V. Cytomegalovirus infection and disease reduce 10-year cardiac allograft vasculopathy-free survival in heart transplant recipients. *BMC Infect. Dis.* **2015**, *15*, 1–9, doi:10.1186/s12879-015-1321-1.
 22. Ramanan, P.; Razonable, R.R. Cytomegalovirus infections in solid organ transplantation: a review. *Infect. Chemother.* **2013**, *45*, 260–71, doi:10.3947/ic.2013.45.3.260.
 23. Humar, A.; St. Louis, P.; Mazzulli, T.; Mcgeer, A.; Lipton, J.; Messner, H.; MacDonald, K.S.S.; Louis, P.S.; Mazzulli, T.; Mcgeer, A.; et al. Elevated Serum

- Cytokines Are Associated with Cytomegalovirus Infection and Disease in Bone Marrow Transplant Recipients. *J. Infect. Dis.* **1999**, *179*, 484–488, doi:10.1086/314602.
24. Ciaurriz, M.; Zabalza, A.; Beloki, L.; Mansilla, C.; Pérez-Valderrama, E.; Lachén, M.; Bandrés, E.; Olavarria, E.; Ramirez, N. The immune response to cytomegalovirus in allogeneic hematopoietic stem cell transplant recipients. *Cell. Mol. Life Sci.* **2015**, *72*, 4049–4062, doi:10.1007/s00018-015-1986-z.
25. Tao, R.; Xu, J.; Gao, H.; Zhao, W.; Shang, S. Characteristics and functions of human cytomegalovirus UL128 gene / protein. *Acta Virol.* **2014**, *58*, 103–107, doi:10.4149/av.
26. Farrell, H.E.; Lawler, C.; Oliveira, M.T.; Davis-Poynter, N.; Stevenson, P.G. Alveolar Macrophages Are a Prominent but Nonessential Target for Murine Cytomegalovirus Infecting the Lungs. *J. Virol.* **2016**, *90*, 2756–2766, doi:10.1128/JVI.02856-15.
27. Farrell, H.E.; Bruce, K.; Lawler, C.; Stevenson, P.G. Murine Cytomegalovirus Spread Depends on the Infected Myeloid Cell Type. *J. Virol.* **2019**, *93*, 1–12, doi:10.1128/JVI.00540-19.
28. Farrell, H.E.; Bruce, K.; Lawler, C.; Oliveira, M.; Cardin, R.; Davis-Poynter, N.; Stevenson, P.G. Murine Cytomegalovirus Spreads by Dendritic Cell Recirculation. *MBio* **2017**, *8*, 1–13, doi:10.1128/mBio.01264-17.
29. Farrell, H.E.; Bruce, K.; Ma, J.; Davis-Poynter, N.; Stevenson, P.G. Human cytomegalovirus US28 allows dendritic cell exit from lymph nodes. *J. Gen. Virol.* **2018**, *99*, 1509–1514, doi:10.1099/jgv.0.001154.

30. Beisser, P.S.; Vink, C.; Van Dam, J.G.; Grauls, G.; Vanherle, S.J. V.; Bruggeman, C.A. The R33 G Protein-Coupled Receptor Gene of Rat Cytomegalovirus Plays an Essential Role in the Pathogenesis of Viral Infection. *J. Virol.* **1998**, *72*, 2352–2363, doi:10.1128/JVI.72.3.2352-2363.1998.
31. Streblow, D.N.; Kreklywich, C.N.; Smith, P.; Soule, J.L.; Meyer, C.; Yin, M.; Beisser, P.; Vink, C.; Nelson, J.A.; Orloff, S.L. Rat Cytomegalovirus-Accelerated Transplant Vascular Sclerosis Is Reduced with Mutation of the Chemokine Receptor R33. *Am. J. Transplant.* **2005**, *5*, 436–442, doi:10.1111/j.1600-6143.2004.00711.x.
32. Farrell, H.E.; Abraham, A.M.; Cardin, R.D.; Sparre-Ulrich, A.H.; Rosenkilde, M.M.; Spiess, K.; Jensen, T.H.; Kledal, T.N.; Davis-Poynter, N. Partial Functional Complementation between Human and Mouse Cytomegalovirus Chemokine Receptor Homologues. *J. Virol.* **2011**, *85*, 6091–6095, doi:10.1128/JVI.02113-10.
33. Gugliesi, F.; Coscia, A.; Griffante, G.; Galitska, G.; Pasquero, S.; Albano, C.; Biolatti, M. Where do we stand after decades of studying human cytomegalovirus? *Microorganisms* **2020**, *8*, 685.
34. Crumpacker, C.S. Ganciclovir. *Drug Ther. (NY)*. **1996**, *335*, 721–729.
35. Chrisp, P.; Clissold, S.P. Foscarnet: A Review of its Antiviral Activity, Pharmacokinetic Properties and Therapeutic Use in Immunocompromised Patients with Cytomegalovirus Retinitis. *Drugs* **1991**, *41*, 104–129, doi:10.2165/00003495-199141010-00009.
36. Orloff, S.L.; Hwee, Y.-K.K.; Kreklywich, C.; Andoh, T.F.; Hart, E.; Smith, P.A.; Messaoudi, I.; Streblow, D.N. Cytomegalovirus latency promotes cardiac lymphoid

- neogenesis and accelerated allograft rejection in CMV Naive recipients. *Am. J. Transplant.* **2011**, *11*, 45–55, doi:10.1111/j.1600-6143.2010.03365.x.
37. de Smet, M.D.; Meenken, C.; Van Den Horn, G.J. Fomivirsen – a phosphorothioate oligonucleotide for the treatment of CMV retinitis. *Ocul. Immunol. Inflamm.* **1999**, *7*, 189–198, doi:10.1076/ocii.7.3.189.4007.
38. Anderholm, K.M.; Bierle, C.J.; Schleiss, M.R. Cytomegalovirus Vaccines: Current Status and Future Prospects. *Drugs* **2016**, *76*, 1625–1645, doi:10.1007/s40265-016-0653-5.
39. ELEK, S.D.; STERN, H. DEVELOPMENT OF A VACCINE AGAINST MENTAL RETARDATION CAUSED BY CYTOMEGALOVIRUS INFECTION IN UTERO. *Obstet. Gynecol. Surv. Lancet* **1974**, *29*, 534–535, doi:10.1097/00006254-197408000-00005.
40. Wang, D.; Freed, D.C.; He, X.; Li, F.; Tang, A.; Cox, K.S.; Dubey, S.A.; Cole, S.; Medi, M.B.; Liu, Y.; et al. A replication-defective human cytomegalovirus vaccine for prevention of congenital infection. *Sci. Transl. Med.* **2016**, *8*, 362ra145-362ra145, doi:10.1126/scitranslmed.aaf9387.
41. Liu, Y.; Freed, D.C.; Li, L.; Tang, A.; Li, F.; Murray, E.M.; Adler, S.P.; McVoy, M.A.; Rupp, R.E.; Barrett, D.; et al. A Replication-Defective Human Cytomegalovirus Vaccine Elicits Humoral Immune Responses Analogous to Those with Natural Infection. *J. Virol.* **2019**, *93*, 1–19, doi:10.1128/JVI.00747-19.
42. Cui, X.; Meza, B.P.; Adler, S.P.; McVoy, M.A. Cytomegalovirus vaccines fail to induce epithelial entry neutralizing antibodies comparable to natural infection. *Vaccine* **2008**, *26*, 5760–5766, doi:10.1016/j.vaccine.2008.07.092.

43. Adler, S.P.; Manganello, A.-M.; Lee, R.; McVoy, M.A.; Nixon, D.E.; Plotkin, S.; Mocarski, E.; Cox, J.H.; Fast, P.E.; Nesterenko, P.A.; et al. A Phase 1 Study of 4 Live, Recombinant Human Cytomegalovirus Towne/Toledo Chimera Vaccines in Cytomegalovirus–Seronegative Men. *J. Infect. Dis.* **2016**, *214*, 1341–1348, doi:10.1093/infdis/jiw365.
44. Fouts, A.E.; Chan, P.; Stephan, J.-P.; Vandlen, R.; Feierbach, B. Antibodies against the gH/gL/UL128/UL130/UL131 Complex Comprise the Majority of the Anti-Cytomegalovirus (Anti-CMV) Neutralizing Antibody Response in CMV Hyperimmune Globulin. *J. Virol.* **2012**, *86*, 7444–7447, doi:10.1128/JVI.00467-12.
45. Wussow, F.; Chiuppesi, F.; Martinez, J.; Campo, J.; Johnson, E.; Flechsig, C.; Newell, M.; Tran, E.; Ortiz, J.; La Rosa, C.; et al. Human Cytomegalovirus Vaccine Based on the Envelope gH/gL Pentamer Complex. *PLoS Pathog.* **2014**, *10*, doi:10.1371/journal.ppat.1004524.
46. Wussow, F.; Yue, Y.; Martinez, J.; Deere, J.D.; Longmate, J.; Herrmann, A.; Barry, P.A.; Diamond, D.J. A vaccine based on the rhesus cytomegalovirus UL128 complex induces broadly neutralizing antibodies in rhesus macaques. *J. virol* **2013**, *87*, 1322–32, doi:10.1128/JVI.01669-12.
47. Gonczol, E.; Ianacone, J.; Ho, W.; Starr, S.; Meignier, B.; Plotkin, S. Isolated gA/gB glycoprotein complex of human cytomegalovirus envelope induces humoral and cellular immune-responses in human volunteers. *Vaccine* **1990**, *8*, 130–136, doi:10.1016/0264-410X(90)90135-9.
48. Oram, J.D.; Downing, R.G.; Akrigg, A.; Dollery, A.A.; Duggleby, C.J.; Wilkinson, G.W.G.; Greenaway, P.J. Use of Recombinant Plasmids to Investigate the Structure

- of the Human Cytomegalovirus Genome. *J. Gen. Virol.* **1982**, *59*, 111–129, doi:10.1099/0022-1317-59-1-111.
49. Sijmons, S.; Van Ranst, M.; Maes, P. Genomic and Functional Characteristics of Human Cytomegalovirus Revealed by Next-Generation Sequencing. *Viruses* **2014**, *6*, 1049–1072, doi:10.3390/v6031049.
50. Meijer, H.; Dreesen, J.C.F.M.; van Boven, C.P.A. Molecular Cloning and Restriction Endonuclease Mapping of the Rat Cytomegalovirus Genome. *J. Gen. Virol.* **1986**, *67*, 1327–1342, doi:10.1099/0022-1317-67-7-1327.
51. Tandon, R.; Mocarski, E.S. Viral and host control of cytomegalovirus maturation. *Trends Microbiol.* **2012**, *20*, 392–401, doi:10.1016/j.tim.2012.04.008.
52. Reyda, S.; Tenzer, S.; Navarro, P.; Gebauer, W.; Saur, M.; Krauter, S.; Buscher, N.; Plachter, B. The Tegument Protein pp65 of Human Cytomegalovirus Acts as an Optional Scaffold Protein That Optimizes Protein Uploading into Viral Particles. *J. Virol.* **2014**, *88*, 9633–9646, doi:10.1128/jvi.01415-14.
53. Varnum, S.M.; Streblow, D.N.; Monroe, M.E.; Smith, P.; Auberry, K.J.; Paša-Tolić, L.; Wang, D.; Camp, D.G.; Rodland, K.; Wiley, S.; et al. Identification of Proteins in Human Cytomegalovirus (HCMV) Particles: the HCMV Proteome. *J. Virol.* **2004**, *78*, 10960–10966, doi:10.1128/JVI.78.20.10960-10966.2004.
54. Yu, X.; Jih, J.; Jiang, J.; Zhou, Z.H. Atomic structure of the human cytomegalovirus capsid with its securing tegument layer of pp150. *Science (80-.)*. **2017**, *356*, eaam6892, doi:10.1126/science.aam6892.
55. Kattenhorn, L.M.; Mills, R.; Wagner, M.; Lomsadze, A.; Makeev, V.; Borodovsky, M.; Ploegh, H.L.; Kessler, B.M. Identification of Proteins Associated with Murine

- Cytomegalovirus Virions. *J. Virol.* **2004**, 78, 11187–11197, doi:10.1128/JVI.78.20.11187-11197.2004.
56. Kalejta, R.F. Tegument Proteins of Human Cytomegalovirus. *Microbiol. Mol. Biol. Rev.* **2008**, 72, 249–265, doi:10.1128/MMBR.00040-07.
57. Nguyen, C.C.; Kamil, J.P. Pathogen at the gates: Human cytomegalovirus entry and cell tropism. *Viruses* 2018, 10.
58. Gardner, T.J.; Tortorella, D. Virion Glycoprotein-Mediated Immune Evasion by Human Cytomegalovirus: a Sticky Virus Makes a Slick Getaway. *Microbiol. Mol. Biol. Rev.* **2016**, 80, 663–677, doi:10.1128/MMBR.00018-16.
59. Kari, B.; Gehrz, R. A human cytomegalovirus glycoprotein complex designated gC-II is a major heparin-binding component of the envelope. *J. Virol.* **1992**, 66, 1761–1764, doi:10.1128/JVI.66.3.1761-1764.1992.
60. Mach, M.; Osinski, K.; Kropff, B.; Schloetzer-Schrehardt, U.; Krzyzaniak, M.; Britt, W. The Carboxy-Terminal Domain of Glycoprotein N of Human Cytomegalovirus Is Required for Virion Morphogenesis. *J. Virol.* **2007**, 81, 5212–5224, doi:10.1128/JVI.01463-06.
61. Krzyzaniak, M.; Mach, M.; Britt, W.J. The Cytoplasmic Tail of Glycoprotein M (gpUL100) Expresses Trafficking Signals Required for Human Cytomegalovirus Assembly and Replication. *J. Virol.* **2007**, 81, 10316–10328, doi:10.1128/JVI.00375-07.
62. Wille, P.T.; Wisner, T.W.; Ryckman, B.; Johnson, D.C. Human Cytomegalovirus (HCMV) Glycoprotein gB Promotes Virus Entry In Trans Acting as the Viral Fusion Protein Rather than as a Receptor-Binding Protein. *MBio* **2013**, 4, e00332-13,

doi:10.1128/mbio.00332-13.

63. Sharma, S.; Wisner, T.W.; Johnson, D.C.; Heldwein, E.E. HCMV gB shares structural and functional properties with gB proteins from other herpesviruses. *Virology* **2013**, *435*, 239–249, doi:10.1016/j.virol.2012.09.024.
64. Soroceanu, L.; Akhavan, A.; Cobbs, C.S. Platelet-derived growth factor- α receptor activation is required for human cytomegalovirus infection. *Nature* **2008**, *455*, 391–395, doi:10.1038/nature07209.
65. Feire, A.L.; Koss, H.; Compton, T. Cellular integrins function as entry receptors for human cytomegalovirus via a highly conserved disintegrin-like domain. *Proc. Natl. Acad. Sci. U. S. A.* **2004**, *101*, 15470–5, doi:10.1073/pnas.0406821101.
66. Feire, A.L.; Roy, R.M.; Manley, K.; Compton, T. The Glycoprotein B Disintegrin-Like Domain Binds Beta 1 Integrin To Mediate Cytomegalovirus Entry. *J. Virol.* **2010**, *84*, 10026–10037, doi:10.1128/JVI.00710-10.
67. Campadelli-Fiume, G.; Collins-McMillen, D.; Gianni, T.; Yurochko, A.D. Integrins as Herpesvirus Receptors and Mediators of the Host Signalosome. *Annu. Rev. Virol.* **2016**, *3*, 215–236, doi:10.1146/annurev-virology-110615-035618.
68. Wang, X.; Huong, S.-M.; Chiu, M.L.; Raab-Traub, N.; Huang, E.-S. Epidermal growth factor receptor is a cellular receptor for human cytomegalovirus. *Nature* **2003**, *424*, 456–461, doi:10.1038/nature01818.
69. Vanarsdall, A.L.; Ryckman, B.J.; Chase, M.C.; Johnson, D.C. Human Cytomegalovirus Glycoproteins gB and gH/gL Mediate Epithelial Cell-Cell Fusion When Expressed either in cis or in trans. *J. Virol.* **2008**, *82*, 11837–11850, doi:10.1128/JVI.01623-08.

70. Huber, M.T.; Compton, T. The Human Cytomegalovirus UL74 Gene Encodes the Third Component of the Glycoprotein H-Glycoprotein L-Containing Envelope Complex. *J. Virol.* **1998**, *72*, 8191–8197, doi:10.1128/JVI.72.10.8191-8197.1998.
71. Ryckman, B.J.; Rainish, B.L.; Chase, M.C.; Borton, J.A.; Nelson, J.A.; Jarvis, M.A.; Johnson, D.C. Characterization of the human cytomegalovirus gH/gL/UL128-131 complex that mediates entry into epithelial and endothelial cells. *J. Virol.* **2008**, *82*, 60–70, doi:10.1128/JVI.01910-07.
72. Caló, S.; Cortese, M.; Ciferri, C.; Bruno, L.; Gerrein, R.; Benucci, B.; Monda, G.; Gentile, M.; Kessler, T.; Uematsu, Y.; et al. The Human Cytomegalovirus UL116 Gene Encodes an Envelope Glycoprotein Forming a Complex with gH Independently from gL. *J. Virol.* **2016**, *90*, 4926–4938, doi:10.1128/jvi.02517-15.
73. Li, L.; Nelson, J.A.; Britt, W.J. Glycoprotein H-related complexes of human cytomegalovirus: identification of a third protein in the gCIII complex. *J. Virol.* **1997**, *71*, 3090–3097, doi:10.1128/JVI.71.4.3090-3097.1997.
74. Ciferri, C.; Chandramouli, S.; Donnarumma, D.; Nikitin, P.A.; Cianfrocco, M.A.; Gerrein, R.; Feire, A.L.; Barnett, S.W.; Lilja, A.E.; Rappuoli, R.; et al. Structural and biochemical studies of HCMV gH/gL/gO and Pentamer reveal mutually exclusive cell entry complexes. *Proc. Natl. Acad. Sci. U. S. A.* **2015**, *112*, 1767–1772, doi:10.1073/pnas.1424818112.
75. Li, G.; Nguyen, C.C.; Ryckman, B.J.; Britt, W.J.; Kamil, J.P. A viral regulator of glycoprotein complexes contributes to human cytomegalovirus cell tropism. *Proc. Natl. Acad. Sci.* **2015**, *112*, 4471–4476, doi:10.1073/pnas.1419875112.
76. Liu, J.; Jardetzky, T.S.; Chin, A.L.; Johnson, D.C.; Vanarsdall, A.L. The Human

- Cytomegalovirus Trimer and Pentamer Promote Sequential Steps in Entry into Epithelial and Endothelial Cells at Cell Surfaces and Endosomes. *J. Virol.* **2018**, *92*, 1–15, doi:10.1128/JVI.01336-18.
77. Li, Q.; Wilkie, A.R.; Weller, M.; Liu, X.; Cohen, J.I. THY-1 Cell Surface Antigen (CD90) Has an Important Role in the Initial Stage of Human Cytomegalovirus Infection. *PLoS Pathog.* **2015**, *11*, 1–26, doi:10.1371/journal.ppat.1004999.
78. Li, Q.; Fischer, E.; Cohen, J.I. Cell Surface THY-1 Contributes to Human Cytomegalovirus Entry via a Macropinocytosis-Like Process. *J. Virol.* **2016**, *90*, 9766–9781, doi:10.1128/jvi.01092-16.
79. Nogalski, M.T.; Chan, G.; Stevenson, E. V.; Gray, S.; Yurochko, A.D. Human Cytomegalovirus-Regulated Paxillin in Monocytes Links Cellular Pathogenic Motility to the Process of Viral Entry. *J. Virol.* **2011**, *85*, 1360–1369, doi:10.1128/jvi.02090-10.
80. Wang, X.; Huang, D.Y.; Huong, S.M.; Huang, E.S. Integrin $\alpha\text{v}\beta\text{3}$ is a coreceptor for human cytomegalovirus. *Nat. Med.* **2005**, *11*, 515–521, doi:10.1038/nm1236.
81. Hochdorfer, D.; Florin, L.; Sinzger, C.; Lieber, D. Tetraspanin CD151 Promotes Initial Events in Human Cytomegalovirus Infection. *J. Virol.* **2016**, *90*, 6430–6442, doi:10.1128/jvi.00145-16.
82. Viswanathan, K.; Verweij, M.C.; John, N.; Malouli, D.; Früh, K. Quantitative membrane proteomics reveals a role for tetraspanin enriched microdomains during entry of human cytomegalovirus. *PLoS One* **2017**, *12*, 1–27, doi:10.1371/journal.pone.0187899.
83. Gatault, P.; Jones, I.K.A.; Meyer, C.; Kreklywich, C.N.; Alexander, T.; Smith, P.;

- Denton, M.; Powell, J.; Orloff, S.L.; Streblow, D.N. Rat and Human Cytomegalovirus ORF116 Encodes a Virion Envelope Glycoprotein Required for Infectivity. *Viol. Submitt. Sept. 2020* **2020**.
84. Gardner, T.J.; Hernandez, R.E.; Noriega, V.M.; Tortorella, D. Human cytomegalovirus gH stability and trafficking are regulated by ER-associated degradation and transmembrane architecture. *Sci. Rep.* **2016**, *6*, 23692, doi:10.1038/srep23692.
85. Vanarsdall, A.L.; Chase, M.C.; Johnson, D.C. Human Cytomegalovirus Glycoprotein gO Complexes with gH/gL, Promoting Interference with Viral Entry into Human Fibroblasts but Not Entry into Epithelial Cells. *J. Virol.* **2011**, *85*, 11638–11645, doi:10.1128/jvi.05659-11.
86. Hetzenecker, S.; Helenius, A.; Krzyzaniak, M.A. HCMV Induces Macropinocytosis for Host Cell Entry in Fibroblasts. *Traffic* **2016**, *17*, 351–368, doi:10.1111/tra.12355.
87. Zhou, M.; Lanchy, J.-M.; Ryckman, B.J. Human Cytomegalovirus gH/gL/gO Promotes the Fusion Step of Entry into All Cell Types, whereas gH/gL/UL128-131 Broadens Virus Tropism through a Distinct Mechanism. *J. Virol.* **2015**, *89*, 8999–9009, doi:10.1128/JVI.01325-15.
88. Stegmann, C.; Hochdorfer, D.; Lieber, D.; Subramanian, N.; Stöhr, D.; Laib Sampaio, K.; Sinzger, C. A derivative of platelet-derived growth factor receptor alpha binds to the trimer of human cytomegalovirus and inhibits entry into fibroblasts and endothelial cells. *PLoS Pathog.* **2017**, *13*, 1–27, doi:10.1371/journal.ppat.1006273.

89. Kabanova, A.; Marcandalli, J.; Zhou, T.; Bianchi, S.; Baxa, U.; Tsybovsky, Y.; Lilleri, D.; Silacci-Fregni, C.; Foglierini, M.; Fernandez-Rodriguez, B.M.; et al. Platelet-derived growth factor- α receptor is the cellular receptor for human cytomegalovirus gH/gL/gO trimer. *Nat. Microbiol.* **2016**, *1*, 16082, doi:10.1038/nmicrobiol.2016.82.
90. Wu, Y.; Prager, A.; Boos, S.; Resch, M.; Brizic, I.; Mach, M.; Wildner, S.; Scrivano, L.; Adler, B. Human cytomegalovirus glycoprotein complex gH/gL/gO uses PDGFR- α as a key for entry. *PLoS Pathog.* **2017**, *13*, 1–24, doi:10.1371/journal.ppat.1006281.
91. Patrone, M.; Secchi, M.; Fiorina, L.; Ierardi, M.; Milanesi, G.; Gallina, A. Human cytomegalovirus UL130 protein promotes endothelial cell infection through a producer cell modification of the virion. *J. Virol.* **2005**, *79*, 8361–8373, doi:10.1128/JVI.79.13.8361-8373.2005.
92. Adler, B.; Scrivano, L.; Ruzcics, Z.; Rupp, B.; Sinzger, C.; Koszinowski, U. Role of human cytomegalovirus UL131A in cell type-specific virus entry and release. *J. Gen. Virol.* **2006**, *87*, 2451–2460, doi:10.1099/vir.0.81921-0.
93. Hahn, G.; Revello, M.G.; Patrone, M.; Percivalle, E.; Campanini, G.; Sarasini, A.; Wagner, M.; Gallina, A.; Milanesi, G.; Koszinowski, U.; et al. Human Cytomegalovirus UL131-128 Genes Are Indispensable for Virus Growth in Endothelial Cells and Virus Transfer to Leukocytes. *J. Virol.* **2004**, *78*, 10023–10033, doi:10.1128/JVI.78.18.10023.
94. Martinez-Martin, N.; Marcandalli, J.; Huang, C.S.; Arthur, C.P.; Perotti, M.; Foglierini, M.; Ho, H.; Dosey, A.M.; Shriver, S.; Payandeh, J.; et al. An Unbiased

- Screen for Human Cytomegalovirus Identifies Neuropilin-2 as a Central Viral Receptor. *Cell* **2018**, *174*, 1158-1171.e19, doi:10.1016/j.cell.2018.06.028.
95. Ryckman, B.J.; Jarvis, M.A.; Drummond, D.D.; Nelson, J.A.; Johnson, D.C. Human Cytomegalovirus Entry into Epithelial and Endothelial Cells Depends on Genes UL128 to UL150 and Occurs by Endocytosis and Low-pH Fusion. *J. Virol.* **2006**, *80*, 710–722, doi:10.1128/JVI.80.2.710-722.2006.
96. Gerna, G.; Percivalle, E.; Lilleri, D.; Lozza, L.; Fornara, C.; Hahn, G.; Baldanti, F.; Revello, M.G. Dendritic-cell infection by human cytomegalovirus is restricted to strains carrying functional UL131-128 genes and mediates efficient viral antigen presentation to CD8+ T cells. *J. Gen. Virol.* **2005**, *86*, 275–284, doi:10.1099/vir.0.80474-0.
97. Ryckman, B.J.; Chase, M.C.; Johnson, D.C. HCMV gH/gL/UL128-131 interferes with virus entry into epithelial cells: evidence for cell type-specific receptors. *Proc. Natl. Acad. Sci. U. S. A.* **2008**, *105*, 14118–23, doi:10.1073/pnas.0804365105.
98. Nogalski, M.T.; Chan, G.C.T.; Stevenson, E. V.; Collins-McMillen, D.K.; Yurochko, A.D. The HCMV gH/gL/UL128-131 Complex Triggers the Specific Cellular Activation Required for Efficient Viral Internalization into Target Monocytes. *PLoS Pathog.* **2013**, *9*, e1003463, doi:10.1371/journal.ppat.1003463.
99. Xiaofei, E.; Meraner, P.; Lu, P.; Perreira, J.M.; Aker, A.M.; McDougall, W.M.; Zhuge, R.; Chan, G.C.; Gerstein, R.M.; Caposio, P.; et al. OR14I1 is a receptor for the human cytomegalovirus pentameric complex and defines viral epithelial cell tropism. *Proc. Natl. Acad. Sci. U. S. A.* **2019**, *116*, 7043–7052, doi:10.1073/pnas.1814850116.

100. Vanarsdall, A.L.; Pritchard, S.R.; Wisner, T.W.; Liu, J.; Jardetzky, T.S.; Johnson, D.C. CD147 Promotes Entry of Pentamer-Expressing Human Cytomegalovirus into Epithelial and Endothelial Cells. *MBio* **2018**, *9*, 1–19, doi:10.1128/mbio.00781-18.
101. Lilja, A.E.; Shenk, T. Efficient replication of rhesus cytomegalovirus variants in multiple rhesus and human cell types. *Proc. Natl. Acad. Sci.* **2008**, *105*, 19950–19955, doi:10.1073/pnas.0811063106.
102. Auerbach, M.; Yan, D.; Fouts, A.; Xu, M.; Estevez, A.; Austin, C.D.; Bazan, F.; Feierbach, B. Characterization of the guinea pig CMV gH/gL/GP129/GP131/GP133 complex in infection and spread. *Virology* **2013**, *441*, 75–84, doi:10.1016/j.virol.2013.03.008.
103. Yamada, S.; Fukuchi, S.; Hashimoto, K.; Fukui, Y.; Tsuda, M.; Kataoka, M.; Katano, H.; Inoue, N. Guinea pig cytomegalovirus GP129/131/133, homologues of human cytomegalovirus UL128/130/131A, are necessary for infection of monocytes and macrophages. *J. Gen. Virol.* **2014**, *95*, 1376–1382, doi:10.1099/vir.0.064527-0.
104. Saederup, N.; Aguirre, S.A.; Sparer, T.E.; Bouley, D.M.; Mocarski, E.S. Murine Cytomegalovirus CC Chemokine Homolog MCK-2 (m131-129) Is a Determinant of Dissemination That Increases Inflammation at Initial Sites of Infection. *J. Virol.* **2001**, *75*, 9966–9976, doi:10.1128/JVI.75.20.9966-9976.2001.
105. Wagner, F.M.; Brizic, I.; Prager, A.; Trsan, T.; Arapovic, M.; Lemmermann, N.A.W.; Podlech, J.; Reddehase, M.J.; Lemnitzer, F.; Bosse, J.B.; et al. The Viral Chemokine MCK-2 of Murine Cytomegalovirus Promotes Infection as Part of a gH/gL/MCK-2 Complex. *PLoS Pathog.* **2013**, *9*, e1003493, doi:10.1371/journal.ppat.1003493.

106. Scrivano, L.; Esterlechner, J.; Mühlbach, H.; Ettischer, N.; Hagen, C.; Grünewald, K.; Mohr, C.A.; Ruzsics, Z.; Koszinowski, U.; Adler, B. The m74 Gene Product of Murine Cytomegalovirus (MCMV) Is a Functional Homolog of Human CMV gO and Determines the Entry Pathway of MCMV. *J. Virol.* **2010**, *84*, 4469–4480, doi:10.1128/JVI.02441-09.
107. Coleman, S.; Hornig, J.; Maddux, S.; Choi, K.Y.; McGregor, A. Viral Glycoprotein Complex Formation, Essential Function and Immunogenicity in the Guinea Pig Model for Cytomegalovirus. *PLoS One* **2015**, *10*, e0135567, doi:10.1371/journal.pone.0135567.
108. Wang, H.; Yao, Y.; Huang, C.; Chen, Q.; Chen, J.; Chen, Z. Immunization with cytomegalovirus envelope glycoprotein M and glycoprotein N DNA vaccines can provide mice with complete protection against a lethal murine cytomegalovirus challenge. *Virol. Sin.* **2013**, *28*, 174–182, doi:10.1007/s12250-013-3330-9.
109. Scalzo, A.A.; Dallas, P.B.; Forbes, C.A.; Mikosza, A.S.J.; Fleming, P.; Lathbury, L.J.; Lyons, P.A.; Laferté, S.; Craggs, M.M.; Loh, L.C. The murine cytomegalovirus M73.5 gene, a member of a 3' co-terminal alternatively spliced gene family, encodes the gp24 virion glycoprotein. *Virology* **2004**, *329*, 234–250, doi:10.1016/j.virol.2004.08.015.
110. Scalzo, A.A.; Forbes, C.A.; Davis-Poynter, N.J.; Farrell, H.E.; Lyons, P.A. DNA sequence and transcriptional analysis of the glycoprotein M gene of murine cytomegalovirus. *J. Gen. Virol.* **1995**, *76*, 2895–2901, doi:10.1099/0022-1317-76-11-2895.
111. El-Hamdi, N.S.; Choi, K.Y.; McGregor, A. Guinea pig cytomegalovirus trimer

- complex gH/gL/gO uses PDGFRA as universal receptor for cell fusion and entry. *Virology* **2020**, *548*, 236–249, doi:10.1016/j.virol.2020.05.012.
112. Yue, Y.; Kaur, A.; Lilja, A.; Diamond, D.J.; Walter, M.R.; Barry, P.A. The susceptibility of primary cultured rhesus macaque kidney epithelial cells to rhesus cytomegalovirus strains. *J. Gen. Virol.* **2016**, *97*, 1426–1438, doi:10.1099/jgv.0.000455.
113. Oxford, K.L.; Eberhardt, M.K.; Yang, K.; Strelow, L.; Kelly, S.; Zhou, S.-S.; Barry, P.A. Protein coding content of the ULb' region of wild-type rhesus cytomegalovirus. *Virology* **2008**, *373*, 181–188, doi:10.1016/j.virol.2007.10.040.
114. Miura, T.; Makino, R.; Yamada, K.; Matsuura, M.; Okumura, M.; Yamada, S.; Watanabe, S.; Inoue, N. Differences in the effects of mutations in GP131, a guinea pig cytomegalovirus homologue of pentameric complex component UL130, on macrophage and epithelial cell infection. *J. Gen. Virol.* **2018**, *99*, 1425–1431, doi:10.1099/jgv.0.001137.
115. Coleman, S.; Choi, K.Y.; Root, M.; McGregor, A. A Homolog Pentameric Complex Dictates Viral Epithelial Tropism, Pathogenicity and Congenital Infection Rate in Guinea Pig Cytomegalovirus. *PLoS Pathog.* **2016**, *12*, 1–38, doi:10.1371/journal.ppat.1005755.
116. Coleman, S.; Choi, K.Y.; McGregor, A. Cytomegalovirus UL128 homolog mutants that form a pentameric complex produce virus with impaired epithelial and trophoblast cell tropism and altered pathogenicity in the guinea pig. *Virology* **2017**, *509*, 205–221, doi:10.1016/j.virol.2017.06.008.
117. McVoy, M.A.; Wang, J. Ben; Dittmer, D.P.; Bierle, C.J.; Swanson, E.C.; Fernández-

- Alarcón, C.; Hernandez-Alvarado, N.; Zabeli, J.C.; Schleiss, M.R. Repair of a Mutation Disrupting the Guinea Pig Cytomegalovirus Pentameric Complex Acquired during Fibroblast Passage Restores Pathogenesis in Immune-Suppressed Guinea Pigs and in the Context of Congenital Infection. *J. Virol.* **2016**, *90*, 7715–7727, doi:10.1128/JVI.00320-16.
118. Lagenaur, L.A.; Manning, W.C.; Vieira, J.; Martens, C.L.; Mocarski, E.S. Structure and function of the murine cytomegalovirus *sgg1* gene: a determinant of viral growth in salivary gland acinar cells. *J. Virol.* **1994**, *68*, 7717–7727, doi:10.1128/JVI.68.12.7717-7727.1994.
119. Manning, W.C.; Stoddart, C.A.; Lagenaur, L.A.; Abenes, G.B.; Mocarski, E.S. Cytomegalovirus determinant of replication in salivary glands. *J. Virol.* **1992**, *66*, 3794–3802, doi:10.1128/JVI.66.6.3794-3802.1992.
120. Stahl, F.R.; Keyser, K.A.; Heller, K.; Bischoff, Y.; Halle, S.; Wagner, K.; Messerle, M.; Förster, R. Mck2-dependent infection of alveolar macrophages promotes replication of MCMV in nodular inflammatory foci of the neonatal lung. *Mucosal Immunol.* **2015**, *8*, 57–67, doi:10.1038/mi.2014.42.
121. Farrell, H.E.; Bruce, K.; Redwood, A.J.; Stevenson, P.G. Murine cytomegalovirus disseminates independently of CX3CR1, CCL2 or its m131/m129 chemokine homologue. *J. Gen. Virol.* **2019**, *100*, 1695–1700, doi:10.1099/jgv.0.001333.
122. Fleming, P.; Davis-Poynter, N.; Degli-Esposti, M.; Densley, E.; Papadimitriou, J.; Shellam, G.; Farrell, H. The murine cytomegalovirus chemokine homolog, m131/129, is a determinant of viral pathogenicity. *J. Virol.* **1999**, *73*, 6800–9.
123. Kaptein, S.J.F.; Van Cleef, K.W.R.; Gruijthuijsen, Y.K.; Beuken, E.V.H.; Van

- Buggenhout, L.; Beisser, P.S.; Stassen, F.R.M.; Bruggeman, C.A.; Vink, C. The r131 gene of rat cytomegalovirus encodes a proinflammatory CC chemokine homolog which is essential for the production of infectious virus in the salivary glands. *Virus Genes* **2004**, *29*, 43–61, doi:10.1023/B:VIRU.0000032788.53592.7c.
124. Oxford, K.L.; Strelow, L.; Yue, Y.; Chang, W.L.W.; Schmidt, K.A.; Diamond, D.J.; Barry, P.A. Open Reading Frames Carried on UL/b' Are Implicated in Shedding and Horizontal Transmission of Rhesus Cytomegalovirus in Rhesus Monkeys. *J. Virol.* **2011**, *85*, 5105–5114, doi:10.1128/JVI.02631-10.
125. MacDonald, M.R.; Burney, M.W.; Resnick, S.B.; Virgin, H.W. Spliced mRNA Encoding the Murine Cytomegalovirus Chemokine Homolog Predicts a β Chemokine of Novel Structure. *J. Virol.* **1999**, *73*, 3682–3691, doi:10.1128/JVI.73.5.3682-3691.1999.
126. Marcinowski, L.; Lidschreiber, M.; Windhager, L.; Rieder, M.; Bosse, J.B.; Rädle, B.; Bonfert, T.; Györy, I.; de Graaf, M.; da Costa, O.P.; et al. Real-time Transcriptional Profiling of Cellular and Viral Gene Expression during Lytic Cytomegalovirus Infection. *PLoS Pathog.* **2012**, *8*, e1002908, doi:10.1371/journal.ppat.1002908.
127. Yamada, S.; Nozawa, N.; Katano, H.; Fukui, Y.; Tsuda, M.; Tsutsui, Y.; Kurane, I.; Inoue, N. Characterization of the guinea pig cytomegalovirus genome locus that encodes homologs of human cytomegalovirus major immediate-early genes, UL128, and UL130. *Virology* **2009**, *391*, 99–106, doi:10.1016/j.virol.2009.05.034.
128. Akter, P.; Cunningham, C.; McSharry, B.P.; Dolan, A.; Addison, C.; Dargan, D.J.; Hassan-Walker, A.F.; Emery, V.C.; Griffiths, P.D.; Wilkinson, G.W.G.; et al. Two

- novel spliced genes in human cytomegalovirus. *J. Gen. Virol.* **2003**, *84*, 1117–1122, doi:10.1099/vir.0.18952-0.
129. Jordan, S.; Krause, J.; Prager, A.; Mitrovic, M.; Jonjic, S.; Koszinowski, U.H.; Adler, B. Virus Progeny of Murine Cytomegalovirus Bacterial Artificial Chromosome pSM3fr Show Reduced Growth in Salivary Glands due to a Fixed Mutation of MCK-2. *J. Virol.* **2011**, *85*, 10346–10353, doi:10.1128/JVI.00545-11.
130. Kanai, K.; Yamada, S.; Yamamoto, Y.; Fukui, Y.; Kurane, I.; Inoue, N. Re-evaluation of the genome sequence of guinea pig cytomegalovirus. *J. Gen. Virol.* **2011**, *92*, 1005–1020, doi:10.1099/vir.0.027789-0.
131. Straschewski, S.; Patrone, M.; Walther, P.; Gallina, A.; Mertens, T.; Frascaroli, G. Protein pUL128 of Human Cytomegalovirus Is Necessary for Monocyte Infection and Blocking of Migration. *J. Virol.* **2011**, *85*, 5150–5158, doi:10.1128/JVI.02100-10.
132. Vink, C.; Beuken, E.; Bruggeman, C.A. Complete DNA sequence of the rat cytomegalovirus genome. *J. Virol.* **2000**, *74*, 7656–7665, doi:10.1128/JVI.74.16.7656-7665.2000.Updated.
133. Vomaske, J.; Denton, M.; Kreklywich, C.; Andoh, T.; Osborn, J.M.; Chen, D.; Messaoudi, I.; Orloff, S.L.; Streblow, D.N. Cytomegalovirus CC chemokine promotes immune cell migration. *J. Virol.* **2012**, *86*, 11833–11844, doi:10.1128/JVI.00452-12.
134. Hui-hui, G.; Ran, T.; Qi, Z.; Jun, X.; Shi-qiang, S. Recombinant HCMV UL128 expression and functional identification of PBMC-attracting activity in vitro. *Arch. Virol.* **2013**, *158*, 173–177, doi:10.1007/s00705-012-1378-8.

135. Malkowska, M.; Kokoszynska, K.; Dymecka, M.; Rychlewski, L.; Wyrwicz, L.S. Alphaherpesvirinae and Gammaherpesvirinae glycoprotein L and CMV UL130 originate from chemokines. *Viol. J.* **2013**, *10*, 1, doi:10.1186/1743-422X-10-1.
136. Frascaroli, G.; Varani, S.; Moepps, B.; Sinzger, C.; Landini, M.P.; Mertens, T. Human Cytomegalovirus Subverts the Functions of Monocytes, Impairing Chemokine-Mediated Migration and Leukocyte Recruitment. *J. Virol.* **2006**, *80*, 7578–7589, doi:10.1128/JVI.02421-05.
137. Saederup, N.; Lin, Y.C.; Dairaghi, D.J.; Schall, T.J.; Mocarski, E.S. Cytomegalovirus-encoded beta chemokine promotes monocyte-associated viremia in the host. *Proc. Natl. Acad. Sci.* **1999**, *96*, 10881–10886, doi:10.1073/pnas.96.19.10881.
138. Bechtel, J.T.; Shenk, T. Human Cytomegalovirus UL47 Tegument Protein Functions after Entry and before Immediate-Early Gene Expression. *J. Virol.* **2002**, *76*, 1043–1050, doi:10.1128/JVI.76.3.1043–1050.2002.
139. Ogawa-Goto, K.; Tanaka, K.; Gibson, W.; Moriishi, E.; Miura, Y.; Kurata, T.; Irie, S.; Sata, T. Microtubule Network Facilitates Nuclear Targeting of Human Cytomegalovirus Capsid. *J. Virol.* **2003**, *77*, 8541–8547, doi:10.1128/JVI.77.15.8541-8547.2003.
140. Maurer, U.E.; Sodeik, B.; Grunewald, K. Native 3D intermediates of membrane fusion in herpes simplex virus 1 entry. *Proc. Natl. Acad. Sci.* **2008**, *105*, 10559–10564, doi:10.1073/pnas.0801674105.
141. Kilcher, S.; Mercer, J. DNA virus uncoating. *Virology* **2015**, *479–480*, 578–590, doi:10.1016/j.virol.2015.01.024.

142. Sodeik, B.; Ebersold, M.W.; Helenius, A. Microtubule-mediated Transport of Incoming Herpes Simplex Virus 1 Capsids to the Nucleus. *J. Cell Biol.* **1997**, *136*, 1007–1021, doi:10.1083/jcb.136.5.1007.
143. Xu, Y.; Cei, S.A.; Rodriguez Huete, A.; Colletti, K.S.; Pari, G.S. Human Cytomegalovirus DNA Replication Requires Transcriptional Activation via an IE2- and UL84-Responsive Bidirectional Promoter Element within oriLyt. *J. Virol.* **2004**, *78*, 11664–11677, doi:10.1128/jvi.78.21.11664-11677.2004.
144. Plafker, S.M.; Gibson, W. Cytomegalovirus Assembly Protein Precursor and Proteinase Precursor Contain Two Nuclear Localization Signals That Mediate Their Own Nuclear Translocation and That of the Major Capsid Protein. *J. Virol.* **1998**, *72*, 7722–7732, doi:10.1128/JVI.72.10.7722-7732.1998.
145. Mettenleiter, T.C. Herpesvirus Assembly and Egress. *J. Virol.* **2002**, *76*, 1537–1547, doi:10.1128/JVI.76.4.1537-1547.2002.
146. Marschall, M.; Muller, Y.A.; Diewald, B.; Sticht, H.; Milbradt, J. The human cytomegalovirus nuclear egress complex unites multiple functions: Recruitment of effectors, nuclear envelope rearrangement, and docking to nuclear capsids. *Rev. Med. Virol.* **2017**, *27*, e1934, doi:10.1002/rmv.1934.
147. Milbradt, J.; Sonntag, E.; Wagner, S.; Strojjan, H.; Wangen, C.; Lenac Rovis, T.; Lisnic, B.; Jonjic, S.; Sticht, H.; Britt, W.; et al. Human Cytomegalovirus Nuclear Capsids Associate with the Core Nuclear Egress Complex and the Viral Protein Kinase pUL97. *Viruses* **2018**, *10*, 35, doi:10.3390/v10010035.
148. Kuan, M.I.; O’Dowd, J.M.; Chughtai, K.; Hayman, I.; Brown, C.J.; Fortunato, E.A. Human Cytomegalovirus nuclear egress and secondary envelopment are negatively

- affected in the absence of cellular p53. *Virology* **2016**, *497*, 279–293, doi:10.1016/j.virol.2016.07.021.
149. Close, W.L.; Glassbrook, J.E.; Gurczynski, S.J.; Pellett, P.E. Infection-Induced Changes Within the Endocytic Recycling Compartment Suggest a Roadmap of Human Cytomegalovirus Egress. *Front. Microbiol.* **2018**, *9*, 1–15, doi:10.3389/fmicb.2018.01888.
150. Sanchez, V.; Greis, K.D.; Sztul, E.; Britt, W.J. Accumulation of Virion Tegument and Envelope Proteins in a Stable Cytoplasmic Compartment during Human Cytomegalovirus Replication: Characterization of a Potential Site of Virus Assembly. *J. Virol.* **2000**, *74*, 975–986, doi:10.1128/JVI.74.2.975-986.2000.
151. Cappadona, I.; Villinger, C.; Schutzius, G.; Mertens, T.; von Einem, J. Human Cytomegalovirus pUL47 Modulates Tegumentation and Capsid Accumulation at the Viral Assembly Complex. *J. Virol.* **2015**, *89*, 7314–7328, doi:10.1128/JVI.00603-15.
152. Johnson, D.C.; Baines, J.D. Herpesviruses remodel host membranes for virus egress. *Nat. Rev. Microbiol.* **2011**, *9*, 382–394, doi:10.1038/nrmicro2559.
153. Ahlqvist, J.; Mocarski, E. Cytomegalovirus UL103 Controls Virion and Dense Body Egress. *J. Virol.* **2011**, *85*, 5125–5135, doi:10.1128/JVI.01682-10.
154. Collins-McMillen, D.; Buehler, J.; Peppenelli, M.; Goodrum, F. Molecular Determinants and the Regulation of Human Cytomegalovirus Latency and Reactivation. *Viruses* **2018**, *10*, 444, doi:10.3390/v10080444.
155. Goodrum, F.D.; Jordan, C.T.; High, K.; Shenk, T. Human cytomegalovirus gene expression during infection of primary hematopoietic progenitor cells: A model for

- latency. *Proc. Natl. Acad. Sci.* **2002**, *99*, 16255–16260, doi:10.1073/pnas.252630899.
156. Crawford, L.B.; Caposio, P.; Kreklywich, C.; Pham, A.H.; Hancock, M.H.; Jones, T.A.; Smith, P.P.; Yurochko, A.D.; Nelson, J.A.; Streblow, D.N. Human Cytomegalovirus US28 Ligand Binding Activity Is Required for Latency in CD34 + Hematopoietic Progenitor Cells and Humanized NSG Mice. *MBio* **2019**, *10*, doi:10.1128/mBio.01889-19.
157. Mikell, I.; Crawford, L.B.; Hancock, M.H.; Mitchell, J.; Buehler, J.; Goodrum, F.; Nelson, J.A. HCMV miR-US22 down-regulation of EGR-1 regulates CD34+ hematopoietic progenitor cell proliferation and viral reactivation. *PLOS Pathog.* **2019**, *15*, e1007854, doi:10.1371/journal.ppat.1007854.
158. Streblow, D.N.; Nelson, J.A. Models of HCMV latency and reactivation. *Trends Microbiol.* **2003**, *11*, 293–295, doi:10.1016/S0966-842X(03)00149-5.
159. Krishna, B.A.; Poole, E.L.; Jackson, S.E.; Smit, M.J.; Wills, M.R.; Sinclair, J.H. Latency-Associated Expression of Human Cytomegalovirus US28 Attenuates Cell Signaling Pathways To Maintain Latent Infection. *MBio* **2017**, *8*, 1–21, doi:10.1128/mBio.01754-17.
160. Humby, M.S.; O'Connor, C.M. Human Cytomegalovirus US28 Is Important for Latent Infection of Hematopoietic Progenitor Cells. *J. Virol.* **2015**, *90*, 2959–2970, doi:10.1128/jvi.02507-15.
161. Fischer, S.; Glas, K.E. A Review of cardiac transplantation. *Anesthesiol. Clin.* **2013**, *31*, 383–403, doi:10.1016/j.anclin.2013.01.003.
162. Southard, M.D, J.H.; Belzer, M.D, F.O. ORGAN PRESERVATION. *Annu. Rev.*

- Med.* **1995**, *46*, 235–247, doi:10.1146/annurev.med.46.1.235.
163. Lutz, J.; Thürmel, K.; Heemann, U. Anti-inflammatory treatment strategies for ischemia/reperfusion injury in transplantation. *J. Inflamm. (Lond)*. **2010**, *7*, 27, doi:10.1186/1476-9255-7-27.
164. Cavalera, M.; Frangogiannis, N. Targeting the Chemokines in Cardiac Repair. *Curr. Pharm. Des.* **2014**, *20*, 1971–1979, doi:10.2174/13816128113199990449.
165. Davis, M.K.; Hunt, S.A. State of the art: Cardiac transplantation. *Trends Cardiovasc. Med.* **2014**, *24*, 341–349, doi:10.1016/j.tcm.2014.08.004.
166. Colvin-Adams, M.; Agnihotri, A. Cardiac allograft vasculopathy: Current knowledge and future direction. *Clin. Transplant.* **2011**, *25*, 175–184, doi:10.1111/j.1399-0012.2010.01307.x.
167. Costello, J.P.; Mohanakumar, T.; Nath, D.S. Mechanisms of chronic cardiac allograft rejection. *Texas Hear. Inst. J.* **2013**, *40*, 395–399.
168. Loupy, A.; Toquet, C.; Rouvier, P.; Beuscart, T.; Bories, M.C.; Varnous, S.; Guillemain, R.; Pattier, S.; Suberbielle, C.; Leprince, P.; et al. Late failing heart allografts: Pathology of cardiac allograft vasculopathy and association with antibody-mediated rejection. *Am. J. Transplant.* **2016**, *16*, 111–120, doi:10.1111/ajt.13529.
169. Hasegawa, T.; Visovatti, S.H.; Hyman, M.C.; Hayasaki, T.; Pinsky, D.J. Heterotopic vascularized murine cardiac transplantation to study graft arteriopathy. **2007**, *2*, 471–480, doi:10.1038/nprot.2007.48.
170. Sozzani, S.; Allavena, P.; Vecchi, A.; Damme, J. Van; Mantovani, A. Chemokine receptors: interaction with HIV-1 and viral-encoded chemokines. *Pharmacochem.*

- Libr.* **2000**, *31*, 305–312, doi:10.1016/S0165-7208(00)80034-3.
171. Carolina, D.; Palomino, T.; Marti, L.C. Chemokines and immunity. *Einstein* **2015**, *13*, 469–473, doi:10.1590/S1679-45082015RB3438.
172. Mortier, A.; Van Damme, J.; Proost, P. Overview of the mechanisms regulating chemokine activity and availability. *Immunol. Lett.* **2012**, *145*, 2–9, doi:10.1016/j.imlet.2012.04.015.
173. Stievano, L.; Piovan, E.; Amadori, A. C and CX3C chemokines: Cell sources and physiopathological implications. *Crit. Rev. Immunol.* **2004**, *24*, 205–228, doi:10.1615/CritRevImmunol.v24.i3.40.
174. Clark, A.K.; Staniland, A.A.; Malcangio, M. Fractalkine/CX3CR1 signalling in chronic pain and inflammation. *Curr. Pharm. Biotechnol.* **2011**, *12*, 1707–1714.
175. Pattison, J.M.; Nelson, P.J.; Huie, P.; Sibley, R.K.; Krensky, A.M. RANTES chemokine expression in transplant-associated accelerated atherosclerosis. *J. Heart Lung Transplant.* **1996**, *15*, 1194–1199.
176. Kalnins, A.; Thomas, M.N.; Andrassy, M.; Müller, S.; Wagner, A.; Pratschke, S.; Rentsch, M.; Klussmann, S.; Kauke, T.; Angele, M.K.; et al. Spiegelmer Inhibition of MCP-1/CCR2 - Potential as an Adjunct Immunosuppressive Therapy in Transplantation. *Scand. J. Immunol.* **2015**, *82*, 102–109, doi:10.1111/sji.12310.
177. Thomas, M.N.; Kalnins, A.; Andrassy, M.; Wagner, A.; Klussmann, S.; Rentsch, M.; Habicht, A.; Pratschke, S.; Stangl, M.; Bazhin, A. V; et al. SDF-1/CXCR4/CXCR7 is pivotal for vascular smooth muscle cell proliferation and chronic allograft vasculopathy. *Transpl. Int.* **2015**, *28*, 1426–1435, doi:10.1111/tri.12651.

178. Zhang, S.-J.; Song, X.-Y.; He, M.; Yu, S.-B. Effect of TGF-beta1/SDF-1/CXCR4 signal on BM-MSCs homing in rat heart of ischemia/perfusion injury. *Eur. Rev. Med. Pharmacol. Sci.* **2016**, *20*, 899–905.
179. Komarowska, I.; Coe, D.; Wang, G.; Haas, R.; Mauro, C.; Kishore, M.; Cooper, D.; Nadkarni, S.; Fu, H.; Steinbruchel, D.A.; et al. Hepatocyte Growth Factor Receptor c-Met Instructs T Cell Cardiotropism and Promotes T Cell Migration to the Heart via Autocrine Chemokine Release. *Immunity* **2015**, *42*, 1087–1099, doi:10.1016/j.immuni.2015.05.014.
180. Schnickel, G.T.; Bastani, S.; Hsieh, G.R.; Shefizadeh, A.; Bhatia, R.; Fishbein, M.C.; Belperio, J.; Ardehali, A. Combined CXCR3/CCR5 blockade attenuates acute and chronic rejection. *J. Immunol.* **2008**, *180*, 4714–4721.
181. Huser, N.; Tertilt, C.; Gerauer, K.; Maier, S.; Traeger, T.; Assfalg, V.; Reiter, R.; Heidecke, C.-D.; Pfeffer, K. CCR4-deficient mice show prolonged graft survival in a chronic cardiac transplant rejection model. *Eur. J. Immunol.* **2005**, *35*, 128–138, doi:10.1002/eji.200324745.
182. Melter, M.; Exeni, A.; Reinders, M.E.; Fang, J.C.; McMahon, G.; Ganz, P.; Hancock, W.W.; Briscoe, D.M. Expression of the chemokine receptor CXCR3 and its ligand IP-10 during human cardiac allograft rejection. *Circulation* **2001**, *104*, 2558–2564.
183. Bao, C.; Lv, Z.; Zhang, X.; Zhu, J.; Ding, F.; Zhang, Y.; Mei, J. Suppression of cardiac allograft vasculopathy in mice by inhibition of CC-motif chemokine receptor 5. *Transpl. Immunol.* **2012**, *26*, 128–132, doi:10.1016/j.trim.2011.11.005.
184. Hancock, W.W.; Gao, W.; Csizmadia, V.; Faia, K.L.; Shemmeri, N.; Luster, A.D.

- Donor-derived IP-10 initiates development of acute allograft rejection. *J. Exp. Med.* **2001**, *193*, 975–80, doi:10.1084/jem.193.8.975.
185. Rosenblum, J.M.; Shimoda, N.; Schenk, A.D.; Zhang, H.; Kish, D.D.; Keslar, K.; Farber, J.M.; Fairchild, R.L. CXC chemokine ligand (CXCL) 9 and CXCL10 are antagonistic costimulation molecules during the priming of alloreactive T cell effectors. *J. Immunol.* **2010**, *184*, 3450–3460, doi:10.4049/jimmunol.0903831.
186. Hancock, W.W.; Lu, B.; Gao, W.; Csizmadia, V.; Faia, K.; King, J.A.; Smiley, S.T.; Ling, M.; Gerard, N.P.; Gerard, C. Requirement of the chemokine receptor CXCR3 for acute allograft rejection. *J. Exp. Med.* **2000**, *192*, 1515–1520.
187. Ma, T.; Xu, J.; Zhuang, J.; Zhou, X.; Lin, L.; Shan, Z.; Qi, Z. Combination of C-X-C motif chemokine 9 and C-X-C motif chemokine 10 antibodies with FTY720 prolongs the survival of cardiac retransplantation allografts in a mouse model. *Exp. Ther. Med.* **2015**, *9*, 1006–1012, doi:10.3892/etm.2015.2204.
188. Xu, J.; Ma, T.; Deng, G.; Zhuang, J.; Li, C.; Wang, S.; Dai, C.; Zhou, X.; Shan, Z.; Qi, Z. Inhibition of C-X-C motif chemokine 10 reduces graft loss mediated by memory CD8(+) T cells in a rat cardiac re-transplant model. *Exp. Ther. Med.* **2018**, *15*, 1560–1567, doi:10.3892/etm.2017.5585.
189. Tatapudi, R.R.; Muthukumar, T.; Dadhania, D.; Ding, R.; Li, B.; Sharma, V.K.; Lozada-Pastorio, E.; Seetharamu, N.; Hartono, C.; Serur, D.; et al. Noninvasive detection of renal allograft inflammation by measurements of mRNA for IP-10 and CXCR3 in urine. *Kidney Int.* **2004**, *65*, 2390–2397, doi:10.1111/j.1523-1755.2004.00663.x.
190. Altara, R.; Manca, M.; Brandao, R.D.; Zeidan, A.; Booz, G.W.; Zouein, F.A.

- Emerging importance of chemokine receptor CXCR3 and its ligands in cardiovascular diseases. *Clin. Sci. (Lond)*. **2016**, *130*, 463–478, doi:10.1042/CS20150666.
191. Camargo, J.F.; Resende, M.R.; Zamel, R.; Klement, W.; Bhimji, A.; Huibner, S.; Kumar, D.; Humar, A.; Jurisica, I.; Keshavjee, S.; et al. Potential role of CC chemokine receptor 6 in prediction of late-onset cytomegalovirus infection following solid organ transplant. *Clin. Transplant*. **2015**, *29*, 492–498, doi:10.1111/ctr.12531.
192. Lisboa, L.F.; Egli, A.; Fairbanks, J.; O’Shea, D.; Manuel, O.; Husain, S.; Kumar, D.; Humar, A.; Shea, D.O.; Manuel, O.; et al. CCL8 and the Immune Control of Cytomegalovirus in Organ Transplant Recipients. *Am. J. Transplant*. **2015**, *15*, 1882–1892, doi:10.1111/ajt.13207.
193. Sharpe, H.R.; Bowyer, G.; Brackenridge, S.; Lambe, T. HLA-E: exploiting pathogen-host interactions for vaccine development. *Clin. Exp. Immunol*. **2019**, *196*, cei.13292, doi:10.1111/cei.13292.
194. Streblow, D.N.; Kreklywich, C.; Yin, Q.; De La Melena, V.T.; Corless, C.L.; Smith, P.A.; Brakebill, C.; Cook, J.W.; Vink, C.; Bruggeman, C.A.; et al. Cytomegalovirus-mediated upregulation of chemokine expression correlates with the acceleration of chronic rejection in rat heart transplants. *J. Virol*. **2003**, *77*, 2182–94, doi:10.1128/jvi.77.3.2182-2194.2003.
195. Dumortier, J.; Streblow, D.N.; Moses, A. V.; Jacobs, J.M.; Kreklywich, C.N.; Camp, D.; Smith, R.D.; Orloff, S.L.; Nelson, J.A. Human Cytomegalovirus Secretome Contains Factors That Induce Angiogenesis and Wound Healing. *J. Virol*. **2008**, *82*,

6524–6535, doi:10.1128/JVI.00502-08.

196. Naing, Z.; Webel, R.; Hamilton, S.; Schmeiser, C.; Scott, G.; Marschall, M.; Rawlinson, W. Stimulatory effects of human cytomegalovirus tegument protein pp71 lead to increased expression of CCL2 (monocyte chemotactic protein-1) during infection. *J. Gen. Virol.* **2015**, *96*, 1855–1862, doi:10.1099/vir.0.000101.
197. Hamilton, S.T.; Scott, G.M.; Naing, Z.; Rawlinson, W.D. Human cytomegalovirus directly modulates expression of chemokine CCL2 (MCP-1) during viral replication. *J. Gen. Virol.* **2013**, *94*, 2495–2503, doi:10.1099/vir.0.052878-0.
198. Hsu, J.L.; van den Boomen, D.J.H.; Tomasec, P.; Weekes, M.P.; Antrobus, R.; Stanton, R.J.; Ruckova, E.; Sugrue, D.; Wilkie, G.S.; Davison, A.J.; et al. Plasma Membrane Profiling Defines an Expanded Class of Cell Surface Proteins Selectively Targeted for Degradation by HCMV US2 in Cooperation with UL141. *PLoS Pathog.* **2015**, *11*, 1–24, doi:10.1371/journal.ppat.1004811.
199. Tu, C.C.; Arnolds, K.L.; O'Connor, C.M.; Spencer, J. V Human Cytomegalovirus UL111A and US27 Gene Products Enhance the CXCL12/CXCR4 Signaling Axis via Distinct Mechanisms. *J. Virol.* **2018**, *92*, doi:10.1128/JVI.01981-17.
200. Varani, S.; Frascaroli, G.; Homman-Loudiyi, M.; Feld, S.; Landini, M.P.; Söderberg-Nauclér, C. Human cytomegalovirus inhibits the migration of immature dendritic cells by down-regulating cell-surface CCR1 and CCR5. *J. Leukoc. Biol.* **2005**, *77*, 219–228, doi:10.1189/jlb.0504301.
201. Frascaroli, G.; Varani, S.; Blankenhorn, N.; Pretsch, R.; Bacher, M.; Leng, L.; Bucala, R.; Landini, M.P.; Mertens, T. Human Cytomegalovirus Paralyzes Macrophage Motility through Down-Regulation of Chemokine Receptors,

- Reorganization of the Cytoskeleton, and Release of Macrophage Migration Inhibitory Factor. *J. Immunol.* **2009**, *182*, 477–488, doi:10.4049/jimmunol.182.1.477.
202. Caldeira-Dantas, S.; Furmanak, T.; Smith, C.; Quinn, M.; Teos, L.Y.; Ertel, A.; Kurup, D.; Tandon, M.; Alevizos, I.; Snyder, C.M. The Chemokine Receptor CXCR3 Promotes CD8(+) T Cell Accumulation in Uninfected Salivary Glands but Is Not Necessary after Murine Cytomegalovirus Infection. *J. Immunol.* **2018**, *200*, 1133–1145, doi:10.4049/jimmunol.1701272.
203. O'Connor, C.M.; Shenk, T. Human cytomegalovirus pUL78 G protein-coupled receptor homologue is required for timely cell entry in epithelial cells but not fibroblasts. *J. Virol.* **2012**, *86*, 11425–33, doi:10.1128/JVI.05900-11.
204. Beisser, P.S.; Grauls, G.; Bruggeman, C.A.; Vink, C. Deletion of the R78 G protein-coupled receptor gene from rat cytomegalovirus results in an attenuated, syncytium-inducing mutant strain. *J. Virol.* **1999**, *73*, 7218–30.
205. Lüttichau, H.R. The Cytomegalovirus UL146 Gene Product vCXCL1 Targets Both CXCR1 and CXCR2 as an Agonist. *J. Biol. Chem.* **2010**, *285*, 9137–9146, doi:10.1074/jbc.M109.002774.
206. Penfold, M.E.T.; Dairaghi, D.J.; Duke, G.M.; Saederup, N.; Mocarski, E.S.; Kemble, G.W.; Schall, T.J. Cytomegalovirus encodes a potent alpha chemokine. *Proc. Natl. Acad. Sci.* **1999**, *96*, 9839–9844, doi:10.1073/pnas.96.17.9839.
207. Heo, J.; Dogra, P.; Masi, T.J.; Pitt, E.A.; de Kruijf, P.; Smit, M.J.; Sparer, T.E. Novel Human Cytomegalovirus Viral Chemokines, vCXCL-1s, Display Functional Selectivity for Neutrophil Signaling and Function. *J. Immunol.* **2015**, *195*, 227–236,

doi:10.4049/jimmunol.1400291.

208. Noda, S.; Aguirre, S.A.; Bitmansour, A.; Brown, J.M.; Sparer, T.E.; Huang, J.; Mocarski, E.S. Cytomegalovirus MCK-2 controls mobilization and recruitment of myeloid progenitor cells to facilitate dissemination. *Blood* **2006**, *107*, 30–38, doi:10.1182/blood-2005-05-1833.
209. Daley-Bauer, L.P.; Wynn, G.M.; Mocarski, E.S. Cytomegalovirus impairs antiviral CD8+ T cell immunity by recruiting inflammatory monocytes. **2012**, *37*, 122–133, doi:10.1161/CIRCULATIONAHA.111.087940.The.
210. Hilterbrand, A.T.; Boutz, D.R.; Marcotte, E.M.; Upton, J.W. Murine Cytomegalovirus Deubiquitinase Regulates Viral Chemokine Levels To Control Inflammation and Pathogenesis. *MBio* **2017**, *8*, doi:10.1128/mBio.01864-16.
211. Leviton, M.P.; Lacayo, J.C.; Choi, K.Y.; Hernandez-Alvarado, N.; Wey, A.; Schleiss, M.R. An attenuated cytomegalovirus vaccine with a deletion of a viral chemokine gene is protective against congenital CMV transmission in a guinea pig model. *Clin. Dev. Immunol.* **2013**, *2013*, 906948, doi:10.1155/2013/906948.
212. Geyer, H.; Hartung, E.; Mages, H.W.; Weise, C.; Beluzic, R.; Vugrek, O.; Jonjic, S.; Kroczeck, R. a; Voigt, S. Cytomegalovirus Expresses the Chemokine Homologue vXCL1 Capable of Attracting XCR1+ CD4- Dendritic Cells. *J. Virol.* **2014**, *88*, 292–302, doi:10.1128/JVI.02330-13.
213. Randolph-Habecker, J.; Rahill, B.; Torok-Storb, B.; Vieira, J.; Kolattukudy, P.E.; Rovin, B.H.; Sedmak, D.D. The Expression of the Cytomegalovirus Chemokine Receptor Homolog Us28 Sequesters Biologically Active Cc Chemokines and Alters Il-8 Production. *Cytokine* **2002**, *19*, 37–46, doi:10.1006/cyto.2002.0874.

214. Billstrom, M.A.; Johnson, G.L.; Avdi, N.J.; Worthen, G.S. Intracellular signaling by the chemokine receptor US28 during human cytomegalovirus infection. *J. Virol.* **1998**, *72*, 5535–44.
215. Hirsch, A.J.; Shenk, T. Human Cytomegalovirus Inhibits Transcription of the CC Chemokine MCP-1 Gene Human Cytomegalovirus Inhibits Transcription of the CC Chemokine MCP-1 Gene. **1999**, *73*, 404–410.
216. Streblow, D.N.; Soderberg-Naucler, C.; Vieira, J.; Smith, P.; Wakabayashi, E.; Ruchti, F.; Mattison, K.; Altschuler, Y.; Nelson, J.A. The Human Cytomegalovirus Chemokine Receptor US28 Mediates Vascular Smooth Muscle Cell Migration. *Cell* **1999**, *99*, 511–520, doi:10.1016/S0092-8674(00)81539-1.
217. Vomaske, J.; Melnychuk, R.M.; Smith, P.P.; Powell, J.; Hall, L.; DeFilippis, V.; Früh, K.; Smit, M.; Schlaepfer, D.D.; Nelson, J.A.; et al. Differential Ligand Binding to a Human Cytomegalovirus Chemokine Receptor Determines Cell Type–Specific Motility. *PLoS Pathog.* **2009**, *5*, e1000304, doi:10.1371/journal.ppat.1000304.
218. Melnychuk, R.M.; Streblow, D.N.; Smith, P.P.; Hirsch, A.J.; Pancheva, D.; Nelson, J.A. Human Cytomegalovirus-Encoded G Protein-Coupled Receptor US28 Mediates Smooth Muscle Cell Migration through $G\alpha_{12}$. *J. Virol.* **2004**, *78*, 8382–8391, doi:10.1128/JVI.78.15.8382-8391.2004.
219. Streblow, D.N.; Vomaske, J.; Smith, P.; Melnychuk, R.; Hall, L.; Pancheva, D.; Smit, M.; Casarosa, P.; Schlaepfer, D.D.; Nelson, J.A. Human Cytomegalovirus Chemokine Receptor US28-induced Smooth Muscle Cell Migration Is Mediated by Focal Adhesion Kinase and Src. *J. Biol. Chem.* **2003**, *278*, 50456–50465, doi:10.1074/jbc.M307936200.

220. Hjortø, G.M.; Kiilerich-Pedersen, K.; Selmeczi, D.; Kledal, T.N.; Larsen, N.B. Human cytomegalovirus chemokine receptor US28 induces migration of cells on a CX3CL1-presenting surface. *J. Gen. Virol.* **2013**, *94*, 1111–1120, doi:10.1099/vir.0.047290-0.
221. Scarborough, J.A.; Paul, J.R.; Spencer, J. V Evolution of the ability to modulate host chemokine networks via gene duplication in human cytomegalovirus (HCMV). *Infect. Genet. Evol.* **2017**, *51*, 46–53, doi:10.1016/j.meegid.2017.03.013.
222. Melnychuk, R.M.; Smith, P.; Kreklywich, C.N.; Ruchti, F.; Vomaske, J.; Hall, L.; Loh, L.; Nelson, J. a; Orloff, S.L.; Streblow, D.N. Mouse cytomegalovirus M33 is necessary and sufficient in virus-induced vascular smooth muscle cell migration. *J. Virol.* **2005**, *79*, 10788–10795, doi:10.1128/JVI.79.16.10788.
223. Waldhoer, M.; Kledal, T.N.; Farrell, H.; Schwartz, T.W. Murine cytomegalovirus (CMV) M33 and human CMV US28 receptors exhibit similar constitutive signaling activities. *J. Virol.* **2002**, *76*, 8161–8, doi:10.1128/JVI.76.16.8161.
224. Yang, Z.; Bjorkman, P.J. Structure of UL18, a peptide-binding viral MHC mimic, bound to a host inhibitory receptor. *Proc. Natl. Acad. Sci. U. S. A.* **2008**, *105*, 10095–10100, doi:10.1073/pnas.0804551105.
225. Beck, S.; Barrell, B.G. Human cytomegalovirus encodes a glycoprotein homologous to MHC class-I antigens. *Nature* **1988**, *331*, 269–272, doi:10.1038/331269a0.
226. Chen, K.; Stanton, R.; Banat, J.; Wills, M. Leukocyte Immunoglobulin-Like Receptor 1-Expressing Human Natural Killer Cell Subsets Differentially Recognize Isolates of Human Cytomegalovirus through the. *J. Virol.* **2016**, *90*, 3123–3137, doi:10.1128/JVI.02614-15.Editor.

227. Cosman, D.; Fanger, N.; Borges, L.; Kubin, M.; Chin, W.; Peterson, L.; Hsu, M.L. A novel immunoglobulin superfamily receptor for cellular and viral MHC class I molecules. *Immunity* **1997**, *7*, 273–282, doi:10.1016/S1074-7613(00)80529-4.
228. Fahnestock, M.L.; Johnson, J.L.; Renny Feldman, R.M.; Neveu, J.M.; Lane, W.S.; J. Bjorkman, P. The MHC class I homolog encoded by human cytomegalovirus binds endogenous peptides. *Immunity* **1995**, *3*, 583–590, doi:10.1016/1074-7613(95)90129-9.
229. Wilkinson, G.W.G.; Tomasec, P.; Stanton, R.J.; Armstrong, M.; Prod'homme, V.; Aicheler, R.; McSharry, B.P.; Rickards, C.R.; Cochrane, D.; Llewellyn-Lacey, S.; et al. Modulation of natural killer cells by human cytomegalovirus. *J. Clin. Virol.* **2008**, *41*, 206–212, doi:10.1016/j.jcv.2007.10.027.
230. Prod'homme, V.; Griffin, C.; Aicheler, R.J.; Wang, E.C.Y.; McSharry, B.P.; Rickards, C.R.; Stanton, R.J.; Borysiewicz, L.K.; López-Botet, M.; Wilkinson, G.W.G.; et al. The Human Cytomegalovirus MHC Class I Homolog UL18 Inhibits LIR-1 + but Activates LIR-1 – NK Cells. *J. Immunol.* **2007**, *178*, 4473–4481, doi:10.4049/jimmunol.178.7.4473.
231. Browne, H.; Churcher, M.; Minson, T. Construction and characterization of a human cytomegalovirus mutant with the UL18 (class I homolog) gene deleted. *J. Virol.* **1992**, *66*, 6784–6787, doi:10.1128/JVI.66.11.6784-6787.1992.
232. Hassan-Walker, A.F.; Cope, A. V.; Griffiths, P.D.; Emery, V.C. Transcription of the human cytomegalovirus natural killer decoy gene, UL18, in vitro and in vivo. *J. Gen. Virol.* **1998**, *79*, 2113–2116, doi:10.1099/0022-1317-79-9-2113.
233. Jones, T.R.; Wiertz, E.J.H.J.; Sun, L.; Fish, K.N.; Nelson, J.A.; Ploegh, H.L. Human

- cytomegalovirus US3 impairs transport and maturation of major histocompatibility complex class I heavy chains. *Proc. Natl. Acad. Sci. U. S. A.* **1996**, *93*, 11327–33, doi:10.1073/pnas.93.21.11327.
234. Hewitt, E.W.; Gupta, S. Sen; Lehner, P.J. The human cytomegalovirus gene product US6 inhibits ATP binding by TAP. *EMBO J.* **2001**, *20*, 387–396, doi:10.1093/emboj/20.3.387.
235. Kim, Y.; Park, B.; Cho, S.; Shin, J.; Cho, K.; Jun, Y.; Ahn, K. Human cytomegalovirus UL18 utilizes US6 for evading the NK and T-cell responses. *PLoS Pathog.* **2008**, *4*, e1000123, doi:10.1371/journal.ppat.1000123.
236. Patro, A.R.K. Subversion of Immune Response by Human Cytomegalovirus. *Front. Immunol.* **2019**, *10*, 1–7, doi:10.3389/fimmu.2019.01155.
237. Hansen, S.G.; Wu, H.L.; Burwitz, B.J.; Hughes, C.M.; Katherine, B.; Ventura, A.B.; Reed, J.S.; Gilbride, R.M.; Ainslie, E.; Morrow, D.W.; et al. Broadly targeted CD8+ T cell responses restricted by major histocompatibility complex-E. *Science (80-.).* **2016**, *351*, 714–720, doi:10.1126/science.aac9475.Broadly.
238. Hansen, S.G.; Sacha, J.B.; Hughes, C.M.; Ford, J.C.; Benjamin, J.; Scholz, I.; Gilbride, R.M.; Lewis, M.S.; Gilliam, A.N.; Ventura, A.B.; et al. Cytomegalovirus vectors violate CD8+ T cell epitope recognition paradigms. *Science (80-.).* **2013**, *340*, doi:10.1126/science.1237874.CYTOMEGALOVIRUS.
239. Abdulhaqq, S.A.; Wu, H.; Schell, J.B.; Hammond, K.B.; Reed, J.S.; Legasse, A.W.; Axthelm, M.K.; Park, B.S.; Asokan, A.; Früh, K.; et al. Vaccine-Mediated Inhibition of the Transporter Associated with Antigen Processing Is Insufficient To Induce Major Histocompatibility Complex E-Restricted CD8 + T Cells in Nonhuman

- Primates. *J. Virol.* **2019**, *93*, 1–14, doi:10.1128/JVI.00592-19.
240. Murray, S.E.; Nesterenko, P.A.; Vanarsdall, A.L.; Munks, M.W.; Smart, S.M.; Veziroglu, E.M.; Sagario, L.C.; Lee, R.; Claas, F.H.J.; Doxiadis, I.I.N.; et al. Fibroblast-adapted human CMV vaccines elicit predominantly conventional CD8 T cell responses in humans. *J. Exp. Med.* **2017**, *214*, 1889–1899, doi:10.1084/jem.20161988.
241. Rawlinson, W.D.; Farrell, H.E.; Barrell, B.G. Analysis of the complete DNA sequence of murine cytomegalovirus. *J. Virol.* **1996**, *70*, 8833–8849, doi:10.1128/jvi.70.12.8833-8849.1996.
242. Mans, J.; Zhi, L.; Revilleza, M.J.R.; Smith, L.; Redwood, A.; Natarajan, K.; Margulies, D.H. Structure and function of murine cytomegalovirus MHC-I-like molecules: how the virus turned the host defense to its advantage. *Immunol. Res.* **2010**, *43*, 264–279, doi:10.1007/s12026-008-8081-6.
243. Smith, H.R.C.; Heusel, J.W.; Mehta, I.K.; Kim, S.; Dorner, B.G.; Naidenko, O. V.; Iizuka, K.; Furukawa, H.; Beckman, D.L.; Pingel, J.T.; et al. Recognition of a virus-encoded ligand by a natural killer cell activation receptor. *Proc. Natl. Acad. Sci.* **2002**, *99*, 8826–8831, doi:10.1073/pnas.092258599.
244. Natarajan, K.; Hicks, A.; Mans, J.; Robinson, H.; Guan, R.; Mariuzza, R.A.; Margulies, D.H. Crystal structure of the murine cytomegalovirus MHC-I homolog m144. *J. Mol. Biol.* **2006**, *358*, 157–171, doi:10.1016/j.jmb.2006.01.068.
245. Mans, J.; Natarajan, K.; Balbo, A.; Schuck, P.; Eike, D.; Hess, S.; Robinson, H.; Šimić, H.; Jonjić, S.; Tiemessen, C.T.; et al. Cellular expression and crystal structure of the murine cytomegalovirus major histocompatibility complex class I-like

- glycoprotein, m153. *J. Biol. Chem.* **2007**, *282*, 35247–35258, doi:10.1074/jbc.M706782200.
246. Adams, E.J.; Juo, Z.S.; Venook, R.T.; Boulanger, M.J.; Arase, H.; Lanier, L.L.; Garcia, K.C. Structural elucidation of the m157 mouse cytomegalovirus ligand for Ly49 natural killer cell receptors. *Proc. Natl. Acad. Sci. U. S. A.* **2007**, *104*, 10128–10133, doi:10.1073/pnas.0703735104.
247. Streblow, D.N.; van Cleef, K.W.R.; Kreklywich, C.N.; Meyer, C.; Smith, P.; Defilippis, V.; Grey, F.; Fruh, K.; Searles, R.; Bruggeman, C.; et al. Rat Cytomegalovirus Gene Expression in Cardiac Allograft Recipients Is Tissue Specific and Does Not Parallel the Profiles Detected In Vitro. *J. Virol.* **2007**, *81*, 3816–3826, doi:10.1128/JVI.02425-06.
248. Pinto, A.K.; Munks, M.W.; Koszinowski, U.H.; Hill, A.B. Coordinated Function of Murine Cytomegalovirus Genes Completely Inhibits CTL Lysis. *J. Immunol.* **2006**, *177*, 3225–3234, doi:10.4049/jimmunol.177.5.3225.
249. Kavanagh, D.G.; Gold, M.C.; Wagner, M.; Koszinowski, U.H.; Hill, A.B. The multiple immune-evasion genes of murine cytomegalovirus are not redundant: m4 and m152 inhibit antigen presentation in a complementary and cooperative fashion. *J. Exp. Med.* **2001**, *194*, 967–977, doi:10.1084/jem.194.7.967.
250. Holtappels, R.; Gillert-Marien, D.; Thomas, D.; Podlech, J.; Deegen, P.; Herter, S.; Oehrlein-Karpi, S.A.; Strand, D.; Wagner, M.; Reddehase, M.J. Cytomegalovirus Encodes a Positive Regulator of Antigen Presentation. *J. Virol.* **2006**, *80*, 7613–7624, doi:10.1128/JVI.00723-06.
251. Lu, X.; Pinto, A.K.; Kelly, A.M.; Cho, K.S.; Hill, A.B. Murine Cytomegalovirus

- Interference with Antigen Presentation Contributes to the Inability of CD8 T Cells To Control Virus in the Salivary Gland. *J. Virol.* **2006**, *80*, 4200–4202, doi:10.1128/JVI.80.8.4200-4202.2006.
252. Gold, M.C.; Munks, M.W.; Wagner, M.; McMahon, C.W.; Kelly, A.; Kavanagh, D.G.; Slifka, M.K.; Koszinowski, U.H.; Raulet, D.H.; Hill, A.B. Murine Cytomegalovirus Interference with Antigen Presentation Has Little Effect on the Size or the Effector Memory Phenotype of the CD8 T Cell Response. *J. Immunol.* **2004**, *172*, 6944–6953, doi:10.4049/jimmunol.172.11.6944.
253. Kern, E.R. Pivotal role of animal models in the development of new therapies for cytomegalovirus infections. *Antiviral Res.* **2006**, *71*, 164–171, doi:10.1016/j.antiviral.2006.05.018.
254. Powers, C.; Früh, K. Rhesus CMV: an emerging animal model for human CMV. *Med. Microbiol. Immunol.* **2008**, *197*, 109–115, doi:10.1038/mp.2011.182.doi.
255. Schleiss, M.R.; McGregor, A.; Choi, K.Y.; Date, S. V.; Cui, X.; McVoy, M.A. Analysis of the nucleotide sequence of the guinea pig cytomegalovirus (GPCMV) genome. *Virol. J.* **2008**, *5*, 139, doi:10.1186/1743-422X-5-139.
256. Terrazzini, N.; Kern, F. Cell-mediated immunity to human CMV infection: a brief overview. *F1000Prime Rep.* **2014**, *6*, 28, doi:10.12703/P6-28.
257. Ettinger, J.; Geyer, H.; Nitsche, A.; Zimmermann, A.; Brune, W.; Sandford, G.R.; Hayward, G.S.; Voigt, S. Complete genome sequence of the english isolate of rat cytomegalovirus (murid herpesvirus 8). *J. Virol.* **2012**, *86*, 13838, doi:10.1128/JVI.02614-12.
258. Loh, H.S.; Mohd-Azmi, M.L.; Lai, K.Y.; Sheikh-Omar, A.R.; Zamri-Saad, M.

- Characterization of a novel rat cytomegalovirus (RCMV) infecting placenta-uterus of *Rattus rattus diardii*. *Arch. Virol.* **2003**, *148*, 2353–2367, doi:10.1007/s00705-003-0173-y.
259. Balakrishnan, K.N.; Abdullah, A.A.; Bala, J.; Abba, Y.; Sarah, S.A.; Jesse, F.F.A.; Nazariah, Z.A.; Noordin, M.M.; Mohd-Azmi, M.L. Identification and comparison of RCMV ALL 03 open reading frame (ORF) among several different strains of cytomegalovirus worldwide. *Infect. Genet. Evol.* **2017**, *54*, 81–90, doi:10.1016/j.meegid.2017.06.020.
260. Camalxaman, S.N.; Zeenathul, N.A.; Quah, Y.W.; Loh, H.S.; Zuridah, H.; Sheikh-Omar, A.R.; Mohd-Azmi, M.L. Cross-reactivity of Malaysian rat cytomegalovirus strains with its human counterpart. *Trop. Biomed.* **2011**, *28*, 661–7.
261. Beisser, P.S.; Kaptein, S.J.; Beuken, E.; Bruggeman, C.A.; Vink, C. The Maastricht strain and England strain of rat cytomegalovirus represent different betaherpesvirus species rather than strains. *Virology* **1998**, *246*, 341–51, doi:10.1006/viro.1998.9196.
262. Lemström, K.; Koskinen, P.; Krogerus, L.; Daemen, M.; Bruggeman, C.; Häyry, P. Cytomegalovirus Antigen Expression, Endothelial Cell Proliferation, and Intimal Thickening in Rat Cardiac Allografts After Cytomegalovirus Infection. *Circulation* **1995**, *92*, 2594–2604, doi:10.1161/01.cir.92.9.2594.
263. Streblov, D.N.; Kreklywich, C.N.; Andoh, T.; Moses, A. V.; Dumortier, J.; Smith, P.P.; Defilippis, V.; Fruh, K.; Nelson, J.A.; Orloff, S.L. The Role of Angiogenic and Wound Repair Factors During CMV-Accelerated Transplant Vascular Sclerosis in Rat Cardiac Transplants. *Am. J. Transplant.* **2008**, *8*, 277–287, doi:10.1111/j.1600-

6143.2007.02062.x.

264. De La Melena, V.T.; Kreklywich, C.N.; Streblow, D.N.; Yin, Q.; Cook, J.W.; Soderberg-Naucler, C.; Bruggeman, C.A.; Nelson, J.A.; Orloff, S.L. Kinetics and development of CMV-accelerated transplant vascular sclerosis in rat cardiac allografts is linked to early increase in chemokine expression and presence of virus. *Transplant. Proc.* **2001**, *33*, 1822–1823, doi:10.1016/S0041-1345(00)02729-9.
265. Orloff, S.L.; Streblow, D.N.; Soderberg-Naucler, C.; Yin, Q.; Kreklywich, C.; Corless, C.L.; Smith, Patricia, A.; Loomis, C.B.; Mills, L.K.; Cook, J.W.; et al. Elimination of donor-specific alloreactivity prevents cytomegalovirus-accelerated chronic rejection in rat small bowel and heart transplants. *Transplantation* **2002**, *73*, 679–688.
266. Shrestha, B.; Haylor, J. Experimental rat models of chronic allograft nephropathy: a review. *Int. J. Nephrol. Renovasc. Dis.* **2014**, *7*, 315, doi:10.2147/IJNRD.S65604.
267. Fietze, E.; Prösch, S.; Reinke, P.; Stein, J.; Döcke, W.D.; Staffa, G.; Löning, S.; Devaux, S.; Emmrich, F.; von Baehr, R.; et al. Cytomegalovirus infection in transplant recipients: The role of tumor necrosis factor. *Transplantation* **1994**, *58*, 675–680, doi:10.1097/00007890-199409000-00007.
268. Zhang, Z.; Qiu, L.; Yan, S.; Wang, J.-J.J.; Thomas, P.M.; Kandpal, M.; Zhao, L.; Iovane, A.; Liu, X. feng; Thorp, E.B.; et al. A clinically relevant murine model unmasks a “two-hit” mechanism for reactivation and dissemination of cytomegalovirus after kidney transplant. *Am. J. Transplant.* **2019**, *19*, 2421–2433, doi:10.1111/ajt.15376.
269. Onai, Y.; Suzuki, J.I.; Kakuta, T.; Maejima, Y.; Haraguchi, G.; Fukasawa, H.; Muto,

- S.; Itai, A.; Isobe, M. Inhibition of I κ B phosphorylation in cardiomyocytes attenuates myocardial ischemia/reperfusion injury. *Cardiovasc. Res.* **2004**, *63*, 51–59, doi:10.1016/j.cardiores.2004.03.002.
270. Zingarelli, B.; Hake, P.W.; Denenberg, A.; Wong, H.R. Sesquiterpene Lactone Parthenolide , an Inhibitor of I κ B Kinase Complex and Nuclear Factor- κ B , Exerts Beneficial Effects in Myocardial Reperfusion Injury. *SHOCK* **2002**, *17*, 127–134.
271. Wanderer, A.A. Rationale and timeliness for IL-1 β -targeted therapy to reduce allogeneic organ injury at procurement and to diminish risk of rejection after transplantation. *Clin. Transplant.* **2010**, *24*, 307–311, doi:10.1111/j.1399-0012.2010.01256.x.
272. Rusai, K.; Huang, H.; Sayed, N.; Strobl, M.; Roos, M.; Schmaderer, C.; Heemann, U.; Lutz, J. Administration of interleukin-1 receptor antagonist ameliorates renal ischemia-reperfusion injury. *Transpl. Int.* **2008**, *21*, 572–580, doi:10.1111/j.1432-2277.2008.00651.x.
273. Vallejo, S.; Palacios, E.; Romacho, T.; Villalobos, L.; Peiró, C.; Sánchez-Ferrer, C.F. The interleukin-1 receptor antagonist anakinra improves endothelial dysfunction in streptozotocin-induced diabetic rats. *Cardiovasc. Diabetol.* **2014**, *13*, 1–13, doi:10.1186/s12933-014-0158-z.
274. Abbate, A.; Salloum, F.N.; Vecile, E.; Das, A.; Hoke, N.N.; Straino, S.; Giuseppe, G.L.; Biondi-Zoccai; Houser, J.E.; Qureshi, I.Z.; et al. Anakinra, a recombinant human interleukin-1 receptor antagonist, inhibits apoptosis in experimental acute myocardial infarction. *Circulation* **2008**, *117*, 2670–2683, doi:10.1161/CIRCULATIONAHA.107.740233.

275. Dinarello, C.A.; Simon, A.; Meer, J.W.M. van der Treating inflammation by blocking interleukin-1 in a broad spectrum of diseases. *Nat. Rev. Drug Discov.* **2012**, *11*, 633–652, doi:10.1038/jnrd3800.
276. Dong, L.; Qiao, H.; Zhang, X.; Zhang, X.; Wang, C.; Wang, L.; Cui, L.; Zhao, J.; Xing, Y.; Li, Y.; et al. Parthenolide is neuroprotective in rat experimental stroke model: Downregulating NF- B, phospho-p38MAPK, and caspase-1 and ameliorating BBB permeability. *Mediators Inflamm.* **2013**, *2013*, doi:10.1155/2013/370804.
277. Liu, Q.; Zhao, J.; Tan, R.; Zhou, H.; Lin, Z.; Zheng, M.; Romas, E.; Xu, J.; Sims, N.A. Parthenolide inhibits pro-inflammatory cytokine production and exhibits protective effects on progression of collagen-induced arthritis in a rat model. *Scand. J. Rheumatol.* **2015**, *44*, 182–191, doi:10.3109/03009742.2014.938113.
278. Valantine, H.A.; Gao, S.-Z.; Menon, S.G.; Renlund, D.G.; Hunt, S.A.; Oyer, P.; Stinson, E.B.; Brown, B.W.; Merigan, T.C.; Schroeder, J.S. Impact of Prophylactic Immediate Posttransplant Ganciclovir on Development of Transplant Atherosclerosis: A Post Hoc Analysis of a Randomized, Placebo-Controlled Study. *Circ. Am. Hear. Assoc.* **1999**, *100*, 61–66, doi:10.1161/01.CIR.100.1.61.
279. Merigan, T.C.; Renlund, D.G.; Keay, S.; Bristow, M.R.; Starnes, V.; O’Connell, J.B.; Richenbacher, W.E.; Millar, R.C.; DuMond, C.; DeAmond, B.; et al. A Controlled Trial of Ganciclovir to Prevent Cytomegalovirus Disease After Heart Transplantation. *N. Engl. J. Med.* **1992**, *326*, 1182–1186, doi:10.1056/NEJM199204303261803.
280. Abbate, A.; Kontos, M.C.; Grizzard, J.D.; Biondi-Zoccai, G.G.L.; Van Tassell,

- B.W.; Robati, R.; Roach, L.M.; Arena, R.A.; Roberts, C.S.; Varma, A.; et al. Interleukin-1 Blockade With Anakinra to Prevent Adverse Cardiac Remodeling After Acute Myocardial Infarction (Virginia Commonwealth University Anakinra Remodeling Trial [VCU-ART] Pilot Study). *Am. J. Cardiol.* **2010**, *105*, 1371-1377.e1, doi:10.1016/j.amjcard.2009.12.059.
281. Saxena, A.; Chen, W.; Su, Y.; Rai, V.; Olisambu, U.U.; Li, N.; Frangogiannis, N.G. IL-1 Induces Proinflammatory Leukocyte Infiltration and Regulates Fibroblast Phenotype in the Infarcted Myocardium. *J. Immunol.* **2013**, doi:10.4049/jimmunol.1300725.
282. Rao, D.A.; Eid, R.E.; Qin, L.; Yi, T.; Kirkiles-Smith, N.C.; Tellides, G.; Pober, J.S. Interleukin (IL)-1 promotes allogeneic T cell intimal infiltration and IL-17 production in a model of human artery rejection. *J. Exp. Med.* **2008**, *205*, 3145–3158, doi:10.1084/jem.20081661.
283. Westman, P.C.; Lipinski, M.J.; Luger, D.; Waksman, R.; Bonow, R.O.; Wu, E.; Epstein, S.E. Inflammation as a Driver of Adverse Left Ventricular Remodeling after Acute Myocardial Infarction. *J. Am. Coll. Cardiol.* **2016**, *67*, 2050–2060, doi:10.1016/j.jacc.2016.01.073.
284. Mulders-manders, C.M.; Baas, M.C.; Molenaar, F.M.; Simon, A. Peri- and Postoperative Treatment with the Interleukin-1 Receptor Antagonist Anakinra Is Safe in Patients Undergoing Renal Transplantation : Case Series and Review of the Literature. *Front. Pharmacol.* **2017**, *8*, 1–6, doi:10.3389/fphar.2017.00342.
285. Kreklywich, C.N.; Smith, P.P.; Jones, C.B.; Cornea, A.; Orloff, S.L.; Streblov, D.N. Fluorescence-Based Laser Capture Microscopy Technology Facilitates

- Identification of Critical In Vivo Cytomegalovirus Transcriptional Programs. In *Human Cytomegaloviruses: Methods and Protocols*; Yurochko, A.D., Miller, W.E., Eds.; 2014; pp. 217–237 ISBN 9781627037884.
286. Yamada, J. Interleukin 1 Receptor Antagonist Suppresses Allosensitization in Corneal Transplantation. *Arch. Ophthalmol.* **1998**, *116*, 1351, doi:10.1001/archophth.116.10.1351.
287. Dana, R. Comparison of topical interleukin-1 vs tumor necrosis factor-alpha blockade with corticosteroid therapy on murine corneal inflammation, neovascularization, and transplant survival (an American Ophthalmological Society thesis). *Trans. Am. Ophthalmol. Soc.* **2007**, *105*, 330–343.
288. Dana, M.R.; Yamada, J.; Streilein, J.W. Topical Interleukin 1 Receptor Antagonist Promotes Corneal Transplant Survival. *Transplantation* **1997**, *63*, 1501–1507, doi:10.1097/00007890-199705270-00022.
289. Lemström, K.; Sihvola, R.; Bruggeman, C.; Häyry, P.; Koskinen, P. Cytomegalovirus infection-enhanced cardiac allograft vasculopathy is abolished by DHPG Prophylaxis in the Rat. *Circ. Am. Hear. Assoc.* **1997**, *95*, 2614–2616, doi:10.1161/01.CIR.95.12.2614.
290. Lemström, K.; Bruning, J.H.; Bruggeman, C.A.; Koskinen, P.K.; Aho, P.T.; Yilmaz, S.; Lautenschlager, I.T.; Häyry, P.J. Cytomegalovirus Infection-Enhanced Allograft Arteriosclerosis Is Prevented by DHPG Prophylaxis in the Rat. *Circulation* **1994**, *90*, 1969–1978, doi:10.1161/01.CIR.90.4.1969.
291. Armstrong, A.T.; Strauch, A.R.; Starling, R.G.C.; Sedmak, D.D.; Orosz, C.G. Morphometric analysis of neointimal formation in murine cardiac allografts.

- Transplantation* **1997**, *63*, 941–947, doi:10.1097/00007890-199704150-00006.
292. Andrews, S. FastQC: A quality control tool for high throughput sequence data 2010.
293. Ewels, P.; Magnusson, M.; Lundin, S.; Källner, M. MultiQC: Summarize analysis results for multiple tools and samples in a single report. *Bioinformatics* **2016**, *32*, 3047–3048, doi:10.1093/bioinformatics/btw354.
294. Bimber, B. DISCVR-Seq: LabKey Server Extensions for Management and Analysis of Sequencing Data 2015.
295. Nelson, E.K.; Piehler, B.; Eckels, J.; Rauch, A.; Bellew, M.; Hussey, P.; Ramsay, S.; Nathe, C.; Lum, K.; Krouse, K.; et al. LabKey Server: An open source platform for scientific data integration, analysis and collaboration. *BMC Bioinformatics* **2011**, *12*, 71, doi:10.1186/1471-2105-12-71.
296. Bolger, A.M.; Lohse, M.; Usadel, B. Trimmomatic: A flexible trimmer for Illumina sequence data. *Bioinformatics* **2014**, *30*, 2114–2120, doi:10.1093/bioinformatics/btu170.
297. Dobin, A.; Davis, C.A.; Schlesinger, F.; Drenkow, J.; Zaleski, C.; Jha, S.; Batut, P.; Chaisson, M.; Gingeras, T.R. STAR: ultrafast universal RNA-seq aligner. *Bioinformatics* **2012**, *29*, 15–21, doi:10.1093/bioinformatics/bts635.
298. DeLuca, D.S.; Levin, J.Z.; Sivachenko, A.; Fennell, T.; Nazaire, M.-D.; Williams, C.; Reich, M.; Winckler, W.; Getz, G. RNA-SeQC: RNA-seq metrics for quality control and process optimization. *Bioinformatics* **2012**, *28*, 1530–1532, doi:10.1093/bioinformatics/bts196.
299. R Core Team R: A language and environment for statistical computing. 2017.
300. Chen, Y.; Lun, A.T.L.; Smyth, G.K. From reads to genes to pathways: differential

- expression analysis of RNA-Seq experiments using Rsubread and the edgeR quasi-likelihood pipeline. *F1000Research* **2016**, *5*, 1438, doi:10.12688/f1000research.8987.2.
301. Robinson, M.D.; Oshlack, A. A scaling normalization method for differential expression analysis of RNA-seq data. *Genome Biol.* **2010**, *11*, doi:10.1186/gb-2010-11-3-r25.
302. Law, C.W.; Chen, Y.; Shi, W.; Smyth, G.K. voom: precision weights unlock linear model analysis tools for RNA-seq read counts. *Genome Biol.* **2014**, *22*, 561–564, doi:10.1186/gb-2014-15-2-r29.
303. Ritchie, M.E.; Phipson, B.; Wu, D.; Hu, Y.; Law, C.W.; Shi, W.; Smyth, G.K. limma powers differential expression analyses for RNA-sequencing and microarray studies. *Nucleic Acids Res.* **2015**, *43*, e47–e47, doi:10.1093/nar/gkv007.
304. Benjamini, Y.; Hochberg, Y. Controlling the False Discovery Rate: A Practical and Powerful Approach to Multiple Testing. *J. R. Stat. Soc.* **1995**, doi:10.2307/2346101.
305. Melter, M.; McMahon, G.; Fang, J.; Ganz, P.; Briscoe, D.M. Current understanding of chemokine involvement in allograft transplantation. *Pediatr. Transplant.* **1999**, *3*, 10–21, doi:10.1034/j.1399-3046.1999.00023.x.
306. Russell, M.E.; Hancock, W.W.; Wallace, A.F.; Wyner, L.R.; Karnovsky, M.J. Modulation of inflammatory activation pathways in the Lewis-to-F-344 rat chronic cardiac rejection model. *Transplant. Proc.* **1995**, *27*, 2100–4.
307. Ahuja, S.K.; Murphy, P.M. Molecular piracy of mammalian interleukin-8 receptor type B by herpesvirus saimiri. *J. Biol. Chem.* **1993**, *268*, 20691–4.
308. Arvanitakis, L.; Geras-Raaka, E.; Varma, A.; Gershengorn, M.C.; Cesarman, E.

- Human herpesvirus KSHV encodes a constitutively active G-protein-coupled receptor linked to cell proliferation. *Nature* **1997**, 385, 347–350, doi:10.1038/385347a0.
309. Bais, C.; Santomasso, B.; Coso, O.; Arvanitakis, L.; Raaka, E.G.; Gutkind, J.S.; Asch, A.S.; Cesarman, E.; Gershengorn, M.C.; Mesri, E.A. G-protein-coupled receptor of Kaposi's sarcoma-associated herpesvirus is a viral oncogene and angiogenesis activator. *Nature* **1998**, 392, 210–210, doi:10.1038/32472.
310. Chee, M.S.; Bankier, A.T.; Beck, S.; Bohni, R.; Brown, C.M.; Cerny, R.; Horsnell, T.; Hutchison, C.A.; Kouzarides, T.; Martignetti, J.A.; et al. Analysis of the Protein-Coding Content of the Sequence of Human Cytomegalovirus Strain AD169. In *Current topics in microbiology and immunology*; 1990; Vol. 154, pp. 125–169.
311. Chee, M.S.; Satchwell, S.C.; Preddie, E.; Weston, K.M.; Barrell, B.G. Human cytomegalovirus encodes three G protein-coupled receptor homologues. *Nature* **1990**, 344, 774–777, doi:10.1038/344774a0.
312. Gompels, U.A.; Nicholas, J.; Lawrence, G.; Jones, M.; Thomson, B.J.; Martin, M.E.D.; Efstathiou, S.; Craxton, M.; Macaulay, H.A. The DNA Sequence of Human Herpesvirus-6: Structure, Coding Content, and Genome Evolution. *Virology* **1995**, 209, 29–51, doi:10.1006/viro.1995.1228.
313. Nicholas, J.; Cameron, K.R.; Honess, R.W. Herpesvirus saimiri encodes homologues of G protein-coupled receptors and cyclins. *Nature* **1992**, 355, 362–365, doi:10.1038/355362a0.
314. Voigt, S.; Sandford, G.R.; Hayward, G.S.; Burns, W.H. The English strain of rat cytomegalovirus (CMV) contains a novel captured CD200 (vOX2) gene and a

- spliced CC chemokine upstream from the major immediate-early region: Further evidence for a separate evolutionary lineage from that of a rat CMV Maastricht. *J. Gen. Virol.* **2005**, *86*, 263–274, doi:10.1099/vir.0.80539-0.
315. Penfold, M.E.T.; Schmidt, T.L.; Dairaghi, D.J.; Barry, P.A.; Schall, T.J. Characterization of the rhesus cytomegalovirus US28 locus. *J. Virol.* **2003**, *77*, 10404–13, doi:10.1128/JVI.77.19.10404-10413.2003.
316. Bongers, G.; Maussang, D.; Muniz, L.R.; Noriega, V.M.; Fraile-Ramos, A.; Barker, N.; Marchesi, F.; Thirunarayanan, N.; Vischer, H.F.; Qin, L.; et al. The cytomegalovirus-encoded chemokine receptor US28 promotes intestinal neoplasia in transgenic mice. *J. Clin. Invest.* **2010**, *120*, 3969–3978, doi:10.1172/JCI42563.
317. van Senten, J.R.; Bebelman, M.P.; van Gasselt, P.; Bergkamp, N.D.; van den Bor, J.; Siderius, M.; Smit, M.J. Human Cytomegalovirus-Encoded G Protein-Coupled Receptor UL33 Facilitates Virus Dissemination via the Extracellular and Cell-to-Cell Route. *Viruses* **2020**, *12*, 594, doi:10.3390/v12060594.
318. Vanarsdall, A.L.; Howard, P.W.; Wisner, T.W.; Johnson, D.C. Human Cytomegalovirus gH/gL Forms a Stable Complex with the Fusion Protein gB in Virions. *PLoS Pathog.* **2016**, *12*, e1005564, doi:10.1371/journal.ppat.1005564.
319. Jones, I.K.A.; Streblow, D.N. Antibody-Independent Quantification of Cytomegalovirus Virion Protein Incorporation Using HiBiT. In *Human Cytomegaloviruses: Methods and Protocols*; Yurochko, A.D., Ed.; Springer, Accepted 2020: New York.
320. Schuessler, A.; Sampaio, K.L.; Sinzger, C. Charge Cluster-to-Alanine Scanning of UL128 for Fine Tuning of the Endothelial Cell Tropism of Human

- Cytomegalovirus. *J. Virol.* **2008**, *82*, 11239–11246, doi:10.1128/JVI.01069-08.
321. Schuessler, A.; Sampaio, K.L.; Scrivano, L.; Sinzger, C. Mutational Mapping of UL130 of Human Cytomegalovirus Defines Peptide Motifs within the C-Terminal Third as Essential for Endothelial Cell Infection. *J. Virol.* **2010**, *84*, 9019–9026, doi:10.1128/JVI.00572-10.
322. Dixon, A.S.; Schwinn, M.K.; Hall, M.P.; Zimmerman, K.; Otto, P.; Lubben, T.H.; Butler, B.L.; Binkowski, B.F.; Machleidt, T.; Kirkland, T.A.; et al. NanoLuc Complementation Reporter Optimized for Accurate Measurement of Protein Interactions in Cells. *ACS Chem. Biol.* **2016**, *11*, 400–408, doi:10.1021/acscchembio.5b00753.
323. Farrell, H.E.; Stevenson, P.G. Cytomegalovirus host entry and spread. *J. Gen. Virol.* **2019**, *100*, 545–553, doi:10.1099/jgv.0.001230.
324. Lee, J.; Kalejta, R.F. Human Cytomegalovirus Enters the Primary CD34 + Hematopoietic Progenitor Cells Where It Establishes Latency by Macropinocytosis. *J. Virol.* **2019**, *93*, 1–14, doi:10.1128/JVI.00452-19.
325. Liu, X.-F.; Swaminathan, S.; Yan, S.; Engelmann, F.; Abbott, D.A.; VanOsdol, L.A.; Heald-Sargent, T.; Qiu, L.; Chen, Q.; Iovane, A.; et al. A novel murine model of differentiation-mediated cytomegalovirus reactivation from latently infected bone marrow haematopoietic cells. *J. Gen. Virol.* **2019**, *100*, 1680–1694, doi:10.1099/jgv.0.001327.
326. Beucler, M.J.; Miller, W.E. Isolation of Salivary Epithelial Cells from Human Salivary Glands for In Vitro Growth as Salispheres or Monolayers. *J. Vis. Exp.* **2019**, *2019*, 1–7, doi:10.3791/59868.

327. Baca Jones, C.C.; Kreklywich, C.N.; Messaoudi, I.; Vomasse, J.; McCartney, E.; Orloff, S.L.; Nelson, J.A.; Streblow, D.N. Rat cytomegalovirus infection depletes MHC II in bone marrow derived dendritic cells. *Virology* **2009**, *388*, 78–90, doi:10.1016/j.virol.2009.02.050.
328. Streblow, D.N.; Hwee, Y.K.; Kreklywich, C.N.; Andoh, T.; Denton, M.; Smith, P.; Hart, E.; Broekel, R.; Pallett, C.; Rogers, K.; et al. Rat cytomegalovirus vaccine prevents accelerated chronic rejection in CMV-Naïve recipients of infected donor allograft hearts. *Am. J. Transplant.* **2015**, *15*, 1805–1816, doi:10.1111/ajt.13188.
329. Boeckh, M.; Geballe, A.P. Cytomegalovirus: pathogen, paradigm, and puzzle. *J. Clin. Invest.* **2011**, *121*, 1673–1680, doi:10.1172/JCI45449.
330. Helanterä, I.; Koskinen, P.; Finne, P.; Loginov, R.; Kyllönen, L.; Salmela, K.; Grönhagen-Riska, C.; Lautenschlager, I. Persistent cytomegalovirus infection in kidney allografts is associated with inferior graft function and survival. *Transpl. Int.* **2006**, *19*, 893–900, doi:10.1111/j.1432-2277.2006.00364.x.
331. Dzabic, M.; Rahbar, A.; Yaiw, K.-C.; Naghibi, M.; Religa, P.; Fellstrom, B.; Larsson, E.; Soderberg-Naucler, C. Intragraft Cytomegalovirus Protein Expression Is Associated With Reduced Renal Allograft Survival. *Clin. Infect. Dis.* **2011**, *53*, 969–976, doi:10.1093/cid/cir619.
332. Leeaphorn, N.; Garg, N.; Thamcharoen, N.; Khankin, E. V.; Cardarelli, F.; Pavlakis, M. Cytomegalovirus mismatch still negatively affects patient and graft survival in the era of routine prophylactic and preemptive therapy: A paired kidney analysis. *Am. J. Transplant.* **2018**, *19*, ajt.15183, doi:10.1111/ajt.15183.
333. Gatault, P.; Halimi, J.; Forconi, C.; Thibault, G.; Barbet, C.; Mérieau, E.; Graffin-

- Gaudy, C.; Marlière, J.-F.; Goudeau, A.; Bruyère, F.; et al. CMV Infection in the Donor and Increased Kidney Graft Loss : Impact of Full HLA-I Mismatch and Posttransplantation CD8+ Cell Reduction. *Am. J. Transplant.* **2013**, 2119–2129, doi:10.1002/ajt.12298.
334. Committee to Study Priorities for Vaccine Development; Division of Health Promotion and Disease Prevention; Institute of Medicine *Vaccines for the 21st Century*; Stratton, K.R., Durch, J.S., Lawrence, R.S., Eds.; National Academies Press: Washington, D.C., 2000; ISBN 978-0-309-05646-5.
335. Macagno, A.; Bernasconi, N.L.; Vanzetta, F.; Dander, E.; Sarasini, A.; Revello, M.G.; Gerna, G.; Sallusto, F.; Lanzavecchia, A. Isolation of Human Monoclonal Antibodies That Potently Neutralize Human Cytomegalovirus Infection by Targeting Different Epitopes on the gH/gL/UL128-131A Complex. *J. Virol.* **2010**, *84*, 1005–1013, doi:10.1128/JVI.01809-09.
336. Wussow, F.; Chiuppesi, F.; Contreras, H.; Diamond, D. Neutralization of Human Cytomegalovirus Entry into Fibroblasts and Epithelial Cells. *Vaccines* **2017**, *5*, 39, doi:10.3390/vaccines5040039.
337. Shen, S.; Wang, S.; Britt, W.J.; Lu, S. DNA vaccines expressing glycoprotein complex II antigens gM and gN elicited neutralizing antibodies against multiple human cytomegalovirus (HCMV) isolates. *Vaccine* **2007**, *25*, 3319–3327, doi:10.1016/j.vaccine.2007.01.011.
338. Shimamura, M.; Mach, M.; Britt, W.J. Human Cytomegalovirus Infection Elicits a Glycoprotein M (gM)/gN-Specific Virus-Neutralizing Antibody Response. *J. Virol.* **2006**, *80*, 4591–4600, doi:10.1128/JVI.80.9.4591-4600.2006.

339. Stegmann, C.; Abdellatif, M.E.A.; Laib Sampaio, K.; Walther, P.; Sinzger, C. Importance of Highly Conserved Peptide Sites of Human Cytomegalovirus gO for Formation of the gH/gL/gO Complex. *J. Virol.* **2017**, *91*, 1–22, doi:10.1128/JVI.01339-16.
340. Schulz, U.; Solidoro, P.; Müller, V.; Szabo, A.; Gottlieb, J.; Wilkens, H.; Enseleit, F. CMV Immunoglobulins for the Treatment of CMV Infections in Thoracic Transplant Recipients. *Transplantation* **2016**, *100*, S5–S10, doi:10.1097/TP.0000000000001097.
341. Chandramouli, S.; Malito, E.; Nguyen, T.; Luisi, K.; Donnarumma, D.; Xing, Y.; Norais, N.; Yu, D.; Carfi, A. Structural basis for potent antibody-mediated neutralization of human cytomegalovirus. *Sci. Immunol.* **2017**, *2*, eaan1457, doi:10.1126/sciimmunol.aan1457.
342. Chowdary, T.K.; Cairns, T.M.; Atanasiu, D.; Cohen, G.H.; Eisenberg, R.J.; Heldwein, E.E. Crystal structure of the conserved herpesvirus fusion regulator complex gH–gL. *Nat. Struct. Mol. Biol.* **2010**, *17*, 882–888, doi:10.1038/nsmb.1837.
343. Fouts, A.E.; Comps-Agrar, L.; Stengel, K.F.; Ellerman, D.; Schoeffler, A.J.; Warming, S.; Eaton, D.L.; Feierbach, B. Mechanism for neutralizing activity by the anti-CMV gH/gL monoclonal antibody MSL-109. *Proc. Natl. Acad. Sci.* **2014**, *111*, 8209–8214, doi:10.1073/pnas.1404653111.
344. Omerović, J.; Lev, L.; Longnecker, R. The Amino Terminus of Epstein-Barr Virus Glycoprotein gH Is Important for Fusion with Epithelial and B Cells. *J. Virol.* **2005**, *79*, 12408–12415, doi:10.1128/JVI.79.19.12408-12415.2005.
345. Plate, A.E.; Smajlović, J.; Jardetzky, T.S.; Longnecker, R. Functional Analysis of

- Glycoprotein L (gL) from Rhesus Lymphocryptovirus in Epstein-Barr Virus-Mediated Cell Fusion Indicates a Direct Role of gL in gB-Induced Membrane Fusion. *J. Virol.* **2009**, *83*, 7678–7689, doi:10.1128/JVI.00457-09.
346. Hua, H.; Kong, Q.; Zhang, H.; Wang, J.; Luo, T.; Jiang, Y. Targeting mTOR for cancer therapy. *J. Hematol. Oncol.* **2019**, *12*, 71, doi:10.1186/s13045-019-0754-1.
347. Yamaoka, T.; Kusumoto, S.; Ando, K.; Ohba, M.; Ohmori, T. Receptor Tyrosine Kinase-Targeted Cancer Therapy. *Int. J. Mol. Sci.* **2018**, *19*, 3491, doi:10.3390/ijms19113491.
348. Kang, B.W.; Chau, I. Molecular target: pan-AKT in gastric cancer. *ESMO Open* **2020**, *5*, e000728, doi:10.1136/esmoopen-2020-000728.
349. Gilic, M.B.; Tyner, A.L. Targeting protein tyrosine kinase 6 in cancer. *Biochim. Biophys. Acta - Rev. Cancer* **2020**, *1874*, 188432, doi:10.1016/j.bbcan.2020.188432.
350. Meineke, R.; Rimmelzwaan, G.; Elbahesh, H. Influenza Virus Infections and Cellular Kinases. *Viruses* **2019**, *11*, 171, doi:10.3390/v11020171.
351. Weisberg, E.; Parent, A.; Yang, P.L.; Sattler, M.; Liu, Q.; Liu, Q.; Wang, J.; Meng, C.; Buhrlage, S.J.; Gray, N.; et al. Repurposing of Kinase Inhibitors for Treatment of COVID-19. *Pharm. Res.* **2020**, *37*, 167, doi:10.1007/s11095-020-02851-7.
352. Palma, G.; Pasqua, T.; Silvestri, G.; Rocca, C.; Gualtieri, P.; Barbieri, A.; De Bartolo, A.; De Lorenzo, A.; Angelone, T.; Avolio, E.; et al. PI3K δ Inhibition as a Potential Therapeutic Target in COVID-19. *Front. Immunol.* **2020**, *11*, 1–9, doi:10.3389/fimmu.2020.02094.
353. Colombel, J.-F. Herpes Zoster in Patients Receiving JAK Inhibitors For Ulcerative Colitis: Mechanism, Epidemiology, Management, and Prevention. *Inflamm. Bowel*

- Dis.* **2018**, *24*, 2173–2182, doi:10.1093/ibd/izy150.
354. Pascual, J.; Royuela, A.; Fernández, A.M.; Herrero, I.; Delgado, J.F.; Solé, A.; Guirado, L.; Serrano, T.; de la Torre-Cisneros, J.; Moreno, A.; et al. Role of mTOR inhibitors for the control of viral infection in solid organ transplant recipients. *Transpl. Infect. Dis.* **2016**, *18*, 819–831, doi:10.1111/tid.12601.
355. Miller-Kittrell, M.; Sparer, T.E. Feeling manipulated: cytomegalovirus immune manipulation. *Viol. J.* **2009**, *6*, 4, doi:10.1186/1743-422X-6-4.
356. Haese, N.N.; Burg, J.M.; Andoh, T.F.; Jones, I.K.A.; Kreklywich, C.N.; Smith, P.P.; Orloff, S.L.; Streblow, D.N. Macrophage Depletion Of CMV-Latently Infected Donor Hearts Ameliorates Recipient Accelerated Chronic Rejection. *Transpl. Infect. Dis.* **2020**, doi:10.1111/tid.13514.
357. Gilbert, M.J.; Riddell, S.R.; Plachter, B.; Greenberg, P.D. Cytomegalovirus selectively blocks antigen processing and presentation of its immediate-early gene product. *Nature* **1996**, *383*, 720–722, doi:10.1038/383720a0.
358. Hansen, S.G.; Powers, C.J.; Richards, R.; Ventura, A.B.; Ford, J.C.; Siess, D.; Axthelm, M.K.; Nelson, J.A.; Jarvis, M.A.; Picker, L.J.; et al. Evasion of CD8+ T Cells Is Critical for Superinfection by Cytomegalovirus. *Science (80-.)*. **2010**, *328*, 102–106, doi:10.1126/science.1185350.
359. Cook, J.D.; Lee, J.E. The Secret Life of Viral Entry Glycoproteins: Moonlighting in Immune Evasion. *PLoS Pathog.* **2013**, *9*, e1003258, doi:10.1371/journal.ppat.1003258.
360. Schwinn, M.K.; Machleidt, T.; Zimmerman, K.; Eggers, C.T.; Dixon, A.S.; Hurst, R.; Hall, M.P.; Encell, L.P.; Binkowski, B.F.; Wood, K. V CRISPR-Mediated

- Tagging of Endogenous Proteins with a Luminescent Peptide. *ACS Chem. Biol.* **2017**, *13*, 467–474, doi:10.1021/acscchembio.7b00549.
361. Landreman, A.; Eggers, C. Quantifying Protein Abundance at Endogenous Levels Available online: <https://www.promega.com/resources/pubhub/2017/quantifying-protein-abundance-at-endogenous-levels/> (accessed on Jun 19, 2018).
362. Davis, T.A.; Loos, B.; Engelbrecht, A.-M. AHNAK: The giant jack of all trades. *Cell. Signal.* **2014**, *26*, 2683–2693, doi:10.1016/j.cellsig.2014.08.017.
363. Nieswandt, B.; Varga-szabo, D.; Elvers, M. Integrins in platelet activation. *J. Thromb. Haemost.* **2009**, *7*, 206–209, doi:10.1111/j.1538-7836.2009.03370.x.
364. Demirkan, A.; van Duijn, C.M.; Ugocsai, P.; Isaacs, A.; Pramstaller, P.P.; Liebisch, G.; Wilson, J.F.; Johansson, Å.; Rudan, I.; Aulchenko, Y.S.; et al. Genome-Wide Association Study Identifies Novel Loci Associated with Circulating Phospho- and Sphingolipid Concentrations. *PLoS Genet.* **2012**, *8*, e1002490, doi:10.1371/journal.pgen.1002490.
365. Branon, T.C.; Bosch, J.A.; Sanchez, A.D.; Udeshi, N.D.; Svinkina, T.; Carr, S.A.; Feldman, J.L.; Perrimon, N.; Ting, A.Y. Efficient proximity labeling in living cells and organisms with TurboID. *Nat. Biotechnol.* **2018**, *36*, 880–887, doi:10.1038/nbt.4201.

Appendix I – Antibody-Independent Quantification of Cytomegalovirus Virion Protein Incorporation Using HiBiT

Iris K. A. Jones^{1,2} and Daniel N. Streblow^{1,2}

¹ *The Vaccine & Gene Therapy Institute, Oregon Health & Science University, Beaverton, OR 97006*

² *Division of Pathobiology & Immunology, Oregon National Primate Research Center, Oregon Health & Science University, Beaverton, OR 97006*

This chapter is adapted from:

Human Cytomegaloviruses: Methods and Protocols, 2nd Edition, Chapter 11 (2020)

AI.1 Abstract

HCMV is a large double stranded DNA virus and member of the β -herpesvirus family. HCMV is ubiquitous in the human population and causes lifelong infections. HCMV infection is associated with high morbidity and mortality in immunocompromised individuals and the virus is a major cause of virus-mediated congenital disease. There have been a number of HCMV entry receptors identified that use one of two viral receptor binding complexes, including the gH/gL/gO complex and the pentamer made up of gH/gL/UL128/UL130/UL131A. CMVs are typically host-restricted requiring the use of species-specific modeling and culture conditions. We use RCMV to study CMV-accelerated vascular disease and chronic allograft rejection. RCMV encodes homologous versions of the entry complex proteins but their incorporation and copy number per virion are still unknown. In this methods article, we describe a novel approach of HiBiT tagging viral proteins in order to detect and quantify protein incorporation into particles. This method is independent of protein-specific antibodies and can be standardized using a commercially available HiBiT protein standard. Using BAC recombineering, we have constructed two individual viruses containing a HiBiT tag fused to the C'-terminus of either the UL128 homologue (R129) or the UL130 homologue (R131). Viruses containing these mutations were rescued, purified and analyzed. Our data demonstrate that R129 and R131 are both incorporated into RCMV virions at equimolar ratios relative to genome copy number, supporting this antibody-free approach for quantifying viral protein incorporation and its application towards the identification of domains required for incorporation.

AI.2 Introduction

HCMV requires a minimum of two membrane glycoprotein complexes for entry into cells including a gH/gL receptor binding complex and the viral fusion protein gB [62]. The gH/gL complex exists in at least three forms: 1) trimeric gH/gL/gO is required for entry into fibroblasts [71]; pentameric gH/gL/UL128/UL130/UL131A is required for entry into epithelial cells, endothelial cells and macrophages [71]; 3) gH/UL116 [72] has yet unknown functions but the homologous complex is required for RCMV entry into fibroblasts. The gH/gL binding region for the ULs is similar to gO but little is known about the structural binding requirements for UL116. Receptor binding induces conformational changes to the gH/gL complex that allow for interactions and triggering of the gB fusion machinery [62,318]. While many recent advances have increased our knowledge about the gH/gL receptor binding complexes, there is still much to learn about their function, receptor specificity, and stoichiometry. In addition, we have limited information regarding binding of entry proteins from CMV species other than HCMV.

Due to strict species specificity of CMVs, many investigators utilize animal models to study mechanisms of CMV dissemination and pathogenesis [360]. We have utilized RCMV infection in rats to examine the role of CMV infection in cardiac transplant rejection and cardiovascular disease. RCMV encodes proteins involved in the formation of all three of the gH/gL complexes. An interesting feature of the HCMV pentamer complex is the finding that UL128 and UL130 have characteristic chemokine folds at their N'-terminal region that extend away from the protein body [128,135]. The functional relationship between this chemokine structure and their role in entry is still unclear. Both proteins also contain unstructured regions at their C'-terminus with various charged

clusters involved in protein:protein interactions important for pentamer complex formation [320,321]. We were interested in dissecting the pentamer receptor binding versus chemokine activities in viral pathogenesis and cardiac transplant-related disease for the UL128 and UL130 homologues, R129 and R131, respectively. However, an important concern with our mutational strategy was to determine how mutations in the N'-terminal chemokine or C'-terminal pentamer binding regions affect pentamer formation. Because of this need, we sought to develop an assay to empirically determine the number of R129 and R131 molecules present in virus particles. However, developing antibodies to detect R129 and R131 is labor intensive and fraught with additional problems. The biggest issue being that the sensitivity of antibody-based assays is set by the binding affinity of the antibody towards the antigen. This feature of antibody binding often limits applications requiring the comparison of different proteins unless they share a common epitope or protein tag.

In this chapter, we detail the techniques used for the molecular tagging and detection of the RCMV pentamer complex proteins R129 and R131 using the HiBiT detection system. NanoLuciferase (NanoLuc) is a 19 kDa protein that generates luminescence with a higher dynamic range than conventional firefly luciferase. While the relatively small size of NanoLuc can be useful for quantifying levels of tagged protein expression or as a reporter for expression studies; the size is still considered prohibitive when studying proteins that form tight complexes wherein steric interference may affect protein interactions. The adoption of a split form of NanoLuc called NanoBiT was developed that contains two fragments of NanoLuc [360]. The small portion that consists of 11 amino acids of NanoLuc

is called HiBiT, and this is the portion that is fused to the protein of interest to be detected. The larger fragment of NanoLuc, called LgBiT, is present in the lytic and extracellular infection detection kits, as well as the HiBiT blotting system, from Promega. While these components are encoded and produced separately, they can associate to reconstitute the NanoBiT enzyme to release a bioluminescent signal following addition of substrate. Using this method, we demonstrate that this approach can be applied to full-length and truncated proteins to quantify the number of molecules incorporated into the virion. This approach could be used to quantify levels of virion incorporation of any viral or host protein, and the effect that mutations in those proteins have on their rate of incorporation into virions.

AI.3 Materials

AI.3.1 RCMV BAC recombineering

1. RCMV Maastricht strain BAC in SW102 *E.coli*
2. pc255-*Galk/Kan* plasmid
3. Prepare 50 mg/ml Kan stock solution in dH₂O. Filter sterilize through a 0.22 µm filter. Store at 4°C.
4. Prepare 12.5 mg/ml Chloramphenicol (Chlor) stock solution in ethanol, store at -20°C.
5. MacConkey agar plates: add 40 g of Difco MacConkey agar base without lactose plus 4 g D-(+)-Galactose to a 1 L bottle and Quantum sufficit (QS) to 1 L with dH₂O. Mix and autoclave to sterilize. Allow the solution to cool until warm to the touch, but not cool enough to solidify. Add Chlor to a final concentration of 12.5 µg/mL and Kan to a final concentration of 50 µg/mL.

Pour 20 mL of agar solution per plate and allow to solidify at room temperature overnight. Store at 4°C.

6. Cloning and sequencing primers are listed in Table 12.
7. DOG selection plates: M63 agar plates with 12.5 µg/mL Chlor.
8. M9 salts: 6 g Na₂HPO₄, 3 g KH₂PO₄, 1 g NH₄Cl, 0.5 g NaCl, QS to 1 L dH₂O.
Autoclave to sterilize.
9. PCR master mix for PCR screening of BAC clones: 2X PCR Platinum master mix.
10. PCR master mix for PCR amplification of genes for sequencing and cloning:
Platinum Supermix HiFi master mix.
11. DpnI (20,000 U/mL).
12. Molecular Biology Grade DNase/RNase-free water.
13. PCR machine.
14. Ultrapure agarose.
15. 50x TAE buffer: 242 g Tris base, 57.1 mL glacial acetic acid, 100 mL 0.5 M EDTA (pH 8.0), QS to 1 L dH₂O. pH to 8.4. Dilute to 1x with dH₂O prior to use. Store at room temperature.
16. SYBR safe DNA gel stain.
17. DNA gels: 1 % Ultrapure Agarose in TAE buffer with 2.5 µL SYBR Safe DNA gel stain per 40 mL gel.
18. Nucleic acids gel electrophoresis unit and power supply.
19. Gel extraction kit.
20. Spectrophotometer machine.

21. 0.1 cm electroporation cuvettes.
22. Electroporation system.
23. Centrifuge and microfuge.
24. 2X YT broth: 31 g broth powder dissolved in 1 L dH₂O. Autoclave to sterilize.
25. 15 mL conical tubes.
26. 50 mL conical tubes.
27. 14 mL polypropylene round-bottom culture tubes.
28. Erlenmeyer flasks (125 mL and 500 mL).
29. Plasmid DNA Midiprep kit.

Insertion/Detection	RCMV R131 HiBiT	RCMV R129_(short)HiBiT
Forward <i>Galk/Kan</i>	5'GTTGTCTCGGTTGC	5'AACTTTGATGGACAAGA
Homology primer	CTATTCCGAACGGCT ATTCTCTGTTGTCTG GGCAGCGGCCTGTTG ACAATTAATCATCGG CATAG	TCCA ACTATCCTGCAGAGA GTCCCTGCTCTATGTGGAT GTTCAAGGGGAAATTCAG TGTGTGGAAGATAGGTGTT CAGAAGGGCCTGTTGACA ATTAATCATCGGCATAG
Reverse <i>Galk/Kan</i>	5'TAAGAACGGAAAC	5'ACCTTCTCTGATAAGTTT
Homology Primer	GTAGTCTTAGGCGTC GGGAACGTCACACC GTACGTCATCGTTGT CACTCAGCAAAAGTT CGATTTA	TCTGAAGGAAAGGAAACA TATACACAAACATATAGA ACATAAGCATGTACACGT GTTAGATATCTAATAAAA ACTATACCTACTCAGCAAA AGTTCGATTTA
Forward Screening Primer	5'CGACTTATTTACCA GATGTACTCATAACC ATCTGTATGCTCAAG ATGTGTTGTCTCGGT TGCCTATTCCGAACG GCTAT	5'AACTTTGATGGACAAGA TCCA ACTATCCTGCAGAGA GTCCCTGCTCTATGTGGAT GTTCAAGGGGAAATTCAG TGTGTG
Reverse Screening Primer	5'CAAAACCTGGCGA CGGATGTGAACGAA	5'CCTTCTCTGATAAGTTTT CTGAAGGAAAGGAAACAT

	TGGCATAGGAGAAG	ATACACAAACATATAGAA
	TAAGAACGGAAACG	CATAAGCATGTACACGTGT
	TAGTCTTAGGCGTCG	TAGATA
	GGAACGTCA	
HiBiT Tag and	5'CGACTTATTTACCA	5'AACTTTGATGGACAAGA
RCMV Sequences	GATGTACTCATAACC	TCCAACATCCTGCAGAGA
for Recombination	ATCTGTATGCTCAAG	GTCCCTGCTCTATGTGGAT
	ATGTGTTGTCTCGGT	GTTCAAGGGGAAATTCAG
	TGCCTATTCCGAACG	TGTGTGGAAGATAGGTGTT
	GCTATTCTCTGTTGT	CAGAAGGGCATCACCATC
	CTGGGCAGCGGCATC	ACCATCACGTGAGCGGCT
	ACCATCACCATCACG	GGCGGCTGTTCAAGAAGA
	TGAGCGGCTGGCGG	TTAGCTAGGTATAGTTTTT
	CTGTTCAAGAAGATT	ATTAGATATCTAACACGTG
	AGCTGACAACGATG	TACATGCTTATGTTCTATA
	ACGTACGGTGTGACG	TGTTTGTGTATATGTTTCC
	TTCCCGACGCCTAAG	TTTCCTTCAGAAAATTAT
	ACTACGTTTCCGTTT	CAGAGAAGGT
	TACTTCTCCTATGC	
	CATTCGTTACATCC	
	GTCGCCAGGTTTTG	

Table 12. DNA primers.

AI.3.2 Virus rescue

1. BAC-derived DNA for RCMV-R129_(short) and RCMV-R131 HiBiT (described in Section AI.4.1).
2. Lipofectamine 2000 (ThermoFisher Scientific).
3. RFL-6 fibroblasts (ATCC) [*see Note 1*].
4. OptiMEM (ThermoFisher Scientific).
5. DMEM culture medium supplemented with 5% FBS, 100 U/mL penicillin, 100 mg/mL streptomycin, 20 mM L-glutamine.
6. 6-well tissue culture dishes.
7. 1.5 mL microcentrifuge tubes.
8. 2 mL polypropylene micro tube with screw cap.
9. DNA/RNA purification kit: GeneJET Viral DNA/RNA purification kit (ThermoFisher Scientific).

AI.3.3 RCMV growth and purification

1. Vented T175 tissue culture flasks.
2. PBS pH 7.2 without Calcium or Magnesium.
3. 70µm cell strainers (Fisher Scientific)
4. Ultra-clear ultracentrifuge tubes, 1 x 3.5" (Beckman Coulter).
5. Ultra-clear ultracentrifuge tubes, 9/16 x 3.5" (Beckman Coulter).
6. Ultracentrifuge machine and appropriate rotors: e.g. Beckman L7-65.
7. 500 mL Stericup 0.22 µm filter units (Millipore Sigma).

8. 10% D-sorbitol in PBS without Calcium or Magnesium. Filter sterilize through a 0.22 μm filter.
9. Histodenz (Sigma).
10. TNE buffer: 50 mM Tris [pH 7.4], 100 mM NaCl, 10 mM EDTA. Filter sterilize through a 0.22 μm filter.
11. 18-gauge 1 1/2" needles
12. Microcentrifuge machine
13. 0.6 mL micro tubes with snap cap.

AI.3.4 Western blotting

1. Cell culture grade water.
2. 10X Cell lysis buffer (Cell signaling technologies).
3. HALT protease inhibitor cocktail (100x) (ThermoFisher Scientific).
4. Sequencing grade modified trypsin.
5. 10-well Novex 10-20 % Tricine protein gels with 1.0 mm wells (ThermoFisher Scientific).
6. Novex Tricine SDS running buffer (2x) (ThermoFisher Scientific).
7. Mini protein gel electrophoresis tank and power supply.
8. BME.
9. Semi-dry transfer buffer: for 2 L mix 11.6 g Tris Base, 5.86 g Glycine and 400 mL methanol. QS to 2 L with dH₂O.
10. Semi-dry transfer cell and power supply.
11. 0.45 μm pore size Immobilon PVDF membranes (Millipore).

12. Nano-Glo HiBiT blotting system (Promega).
13. West Pico PLUS chemiluminescent solution (ThermoFisher Scientific).
14. Rat anti-gB monoclonal antibody (OHSU-VGTI Monoclonal Antibody Facility).
15. Rabbit anti-Rat IgG (H+L) HRP (Southern Biotech).

AI.3.5 HiBiT in-solution detection

1. Nano-Glo HiBiT lytic detection system (Promega).
2. HiBiT control protein (Promega).
3. 96-well white walled detection plates.
4. Multi-mode microplate reader machine.

AI.3.6 RCMV viral genome quantification

1. DNazol reagent (Invitrogen).
2. 100% and 70% molecular grade Ethanol.
3. qPCR master mix: Taqman fast advanced master mix (Applied biosystems).
4. 384-well qPCR plates
5. Optical adhesive films
6. RCMV qPCR primers and probe recognizing RCMV-R54. Forward primer: 5' CCTCACGGGCTACAACATCA (RCMV nucleotides 64,071-64,090); Reverse: 5' GAGAGTTGACGAAGAACCGACC (Reverse complement of RCMV nucleotides 63,963-63,984); Probe: 5'-VIC-CGGCTTCGATATCAAGTATCTCCTGCACC-TAMRA (RCMV nucleotides 64,041-64,069).

7. Quantification standard: RCMV viral genomic DNA at known concentration.
8. Real-Time PCR machine.

AI.4. Methods

AI.4.1 Generation of RCMV containing R131 or R129_(short) HiBiT fusion tags

The RCMV Maastricht strain genome was captured as a BAC using homologous recombination by replacing ORFs r144-r146 with a BAC cassette [133]. The BAC is resistant to Chlor and contains an eGFP cassette under the control of the HCMV MIEP. A two-step recombination protocol can be used to molecularly tag RCMV ORFs without leaving a sequence scar. Individual RCMV R129 and R131 recombinant viruses were constructed by addition of a C' terminal in-frame fusion tag consisting of 6 Histidine residues and the 11 amino acid HiBiT tag followed by a stop codon [*see Note 2*]. The first recombination step requires the incorporation of a gene cassette expressing *galK* and Kan resistance genes into the RCMV BAC genome at the genomic site for introduction of the tag. PCR is used to generate an amplicon containing 50-100 bp of homology [*see Note 3*] to the RCMV insertion site flanking the *galK/Kan* gene cassette. The amplified DNA is treated with Dpn1, purified and then electroporated into competent RCMV-BAC SW102 cells. Clones are positively selected for gain of resistance against Kan. Resistant clones are screened by PCR and sequenced to identify clones with the proper insertion. For the second step in the recombination process, PCR is used to generate a DNA fragment containing RCMV sequences with the gene-specific in-frame HiBiT tag as shown in Figure 29. The amplicon is electroporated into competent bacteria and negatively selected for *galK* replacement on DOG negative selection plates. At this stage BAC clones are grown and

checked by PCR and sequencing for correct incorporation of the HiBiT tag. DNA from correct clones is prepared for transfection rescue of infectious virus in mammalian cells.

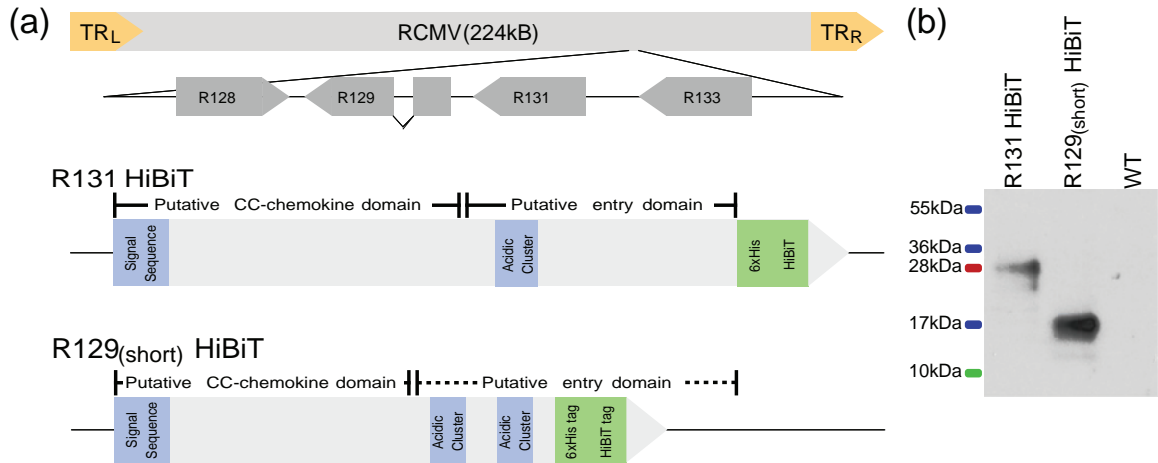


Figure 29. HiBiT tag design for R131 and R129_(short) viral proteins. (a) Schematic depiction of RCMV genome with R131 HiBiT and R129 HiBiT tagged proteins and putative protein domains. (b) HiBiT blot detection of R131-HiBiT (28 kDa) and RCMV R129_(short)-HiBiT (17 kDa) proteins in RCMV-infected cell lysates at the time of maximum cytopathic effect. Nano-Glo HiBiT blotting system was used for luminescence-based detection of proteins. RFL-6 cells infected with a BAC-derived RCMV lacking the fusion HiBiT tag was used as a negative control.

I. Generate PCR fragments for homologous recombination

1. Prepare PCR reaction for amplification of the *galk/Kan* cassette to create the construct for the first recombination step using homology primers and High-Fidelity PCR mix in a total volume of 50 μ L per reaction. Multiple reactions may need to be performed to ensure that enough amplicon is produced.
2. Perform PCR amplification using the following conditions: 3 minutes 95°C then 30 seconds at 95°C / 30 seconds at 58°C / 3 minutes at 72°C for 28 cycles. *These PCR conditions should be optimized for each individual amplicon and primer set.*

3. Treat the PCR product with 1 μ L Dpn1 at 37°C for at least one hour.
4. Run the PCR product on a 1% agarose TAE gel and cut out band corresponding to the PCR product and purify using a commercially available gel extraction kit and elute the final DNA product in 50 μ L Molecular biology-grade water.
5. Determine concentration of DNA product using a spectrophotometer.

II. First recombination step

1. Inoculate 5 mL of 2X YT broth plus 12.5 μ g/mL Chlor with SW102 cells containing the RCMV BAC and grow overnight at 30°C.
2. Add 500 μ L of the overnight culture to 25 mL 2X YT plus 12.5 μ g/mL Chlor and incubate at 30°C for approximately 3 hours (OD_{600} is between 0.55-0.6).
3. Heat-shock the 25 mL culture at 42°C for exactly 17 minutes.
4. Cool the culture on ice and transfer into two prechilled 50 mL conical tubes. Culture must be kept ice cold for steps until the electroporation is complete.
5. Pellet the culture at 650 Xg for 10 minutes at 0°C.
6. Pour off the supernatant and resuspend the pellet in 10 mL of ice-cold water by shaking gently.
7. Repeat wash steps once.
8. Resuspend the bacterial pellet in 1 mL of ice-cold water by shaking gently.
9. Transfer the resuspended bacterial pellet to a 1.5 mL microcentrifuge tube.
10. Pellet the culture at 5,000 Xg for 1 minute.
11. Pipette off the supernatant and wash once more in 1 mL ice-cold water.

12. Pipette off the supernatant and resuspend the bacterial pellet in 240 μ L of molecular biology-grade water.
13. Prechill a 0.1 cm cuvette on ice.
14. Into the cuvette add 300 ng of the PCR product and 60 μ L of electrocompetent cells, mix by gentle flicking.
15. Pulse the *galK/Kan* PCR product / competent cell mixture using the following settings: Voltage = 1.8 kV, Capacitance = 25 μ F, Resistance = 200 Ohms.
16. Immediately following electroporation, add 1 mL 2X YT broth to the cuvette and then transfer to a fresh 50 mL conical containing an additional 9 mL of 2X YT broth and incubate at 30°C for 2 hours.
17. Pellet bacteria and resuspend in 100 μ L of 2X YT broth.
18. Plate recovered bacteria on MacConkey/Kan/Chlor plates and incubate at 30°C for 2 days. Positive colonies should turn red and negative colonies will be white.
19. Pick individual colonies and PCR screen to identify positive colonies (positive PCR product should be around 2.5 kB). [*see Note 4*].

III. Second recombination step

1. Prepare electrocompetent positive clones by repeating steps outlined in AI.4.1.II (Steps 1-8) with the addition of 100 μ g/mL Kan to culture conditions.
2. Prepare PCR fragments containing the HiBiT tag sequence designed to replace the *galK/Kan* cassette [*see Note 5*].

3. Immediately following electroporation, add 1 mL 2X YT broth to the cuvette and then transfer to a fresh 50 mL conical containing an additional 9 mL of 2X YT broth and incubate at 30°C for 5 hours.
4. Pellet 1 mL of recovered bacteria by centrifugation at 10,000 Xg for 1 minute.
5. Resuspend bacterial pellet in 1.5 mL of M9 salts. Repeat this wash step once.
6. Plate the washed bacteria in M9 salts on DOG negative selection plates and incubate at 30°C for 2 days.
7. PCR screen to identify positive colonies, sequence the fragments to confirm proper genetic recombination [*see Note 6*].
8. To prepare BAC DNA for virus rescue transfections, inoculate 100 mL 2X YT broth plus 12.5µg/mL Chloramphenicol with positive clones.
9. Prepare BAC DNA containing the desired tags by DNA midiprep [*see Note 7*].

AI.4.2 Transfection of BAC DNA and rescue of RCMV-R131 and -R129_(short) HiBiT

The recovery of CMVs from BAC DNA requires a cell line that is competent for both the successful transfection of highly pure DNA and the ability of the virus to replicate. For the recovery of the Maastricht strain of RCMV, a rat lung fibroblast cell line called RFL-6 fulfills both requirements. Often it is necessary to use culture conditions that promote slower cell growth to prevent the cells from outgrowing the virus as it begins to propagate. We typically grow RFL-6 cells in 5% FBS for this reason. DNA prepared using a midiprep kit ensures sufficient DNA quantity and quality. Successfully transfected cells become GFP⁺ within 24-48 hours and viral spread to neighboring cells should occur within 7 dpi. Transfection of a range of DNA concentrations (2-10 µg) will allow for optimization of the

conditions necessary for successful rescue. Unless it is possible to identify a virus transfection condition with only one RCMV rescue per well, limiting dilution isolation of culture supernatants harvested at the time of maximum cytopathic effect should be performed to obtain a clonal virus for expansion. Virus mutational analysis and insert validation is accomplished by PCR screening and sequencing of DNA isolated from rescued RCMV.

1. Seed 6-well plates with RFL-6 cells at a density of 5×10^5 cells per well in 2 mL of complete DMEM culture medium at 18 hours before transfection.
2. Mix Lipofectamine 2000 (10 μ L/well) with DNA (2-10 μ g) in OptiMEM (1 mL), in a 1.5 mL microcentrifuge tube. Incubate at room temperature for 15 minutes.
3. Replace DMEM culture medium with 1 mL of OptiMEM containing transfection mixture.
4. At 4 hours post-transfection, replace transfection medium with 2 mL of fresh DMEM medium.
5. Monitor virus recovery and, at maximum cytopathic effect, collect supernatants and cells into 2.0 mL tubes.
6. Freeze at -80°C for further use.
7. In order to validate RCMV-R129_(short) and RCMV-R131 HiBiT insertions, purify viral DNA from 200 μ L of supernatant and extract using a DNA/RNA purification kit.
8. PCR amplify the region of insertion as described above in Section AI.4.1.III (Step 7).

- Sequence PCR products to confirm insertion (at this point the sequence of the entire virus can be performed to confirm virus integrity) [see **Note 8**].

AI.4.3 RCMV purification protocol

There are a number of different protocols for CMV purification. For virion structural studies we routinely infect at least 40 flasks of cells and harvest only supernatant virus at the time of maximum cytopathic effect. Supernatants are clarified of cell debris by centrifugation followed by filtration through a 70 μm filter. The virus is pelleted through a Sorbitol cushion and the pellet is then resuspended and banded using density gradient ultracentrifugation. The banded virus is removed from the gradient and then pelleted to concentrate. This approach yields a highly pure virus preparation with very little cellular contamination. The virus purification workflow is depicted in Figure 30.

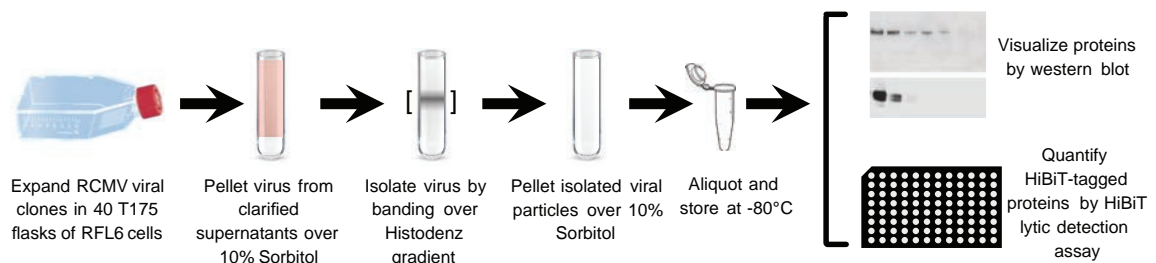


Figure 30. Virus purification and analysis workflow diagram.

- For each RCMV-HiBiT virus and control, infect 40 confluent RFL-6 T175 flasks with a MOI equal to 0.25. Incubate at 37°C until full cytopathic effect is achieved.
- Collect culture medium into 50 mL conical tubes and centrifuge at 1,989 X_g (Beckman GH-3.8 rotor) for 15 minutes.
- Filter supernatants through a 70 μm filter unit.
- Transfer clarified supernatants to SW32 centrifugation tubes (30 mL per tube).

5. Underlay each tube with 5 mL of 10% Sorbitol solution.
6. Add 2 mL of cell-free supernatants to the top of each tube for a total volume of 37 mL per tube. Tubes should be balanced appropriately prior to centrifugation.
7. Centrifuge at 76,755 Xg (Beckman L7-65 ultracentrifuge; SW32 rotor) for 70 minutes at 4°C.
8. Pour off the supernatants and resuspend the virus pellets in TNE buffer (4 mL total volume).
9. Overlay the resuspended pellet on top of thawed SW41Ti ultracentrifuge tubes containing 10%-50% Histodenz gradient, 2 mL per tube. [*see Note 9*]
10. Centrifuge at 111,132 Xg (Beckman ultracentrifuge; SW41Ti rotor) for 2 hours at 4°C.
11. Virions should be visible as a white band. Collect virion band by fractionating the gradient contents by draining from the bottom of the centrifugation tube using an inserted needle.
12. QS the banded virus fractions in PBS up to 32 mL.
13. Pellet virus as described in Section AI.4.3 (Steps 4-7).
14. Pour off the supernatants and resuspend the virus pellet with 300 µL PBS.
15. Store 30 µL aliquots at -80°C until further analysis.

AI.4.4 Virion protein detection

Serial dilutions of the RCMV virion preparations were separated by SDS-PAGE and analyzed by immunoblotting for the presence of HiBiT tagged proteins and gB. Figure 31

demonstrates that R131-HiBiT and R129-HiBiT are present in their respective virion preparations. Staining for gB was used to normalize virion preparations for further studies.

1. To purified virus preparations, add Tricine loading buffer + 2% BME at a ratio of 1:1.
2. Boil samples at 100°C for 5 minutes and allow to cool to room temperature before loading.
3. Separate samples by electrophoresis on 10-20% Tricine gels at 125 V for 1 hour.
4. Transfer the proteins to a PVDF membrane using a semi-dry transfer system at 25V for 25 minutes.
5. In order to stain for both gB and HiBiT, cut across the membrane at the 36 kDa marker.
6. Detect the presence of gB on the upper blot using a monoclonal anti-gB antibody, as follows in steps 7-13.
7. Block with 5% BSA in TBST (0.1% Tween-20) buffer for one hour at room temperature.
8. Incubate the blot with 10 mL of rat anti-gB antibody diluted 1:1,000 in 5% BSA-TBST for one hour at room temperature.
9. Wash the blot 3 times (20 mL) with TBST at room temperature (20, 15, and 5 minutes).
10. Incubate the blot with an anti-rat secondary antibody at 1:5,000 in TBST.
11. Wash 3 times in TBST as in Section AI.4.4 (Step 9). Perform one final wash with 10 mL water.

12. Add 2 mL each of pico chemiluminescent substrate solutions and incubate at room temperature for 3 minutes, shaking gently.
13. Image blot using X-Ray film (Chemiluminescent gel image systems may also be used).
14. Detect presence of HiBiT tag on the lower blot using HiBiT blotting kit, as follows in steps 15-19.
15. Wash the blot for 5 minutes in TBST.
16. Add 1 mL of 10X HiBiT blotting buffer and 50 μ L of LgBiT protein to 9 mL of water and mix.
17. Incubate blot in 10 mL of HiBiT blotting buffer containing LgBiT for 1 hour at room temperature.
18. Add 20 μ L of HiBiT substrate directly to the 1X blotting buffer with LgBiT and rock at room temperature for 5 minutes.
19. Image blot for luminescent signal using X-Ray film (Chemiluminescent gel image systems may also be used).

This detection method was used to confirm the presence of the HiBiT tags in virus particles and to normalize levels of gB staining for wild type RCMV and viruses containing R131-HiBiT or R129_(short)-HiBiT tags for biochemical analyses.

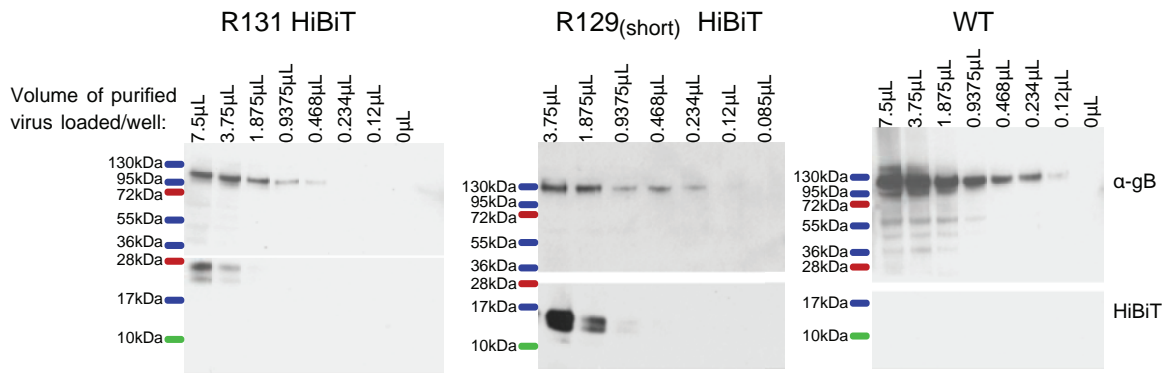


Figure 31. Detection of virion-associated proteins. Histodenz-purified viral preparations of RCMV R131-HiBiT, RCMV R129_(short)-HiBiT, and RCMV WT were generated as described in Section AI.4.3. Varying amounts of viral preparations were separated by SDS-PAGE and analyzed by western or HiBiT blot as described in Section AI.4.4. The extent of gB staining was used to normalize samples when used in Section AI.4.5.

AI.4.5 Trypsin sensitivity of virion-associated R131 and R129_(short) HiBiT

Trypsin treatment of virions is often used to determine whether proteins are present on the outside membrane of the virus particle, accessible to trypsin. In this procedure, we trypsin treated virion preparations that were normalized to levels of gB protein in order to verify that R129 and R131 are on the outside of the virion, similar to the viral glycoprotein gB (Figure 32). Protein analysis procedures were similar to those described in Section AI.4.4.

1. For this analysis, create duplicate samples of virion preparations; one of the duplicates will be treated with trypsin and the other will remain untreated. To produce each sample, pipette equivalent gB levels of each virus into an Eppendorf tube and add PBS to a total volume of 15 μ L. Add 10 μ L of sequencing grade modified trypsin (0.5 mg/mL) or the equivalent volume of PBS and incubate the samples at 37°C for 1 hour.

2. Add 25 μ L of Tricine loading buffer containing 2% BME to each sample and heat at 100°C for 5 minutes.
3. Separate samples by SDS-PAGE using 10-20% Tricine gels with a run time of 1 hour at 125 V.
4. Transfer the proteins to a PVDF membrane using a semi-dry transfer system at 25 V for 25 minutes.
5. Detect RCMV gB by immunoblotting and the HiBiT-tagged proteins using the HiBiT blotting system as described above in Section AI.4.4.

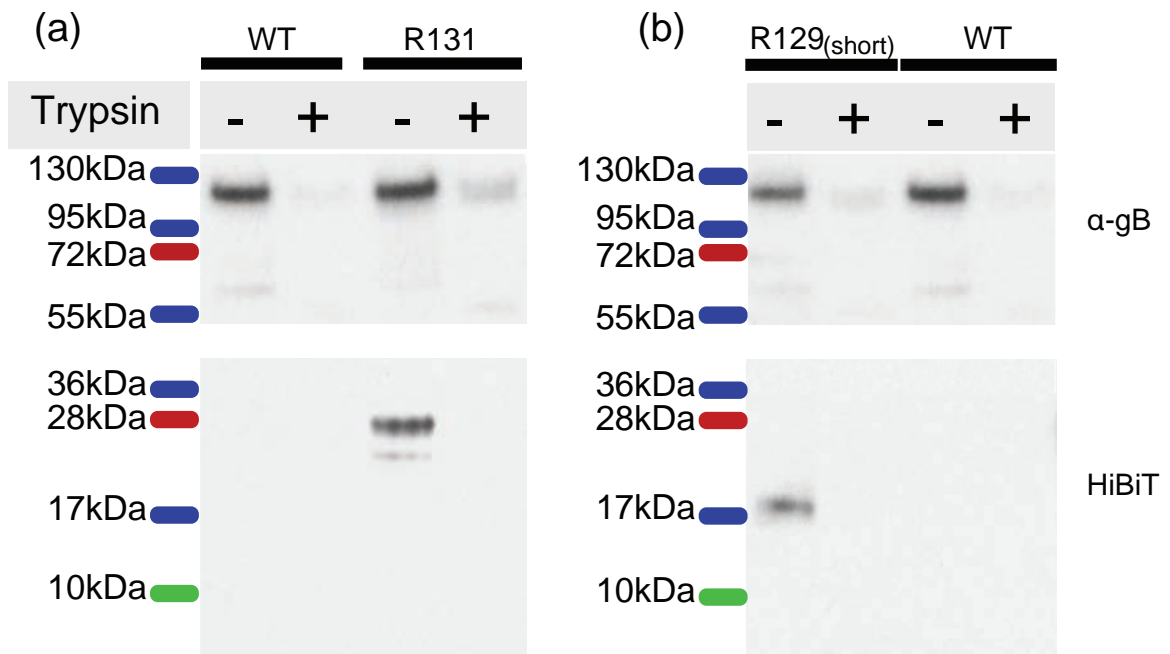


Figure 32. R131 and R129 HiBiT proteins are trypsin sensitive. To demonstrate that the virion incorporated R131 and R129 proteins were present on the outside of the virus particle, wild type RCMV, RCMV R131-HiBiT and RCMV R129_(short)-HiBiT viral preparations, normalized to gB content, were treated with PBS or sequence grade Trypsin for 1 hour at 37°C. Samples were then separated by SDS-PAGE and blotted for gB and HiBiT. Both gB and HiBiT tagged proteins were sensitive to trypsin treatment indicating that they were accessible on the virion surface

AI.4.6 Quantification of virion-associated R131- and R129_(short)-HiBiT-tagged molecules relative to viral genome copy number

In order to quantify the levels of the pentamer complex proteins per virion, we developed a two-pronged strategy. First, we determined the level of virion incorporated HiBiT tagged proteins using an in-solution assay and a commercially available HiBiT control protein standard. In the second step, viral genome levels in equivalent amounts of virion preparations was quantified using real-time PCR. Three different starting amounts of each virus were used in order to assess whether input levels affect the detection and calculation of HiBiT molecular copy number per viral genome. We calculated the relative copy number of virion-associated R129 and R131 and found that they were equimolar. This method could be useful to identify functional domains in R129 and R131 and determine how mutations in these proteins affect the levels of virion-associated pentamer and to correlate how the level of pentamer affects entry activity.

I. In-solution detection of HiBiT

1. Add 7.5 μ L, 3.75 μ L, 1.875 μ L of R131-HiBiT, R129_(short)-HiBiT, and WT RCMV purified viral particles in PBS in duplicates to a white-walled 96-well plate.
2. QS samples to 25 μ L with PBS.
3. Prepare a 7-point standard curve using the HiBiT control protein diluted in PBS, ranging from 1,000 to 15.625 nM. Add 25 μ L of each standard in duplicate to the white-walled 96-well plate.
4. Add 25 μ L of PBS to duplicate wells as a background control.

- Dilute the LgBiT protein 1:100 and the Nano-Glo HiBiT Lytic Substrate 1:50 in Nano-Glo HiBiT Lytic Buffer. Add 25 μL of HiBiT lytic detection reagent to each sample well.
- Seal the plate and shake at medium-low on a plate shaker in the dark for 10 minutes.
- Read sample luminescence on a 96-well plate reader [see **Note 10**]. (Figure 33a).
- Calculate molecules of HiBiT control protein for each standard. Perform a linear fit on a log-log transform of the standard curve using the mean of the standard curve duplicates (Figure 33b). Calculate the molecules of HiBiT-tagged protein in the samples based on the mean luminescence reading for each sample. (Figure 33c).

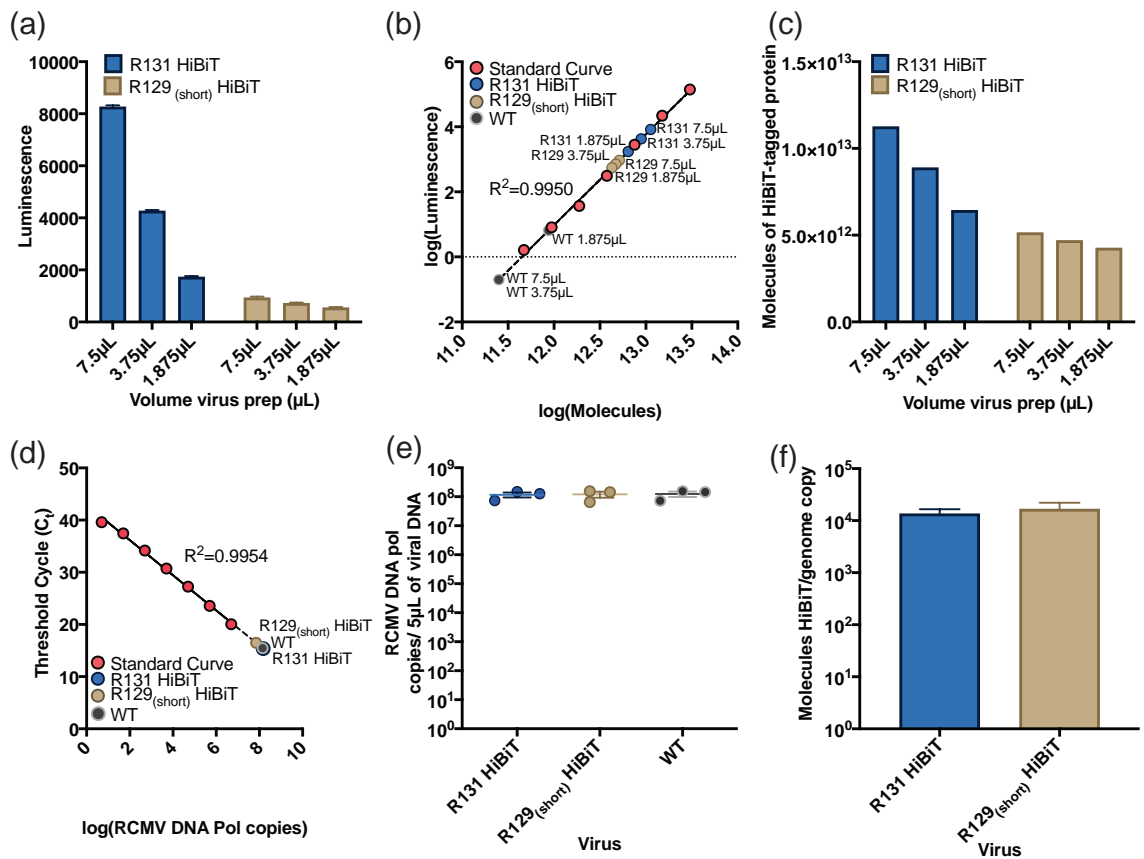


Figure 33. Determination of R131 and R129_(short) HiBiT molecules relative to viral genome copies. (a) In-solution luminescence assay results of HiBiT-tagged viral proteins. Three different volumes of viral particles were diluted to 25 μL and loaded into a 96-well plate in duplicates. (b) Log-log transform of the standard

curve from the HiBiT lytic detection assay with mean of duplicate standards shown in red and unknown sample means shown and labeled. R^2 of the linear regression of the standard curve was 0.9950. Standard curve was defined as a given number of molecules of HiBiT control protein. (c) Molecules of HiBiT-tagged proteins in unknown samples calculated from standard curve using average luminescence of duplicate sample wells. (d) $\log(X)$ transform of qPCR standard curve with mean of technical triplicates shown in red and unknown sample means shown and labeled. R^2 of the linear regression of the standard curve was 0.9954. Standard curve was created using RCMV viral DNA at known genome concentrations in 1:10 dilutions ranging from 5×10^6 – 5 genome copies per well. (e) RCMV DNA Pol copies per 5 μ L of RCMV viral DNA determined by qPCR against a standard curve of known genome copies. (f) Molecules of HiBiT per genome copy as determined in AI.4.6. R131-HiBiT and R129_(short)-HiBiT showed similar levels of protein incorporation per viral genome

II. Quantification of viral DNA genomes

1. Add 1 mL DNazol to 15 μ L of purified virus preparations (*see Note 11*). Add 500 μ L 100% ethanol to each sample. Mix by inverting the tube 10 times.
2. Centrifuge at 5,200 rpm in a microfuge for 15 minutes to pellet the DNA.
3. Wash the DNA pellet twice with 1 mL 70% ethanol. After each wash, spin the sample at maximum speed in a table-top centrifuge for 5 minutes. Carefully pipette off all of the supernatant and air dry the pellet for 15 minutes.
4. Once the pellet is dry, add 30 μ L of molecular biology-grade water to resuspend the DNA.
5. Heat the sample at 55°C in a shaker for 10 minutes.
6. Dilute the viral DNA 1:3 in molecular biology-grade water. Perform qPCR with primers and probes designed against RCMV DNA polymerase (R54) in technical triplicate.

7. Prepare RCMV qPCR standard consisting of 1:10 dilutions ranging from 1×10^6 genome copies/ μL to 1 genome copy/ μL . Use 5 μL /well for samples and standards.
8. Prepare PCR reaction for detection of RCMV genomic DNA. Load 10 μL PCR mix/well plus 5 μL sample DNA/well.
9. CMV qPCR run cycle parameters: 3 minutes at 95°C/s, then 40 cycles of 95°C for 1 second, ramped down at a rate of 1.6°C/s to 60°C, and 60°C for 20 seconds. *These PCR conditions were optimized for this primer and probe set.*
10. Utilize TaqMan software to calculate the number of genome copies/sample (Figure 33d,e).
11. Calculate the number of genome copies/ μL in each original prep (RCMV WT, RCMV R131-HiBiT, and RCMV R129_(short)-HiBiT) as follows:

- *RCMV DNA pol copies = RCMV genome copies*
- *Genome copies per sample = Genome copies per 5 μL*
- $$\frac{\text{Genome copies per } 5\mu\text{L}}{5} = \text{Genome copies per } 1\mu\text{L}$$
- *Genome copies per 1 μL x 3 =*
Original genome concentration from extracted DNA per μL
- *Original genome concentration from extracted DNA per μL x 30 μL =*
Total genome copies in extracted DNA
- $$\frac{\text{Total genome copies in extracted DNA}}{15\mu\text{L}} =$$

Total genomes per μL in initial prepared virus

12. Calculate the Molecules of HiBiT-tagged protein per μL over Genome copies per μL for each virus (Figure 33f).

AI.4.7 Observations

Protein tags are an essential tool of biochemical studies. Here, we have demonstrated that the 11-amino acid HiBiT tag of proteins in CMV BAC-derived viruses enable specific and quantitative detection of proteins. We used this technology to visualize and quantify incorporation of two putative pentamer entry proteins in RCMV, R129 and R131. Furthermore, we were able to quantify the incorporation of these proteins per viral genome by measuring both incorporated proteins and viral genome copies per volume of viral particles. We determined that R129_(short) was incorporated into viral particles at an average of 16,622 molecules per viral genome, and that R131 was incorporated at an average of 13,508 molecules per viral genome. These calculations assume that the number of viral particles was equal to the number of viral genomes and future studies should incorporate infectious virus particles into these equations. Future studies utilizing this technique can be performed to identify the functional domains in the C'-terminal region necessary for formation of the RCMV pentamer and determine the effect of mutations on the number of R129 and R131 proteins incorporated into viral particles. Although, we showed here that R129_(short)-HiBiT is still incorporated into viral particles, we left the predicted necessary charge clusters intact in this mutant (*see* Figure 29a). Next, we intend to design C'-terminal/acidic cluster mutants to determine the impact of these mutations on incorporation of these proteins into the viral particle. This technology could also be employed to

determine the molecular copy number of other virion-associated proteins or to quantify viral protein expression levels in cells.

AI.5 Notes

1. RFL-6 cells were used to transfect, expand, and titer the virus. Cells were maintained in DMEM (Corning) supplemented with 5% FBS, 100 U/mL penicillin, 100 mg/mL streptomycin, 20 mM L-glutamine (PSG).
2. The amino acid sequence of the HiBiT tag is VSGWRLFKKIS (GTG AGC GGC TGG CGG CTG TTC AAG AAG ATT AGC) [360,361]. Location of the HiBiT tag within the protein is an important consideration as placement into a region that is buried upon protein folding will decrease detection of naturally folded protein. The 6x-His tag was added to allow for eventual pull-down of the tagged proteins and their complexes. The 6x-His tag was constructed using alternating CAT-CAC codons.
3. The length of the homology arms should be at least 50 bp each. If the second step of the recombination process (replacing *Galk/Kan* with the gene insert) proves challenging, the homology arms should be extended to 100+ bp each as a first approach.
4. For mixed colonies detected by PCR screening, repeat growth in 2X YT broth plus 12.5 µg/mL Chlor and 100 µg/mL Kan followed by plating onto MacConkey/Kan/Chlor selection plates and rescreen colonies by PCR. If necessary, the concentration of the Kan may be increased up to 200 µg/mL to improve selection.

5. For convenience, we order the 2nd-Step replacement DNA fragment from a commercial vendor. The R129 and R131 HiBiT tag replacement fragments contained a 6x-His/HiBiT fusion tag flanked by 50-100 bp homology to the insertion site in the RCMV genome. These gene fragments may be PCR amplified and cloned to provide a stock of the gene fragment for future PCR reactions.
6. For the 2nd recombination step, positive clones arise through recombination and replacement of the *GalK* gene; however, it is possible that spontaneous mutations that arise in the *GalK* gene can grow on the DOG plates. PCR and sequencing should reveal whether the colonies contain the proper genetic recombination event.
7. DNA midiprep kit was used to prepare BAC DNA for analysis and transfection into mammalian cells. For RCMV BAC recovery, the phenol-chloroform method of DNA isolation failed to successfully rescue RCMV. BAC DNA preparations should be used within 24 hours for best results.
8. PCR amplification and gel purification of the region including the inserted tags prior to sequencing provides cleaner sequencing results. However, it is possible to submit the BAC DNA for sequencing directly. Whole DNA genome sequencing should be performed on viral genomic DNA preparations.
9. A discontinuous 10-50% Histodenz gradient was prepared in TNE buffer (50 mM Tris [pH 7.4], 100 mM NaCl, 10 mM EDTA). The 50% Histodenz layer was at the bottom of an SW41Ti ultracentrifuge tube and individual 5% steps (1 mL) were layered on top. Each layer was frozen prior to addition of the next to prevent mixing of layers and to retain clean step interface lines. Prior to use the centrifuge gradients were completely thawed. Virus particle preparations were resuspended in 2 mL of

TNE buffer (no Histodenz), which was added to the top of the 10% Histodenz layer prior to centrifugation.

10. A Synergy HTX multi-mode microplate BioTeK plate reader was used to read the HiBiT in-solution assay with the following settings: Luminescence endpoint; Integration time (1.00 seconds); Emission (Hole); Optics: (Bottom); Gain (135); Actual Temperature (22.6°C).
11. DNA extraction is necessary to obtain clean DNA for the qPCR reaction. Performing qPCR on the viral preparation alone results in degradation of the PCR product.

AI.6 Acknowledgements

The methods development presented in this manuscript was supported by a grant from the National Institutes of Health NIAID RO1 AI116633. IJ was supported by the OHSU Molecular Microbiology and Immunology Interactions at the Microbe/Host Interface training grant NIH T32 AI007472. We thank Drs. Brock Binkowski, Chris Eggers, and Jessica Rossol-Allison for helpful discussions and advice about the HiBiT system.

Appendix II – Characterizing the RCMV-encoded protein

r152.4

Iris K. A. Jones¹, Zachary J. Streblow¹, Michael Denton¹, Daniel N. Streblow¹

¹ *The Vaccine & Gene Therapy Institute, Oregon Health & Science University, Beaverton, OR 97006*

III.1 Abstract

HCMV is a β -herpesvirus that causes acceleration of TVS and CR in organ transplant recipients. Development of therapeutics or vaccines aimed at minimizing HCMV associated morbidity and mortality in transplant patients will be essential for the improvement in organ rejection rates following transplantation. Due to the high species specificity of CMV the development of such therapies requires the use of animal models with the appropriate CMV for the model chosen. The use of an allogeneic rat transplant model to study cardiac transplantation provides an ideal small animal model because RCMV infection recapitulates the acceleration of TVS and CR seen in transplant recipients. However, there remain identified ORFs in RCMV for which the function remains unknown. One of these genes is r152.4, which is highly expressed in multiple tissues following transplantation [247]. r152.4 has been identified based on sequence homology as an m145 glycoprotein family member, with greatest similarity to m152 [132]. This suggests that it may adopt an MHC-I-like fold. However, any homologous proteins of r152.4 in HCMV have yet to be identified and the function of r152.4 remains to be described. Additionally, to date, no interactions with host proteins have been identified. Here, we show that r152.4 is highly glycosylated like its MCMV m145 family predicted homologues. Additionally, we show that r152.4 is expressed with early viral gene kinetics. This is in contrast to HCMV UL18, which is predicted to have similar functions, and is expressed with late viral gene kinetics, but is consistent with MCMV m152, which is expressed with early gene kinetics. Loss of RCMV r152.4 does not impair multi-step growth curves in rat RFL6 fibroblasts, but does decrease viral loads in tissues during *in vivo* infections. Although extensive work has been done in describing the immune-

modulatory genes of MCMV, this work provides the first characterization of a proposed MHC-I-like protein in RCMV.

AII.2 Introduction

CMV is a β -herpes virus that establishes persistent, latent infection in hosts. HCMV is an opportunistic pathogen, causing disease primarily in immunocompromised patients and congenital infections. Due to the high species specificity of CMV several model systems are commonly used to study HCMV pathogenesis including MCMV, RCMV, RhCMV, and gpCMV models in their respective host species. Functional and sequence conservation of viral ORFs varies greatly between CMV species. As such, it is important to identify the function of ORFs across different model species.

CMV has extensive tools to modulate the host immune response. For example, HCMV encodes several immune-modulation genes that affect or mimic MHC-I. The most notable of these is UL18, which adopts an MHC-I-like fold [224], but has only approximately 25% sequence similarity to classical MHC-I [225]. UL18 binds LILRB-1 on NK cells [224,226,227], and presents peptide similar to host MHC-I [228]. HCMV UL18 contains 13 potential N-linked glycosylation sites, that allow for most of the protein to be shielded by carbohydrate groups, preventing protein-protein interactions beyond binding LILRB-1 and peptide presentation [224]. UL18 was initially proposed to block NK cell-mediated killing; however, further work revealed its function to be more nuanced [229]. LILRB1⁺ NK cells were inhibited by UL18 expressing fibroblasts, whereas LILRB1⁻ NK cells were activated [230]. Importantly, UL18 is not essential for HCMV replication *in vitro* [231],

and is not expressed until approximately 72 hpi [232], suggesting late gene expression kinetics. Additional immune-modulators encoded by HCMV include US3 and US6, which are involved in blocking MHC-I trafficking to the cellular membrane. US3 prevents trafficking of MHC-I out of the ER, resulting in perinuclear accumulation of MHC-I heavy chains [233]. US6 blocks MHC-I antigen presentation by binding to TAP [234]. UL18 interacts with US6 to restore TAP function for loading of peptides on to UL18, while still preventing interaction of MHC-I molecules with TAP [235].

Similarly, MCMV encodes a family of genes consisting of m145, m146, m150-m155, m157, m158, and m17 that are involved in immune modulation [241,242]. Similar to HCMV UL18, MCMV m145 family members typically include a signal peptide, a transmembrane domain, and several N-linked glycosylation sites [242]. Several of these genes are predicted to adopt an MHC-I-like fold [243], and the solved structures of m144 (a relative of the m145 family), m153, and m157 all exhibit MHC-I-like folds [244–246]. RCMV encodes several predicted homologues of these genes including r145, r149, r150, r151, r151.3, r152, r152.2, r152.3, r152.4, r155, and r157 [132,242]. One of these, RCMV r152.4, is of particular interest because it is highly expressed in multiple tissues during *in vivo* infections [247] and is most closely related to m152 [132], which has multiple immune-modulation functions reviewed previously [242]. Briefly, MCMV m152 has been shown to down-regulate Rae-1, a ligand of the activating NK cell receptor NKG2D. In addition, m152 has been shown to down-regulate MHC-I gene expression by retaining the MHC-complex to the ER, similar to the function of US3 in HCMV. This blockade of antigen presentation provides a resistance to cytotoxic T-lymphocyte attack of infected

cells, a process that is regulated by m152 in conjunction with m04 and m06, two additional genes that alter antigen presentation on infected cells [248–250]. These functions provide selective advantage for the virus as an m04/m06/m152 mutant MCMV had a 10-fold reduction in viral titers in salivary glands of mice [251]. However, m152 appears to have no impact on the ability of the virus to infect, persist, or establish latency [252]. Interestingly, transfection experiments showed that m152 is primarily expressed intracellularly with only limited expression at the cell surface [242]. The RCMV homologues of the m145 family members remain less well elucidated than their MCMV counterparts. Here, we characterize the expression of RCMV r152.4 and its role in viral infection.

III.3 Results

III.3.1 Characterization of RCMV r152.4

Previous studies had identified the RCMV r152.4 ORF as being highly expressed at multiple time points following infection *in vivo* [247]. The RCMV viral ORF r152.4 is 1.14kB in length, situated towards the left terminal repeat of the RCMV genome. r152.4 is bordered on either side by the r152.5 and r152.3 ORFs (Figure 34a). MHC-I-like proteins in MCMV and HCMV are heavily glycosylated, suggesting that RCMV r152.4 might also contain several potential glycosylation sites. To verify this, the r152.4 ORF was loaded into the Eukaryotic Linear Motif resource and structural domains and post-translational modifications were predicted. The predicted size of the protein is 43.384 kDa with a predicted signal sequence at amino acids 1-22, a trans-membrane domain at 336-358, and a cytoplasmic tail from 358-379 (Figure 34a). RCMV r152.4 contains 21 potential N-linked

glycosylation sites (Figure 34a). To determine the extent of the glycosylation, RFL6 fibroblasts were infected with RCMV at an MOI=1 and cell lysates were harvested at 48 hpi (Figure 34c). Detection of r152.4 with an anti-r152.4 antibody revealed two bands running at approximately 115kDa and 90kDa. Treatment of cell lysates with Endo H, which cleaves select N-linked glycosyl groups, resulted in 4 clear bands at approximately 105, 50, 43, and 32 kDa and a smear at 20kDa. Treatment with PNGase F, which cleaves all N-linked glycosyl groups, eliminated the higher molecular weight bands and resulted in 3 clear bands at approximately 50, 43, and 30 kDa.

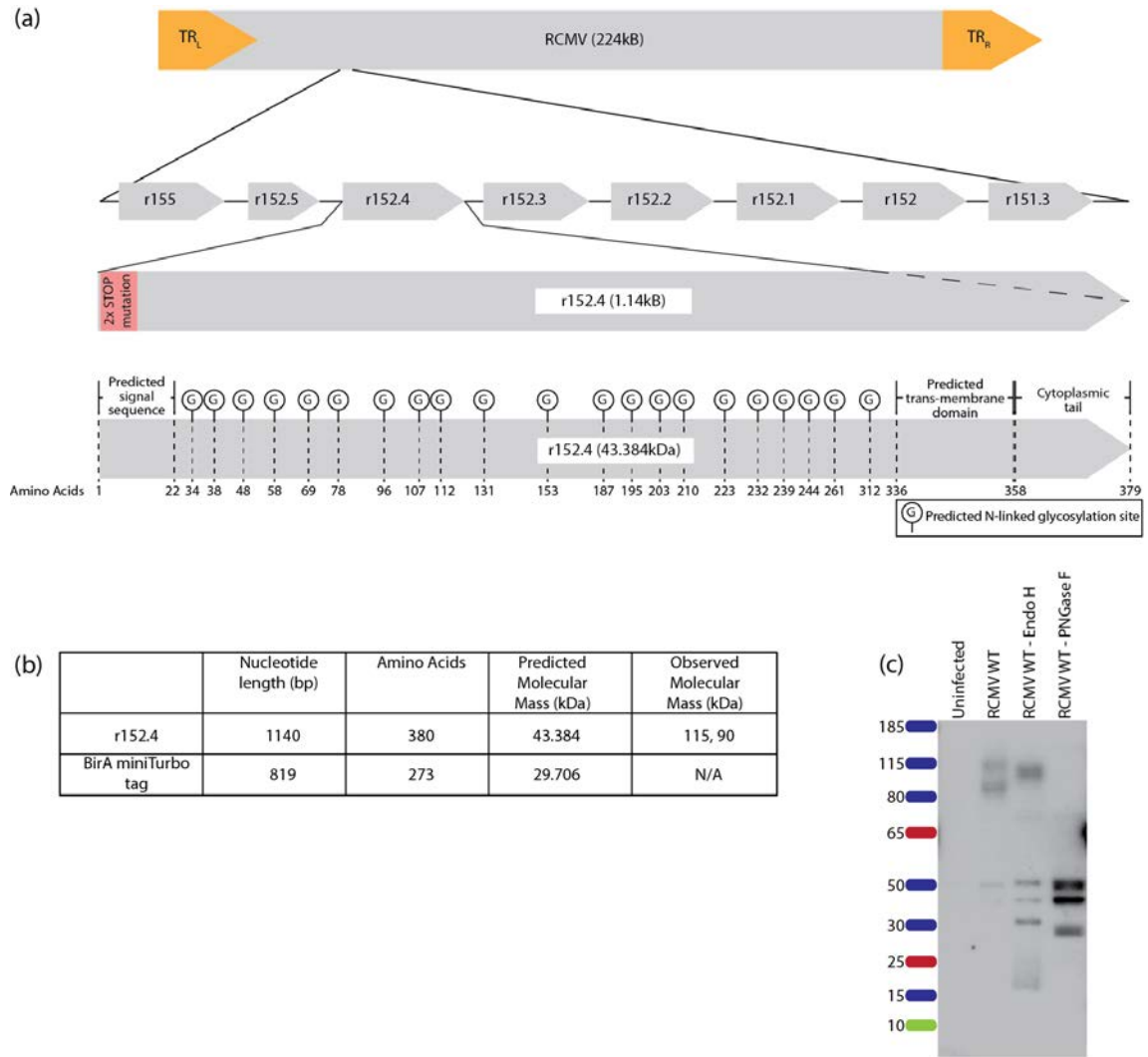


Figure 34. RCMV r152.4 is heavily glycosylated. (a) Diagram of r152.4 and the surrounding area in the RCMV genome. Location of the 2x STOP codons in the r152.4 2x STOP mutant is at the N'terminus of the protein as depicted. The 21 predicted N-linked glycosylation sites are depicted by G markings. (b) Observed size of r152.4 is significantly greater than the predicted size. (c) Glycosidase treatment of infected cell lysates reduces r152.4 to the predicted size. RFL6 cells were plated in 6-well dishes at 5×10^5 cells/well and infected with RCMV GFP at an MOI=1 or left uninfected as a control. Lysates were harvested at 48 hpi then treated with Endo H or PNGase F and a western blot was performed.

To determine the expression kinetics of r152.4, RFL6 fibroblasts were infected in duplicate with RCMV at an MOI of 1 and harvested in cell lysis buffer at 8, 24, 48, and 72 hpi. Additional samples were infected for late timepoints, 48 and 72 hpi, and treated at the time of infection with 100 μ M foscarnet (a DNA polymerase inhibitor that blocks late viral gene expression). Western blots showed expression of r152.4 by 24 hpi, with no impact of Foscarnet on protein levels, indicating that r152.4 is expressed with early viral gene expression kinetics (Figure 35). Viral gB and IE were used as controls for viral protein expression.

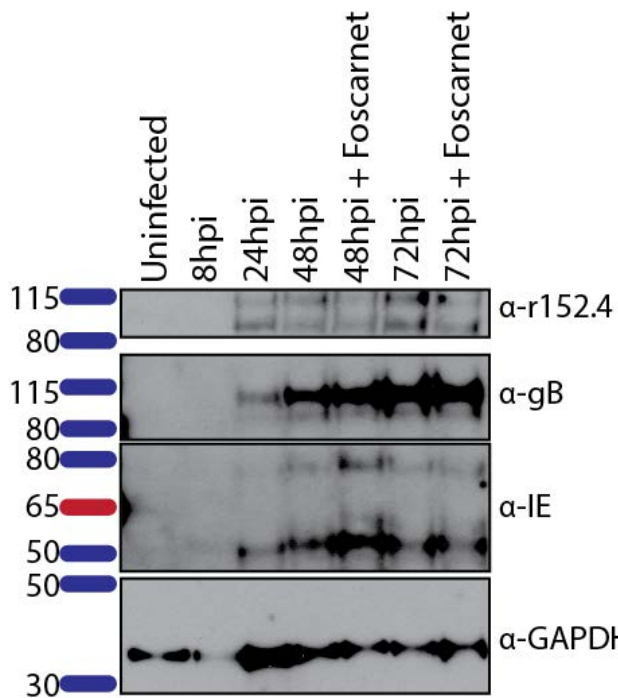


Figure 35. r152.4 is expressed with early viral gene kinetics. Fibroblasts were plated in 6-well dishes at 5×10^5 cells/well and infected with RCMV GFP at an MOI=1 or left uninfected as a control. Foscarnet (100 μ M) was added to samples indicated at the time of infection. Infection groups were performed in duplicate. Samples were harvested in cell lysis buffer containing protease inhibitors and total protein concentrations were determined by BCA assay. Equal quantities of protein were loaded and proteins were detected via western blots with

anti-r152.4, anti-gB, anti-IE, and anti-GAPDH antibodies. The single replicate shown for each timepoint is representative of the duplicate samples. r152.4 was detectable by 24 hpi and was unaffected by Foscarnet treatment.

AII.3.2 r152.4 interacts with the cellular proteins AHNAK, Talin-1, and Pdxdc1

To identify interacting partners of r152.4 during *in vitro* infections, a recombinant RCMV was generated that contained a BirA mini Turbo tag on the C'terminus of r152.4. RFL6 fibroblasts were infected with WT RCMV or RCMV r152.4 BirA mini Turbo at an MOI=1. Labeling was performed by addition of 50µg/mL Biotin to the cell culture at 6 hours prior to harvesting of the cells. At 72 hpi cells were washed in PBS and harvested in cell lysis buffer. Labeled proteins were isolated on Neutravidin beads and analyzed by mass spectrometry. Mass spectrometry analysis revealed three unique proteins in the r152.4 BirA mini Turbo infected samples compared to WT: neuroblast differentiation associated protein AHNAK (AHNAK), Talin-1, and Pyridoxal-dependent decarboxylase domain-containing protein 1 (Pdxdc1). Further work will be necessary to verify interactions between these proteins and r152.4 and to assess their function.

AI.3.3 RCMV lacking r152.4 has normal growth kinetics but displays impaired *in vivo* replication

To determine the impact of r152.4 on viral replication *in vitro* and *in vivo* an RCMV mutant was generated via BAC recombineering containing 2 contiguous stop codons inserted into the N'terminus of the protein (2xSTOP mutation shown in Figure 34a). Correct insertion of the stop codons was determined by sequencing of the BAC viral genomic DNA before viral rescue and of the rescued viruses after expansion in fibroblasts (data not shown). Loss of r152.4 protein expression was verified by western blot in both untreated and PNGase F treated lysates (Figure 36a). Two different mutants were rescued and both lacked r152.4 protein expression. Multi-step growth curves were performed on RFL6 fibroblasts with an MOI=0.1 with both r152.4 2xSTOP mutants and RCMV WT. Supernatant samples were

taken at 0, 24, 48, 96, 120, 144, and 168 hpi and were titered by plaque assay using fibroblasts. There was no significant difference in viral titers at any point in the growth curve (Figure 36b). Growth of r152.4 2xSTOP mutants *in vivo* was determined by i.p. infection of 5 Gy irradiated F344 rats with either r152.4 2xSTOP mutant #2 or RCMV WT at 5×10^5 PFU/animal (Figure 36c). Rats were sacrificed at 5 dpi and tissues were harvested for analysis of viral genome copies as determined by qPCR using primers and probe directed against the RCMV DNA pol (R54). The r152.4 mutant virus showed only a very minor decrease in viral loads in the spleen at 5 dpi, suggesting that the virus has no inherent infection impairment. However, decreased viral loads were seen to varying extents in heart, kidney, liver, lung, SMG, mesenteric lymph node, bone marrow and PBMC, suggesting a decrease in the ability of the virus to disseminate to other tissues.

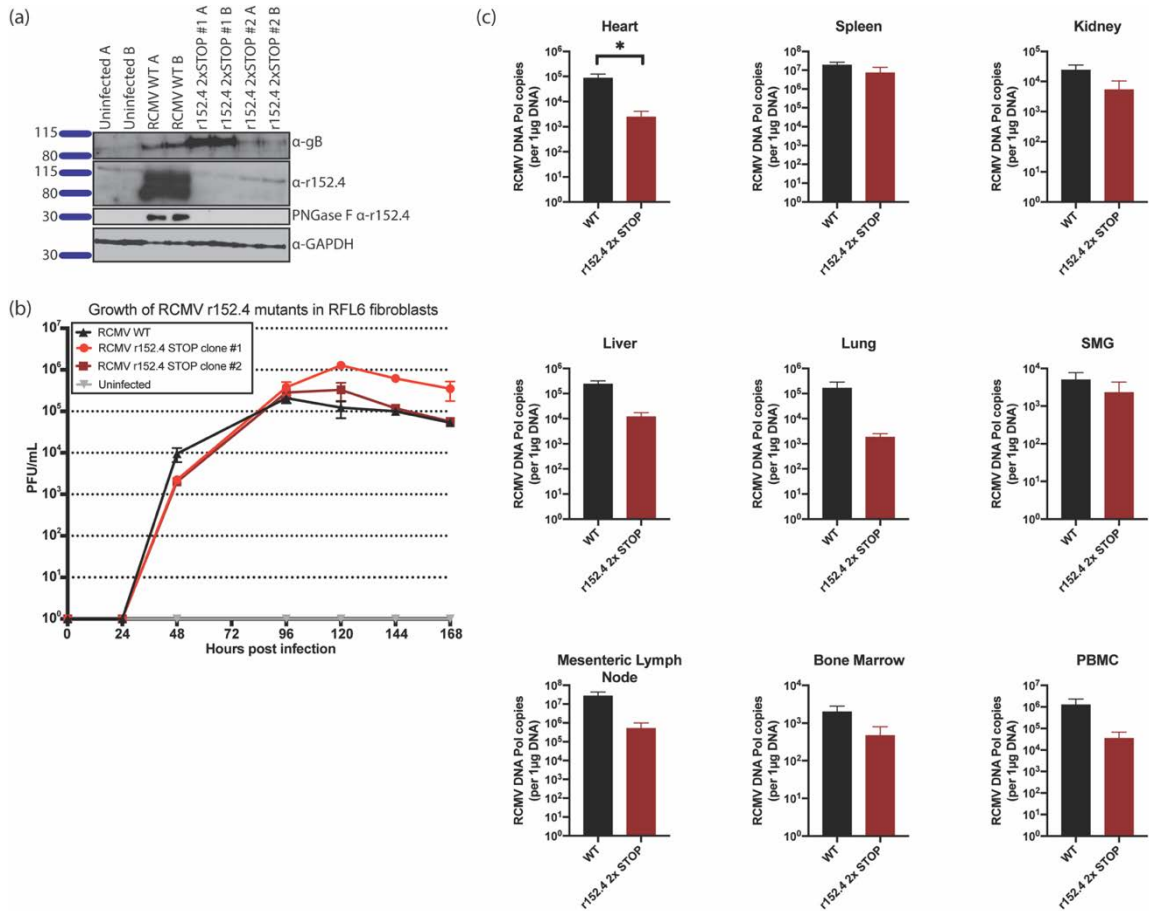


Figure 36. RCMV viruses with 2x STOP mutations in the *r152.4* gene show impaired viral dissemination *in vivo*, but not *in vitro*. (a) RCMV *r152.4* protein expression is eliminated by the addition of 2 STOP codons at the N' terminus of the protein. RFL6 cells were plated in 6-well dishes at 5×10^5 cells/well and infected with RCMV GFP, 2 RCMV *r152.4* 2xSTOP clones at an MOI=1, or left uninfected as a control. At 48 hpi cell lysates were harvested and western blots were performed on untreated lysates and lysates treated with PNGase F per NEBs protocol. (b) RCMV viruses with 2x STOP mutations in the *r152.4* gene show no inherent impairment in replication kinetics compared to WT virus. RFL6 cells were infected in triplicate with RCMV WT or *r152.4* mutant strains at an MOI = 0.1. Growth curve samples were taken at 24-hour intervals as indicated following infection. Viral titers at timepoints were determined by plaque assay on RFL6 cells. (c) F344 rats were irradiated at 5 Gy infected with 5×10^5 PFU/animal by *i.p.* injection with mutant or WT viruses. Tissues were harvested at POD5 and viral loads were determined by qPCR for RCMV viral DNA polymerase. * $p < 0.05$

AI.4 Discussion

Immune modulation is a key strategy employed by CMV to establish persistent infection in hosts. Although the immune-modulatory genes do not necessarily share positional homology between CMV species, the genes do tend to carry similar functions and structural properties. HCMV UL18 is known to adopt an MHC-I-like fold [224], and both m152 and r152.4 are predicted to adopt similar folds. Although, UL18 is predicted to be more similar to m144 than the m145 family members, in combination with US3 and US6, it shares some functionality with m152. These proteins all alter cellular expression of MHC-I molecules and appear to act as decoy ligands to NK-cell activating receptors, preventing NK-mediated killing of CMV infected cells. Similar to other MHC-I-like genes in HCMV and MCMV [224,242], RCMV r152.4 is highly glycosylated. As has been suggested previously for UL18, this may prevent interactions between r152.4 and other host or viral proteins targeting MHC-I-like structures. r152.4 was expressed with early gene kinetics, similar to m152, which has previously been reported to be expressed with exclusively early gene kinetics [126,248]. This is in contrast to UL18, which is typically expressed with late kinetics [232]. Additionally, r152.4 was not essential for viral infection *in vitro*, similar to UL18 [231]. However, loss of r152.4 expression did result in decreased viral loads in multiple tissues during an *in vivo* infection. Similarly, loss of MCMV m152 resulted in lower viral loads in the salivary glands of mice following infection [251]. Proximity sensing using the Biotin-labeling of r152.4-BirA did not identify any immune-related interactors of r152.4 in fibroblasts. The three interacting partners identified here, AHNAK, Talin-1, and Pdxdc1 have roles in scaffolding, integrin attachment to cytoskeletal actin, and phospholipid processing, respectively [362–364]. AHNAK in particular is

involved in countless cellular processes, making identification of a mechanism by which r152.4 might alter normal cell function through interaction with AHNAK challenging [362]. Further work will be necessary to first confirm these interactions and then to identify mechanisms by which RCMV benefits from these interactions. In addition, while this was a proof-of-concept experiment future proximity sensor experiments should be performed in immune cells including macrophages and DC.

III.5 Materials and methods

RCMV Bacterial Artificial Chromosome: The RCMV Maastricht strain genome was captured as a BAC containing eGFP using homologous recombination by replacing ORFs r144-r146 with a BAC cassette [133,319]. A two-step recombination protocol was used to create two mutants of r152.4: r152.4 2xSTOP and r152.4 BirA miniTurbo. The r152.4 2xSTOP mutant was created by insertion of 2 STOP codons into the N' terminus of the RCMV r152.4 ORF. Two RCMV r152.4 2x STOP clones were expanded for use in assays. The r152.4 BirA miniTurbo mutant virus was created by insertion of the BirA miniTurbo tag [365] at the C' terminus of WT r152.4. Following rescue and expansion of RCMV, virus preparations were aliquoted and stored at -80°C. Sequences were confirmed by sequencing and protein expression was verified by western blot. Viruses were titered simultaneously by plaque assay as described below.

Plaque Assays: Viral supernatants and stocks were titered over RFL6 cells in serial dilutions from 10^{-1} to 10^{-6} to determine viral titers in plaque forming units per mL (PFU/mL). RFL6 cells were plated at confluency in 24 well plates and allowed to adhere

overnight. Serial dilutions of the viral supernatants were performed in round-bottom 96 well plates. Media was aspirated from the RFL6 cells and 200µL of each viral dilution was added to the RFL6 cells. Cells were incubated on a rocker at 37°C for 2 hours and 250µL of CMC was added per well. At 7 days, the cells were fixed and stained with methylene blue and plaques were counted to determine viral titers.

RCMV multi-step viral growth curve: RCMV growth *in vitro* was assessed by infection in the RFL6 rat fibroblast cell line (ATCC, CCL-192). RFL6 fibroblasts were maintained in DMEM (ThermoFisher) with 5%FBS and 100U Penicillin/ 100µg Streptomycin/ 292µg/mL Glutamine (Fisher, 10378-016). Cells were plated at 1.5×10^5 cells/well in 6-well plates and allowed to adhere overnight. 24 hours after plating, duplicate wells were trypsinized and counted to determine an average cell count per well. Cells were infected at an MOI of 0.1 with RCMV WT, RCMV r152.4 2x STOP clone 1, RCMV r152.4 2x STOP clone 2, or left uninfected as a control for 2 hours at 37°C. Cells were washed 3 times with PBS to remove unbound virus and fresh complete DMEM was added to the cells. Virus was allowed to replicate in the cells for 7 days at 37°C and 100µL samples of supernatant were taken at 24-hour intervals beginning at 0 hpi. Plaque assays were performed on supernatants to determine virus growth in WT versus r152.4 2x STOP mutants over the time-course. Infections were performed in biological triplicates.

Protein post-translational computational analysis: The amino acid sequence of r152.4 (MATHALTKIVLCVAVCTGLSTAWRCPDTMSLMANQTRNGSFETVTGFNSTFPF VKTVNGTVVQLAPFVNISRMWFELNFTAQKTPLETLLNKHPNLTSAAIIVYNCN

VTTLNCTVACVFKGETTEGSREVVNSDAENGVHVCNDGYHLHRLMNHSHWLE
GRWTHLCEYFVTLQFKEQNLAWMTLIGNETVECAFNTSIPIRYNITLYGYNLTRV
DKECTQRDNQTVFCSITNSTRDIYNMSVLNCTIHRPWPVWINAKFNYSSELM
TYEYDNPDYKYKGDYDEDEDEDEDEDEENEDEYNGNGEELINETTSKPNYA
KQVKDPTNSDVVIPPGSVLLIIGIVALVAVTVLAVTFRKRRGGVREMANYSKRSR
SLY) was uploaded to the Eukaryotic Linear Motif analysis tool with no cellular
localization information provided for the query.

Antibodies: anti-RCMV IE [263] and anti-r152.4 (#J7726) antibodies were generated in rabbits and the rat anti-RCMV gB monoclonal antibody [328] was generated at OHSU-VGTI Monoclonal Antibody Facility. All primary antibodies were used at 1:10,000 overnight at 4°C and detected with an HRP-conjugated secondary antibody (TrueBlot Rabbit anti-Rabbit; Southern Biotech anti-Rat) used at 1:100,000 overnight at 4°C with blocking in 5% BSA-TBST. An HRP-conjugated anti-GAPDH antibody was used at 1:10,000 with blocking in 5% BSA-TBST as a loading control.

r152.4 detection by western blots: RFL6 cells were plated in 6-well dishes at 5×10^5 cells/well and infected with RCMV GFP at an MOI=1 or left uninfected as a control. At 48 hpi, cell lysates were harvested in cell lysis buffer (Cell Signaling Technologies) with 1x HALT (ThermoFisher Scientific) and clarified at 10,000RPM for 10 minutes at 4°C. Proteins were combined 1:1 with NuPage SDS running buffer (ThermoFisher) + 2% BME and boiled for 7 minutes, then spun briefly. Proteins were separated on an SDS-PAGE BOLT gels at 165V for 40 minutes and transferred to a PVDF membrane (Millipore) using

a semi-dry transfer system at 25V for 25 minutes. The membrane was dried overnight and then blocked with 5% BSA in TBST and proteins were detected with anti-r152.4, anti-IE, anti-gB, and anti-GAPDH antibodies as described above. The membrane was detected by autoradiography with chemiluminescent solution (ThermoFisher, West Pico Plus Solution).

PNGase F treatment: PNGase F (NEB) was used to treat lysates from RFL6 cells prior to heat-denaturing. Briefly, 9 μ L of each sample was combined with 1 μ L of 10x glycoprotein denaturing buffer. The glycoproteins were denatured by boiling at 100°C for 10 minutes and then chilled on ice and centrifuged for 10 seconds. A cocktail containing 2 μ L of Glycobuffer 2, 2 μ L of 10% NP-40, and 6 μ L of dH₂O was added to the sample. Then 1 μ L of PNGase F was added and the sample was mixed gently and then incubated at 37°C for 1 hour. To end the enzymatic reaction an equal volume of NuPage running buffer was added to each sample and then they were heated for 7 minutes at 100°C. Samples were spun briefly and run on an SDS -PAGE gel.

Endo H treatment: Endo H (NEB) was used to treat lysates from RFL6 cells prior to heat-denaturing. Briefly, 9 μ L of each sample was combined with 1 μ L of 10x glycoprotein denaturing buffer. The glycoproteins were denatured by heating at 100°C for 10 minutes. 2 μ L of Glycobuffer 3, 1 μ L of Endo H, and 7 μ L of dH₂O were added to the sample, and incubated at 37°C for 1 hour. Samples were incubated in the presence of Endo H at 37°C for 1 hour, then mixed with an equal volume of NuPage running buffer and heated for 7 minutes at 100°C. Samples were spun briefly and run on an SDS -PAGE gel.

Identification of r152.4 interactions by biotin labeling and mass spectrometry: RFL6 cells were plated in 6-well plates at 5×10^5 cells/well. Cells were infected with either RCMV WT or with RCMV expressing a BirA miniTurbo tag on the C'terminus of r152.4, or left uninfected. Cells were treated with $50 \mu\text{g/mL}$ biotin at 66 hpi. Cells were washed once with ice-cold PBS and harvested in cell lysis buffer (Cell Signaling Technologies) with 1x HALT (ThermoFisher) protease inhibitor at 72 hpi. Cell lysates were bound to NeutrAvidin slurry overnight at 4°C on a rocker. Beads were then washed once with urea wash buffer (PBS pH 7.4, 4M Urea), three times with wash buffer (PBS pH 7.4, 1% Triton X-100), twice with 50mM ammonium bicarbonate, twice with PBS, and twice more with 50mM ammonium bicarbonate. For all washes, beads were incubated with rocking for 5 minutes and were spun at $2000 \times g$ for 1 minute at room temperature. Beads were resuspended in 50mM ammonium bicarbonate and incubated for 10 minutes at 70°C with agitation. 6M urea was immediately added to the samples and beads were cooled to room temperature. 0.5M Tris 2-carboxyethyl phosphine (TCEP) was then added and samples were incubated for 30 minutes at room temperature on a rocker. 0.5M iodoacetamide was added and samples were incubated for a further 30 minutes. $3.7 \mu\text{L}$ of 10mM CaCl_2 was added, followed by addition of $20 \mu\text{L}$ of $0.1 \mu\text{g}/\mu\text{L}$ of sequencing grade trypsin. Samples were incubated overnight at 37°C with agitation. Solution was loaded onto a spin column and spun for 1 minute at $1000 \times g$ at room temperature. $20 \mu\text{L}$ of formic acid was added to the eluate and samples were stored at -20°C until analysis by mass spectrometry.

RCMV infection of rats for viral load analysis: F344 rats were irradiated at 5 Gy and infected with 5×10^5 PFU/animal by i.p. injection with WT or r152.4 mutant viruses. Tissues

were harvested at 5 dpi. DNA was extracted from homogenized tissues using DNAzol (ThermoFisher) and viral loads were determined by qPCR for viral DNA polymerase.

* $p < 0.05$ Mann-Whitney Test.

RCMV Quantitative PCR: Viral genome copies in rat tissues were quantified using real-time PCR with standard cycling parameters with a primer and probe set designed against RCMV viral DNA polymerase (R54). P1: CCTCACGGGCTACAACATCA; P2: GAGAGTTGACGAAGAACCGACC; Probe: CGGCTTCGATATCAAGTATCTCCTGCACC. DNA was extracted from tissues homogenized in DNAzol. Quantity of DNA isolated was determined by spectrophotometer and samples were diluted to 250ng/ μ L DNA. qPCR was performed using TaqMan Fast Advanced Master Mix (4444963). RCMV viral DNA at known genome concentrations served as the quantification standard. Samples were analyzed using a QuantStudio 7 Flex Real-Time PCR system.

Appendix III – RNA Deep Sequencing Data

Table 13. Canonical pathway analysis summary for rat cardiac IRI: up-regulated pathways.

Canonical Pathways	Cohort 2 Graft vs. Cohort 1 Control		Cohort 2 Graft vs. Cohort 2 Native		Cohort 2 Native vs. Cohort 1 Control	
	Z-score	-log(BH-p-value)	Z-score	-log(BH-p-value)	Z-score	-log(BH-p-value)
Neuroinflammation Signaling Pathway	6.070	3.939	5.528	2.966	-0.447	0.338
TREM1 Signaling	5.604	6.017	5.754	4.687	N/A	0.000
Dendritic Cell Maturation	4.542	4.728	5.103	4.457	N/A	0.276
Production of Nitric Oxide and Reactive Oxygen Species	4.243	4.573	3.580	5.125	2.236	1.144
Acute Phase Response Signaling	3.742	4.285	3.910	3.536	N/A	0.949
Leukocyte Extravasation Signaling	3.710	8.460	3.579	8.756	N/A	0.000
Fcy Receptor-mediated Phagocytosis in Macrophages	3.709	9.612	4.061	7.947	N/A	0.412
iNOS Signaling	3.638	1.608	3.500	1.467	N/A	0.323
NF-κB Signaling	3.638	3.624	3.491	3.406	N/A	0.000
Colorectal Cancer Metastasis Signaling	3.629	7.413	3.507	7.503	0.000	0.481
Rac Signaling	3.618	3.039	3.464	3.841	0.000	0.969
Inflammasome pathway	3.606	3.613	3.606	3.454	N/A	0.000
Remodeling of Epithelial Adherens Junctions	3.606	5.648	3.742	6.864	N/A	0.202
Role of Pattern Recognition Receptors in Recognition of	3.479	3.512	2.722	2.851	N/A	0.000
Tec Kinase Signaling	3.434	4.195	3.742	4.534	N/A	0.000
GP6 Signaling Pathway	3.414	5.780	3.969	6.008	N/A	0.241
Role of NFAT in Regulation of the Immune Response	3.207	2.729	3.474	2.340	N/A	0.000
Type 1 Diabetes Mellitus Signaling	3.157	3.070	3.024	1.546	N/A	0.000
Cdc42 Signaling	3.087	0.500	3.087	0.000	N/A	0.000
Th1 Pathway	3.086	3.554	2.592	3.446	N/A	0.000
Sirtuin Signaling Pathway	3.085	15.383	2.440	14.097	1.000	0.000
IL-8 Signaling	3.038	7.158	3.313	7.776	0.000	0.716
Ephrin Receptor Signaling	3.000	3.656	2.496	3.710	N/A	0.000
Toll-like Receptor Signaling	2.985	2.556	3.128	2.316	N/A	0.000
CD28 Signaling in T Helper Cells	2.967	3.256	2.592	2.893	N/A	0.244
PDGF Signaling	2.967	4.162	2.846	3.456	N/A	0.000
Actin Nucleation by ARP-WASP Complex	2.837	1.750	3.266	2.749	N/A	0.000
HMGB1 Signaling	2.832	2.415	2.714	3.133	N/A	0.000
STAT3 Pathway	2.777	7.388	3.429	6.798	N/A	0.241
PKCθ Signaling in T Lymphocytes	2.774	3.431	2.429	2.340	N/A	0.000
Regulation of Actin-based Motility by Rho	2.744	2.917	3.000	3.590	N/A	0.000
IL-6 Signaling	2.722	4.931	2.562	4.788	N/A	0.229
Integrin Signaling	2.692	4.340	2.982	4.787	N/A	0.000
Interferon Signaling	2.673	1.250	3.317	0.453	N/A	0.000
Chondroitin Sulfate Degradation (Metazoa)	2.646	1.047	2.121	1.417	N/A	0.000
IL-7 Signaling Pathway	2.600	0.865	2.268	1.444	N/A	0.418
RhoA Signaling	2.598	4.035	2.828	4.623	N/A	0.594
Chemokine Signaling	2.535	4.261	2.333	4.329	N/A	0.000
NGF Signaling	2.530	1.559	2.160	1.916	N/A	0.000
Dermatan Sulfate Biosynthesis	2.524	0.800	2.985	1.337	N/A	0.689
Role of BRCA1 in DNA Damage Response	2.524	1.180	2.746	3.544	-1.890	3.844
Actin Cytoskeleton Signaling	2.524	6.117	2.907	6.009	N/A	0.000
EIF2 Signaling	2.480	2.577	2.546	3.130	0.000	0.629
Gai Signaling	2.469	3.823	2.777	3.147	N/A	0.000
p70S6K Signaling	2.429	3.028	2.941	3.181	N/A	0.000
mTOR Signaling	2.429	3.720	2.496	4.419	N/A	0.415
Mouse Embryonic Stem Cell Pluripotency	2.401	1.060	2.082	1.788	N/A	0.304
B Cell Receptor Signaling	2.357	4.637	2.425	4.929	N/A	0.000
ERK5 Signaling	2.353	2.031	2.558	0.913	N/A	0.000
Complement System	2.324	3.142	1.890	0.408	N/A	1.014
PI3K Signaling in B Lymphocytes	2.292	4.705	2.673	4.247	N/A	0.232
Macropinocytosis Signaling	2.268	2.507	2.556	2.529	N/A	0.000
GM-CSF Signaling	2.263	4.505	2.263	4.151	N/A	0.474
Lymphotoxin β Receptor Signaling	2.236	1.020	1.877	1.552	N/A	0.590
Urea Cycle	2.236	2.279	N/A	0.710	N/A	0.000
Th2 Pathway	2.214	2.825	2.236	3.203	N/A	0.000
Aryl Hydrocarbon Receptor Signaling	2.191	3.296	2.197	4.666	-2.000	0.833
TNFR1 Signaling	2.183	0.924	2.183	0.821	N/A	0.291
Signaling by Rho Family GTPases	2.138	4.752	2.438	6.797	-1.000	0.511
NF-κB Activation by Viruses	2.121	1.999	2.475	1.766	N/A	0.391
PI3K/AKT Signaling	2.082	1.178	3.280	1.477	N/A	0.250
IL-23 Signaling Pathway	2.065	0.748	1.706	1.260	N/A	1.270
JAK/Stat Signaling	2.058	2.613	1.915	2.077	N/A	0.000
ILK Signaling	2.047	4.218	2.393	6.245	N/A	0.477
Telomerase Signaling	2.043	0.995	2.121	1.128	N/A	0.000
Neurotrophin/TRK Signaling	2.041	0.934	1.732	1.344	N/A	0.000
ErbB2-ErbB3 Signaling	2.041	1.180	2.268	1.942	N/A	0.502
p38 MAPK Signaling	2.030	2.458	1.581	2.170	N/A	0.300
Oncostatin M Signaling	2.000	2.195	2.500	2.027	N/A	0.000
Pancreatic Adenocarcinoma Signaling	2.000	3.026	1.441	3.845	0.447	3.396
Huntington's Disease Signaling	1.980	3.181	0.714	3.089	N/A	0.000
IL-17A Signaling in Airway Cells	1.961	1.180	1.671	1.684	N/A	0.502
fMLP Signaling in Neutrophils	1.938	4.047	2.188	3.940	N/A	0.539
SAPK/JNK Signaling	1.915	1.154	1.333	1.706	N/A	0.312
Glioma Invasiveness Signaling	1.915	3.701	2.466	5.320	N/A	0.865
FLT3 Signaling in Hematopoietic Progenitor Cells	1.890	0.936	1.826	1.127	N/A	0.000

Leukotriene Biosynthesis	1.890	1.553	1.633	0.988	N/A	0.770
Regulation of eIF4 and p70S6K Signaling	1.877	1.149	1.961	1.869	N/A	0.000
Gα12/13 Signaling	1.852	1.340	1.697	2.681	N/A	0.000
VEGF Signaling	1.852	3.699	1.677	3.974	N/A	0.316
Role of NANOG in Mammalian Embryonic Stem Cell Plu	1.800	1.472	1.512	1.252	N/A	0.000
Thrombopoietin Signaling	1.800	1.769	1.732	2.117	N/A	0.000
IL-2 Signaling	1.800	2.343	1.732	2.742	N/A	0.000
Salvage Pathways of Pyrimidine Ribonucleotides	1.768	1.188	1.732	0.371	N/A	0.796
Death Receptor Signaling	1.768	1.788	1.768	1.579	N/A	0.000
3-phosphoinositide Biosynthesis	1.767	6.274	0.976	6.570	N/A	0.252
Estrogen-mediated S-phase Entry	1.732	1.721	2.324	3.108	-2.646	7.243
Sphingosine-1-phosphate Signaling	1.732	3.544	1.000	4.361	N/A	0.527
Type II Diabetes Mellitus Signaling	1.715	3.909	1.768	3.211	N/A	0.746
LPS/IL-1 Mediated Inhibition of RXR Function	1.715	5.595	1.567	5.520	N/A	1.381
Induction of Apoptosis by HIV1	1.706	1.593	1.633	2.000	N/A	0.234
Renin-Angiotensin Signaling	1.677	3.639	1.543	2.979	N/A	0.000
Prolactin Signaling	1.671	2.059	1.826	1.827	N/A	0.000
Synaptogenesis Signaling Pathway	1.671	5.457	1.811	6.143	N/A	0.000
Nicotine Degradation II	1.667	0.000	-0.302	0.000	2.000	1.862
Cytotoxic T Lymphocyte-mediated Apoptosis of Target C	1.667	0.533	1.667	0.312	N/A	0.000
Amyotrophic Lateral Sclerosis Signaling	1.667	1.863	1.298	2.069	N/A	0.320
ErbB Signaling	1.667	1.911	1.947	2.133	N/A	0.000
Glioblastoma Multiforme Signaling	1.664	2.920	1.987	4.534	N/A	0.941
Gαq Signaling	1.664	5.491	1.549	4.933	N/A	0.995
Estrogen-Dependent Breast Cancer Signaling	1.633	2.699	1.732	3.376	N/A	0.436
FcγRIIB Signaling in B Lymphocytes	1.633	3.015	1.732	3.728	N/A	0.000
Endocannabinoid Developing Neuron Pathway	1.622	2.215	1.543	2.627	N/A	0.544
HIPPO signaling	1.604	0.604	1.807	0.778	N/A	0.000
Agrin Interactions at Neuromuscular Junction	1.569	2.060	2.449	1.593	N/A	0.000
LPS-stimulated MAPK Signaling	1.567	2.258	1.715	2.539	N/A	0.391
Osteoarthritis Pathway	1.565	2.981	1.673	3.183	N/A	0.000
Pyridoxal 5'-phosphate Salvage Pathway	1.528	0.855	1.528	0.744	N/A	1.186
Small Cell Lung Cancer Signaling	1.528	1.376	1.400	3.048	N/A	2.821
Phospholipase C Signaling	1.477	3.714	1.940	3.601	N/A	0.000
Renal Cell Carcinoma Signaling	1.460	1.883	1.400	1.904	N/A	0.000
HGF Signaling	1.441	2.247	0.949	1.968	N/A	0.277
Methionine Degradation I (to Homocysteine)	1.414	0.743	1.000	0.988	N/A	0.000
ErbB4 Signaling	1.400	1.204	1.569	1.245	N/A	0.000
CCR5 Signaling in Macrophages	1.387	1.361	1.604	1.380	N/A	0.000
iCOS-iCOSL Signaling in T Helper Cells	1.372	3.219	1.234	2.608	N/A	0.274
ATM Signaling	1.342	0.000	1.732	0.584	-0.447	2.580
Cell Cycle Regulation by BTG Family Proteins	1.342	0.000	1.667	1.347	-1.000	2.739
Antiproliferative Role of Somatostatin Receptor 2	1.342	1.195	1.279	1.892	N/A	0.000
Pyrimidine Ribonucleotides De Novo Biosynthesis	1.342	2.189	1.500	0.863	N/A	0.316
Ephrin B Signaling	1.342	2.660	0.894	2.419	N/A	0.000
Apoptosis Signaling	1.333	2.444	0.667	2.180	N/A	0.778
Ovarian Cancer Signaling	1.333	3.093	1.480	3.475	N/A	0.746
Fc Epsilon RI Signaling	1.313	3.335	1.443	2.972	N/A	0.257
CD40 Signaling	1.279	0.933	1.000	1.376	N/A	0.965
Apelin Liver Signaling Pathway	1.265	0.979	2.333	0.630	N/A	0.507
Granzyme B Signaling	1.265	2.691	1.265	2.570	N/A	0.689
Tumoricidal Function of Hepatic Natural Killer Cells	1.265	3.815	1.265	2.998	N/A	0.000
TGF-β Signaling	1.225	1.244	1.706	0.619	N/A	0.000
PAK Signaling	1.219	1.501	1.183	1.690	N/A	0.000
Melanoma Signaling	1.213	1.450	1.091	2.426	N/A	0.618
RANK Signaling in Osteoclasts	1.183	2.291	0.649	2.834	N/A	0.360
Paxillin Signaling	1.183	2.753	1.480	2.691	N/A	0.000
Adrenomedullin signaling pathway	1.179	3.575	1.053	3.558	N/A	0.000
Cholecystokinin/Gastrin-mediated Signaling	1.151	1.906	1.667	1.659	N/A	0.000
UVB-Induced MAPK Signaling	1.147	0.553	1.091	0.766	N/A	0.206
Pyrimidine Ribonucleotides Interconversion	1.147	2.067	1.291	0.776	N/A	0.330
γ-linolenate Biosynthesis II (Animals)	1.134	0.921	1.000	1.733	N/A	0.665
Fatty Acid Activation	1.134	1.553	0.707	2.077	N/A	0.770
NAD Phosphorylation and Dephosphorylation	1.134	1.553	0.816	0.988	N/A	0.000
Urate Biosynthesis/Inosine 5'-phosphate Degradation	1.134	1.553	0.447	0.608	N/A	0.770
UVA-Induced MAPK Signaling	1.134	2.023	1.177	1.563	N/A	0.000
CXCR4 Signaling	1.109	3.418	1.069	3.718	N/A	0.000
Superpathway of Inositol Phosphate Compounds	1.106	8.049	0.198	8.233	N/A	0.000
Growth Hormone Signaling	1.095	2.484	0.557	1.962	N/A	0.000
14-3-3-mediated Signaling	1.093	3.111	1.093	3.546	N/A	0.000
Endometrial Cancer Signaling	1.091	1.282	1.043	2.117	N/A	0.540
Mitotic Roles of Polo-Like Kinase	1.069	1.210	1.291	1.810	-1.265	9.865
Apelin Pancreas Signaling Pathway	1.043	2.084	1.043	1.896	N/A	0.244
CCR3 Signaling in Eosinophils	1.029	2.276	0.845	2.659	N/A	0.226
IL-3 Signaling	1.029	2.709	1.151	3.366	N/A	0.000
Glioma Signaling	1.029	3.515	1.521	4.387	N/A	0.581
T Cell Exhaustion Signaling Pathway	1.021	1.902	1.109	2.116	N/A	0.000
B Cell Activating Factor Signaling	1.000	0.451	1.265	0.556	N/A	0.352

Cysteine Biosynthesis III (mammalia)	1.000	0.860	0.632	1.106	N/A	0.000
Pyrimidine Deoxyribonucleotides De Novo Biosynthesis	1.000	0.958	1.633	0.000	N/A	0.552
Purine Nucleotides Degradation II (Aerobic)	1.000	1.321	0.378	0.576	N/A	0.604
Arginine Biosynthesis IV	1.000	1.385	N/A	0.299	N/A	0.000
Arginine Degradation VI (Arginase 2 Pathway)	1.000	1.385	1.000	1.333	N/A	0.000
Proline Biosynthesis II (from Arginine)	1.000	1.385	N/A	0.710	N/A	0.000
Superpathway of Citrulline Metabolism	1.000	2.295	0.378	1.122	N/A	0.000
Spermine and Spermidine Degradation I	1.000	2.362	1.000	2.303	N/A	0.000
PDF Signaling	0.928	1.533	1.219	2.264	N/A	0.391
Neuregulin Signaling	0.898	1.903	1.461	1.680	N/A	0.000
GDNF Family Ligand-Receptor Interactions	0.898	2.389	1.061	2.426	N/A	0.000
Non-Small Cell Lung Cancer Signaling	0.894	1.114	0.853	1.801	N/A	0.448
Endothelin-1 Signaling	0.894	6.381	0.906	5.125	1.000	0.482
EGF Signaling	0.816	1.397	0.816	1.239	N/A	0.198
Citrulline Biosynthesis	0.816	1.941	0.447	1.207	N/A	0.000
Prostanoid Biosynthesis	0.816	1.941	0.816	1.865	N/A	0.000
Regulation of Cellular Mechanics by Calpain Protease	0.775	1.715	1.291	1.810	2.000	2.607
Cardiac Hypertrophy Signaling (Enhanced)	0.745	10.477	0.606	7.662	-0.447	0.000
ERK/MAPK Signaling	0.728	2.811	0.585	3.711	N/A	0.245
Histamine Degradation	0.707	1.054	0.707	0.982	N/A	0.000
Adenosine Nucleotides Degradation II	0.707	1.333	0.378	0.858	N/A	0.665
Aldosterone Signaling in Epithelial Cells	0.707	3.893	0.354	3.964	N/A	0.000
IL-1 Signaling	0.688	2.602	0.728	1.579	N/A	0.000
Insulin Receptor Signaling	0.687	3.240	0.651	4.866	N/A	0.445
VEGF Family Ligand-Receptor Interactions	0.667	3.034	0.649	3.686	N/A	0.778
Cyclins and Cell Cycle Regulation	0.655	1.557	1.400	2.129	-2.646	4.701
Wnt/ β -catenin Signaling	0.603	0.841	0.420	1.777	N/A	0.000
cAMP-mediated signaling	0.585	2.478	1.254	3.250	N/A	0.000
April Mediated Signaling	0.577	0.544	0.832	0.667	N/A	0.369
Intrinsic Prothrombin Activation Pathway	0.577	0.575	1.155	0.506	N/A	0.922
Ceramide Signaling	0.539	1.799	0.686	2.283	N/A	0.000
IL-9 Signaling	0.535	1.139	0.243	1.897	N/A	0.310
TWEAK Signaling	0.535	1.351	0.775	1.570	N/A	0.404
IGF-1 Signaling	0.507	2.622	0.667	2.851	N/A	0.000
PCP pathway	0.500	0.404	0.243	0.461	N/A	0.000
Thrombin Signaling	0.500	4.569	0.985	4.775	N/A	0.000
D-myo-inositol-5-phosphate Metabolism	0.492	4.731	-0.124	3.947	N/A	0.000
CDK5 Signaling	0.480	2.767	0.480	2.212	N/A	0.000
VDR/RXR Activation	0.471	1.305	0.000	0.954	N/A	0.000
UVC-Induced MAPK Signaling	0.471	1.540	1.414	1.683	N/A	0.000
Triacylglycerol Biosynthesis	0.471	1.621	0.688	1.785	N/A	0.303
Cell Cycle: G1/S Checkpoint Regulation	0.447	1.143	0.000	2.006	2.000	2.578
Wnt/Ca ⁺ pathway	0.408	1.788	1.043	1.352	N/A	0.000
P2Y Purigenic Receptor Signaling Pathway	0.405	5.874	0.412	4.666	N/A	0.000
D-myo-inositol (1,4,5,6)-Tetrakisphosphate Biosynthesis	0.397	3.773	-0.132	3.363	N/A	0.000
D-myo-inositol (3,4,5,6)-tetrakisphosphate Biosynthesis	0.397	3.773	-0.132	3.363	N/A	0.000
Colanic Acid Building Blocks Biosynthesis	0.378	1.359	1.414	1.823	N/A	0.000
nNOS Signaling in Neurons	0.378	1.414	0.378	1.024	N/A	0.310
Sucrose Degradation V (Mammalian)	0.378	2.799	N/A	0.354	N/A	2.169
Mitochondrial L-carnitine Shuttle Pathway	0.333	1.831	0.000	2.302	N/A	0.665
Melanocyte Development and Pigmentation Signaling	0.324	3.060	0.480	3.034	N/A	0.000
Glutathione Redox Reactions I	0.302	1.589	0.000	1.924	N/A	0.000
Fatty Acid α -oxidation	0.302	1.913	0.632	1.360	N/A	0.000
Inhibition of Angiogenesis by TSP1	0.277	1.459	0.535	1.693	N/A	0.000
Putrescine Degradation III	0.277	2.793	0.577	2.107	N/A	0.000
Choline Biosynthesis III	0.277	5.896	0.000	4.620	N/A	0.714
GNRH Signaling	0.272	3.447	0.429	2.152	N/A	0.000
eNOS Signaling	0.140	2.228	0.137	2.949	N/A	0.346
Calcium-induced T Lymphocyte Apoptosis	0.000	0.802	0.500	0.414	N/A	0.000
Retinoate Biosynthesis I	0.000	0.857	0.000	0.775	N/A	0.414
Amyloid Processing	0.000	1.346	0.000	0.972	N/A	0.285
D-myo-inositol (1,4,5)-Trisphosphate Biosynthesis	0.000	1.578	-0.302	1.112	N/A	0.000
NAD Salvage Pathway II	0.000	1.721	0.000	1.607	N/A	0.000
Noradrenaline and Adrenaline Degradation	0.000	1.824	0.258	1.347	N/A	0.000
D-myo-inositol (1,3,4)-trisphosphate Biosynthesis	0.000	2.179	-0.905	2.674	N/A	0.000
PFKFB4 Signaling Pathway	0.000	2.189	-0.447	2.016	N/A	0.316
Melatonin Degradation II	0.000	2.362	N/A	1.222	N/A	0.000
Acute Myeloid Leukemia Signaling	0.000	2.374	0.180	2.932	N/A	0.743
UDP-N-acetyl-D-galactosamine Biosynthesis II	0.000	2.844	0.000	2.739	N/A	0.000
Endocannabinoid Neuronal Synapse Pathway	0.000	4.148	-0.295	2.137	N/A	0.000
Leptin Signaling in Obesity	0.000	5.619	0.218	4.375	N/A	0.000

Table 14. Canonical pathway analysis summary for rat cardiac IRI: down-regulated pathways.

Canonical Pathways	Cohort 2 Graft vs. Cohort 1 Control		Cohort 2 Graft vs. Cohort 2 Native		Cohort 2 Native vs. Cohort 1 Control	
	Z-score	-log ₁₀ (P-value)	Z-score	-log ₁₀ (P-value)	Z-score	-log ₁₀ (P-value)
Oxidative Phosphorylation	-8.778	25.616	-8.858	25.475	N/A	0.000
TCA Cycle II (Eukaryotic)	-4.025	8.280	-4.025	8.004	N/A	0.000
PPAR Signaling	-4.004	1.372	-4.352	1.184	N/A	0.000
Valine Degradation I	-3.357	6.310	-3.357	6.102	N/A	0.000
Apelin Cardiac Fibroblast Signaling Pathway	-3.207	3.712	-3.051	2.888	N/A	0.000
PPARα/RXRα Activation	-3.051	2.977	-2.941	1.988	N/A	0.000
Glycolysis I	-2.887	1.721	-3.000	0.630	N/A	1.282
Apelin Muscle Signaling Pathway	-2.714	2.804	-2.333	1.546	N/A	0.000
Glutaryl-CoA Degradation	-2.714	3.437	-2.887	4.139	N/A	0.689
Isoleucine Degradation I	-2.714	4.286	-2.309	5.197	N/A	0.000
Calcium Signaling	-2.534	4.135	-2.412	3.386	N/A	0.000
Ketolysis	-2.449	1.649	-1.890	2.295	N/A	0.000
Heme Biosynthesis II	-2.449	1.941	-2.449	1.865	N/A	0.918
Inhibition of Matrix Metalloproteases	-2.357	3.270	-1.896	3.095	N/A	0.369
Gluconeogenesis I	-2.324	3.278	-2.496	2.047	N/A	0.507
LXR/RXR Activation	-2.287	3.302	-2.714	3.238	-0.447	1.532
Cardiomyocyte Differentiation via BMP Receptors	-2.236	0.627	-2.000	0.000	N/A	0.000
Acetyl-CoA Biosynthesis I (Pyruvate Dehydrogenase Complex)	-2.236	1.838	-2.236	1.773	N/A	0.000
2-oxobutanoate Degradation I	-2.236	2.953	-2.236	2.679	N/A	0.000
Tryptophan Degradation III (Eukaryotic)	-2.138	2.918	-2.324	3.360	N/A	0.522
Leucine Degradation I	-2.121	3.884	-2.121	3.770	N/A	0.000
Fatty Acid Oxidation	-2.065	4.259	-2.400	5.379	N/A	0.435
Glycine Cleavage Complex	-2.000	1.385	-1.342	2.210	N/A	1.085
Glycogen Biosynthesis II (from UDP-D-Glucose)	-2.000	1.763	-2.000	1.708	N/A	0.000
2-ketoglutarate Dehydrogenase Complex	-2.000	1.763	-2.000	1.708	N/A	0.000
Tetrahydro Biosynthesis I	-2.000	2.362	-2.000	2.303	N/A	0.000
Acetate Conversion to Acetyl-CoA	-2.000	2.362	-2.000	2.303	N/A	0.000
Branched-chain α-keto acid Dehydrogenase Complex	-2.000	2.362	-2.000	2.303	N/A	0.000
Methylmalonyl Pathway	-2.000	2.362	-2.000	2.303	N/A	0.000
Ubiquinol-10 Biosynthesis (Eukaryotic)	-2.189	2.179	-1.897	2.067	N/A	0.644
Ketogenesis	-1.890	2.385	-1.414	3.188	N/A	0.875
AMPK Signaling	-1.432	2.730	-1.134	3.543	0.447	0.982
OX40 Signaling Pathway	-1.342	0.000	-0.816	0.000	N/A	0.000
Superpathway of Geranylgeranyl/diphosphate Biosynthesis I (via Mevalonate)	-1.342	0.345	-0.378	0.658	N/A	1.524
Sperm Motility	-1.234	5.794	-0.617	6.317	N/A	0.000
Opioid Signaling Pathway	-1.166	5.228	-0.530	4.338	N/A	0.000
GPCR-Mediated Nutrient Sensing in Enterendocrine Cells	-1.155	4.261	-1.067	2.395	N/A	0.000
Histidine Degradation VI	-1.134	1.192	-1.134	1.122	N/A	0.714
Progesterone Biosynthesis	-1.134	1.782	-1.134	1.700	N/A	0.802
GPCR-Mediated Integration of Enterendocrine Signaling Exemplified by an L Cell	-1.134	1.940	-1.000	1.047	N/A	0.000
Purine Nucleosides De Novo Biosynthesis II	-1.134	2.054	-1.000	0.481	N/A	0.000
Stearate Biosynthesis I (Animals)	-1.091	2.891	-0.816	4.119	N/A	0.889
Retinol Biosynthesis	-1.069	0.778	-0.728	1.461	-1.000	2.534
Role of CHK Proteins in Cell Cycle Checkpoint Control	-1.069	0.915	-0.943	2.824	1.000	2.891
Ethanol Degradation II	-1.069	1.459	-1.069	1.343	N/A	0.000
BMP signaling pathway	-1.043	0.909	0.229	0.301	N/A	0.000
Mevalonate Pathway I	-1.000	0.958	0.000	0.988	N/A	1.848
Superoxide Radicals Degradation	-1.000	0.909	-1.342	1.454	N/A	0.000
IRNA Splicing	-1.000	1.286	-0.688	2.158	N/A	0.000
Trehalose Degradation II (Trehalase)	-1.000	1.763	-1.000	1.708	N/A	0.000
Phenylethylamine Degradation I (Aerobic)	-1.000	2.362	-1.000	2.303	N/A	0.000
Glucose and Glucose-1-phosphate Degradation	-1.000	3.804	-0.707	2.739	N/A	0.000
Apelin Adipocyte Signaling Pathway	-1.000	3.860	-0.649	4.329	N/A	0.502
Dopamine Receptor Signaling	-1.000	3.877	-0.775	3.956	N/A	0.000
Superpathway of Methionine Degradation	-0.943	2.650	-0.943	2.947	N/A	0.000
Apelin Cardiomyocyte Signaling Pathway	-0.926	2.707	-0.926	2.667	N/A	0.000
Endocannabinoid Cancer Inhibition Pathway	-0.911	3.286	-0.882	3.944	1.000	0.719
Oxidative Ethanol Degradation II	-0.905	2.101	-0.905	1.983	N/A	0.000
D-myo-inositol (1,4,5)-trisphosphate Degradation	-0.885	3.100	-1.000	2.865	N/A	0.000
Phenylethylamine Degradation IV (Mammalian, via Side Chain)	-0.905	4.286	-0.632	3.237	N/A	0.741
Synaptic Long Term Depression	-0.896	2.140	-0.775	1.811	N/A	0.000
Angiopoietin Signaling	-0.894	1.942	-0.655	2.526	N/A	0.875
Sumoylation Pathway VI	-0.853	0.399	-1.732	1.061	N/A	0.365
Ethanol Degradation IV	-0.832	2.366	-0.632	2.229	N/A	0.000
Superpathway of D-myo-inositol (1,4,5)-trisphosphate Metabolism	-0.832	2.793	-1.604	3.257	N/A	0.000
Superpathway of Cholesterol Biosynthesis	-0.816	0.000	0.632	0.730	-1.000	3.204
Aspartate Degradation II	-0.816	2.807	-0.816	2.722	N/A	0.000
Phosphatidylcholine Biosynthesis I	-0.816	2.807	-0.816	2.722	N/A	0.000
Bladder Cancer Signaling	-0.775	2.925	-0.535	2.351	N/A	0.396
PTEN Signaling	-0.745	3.128	-0.885	3.055	N/A	0.000
CD27 Signaling in Lymphocytes	-0.728	1.186	-1.500	0.843	N/A	0.274
The Visual Cycle	-0.707	0.938	0.000	1.674	N/A	1.491
Glycogen Degradation III	-0.707	1.693	-1.000	2.189	N/A	0.000
Glycogen Degradation II	-0.707	2.173	-1.000	2.801	N/A	0.000
GDP-glucose Biosynthesis	-0.707	3.297	-0.707	3.188	N/A	0.000
Role of NFAT in Cardiac Hypertrophy	-0.663	7.268	-0.226	5.056	N/A	0.000
Antioxidant Action of Vitamin C	-0.632	5.128	-0.324	3.984	-1.000	1.132
Cardiac β-adrenergic Signaling	-0.617	3.860	-0.295	5.358	N/A	0.000
Synaptic Long Term Potentiation	-0.577	3.428	0.000	2.067	N/A	0.000
Neuropathic Pain Signaling in Dorsal Horn Neurons	-0.577	4.031	-0.457	2.246	N/A	0.000
Melatonin Signaling	-0.557	3.008	-0.408	1.325	N/A	0.000
FGF Signaling	-0.539	1.487	-0.539	1.300	N/A	0.000
Gas Signaling	-0.522	1.821	-0.174	1.810	N/A	0.000
Nitric Oxide Signaling in the Cardiovascular System	-0.493	1.731	-1.160	1.924	N/A	0.000
Cell Cycle: G2/M DNA Damage Checkpoint Regulation	-0.447	2.566	-0.218	2.763	1.890	6.384
α-Adrenergic Signaling	-0.447	4.179	0.229	3.142	N/A	0.000
Apelin Endothelial Signaling Pathway	-0.429	3.630	0.429	3.537	N/A	0.000
G Beta Gamma Signaling	-0.429	4.638	0.447	3.143	N/A	0.000
p53 Signaling	-0.378	1.255	0.000	1.626	-1.000	1.644
1D-myo-inositol Hexakisphosphate Biosynthesis II (Mammalian)	-0.333	1.640	-1.265	2.067	N/A	0.000
Cardiac Hypertrophy Signaling	-0.325	5.701	-0.325	5.281	N/A	0.000
Glutathione-mediated Detoxification	-0.302	0.755	-0.577	0.933	N/A	0.435
Tryptophan Degradation X (Mammalian, via Tryptamine)	-0.277	2.366	0.000	1.758	N/A	0.000
CREB Signaling in Neurons	-0.267	3.416	0.405	2.542	N/A	0.000
RhoGDI Signaling	-0.267	4.195	-0.896	5.131	N/A	0.000
3-phosphoinositide Degradation	-0.250	4.515	-0.750	4.039	N/A	0.000
Eicosanoid Signaling	-0.243	4.384	-0.728	2.881	N/A	1.139
NRF2-mediated Oxidative Stress Response	-0.180	4.400	0.000	4.656	N/A	0.473
Phospholipases	-0.174	5.402	-0.539	4.114	N/A	1.186
Retelin Signaling	-0.164	3.222	-0.480	4.138	N/A	0.000
Corticotropin Releasing Hormone Signaling	-0.146	2.076	0.149	1.994	N/A	0.000
Dopamine-DARPP32 Feedback in cAMP Signaling	-0.146	2.082	0.000	1.602	N/A	0.000
Protein Kinase A Signaling	-0.088	7.784	-0.258	9.445	0.447	0.466

Table 15. Canonical pathway analysis summary for rat PBMC following IRI: up-regulated pathways.

Canonical Pathways	Cohort 2 vs. Cohort 1	
	Z-score	-log(BH-p-value)
Cardiac Hypertrophy Signaling (Enhanced)	4.903	4.180
Production of Nitric Oxide and Reactive Oxygen Species	4.230	3.545
TREM1 Signaling	4.200	3.545
Dendritic Cell Maturation	4.003	2.383
iNOS Signaling	3.873	2.746
Neuroinflammation Signaling Pathway	3.845	3.209
Role of Pattern Recognition Receptors in Recognition	3.800	2.165
Endothelin-1 Signaling	3.753	3.545
Colorectal Cancer Metastasis Signaling	3.727	3.040
Gαq Signaling	3.651	2.219
Superpathway of Inositol Phosphate Compounds	3.615	4.279
Opioid Signaling Pathway	3.592	0.716
Tec Kinase Signaling	3.536	2.176
NF-κB Signaling	3.501	5.251
Fcγ Receptor-mediated Phagocytosis in Macrophages	3.400	2.352
Acute Phase Response Signaling	3.395	4.006
Th17 Activation Pathway	3.357	0.404
IL-8 Signaling	3.333	1.783
MIF-mediated Glucocorticoid Regulation	3.317	1.788
AMPK Signaling	3.307	0.903
Aldosterone Signaling in Epithelial Cells	3.300	0.934
IL-1 Signaling	3.300	2.525
IL-6 Signaling	3.280	5.527
Type I Diabetes Mellitus Signaling	3.272	4.143
Cardiac Hypertrophy Signaling	3.244	2.022
NGF Signaling	3.182	2.979
Adrenomedullin signaling pathway	3.175	3.713
Synaptogenesis Signaling Pathway	3.151	1.573
G Beta Gamma Signaling	3.130	0.681
Signaling by Rho Family GTPases	3.130	1.883
MIF Regulation of Innate Immunity	3.051	1.892
CCR3 Signaling in Eosinophils	3.024	3.155
P2Y Purigenic Receptor Signaling Pathway	3.024	2.292
EGF Signaling	3.000	1.708
TNFR1 Signaling	3.000	2.350
FGF Signaling	2.982	1.454
3-phosphoinositide Biosynthesis	2.887	3.254
Toll-like Receptor Signaling	2.887	2.526
Phospholipases	2.828	1.991
D-myo-inositol-5-phosphate Metabolism	2.777	3.267
Role of NFAT in Cardiac Hypertrophy	2.722	2.253
Androgen Signaling	2.714	0.427
Gαi Signaling	2.711	1.493
Pancreatic Adenocarcinoma Signaling	2.711	2.197
VEGF Family Ligand-Receptor Interactions	2.711	2.112
14-3-3-mediated Signaling	2.694	3.040

Endocannabinoid Neuronal Synapse Pathway	2.683	0.356
Growth Hormone Signaling	2.668	1.473
Thrombin Signaling	2.667	2.072
D-myo-inositol (1,4,5)-Trisphosphate Biosynt	2.646	0.853
ErbB Signaling	2.646	2.917
RANK Signaling in Osteoclasts	2.646	4.066
CXCR4 Signaling	2.611	2.263
HGF Signaling	2.611	4.038
Ephrin Receptor Signaling	2.600	0.574
IL-3 Signaling	2.600	2.665
PDGF Signaling	2.600	2.526
Th1 Pathway	2.556	3.254
3-phosphoinositide Degradation	2.530	3.038
Phospholipase C Signaling	2.530	1.780
Role of NFAT in Regulation of the Immune Re	2.530	3.634
TNFR2 Signaling	2.530	1.745
Cholecystokinin/Gastrin-mediated Signaling	2.502	1.708
Mouse Embryonic Stem Cell Pluripotency	2.502	2.263
STAT3 Pathway	2.502	3.634
IL-23 Signaling Pathway	2.500	1.991
Triacylglycerol Biosynthesis	2.496	1.496
HMGB1 Signaling	2.475	1.748
Rac Signaling	2.475	3.038
GNRH Signaling	2.466	2.412
D-myo-inositol (1,3,4)-trisphosphate Biosynt	2.449	1.170
Type II Diabetes Mellitus Signaling	2.449	2.483
Glioblastoma Multiforme Signaling	2.414	0.940
LPS-stimulated MAPK Signaling	2.414	4.279
Renin-Angiotensin Signaling	2.414	2.714
PI3K Signaling in B Lymphocytes	2.402	4.038
Apelin Endothelial Signaling Pathway	2.401	3.634
Renal Cell Carcinoma Signaling	2.400	3.548
UVA-Induced MAPK Signaling	2.400	2.626
IL-7 Signaling Pathway	2.357	1.639
FLT3 Signaling in Hematopoietic Progenitor C	2.353	2.568
NF-κB Activation by Viruses	2.353	3.237
Melatonin Signaling	2.333	0.272
Notch Signaling	2.333	1.844
FAT10 Cancer Signaling Pathway	2.309	1.301
Apelin Cardiomyocyte Signaling Pathway	2.294	1.873
CD28 Signaling in T Helper Cells	2.294	2.230
Melanocyte Development and Pigmentation S	2.294	1.702
Sperm Motility	2.294	1.357
p70S6K Signaling	2.268	1.872
ErbB2-ErbB3 Signaling	2.236	2.291
ErbB4 Signaling	2.236	3.264
Role of NANOG in Mammalian Embryonic Ste	2.236	0.864
Synaptic Long Term Depression	2.191	0.633

ERK5 Signaling	2.183	1.346
B Cell Receptor Signaling	2.143	4.066
Wnt/Ca+ pathway	2.138	1.035
D-myo-inositol (1,4,5,6)-Tetrakisphosphate B	2.137	2.965
D-myo-inositol (3,4,5,6)-tetrakisphosphate Bi	2.137	2.965
Cdc42 Signaling	2.132	0.807
PFKFB4 Signaling Pathway	2.121	0.373
Superpathway of D-myo-inositol (1,4,5)-trisph	2.121	1.565
CREB Signaling in Neurons	2.117	1.127
JAK/Stat Signaling	2.117	3.503
CNTF Signaling	2.065	2.348
Thrombopoietin Signaling	2.065	1.994
cAMP-mediated signaling	2.058	0.661
Apelin Adipocyte Signaling Pathway	2.000	0.807
Integrin Signaling	2.000	0.844
Leukocyte Extravasation Signaling	2.000	1.668
Pentose Phosphate Pathway	2.000	0.949
Role of JAK1, JAK2 and TYK2 in Interferon Si	2.000	1.475
Urea Cycle	2.000	1.819
Macropinocytosis Signaling	1.964	2.203
Prolactin Signaling	1.964	2.352
VEGF Signaling	1.964	2.626
IGF-1 Signaling	1.961	2.546
p38 MAPK Signaling	1.961	1.977
Paxillin Signaling	1.961	1.952
PKCθ Signaling in T Lymphocytes	1.947	3.209
fMLP Signaling in Neutrophils	1.915	4.252
1D-myo-inositol Hexakisphosphate Biosynthe	1.890	1.639
Mitochondrial L-carnitine Shuttle Pathway	1.890	1.756
PAK Signaling	1.890	3.034
SAPK/JNK Signaling	1.890	2.590
GM-CSF Signaling	1.877	3.226
IL-17A Signaling in Airway Cells	1.877	3.209
PEDF Signaling	1.877	2.977
Huntington's Disease Signaling	1.826	1.458
Actin Cytoskeleton Signaling	1.809	2.808
Osteoarthritis Pathway	1.808	1.543
Nitric Oxide Signaling in the Cardiovascular S	1.807	0.344
UVB-Induced MAPK Signaling	1.807	2.118
Endocannabinoid Developing Neuron Pathwa	1.800	1.487
GDNF Family Ligand-Receptor Interactions	1.789	1.908
mTOR Signaling	1.768	6.972
Fc Epsilon RI Signaling	1.715	3.348
Estrogen-Dependent Breast Cancer Signaling	1.698	2.292
4-1BB Signaling in T Lymphocytes	1.667	2.379
Inflammasome pathway	1.667	2.383
Choline Biosynthesis III	1.633	1.501
D-myo-inositol (1,4,5)-trisphosphate Degrada	1.633	1.277

IL-17A Signaling in Gastric Cells	1.633	0.982
Leukotriene Biosynthesis	1.633	1.773
Role of IL-17F in Allergic Inflammatory Airway	1.633	0.256
Superpathway of Citrulline Metabolism	1.633	1.501
Glioma Signaling	1.606	1.293
IL-2 Signaling	1.606	2.582
Regulation of eIF4 and p70S6K Signaling	1.606	11.288
Lymphotoxin β Receptor Signaling	1.604	2.053
Death Receptor Signaling	1.528	1.727
Neurotrophin/TRK Signaling	1.528	2.142
Telomerase Signaling	1.528	2.274
CDP-diacylglycerol Biosynthesis I	1.508	2.713
Eicosanoid Signaling	1.508	1.547
Ephrin B Signaling	1.508	0.866
Phosphatidylglycerol Biosynthesis II (Non-pla	1.508	2.489
Agrin Interactions at Neuromuscular Junction	1.500	0.866
Ovarian Cancer Signaling	1.500	0.545
ILK Signaling	1.461	0.504
Endometrial Cancer Signaling	1.414	2.291
TGF- β Signaling	1.414	1.293
ERK/MAPK Signaling	1.406	1.991
CD40 Signaling	1.400	4.066
Oncostatin M Signaling	1.387	1.822
UVC-Induced MAPK Signaling	1.387	1.564
Cytotoxic T Lymphocyte-mediated Apoptosis	1.342	0.244
Fatty Acid Activation	1.342	1.233
Interferon Signaling	1.342	0.172
Neuregulin Signaling	1.342	1.293
γ -linolenate Biosynthesis II (Animals)	1.342	0.837
PI3K/AKT Signaling	1.333	3.798
Chemokine Signaling	1.279	2.291
Sphingosine-1-phosphate Signaling	1.279	0.843
Synaptic Long Term Potentiation	1.279	0.540
Stearate Biosynthesis I (Animals)	1.265	0.837
α -Adrenergic Signaling	1.265	0.729
G α 12/13 Signaling	1.257	2.609
iCOS-iCOSL Signaling in T Helper Cells	1.225	1.906
BMP signaling pathway	1.213	0.840
Non-Small Cell Lung Cancer Signaling	1.213	1.378
IL-9 Signaling	1.155	1.881
Pyridoxal 5'-phosphate Salvage Pathway	1.155	0.533
SPINK1 General Cancer Pathway	1.147	1.756
Hypoxia Signaling in the Cardiovascular Syst	1.134	0.807
Pyrimidine Ribonucleotides De Novo Biosynt	1.134	0.245
Pyrimidine Ribonucleotides Interconversion	1.134	0.274
Relaxin Signaling	1.091	3.243
Cell Cycle: G2/M DNA Damage Checkpoint F	1.069	2.080
Role of PI3K/AKT Signaling in the Pathogenes	1.069	1.247

T Cell Exhaustion Signaling Pathway	1.061	2.592
Apoptosis Signaling	1.043	1.624
Citrulline Biosynthesis	1.000	1.218
GDP-glucose Biosynthesis	1.000	1.067
Guanosine Nucleotides Degradation III	1.000	0.844
IL-22 Signaling	1.000	1.892
Induction of Apoptosis by HIV1	1.000	1.639
Melanoma Signaling	1.000	2.244
Tumoricidal Function of Hepatic Natural Killer	1.000	0.449
Acute Myeloid Leukemia Signaling	0.962	4.066
Glioma Invasiveness Signaling	0.943	1.296
Actin Nucleation by ARP-WASP Complex	0.905	0.272
B Cell Activating Factor Signaling	0.905	2.715
Leptin Signaling in Obesity	0.905	1.624
FcγRIIB Signaling in B Lymphocytes	0.894	2.857
Apelin Muscle Signaling Pathway	0.816	1.170
Cardiac β-adrenergic Signaling	0.816	2.206
Glutathione-mediated Detoxification	0.816	0.401
Granzyme B Signaling	0.816	1.378
NAD Phosphorylation and Dephosphorylation	0.816	1.773
Apelin Pancreas Signaling Pathway	0.775	2.054
Th2 Pathway	0.730	2.590
CD27 Signaling in Lymphocytes	0.728	3.556
Salvage Pathways of Pyrimidine Ribonucleoti	0.728	0.533
Small Cell Lung Cancer Signaling	0.728	2.197
Role of RIG1-like Receptors in Antiviral Innate	0.707	1.106
VDR/RXR Activation	0.632	0.398
NRF2-mediated Oxidative Stress Response	0.626	3.040
Antiproliferative Role of Somatostatin Receptc	0.535	2.292
April Mediated Signaling	0.500	3.328
RhoA Signaling	0.447	0.533
UDP-N-acetyl-D-galactosamine Biosynthesis	0.447	1.502
Endocannabinoid Cancer Inhibition Pathway	0.378	0.989
Remodeling of Epithelial Adherens Junctions	0.378	0.596
Insulin Receptor Signaling	0.343	2.664
Fatty Acid β-oxidation I	0.333	1.216
tRNA Splicing	0.277	1.892
TWEAK Signaling	0.277	2.516
Corticotropin Releasing Hormone Signaling	0.243	0.202
Calcium-induced T Lymphocyte Apoptosis	0.000	0.000
Ceramide Signaling	0.000	1.639
LPS/IL-1 Mediated Inhibition of RXR Function	0.000	2.040
NAD Salvage Pathway II	0.000	0.623
Wnt/β-catenin Signaling	0.000	0.000

Table 16. Canonical pathway analysis summary for rat PBMC following IRI: down-regulated pathways.

Canonical Pathways	Cohort 2 vs. Cohort 1	
	Z-score	-log(BH-p-value)
Antioxidant Action of Vitamin C	-3.900	4.143
PPAR Signaling	-3.651	3.209
EIF2 Signaling	-3.046	22.200
Oxidative Phosphorylation	-2.840	0.000
Cell Cycle: G1/S Checkpoint Regulation	-2.309	1.594
NER Pathway	-2.041	2.180
p53 Signaling	-1.941	0.477
PTEN Signaling	-1.461	2.567
Role of p14/p19ARF in Tumor Suppression	-1.414	1.053
Amyloid Processing	-1.000	1.025
Role of CHK Proteins in Cell Cycle Checkpoint	-1.000	1.873
LXR/RXR Activation	-0.853	1.639
Valine Degradation I	-0.816	1.170
Aryl Hydrocarbon Receptor Signaling	-0.775	0.427
Sirtuin Signaling Pathway	-0.762	2.596
Sumoylation Pathway	-0.688	0.844
Mitotic Roles of Polo-Like Kinase	-0.632	1.374
Role of BRCA1 in DNA Damage Response	-0.577	1.491
ATM Signaling	-0.500	0.843
NAD biosynthesis II (from tryptophan)	-0.447	1.000
Purine Nucleotides De Novo Biosynthesis II	-0.447	1.502
Protein Kinase A Signaling	-0.384	2.698
PPAR α /RXR α Activation	-0.324	3.713
Activation of IRF by Cytosolic Pattern Recognition	-0.302	0.427
Regulation of Cellular Mechanics by Calpain I	-0.302	0.677
Angiopoietin Signaling	-0.243	3.217
CDK5 Signaling	-0.209	1.277

Table 17. Fold-change data, p-values, and FDR-corrected p-values for all genes and comparisons from RNAseq data. FDR p-values determined using the Benjamini-Hochberg method.



Table 17.xlsx